SPILLOVER STABILIZATION IN THE CONTROL OF LARGE FLEXIBLE SPACE STRUCTURES

by

Eva A. Czajkowski

Dissertation submitted to the Faculty of the
Virginia Polytechnic Institute and State University
in partial fulfillment of the requirements for the degree of
Doctor of Philosophy
in
Aerospace Engineering

APPROVED:

Raphael T. Haftka, Chairman

William L. Hallauer, Jr.

Stanoje Bingulac

Rakesh K. Kapania

Liviu Librescu

May, 1988

Blacksburg, Virginia

SPILLOVER STABILIZATION IN THE CONTROL OF LARGE FLEXIBLE SPACE STRUCTURES

by

Eva A. Czajkowski

Raphael T. Haftka, Chairman

Aerospace Engineering

(ABSTRACT)

Active control of large flexible space structures is typically implemented to control only a few known elastic modes. Linear Quadratic Regulators (LQR) and Kalman-Bucy Filter (KBF) observers are usually designed to control the desired modes of vibration. Higher modes, referred to as residual modes, are generally ignored in the analysis and may be excited by the controller to cause a net destabilizing effect on the system. This is referred to as the spillover phenomenon.

This dissertation considers the stabilization of the neglected dynamics of the higher modes of vibration. It aims at designing modal controllers with improved spillover stability properties. It is based on the premise that the structural dynamicist will be able to predict more vibration modes than would be practical to include in the design of the controller. The proposed method calls for designing the observer so as to improve spillover stability with minimum loss in performance. Two formulations are pursued. The first is based on optimizing the noise statistics used in the design of the Kalman-Bucy Filter. The second optimizes directly the gain matrix of the observer.

The influence of the structure of the plant noise intensity matrix of the Kalman-Bucy Filter on the stability margin of the residual modes is demonstrated. An optimization procedure is presented which uses information on the residual modes to minimize spillover (i.e., maximize the stability margin) of known residual modes while preserving robustness vis-à-vis the unknown dynamics. This procedure selects either the optimum plant noise intensity matrix or the optimum observer gain matrix directly to maximize the stability margins of the residual modes and properly place the observer poles. The proposed method is demonstrated for both centralized and decentralized modal control.

Acknowledgements

I wish to express my gratitude to Dr. Raphael T. Haftka for his roles as my advisor and chairman of my doctoral committee under a somewhat unusual trans-Atlantic arrangement. His guidance and helpful suggestions during the course of this project are very much appreciated. His expertise in the area of optimization proved to be invaluable.

I would like to thank Dr. William L. Hallauer, Jr., Dr. Rakesh K. Kapania, Dr. Stanoje Bingulac, and Dr. Liviu Librescu for serving as members of my committee. Their constant encouragement and interest in my research work has been most beneficial. I am especially indebted to Dr. Bingulac for his help with the L-A-S computer program. His constant support in terms of consultations, along with expanding the capabilities of the computer program for my particular research needs, is very much appreciated. Special thanks are also extended to Dr. Harry H. Robertshaw for his association with this project.

I would also like to thank Dr. Douglas K. Lindner for his help in the area of decentralized modal control. His assistance in this segment of my research, along with his help in tracking down and providing some pertinent references, is appreciated.

Special thanks are extended to Dr. André Preumont of the Free University of Brussels (Belgium). Although not formally a member of my committee, this research was initiated under his supervision, some three years ago, while he was a visiting professor at Virginia Polytechnic In-

stitute and State University. After returning to Belgium, he continued to act as my advisor. His persistence, insight, and dedication to this research project proved to be crucial. I am grateful to him for the support he has shown me in terms of guidance, suggestions, and having research discussion meetings with me at various locations in the United States and Belgium. I wish to express my sincere gratitude to the North Atlantic Treaty Organization for helping this research by way of a travel grant (NATO Grant 86-698). This grant enabled me to make two trips to Belgium and for Dr. Preumont to make several trips back to the United States.

This research was funded by the National Aeronautics and Space Administration (NASA Grant NAG-1-603). I gratefully acknowledge and appreciate their financial support. I am also grateful to the Department of Aerospace and Ocean Engineering for the Pratt Presidential Fellowship.

Finally, I would like to take this opportunity to express my sincerest appreciation to my parents and brother who have been a constant source of support and encouragement.

Table of Contents

List of Illustrations

List of Tables

NOMENCLATURE

a	vector elements of $V_1 = aa^T$
a_A	A for the scalar case
a_k	element of K_c in the grid structure example
a_q	element of a_Q in Q_q in the grid structure example
a_Q	vector elements of $Q_q = a_Q a_Q^T$ in the grid structure example
a_v	element of V_1 in the grid structure example
A	system matrix (plant coefficient matrix)
A_c	system matrix of the controlled modes
A_D	system matrix in decentralized modal control
A_D^s	spillover system matrix in decentralized modal control
A_D^x	regulator/observer system matrix in decentralized modal control
A_r	system matrix of the known residual modes
A_R	system matrix of the unknown residual modes
$\overline{A}$	α - shifted system matrix $(A + \alpha I)$
$\overline{A}_i^D$	disabled system matrix in decentralized modal control
$\overline{A}_i^s$	disabled spillover system matrix in decentralized modal control
$\overline{A}_i^x$	disabled regulator/observer system matrix in decentralized modal control

$A(t)$	system matrix for the time-varying system
b	column vector of H
b_B	B for the scalar case
b_k	element of K_c in the grid structure example
b_q	element of a_Q in Q_q in the grid structure example
b_v	element of V_1 in the grid structure example
B	control matrix
B_c	control matrix of the controlled modes
B_r	control matrix of the known residual modes
B_R	control matrix of the unknown residual modes
$B(t)$	control matrix for the time-varying system
c_C	C for the scalar case
c_k	element of K_c in the grid structure example
c_q	element of a_Q in Q_q in the grid structure example
c_v	element of V_1 in the grid structure example
C	output matrix
C_c	output matrix of the controlled modes
C_r	output matrix of the known residual modes
C_R	output matrix of the unknown residual modes
$\underline{C}$	viscous damping matrix
d_k	element of K_c in the grid structure example
d_v	element of V_1 in the grid structure example
$d(s)$	(output) disturbance signal
$D(s)$	(output) disturbance signal vector
$D_{gk}(s)$	denominator of $g(s)k(s)$
e	state estimator error
e_c	state estimator error of the controlled modes
e_k	element of K_c in the grid structure example

e_v	element of V_1 in the grid structure example
$e(s)$	error signal
EI	bending stiffness for Balas beam
$E[.]$	expected value of function [.]
$E(s)$	error signal vector
f	optimization objective function for the deterministic spillover study
$\bar{f}$	applied force vector
f_F	$\bar{F}$ for the scalar case
f_k	element of K_c in the grid structure example
f_v	element of V_1 in the grid structure example
F	optimization objective function for the stochastic spillover study
$\bar{F}$	solution of the LQR Riccati Equation
$F_{\bar{f}}$	applied force distribution matrix
$F_{performance}$	relative performance deterioration of the system under the actual noise statistics
$\bar{F}(t, T)$	solution of the LQR Riccati Equation for the finite-time deterministic regulator - time-varying system
$\bar{F}^{\infty}(t)$	solution of the LQR Riccati Equation for the infinite-time deterministic regulator - time-varying system
$g(s)$	SISO plant transfer function
$[g(s)k(s)]$	open-loop transfer function
$\dfrac{[g(s)k(s)]}{[1+g(s)k(s)]}$	closed-loop transfer function (complementary sensitivity transfer function)
$g^{n}(s)$	nominal plant transfer function
$G(s)$	MIMO plant transfer function matrix
$[G(s)K(s)]$	open-loop transfer matrix
$\tilde{G}(s)$	actual plant transfer function matrix
G_c	feedback/closed-loop regulator gain matrix
GM	gain margin
H	matrix elements of $V_1 = HH^T$

$\mathscr{H}_1(s)$	open-loop transfer function of the LQR relating u and χ
$\mathscr{H}_2(s)$	open-loop transfer function of the KBF relating z and $\hat{u}$
I	identity matrix
$[I + G(s)K(s)]$	return difference matrix
$[I + G(s)K(s)]^{-1}$	inverse return difference matrix
$[I + G(s)K(s)]^{-1}G(s)K(s)$	closed-loop transfer matrix
$[1 + g(s)k(s)]$	return difference transfer function
$[1 + g(s)k(s)]^{-1}$	sensitivity transfer function
j	imaginary number $\sqrt{-1}$
J	performance index
J_{LQR}	performance index for the LQR alone (when the state is perfectly observed)
$J_{LQR+KBF}$	LQG performance index with regulator/observer pair
J_{OPT}	statistically optimum stochastic performance index
J_r	performance index contribution for the known residual modes
k_s	scaling factor in the optimization objective function
$k(s)$	SISO compensator transfer function
K	stiffness matrix
K_c	observer gain matrix
$K(s)$	MIMO compensator transfer function matrix
KBF	Kalman-Bucy Filter
$l_a(\omega)$	upper bound on the magnitude of $\Delta G(s)$
$l_m(\omega)$	upper bound on the magnitude of $L(s)$
L	length of the Balas beam
$L(s)$	relative error of the plant under a multiplicative uncertainty
LQR	Linear Quadratic Regulator
LQG	Linear Quadratic Gaussian
LQG/LTR	Linear Quadratic Gaussian with Loop Transfer Recovery

m	number of modes of the actual known system (large scale model)
$\overline{m}$	mass per unit length of the Balas beam
m_A	number of open-loop zeros of $\mathscr{H}_1(s)$
M	mass matrix
M_C	controllability matrix
M_O	observability matrix
MESS	Model Error Sensitivity Suppression
MIMO	multi-input-multi-output
n	number of controlled modes in the reduced-order system
n_a	number of actuators
n_A	order of the controlled system (order of matrix A), i.e., $n_A = 2n$
n_b	number of columns of H
n_c	number of controlled modes
n_p	number of unstable open-loop SISO system poles
n_s	number of sensors
$n(s)$	sensor noise signal
N_p	number of unstable open-loop MIMO system poles
$N(s)$	sensor noise signal vector
$N_{gk}(s)$	numerator of $g(s)k(s)$
$N(\overline{\beta}; \Phi_c(s); \Gamma)$	number of clockwise encirclements of the point $\overline{\beta}$ by the conformal mapping $\Phi_c(s)$ of contour Γ
p_j	open-loop poles
p_n	number of closed-loop poles of $\phi_{CL}(s)$ in the right half-plane
$ps(\omega)$	performance specification
P	solution of the KBF Riccati Equation
P_L	solution of the Lyapunov Equation
PM	phase margin
q	LQG/LTR scaling factor
q_Q	Q for the scalar case

Q	weighting matrix on the state
Q_c	weighting matrix on the state of the controlled modes
Q_q	LQG/LTR matrix
Q_r	weighting matrix on the state of the known residual modes
$Q(t)$	weighting matrix on the state for the time-varying system
$\overline{Q}(t)$	α - shifted time-varying weighting matrix on the state
r	radius of the Nyquist contour
r_R	R for the scalar case
$r(s)$	input command reference signal
R	weighting matrix on the control
R_r	weighting matrix on the control of the known residual modes
$R(s)$	input command reference signal vector
$R(t)$	weighting matrix on the control for the time-varying system
$\overline{R}(t)$	α - shifted time-varying weighting matrix on the control
s	complex variable ($s = \sigma_s + j\omega$)
S	terminal penalty matrix
$SISO$	single-input-single-output
t	minimum desired system stability margin
t	time
t_f	final time
t_o	initial time
T	terminal time
$T_{CL}(s)$	actual closed-loop transfer function
$T^{\times}_{CL}(s)$	nominal closed-loop transfer function
T_x	matrix of eigenvectors of the matrix A
u	control vector
$u(s)$	control input signal
$\overline{u}$	α - shifted control vector

$\hat{u}$	observer control vector
u^*	optimal control vector
$\bar{u}^*$	α - shifted optimal control vector
$U(s)$	control input signal vector
v_i^2	diagonal elements of $V_1 = diag(v_i^2)$
$\hat{v}$	observer noise $[\hat{v} \equiv (K_e w_2 - w_1)^T]$
V_1	plant noise intensity matrix of the KBF
V_{1_c}	KBF plant noise intensity matrix of the controlled modes
V_{1_r}	KBF plant noise intensity matrix of the known residual modes
V_2	measurement noise intensity matrix of the KBF
V_{2_r}	measurement noise intensity matrix of the known residual modes
w	stationary white noise excitation
w_1	plant noise
w_2	measurement noise
W	stationary white noise intensity matrix
W_1	actual plant noise intensity matrix
W_2	actual measurement noise intensity matrix
W_r	control weighting matrix in MESS
W_{V_r}	noise weighting matrix in MESS
x	state vector
x_c	state vector of the controlled modes
x_f	final state vector
x_o	initial state vector
x_r	state vector of the known residual modes
x_R	state vector of the unknown residual modes
$\hat{x}$	reconstructed state vector
$\bar{x}$	α - shifted state vector

x	position along the length of the Balas beam
y	output vector
$y(s)$	output signal
$y^{*}(s)$	output signal under the nominal plant
$Y(s)$	output signal vector
z	estimator state vector ("transpose" of state estimator error)
z_i	open-loop zeros
z_n	number of closed-loop zeros of $\phi_{CL}(s)$ in the right half-plane
α	prescribed stability margin
α_{LQR}	stability margin of the LQR
α_{OBS}	stability margin of the KBF observer
α_{RES}	stability margin of the residual modes
β	control matrix - coupling effect from control spillover in decentralized modal control
$\bar{\beta}$	encirclement point
γ	output matrix - coupling effect from observation spillover in decentralized modal control
Γ	closed contour
Γ_{gk}	image contour of Γ_s under the mapping $g(s)k(s)$
Γ_s	Nyquist contour (outlines entire right half-plane)
$\bar{\Gamma}_s$	image contour of Γ_s under the mapping $\phi_{CL}(s)$
δ	actual system stability margin
$\delta g(s)$	variation between nominal and actual plants
$\delta y(s)$	variation between nominal and actual outputs
$\Delta G(s)$	absolute model error of the plant under an additive uncertainty
ε	state vector of the composite system
ε_L	percentage of the relative error present in the plant model
ε_o	initial state vector of the composite system
ζ	viscous damping factor

η_k	modal amplitude of mode k
$\frac{\dot{\eta}_k}{\omega_k}$	reduced modal velocity of mode k
λ_i	closed-loop system eigenvalues
λ_{max}	maximum stability margin on the composite system (maximum speed)
μ	weighting parameter used to weight the objectives of spillover stability and performance
ν_i	positive scalar factor in V_2 under the MESS formulation
Ξ	normalized weighting matrix on the control
ρ_i	positive scalar factor in R under the MESS formulation
$\bar{\rho}$	scalar, scaling the relative weight of the control
$\sigma[.]$	singular value of matrix [.]
$\bar{\sigma}$	maximum singular value
$\underline{\sigma}$	minimum singular value
$\bar{\upsilon}$	scalar, scaling the relative weight of the measurement noise intensity matrix
$\bar{\Upsilon}$	normalized measurement noise intensity matrix
$\phi_{CL}(s)$	closed-loop characteristic polynomial
$\phi_k(a)$	mode shape amplitude corresponding to the actuator location
$\phi_k(s)$	mode shape amplitude corresponding to the sensor location
$\phi_{OL}(s)$	open-loop characteristic polynomial
Φ	modal matrix
$\Phi_c(s)$	conformal mapping function
χ	controlled variable
ω	frequency
ω_k	undamped natural frequency

CHAPTER 1. INTRODUCTION

Active control of large flexible space structures is typically implemented to control only a few known elastic modes. Linear state feedback regulators and Kalman-Bucy Filter observers are usually designed to control the desired modes of vibration. Higher modes, referred to as residual modes, are generally ignored in the analysis and may be excited by the controller to cause a net destabilizing effect on the system. This is referred to as the spillover phenomenon [1].

There are two contributions to spillover. The first is observation spillover which entails the contamination of the sensor output signal through the presence of the residual modes. The second is control spillover which entails the excitation of the residual modes by the feedback controller. When both types of spillover are present, the system may become unstable. Spillover moves the eigenvalues of the residual poles from their original locations. Since they usually have a small stability margin, even a slight coupling may destabilize them.

Balas [1 – 5] has demonstrated that spillover instability is one of the major issues in the control of large space structures. This is due to the very large size of the systems involved which results in high modal density and the very light natural damping of such structures.

Spillover can also be an important problem in decentralized modal control. Decentralized modal control involves multi-actuators and sensors which control distinct sets of modes that may be locally dominant. It may be attractive for large space structures because the various compo-

nents, which may be located quite far from each other, are often affected by distinct sets of modes which are locally dominant. For example, the PACOSS (Passive and Active Control of Space Structures program) representative system considered by Morgenthaler and Gehling [6] has 210 modes below 10 Hz, out of which only 34 are global; the others are local, i.e., they affect only one component of Large Space Structures (LSS). By a judicious choice of the actuator and sensor locations, the local nature of the modes can be exploited to make the coupling between the control subsystems as weak as possible.

In the absence of control reconfiguration, independence implies that if one of the controllers is turned off (following a failure or for any other reason) the closed-loop system remains stable. This implies that each individual modal controller provides the set of modes it does not control with a positive stability margin. This is designated as the reliability condition, and it is in this context that spillover is analyzed, i.e., the controlled modes of one controller become the residual modes of the other controller. When a local controller does not operate, the corresponding set of modes has a small stability margin and is a candidate for destabilization. It must remain stable in spite of its interaction with the other subsystems.

Various ways of alleviating spillover have been proposed:

- increasing the passive damping, i.e., selecting certain materials based on their properties, implementing a specific structural design, adding devices such as elastomers and coatings, etc. [7];

- supplementing modal control by direct velocity feedback with colocated sensors and actuators [8 – 13]. This technique was found to guarantee stability and robustness. [12, 13];

- suppressing the residual modes via a transformation in the problem formulation which produces an observer gain matrix which effectively nullifies the observation spillover [14 – 16];

- adding an innovations feedthrough (output feedback) component to the control and a residual mode aggregation component to the observer that restitute the original stability margin to a selected number of residual modes [3, 5]. The scheme requires the knowledge of the residual modes and a number of sensors which is at least twice the number of residual modes to be corrected. There is no guarantee that the spillover in the remaining residual modes will not be increased, and, in fact, this scheme has been found to reduce significantly the robustness of the system. [17];

- using frequency dependent weighting matrices in the quadratic cost function to increase the penalty for the high frequency components of the control [18], reflecting the fact that input in the frequency range, where the model characteristics are poor, is undesirable. This procedure can also be used to achieve some integral action at low frequency.;

- utilizing Loop Transfer Recovery (LTR) techniques by designing a regulator which satisfies a robustness test and make the controller *recover* the loop transfer matrix of the regulator assuming the noise enters the plant at the input [19];

- implementing nonlinear modifications to the control in the vicinity of the equilibrium which makes the composite system (regulator, observer, and residual modes) benefit from the inherent stability properties of the open-loop system [20];

- adding a correction to the control law which nullifies the effect of the truncated modes on the closed-loop system. An estimate of the model deviation, as a result of the truncated modes, is needed and is determined by designing two filters. The first is designed for the controlled system model, and the second is designed for the actual state observation. The control law correction term nullifies the difference between these two filters. This technique decouples the truncated modes from the controlled system model and, therefore, prevents any movement in the eigenvalues from their original designed locations. [21];

- minimizing an objective function which includes the quadratic performance index and a term corresponding to the sum of the closed-loop eigenvalues of the truncated modes. This objective function represents a trade-off between controller performance and truncated mode stability. It assumes that the truncated modes are *much* faster than the controlled system modes, i.e., there is an appreciable *gap* between the controlled and truncated modes; they are not closely spaced. An accurate model of the fast dynamics is not required. The design procedure uses linear output feedback control with constant feedback gain. Thus, no observer is present in the problem formulation. An iterative procedure is presented for the determination of the feedback gain matrix [22].

When the structural model is sufficiently accurate to provide some reliable information about the residual modes, it is possible to include in the control system performance index a penalty in the control spillover which forces the control to be *orthogonal* to a set of residual modes [23, 24]. This method is known under the acronym of MESS (Model Error Sensitivity Suppression). By duality, the method applies to observation spillover as well. In the Kalman-Bucy Filter design, the measurement noise intensity matrix is given a fictitious contribution of the shape of the observation spillover, which tends to produce an observer blind to the residual modes. MESS, however, does not guarantee stability, and it cannot be applied to SISO systems.

Low order controllers insuring the stability of the full-order system have been investigated [25] and applied to flutter control [26, 27]. The controller parameters are obtained as a solution of an optimization problem. The solution is not guaranteed to exist (existence is conditioned on the selection of a set of initial design variables which result in a stable solution), but if it does, it is guaranteed to be stable for the full-order system. By a proper adjustment of the weighting matrix appearing in the performance index, this method can be used to control a limited set of modes while keeping the others barely stable.

There are certain restrictions and limitations on all the above methods.

In general, the active control problem can be viewed as consisting of three types of modes, i.e.,

- the *controlled modes* for which Linear Quadratic Regulators and Kalman-Bucy Filters are designed to control the desired modes of vibration.

- the *marginal residual (uncontrolled) modes* which are found in the transition region just outside the bandwidth of the controller. They either do not satisfy a stability robustness test or have only a small stability margin. These modes are candidates for destabilization and must be considered carefully.

- the *control system robust residual (uncontrolled) modes* (called robust modes hereafter) which satisfy a stability robustness test and are guaranteed to be stable.

Only the controlled and marginal residual modes will have to be considered by the designer; the latter will be called residual modes.

In a number of the above mentioned methods, e.g., LTR and MESS, the noise intensity matrices involved in the design of the Kalman-Bucy Filter are considered as free parameters which can be tuned to achieve desirable properties in the control system. A similar point of view is adopted in this study. Therefore, the objective of the present research is to use information on residual modes to develop a design methodology for the Linear Quadratic Regulator (LQR) and Kalman-Bucy Filter (KBF). The controller design has an appreciable effect on the stability margin of the composite system. The influence of the structure of the plant noise intensity matrix of the Kalman-Bucy Filter on the system stability margin as defined by the residual modes will be demonstrated. The idea of optimizing the stability margin by designing a proper controller becomes readily apparent. The goal is to develop an optimization procedure which minimizes spillover (i.e., maximizes the stability margin) of *known* residual modes while preserving robustness vis-à-vis the *unknown* dynamics. The unknown dynamics are viewed as an unstructured uncertainty. A candidate design method has been developed and is demonstrated on both centralized and decentralized modal control. This design procedure is based on minimizing a composite cost functional which includes a contribution from system stability and from performance. The stability of the unknown

dynamics (viewed as unstructured) is taken care of by a robustness test. It is the robustness test which also decides which modes are robust and which are residual.

CHAPTER 2. BACKGROUND INFORMATION

This chapter outlines the basic concepts of the control theory which will be used in this dissertation. The formulation of the basic structural vibration equation in state-space form is also presented. The reader who is familiar with the concepts of classical and modern control theory may want to skip this chapter.

2.1. EQUATION OF MOTION

The equation of motion for a discretized vibrating structure, which was mathematically modelled with m degrees of freedom, is

$$\underline{M}\ddot{p} + \underline{C}\dot{p} + \underline{K}p = \bar{f} \qquad [2.1.1]$$

where $\underline{M}$ is the mass matrix, $\underline{C}$ is the viscous damping matrix, $\underline{K}$ is the stiffness matrix, p is the physical displacement/coordinate vector, and $\bar{f}$ is the applied force vector. $\underline{M}$, $\underline{C}$, and $\underline{K}$, are of dimension $m \times m$, and p and $\bar{f}$ are of dimension $m \times 1$. Assuming p can be written as a linear combination of vibration modes,

$$p = \Phi\eta \qquad [2.1.2]$$

where η is the modal coordinate vector of dimension $m \times 1$, and Φ is the system modal matrix of dimension $m \times m$ whose columns are the respective normal mode shapes of the entire structure

$$\Phi = [\phi_1, \ldots, \phi_m] \qquad [2.1.3]$$

The orthogonality conditions [28] can be applied where the modal mass matrix and modal stiffness matrix have been normalized according to

$$\Phi^T \underline{M} \Phi = I_m \qquad [2.1.4]$$

and

$$\Phi^T \underline{K} \Phi = diag(\omega_1^2, \ \omega_2^2, \ldots, \omega_m^2) \qquad [2.1.5]$$

respectively. It is assumed that the damping matrix is diagonalizable by the modal transformation, Φ, (classical damping) as

$$\Phi^T \underline{C} \Phi = diag(2\zeta_1\omega_1, \ldots, 2\zeta_m\omega_m) \qquad [2.1.6]$$

The governing equation becomes

$$\ddot{\eta}_k + 2\zeta_k\omega_k\dot{\eta}_k + \omega_k^2\eta_k = \phi_k^T(a)u \qquad [2.1.7]$$

where ω_k is the undamped natural frequency of mode k, and ζ_k is the viscous damping factor of mode k. In this expression, it was assumed that the applied force is implemented by point actuators, where the applied force vector, $\bar{f}$, was represented as

$$\bar{f} = F_{\bar{f}}u \qquad [2.1.8]$$

where $F_{\bar{f}}$ is the applied force distribution matrix of dimension $m \times n_a$, where n_a is the number of actuators, to produce

$$\Phi^T F_{\bar{f}} = \Phi^T(a) \qquad [2.1.9]$$

so u is the reduced force vector of dimension $n_a \times 1$, and $\phi_k(a)$ designates the normal mode shape amplitudes at the actuator locations. To limit the scope of this study, the force vector only considers control forces as opposed to some combination of external forces and control forces.

There are m such equations of the form represented by Equation [2.1.7]. The order of the discretized structural model, m, is typically much larger than would be practical to include in the design of the controller. Therefore, the model will have to be truncated, and a controller will be implemented on only a relatively small number of modes, $n << m$. The controller will be designed for only the first n equations of the form [2.1.7].

Defining the normalized state variables as:

$$x_k = \eta_k \qquad [2.1.10]$$

and

$$x_{n+k} = \frac{\dot{\eta}_k}{\omega_k} = \frac{\dot{x}_k}{\omega_k} \qquad [2.1.11]$$

where η_k is the modal amplitude of mode k, and $\frac{\dot{\eta}_k}{\omega_k}$ is the reduced modal velocity of mode k, the system of equations for mode k can be rewritten as

$$\begin{bmatrix} \dot{x}_k \\ \dot{x}_{n+k} \end{bmatrix} = \begin{bmatrix} 0 & \omega_k \\ -\omega_k & -2\zeta_k\omega_k \end{bmatrix} \begin{bmatrix} x_k \\ x_{n+k} \end{bmatrix} + \begin{bmatrix} 0 \\ \frac{\phi_k^T(a)}{\omega_k} \end{bmatrix} u \qquad [2.1.12]$$

The output vector consists of a displacement sensor model defined as

$$y_k = \begin{bmatrix} \phi_k(s) & 0 \end{bmatrix} \begin{bmatrix} x_k \\ x_{n+k} \end{bmatrix} \qquad [2.1.13]$$

where $\phi_k(s)$ is the mode shape amplitude corresponding to the sensor location. The above equations are in the standard state-space form and can be written for the entire system of n modes as

$$\dot{x} = Ax + Bu \qquad [2.1.14]$$

$$y = Cx \qquad [2.1.15]$$

where

$$A = \begin{bmatrix} 0_n & diag(\omega_1, \ldots, \omega_n) \\ -diag(\omega_1, \ldots, \omega_n) & -2diag(\zeta_1\omega_1, \ldots, \zeta_n\omega_n) \end{bmatrix} \qquad [2.1.16]$$

$$B = \begin{bmatrix} 0_n \\ \frac{\phi_1^T(a)}{\omega_1} \\ \ldots \\ \frac{\phi_n^T(a)}{\omega_n} \end{bmatrix} \qquad [2.1.17]$$

and

$$C = [\phi_1(s), \ldots, \phi_n(s) \quad 0_n] \qquad [2.1.18]$$

A is of dimension $2n \times 2n$. The exact dimensions of B and C are consistent with the number of actuators and displacement sensors, respectively. For n_a actuators, B is of dimension $2n \times n_a$, and, for n_s sensors, C is of dimension $n_s \times 2n$.

2.2. CONTROLLABILITY AND OBSERVABILITY

The concepts of controllability and observability arise as necessary conditions on the existence of a solution in the LQG formulation [19, 29 – 31] to be presented shortly.

Controllability is viewed as the ability to transfer a system from some initial state, $x_o = x(t_o)$, to some final state, $x_f = x(t_f)$, within a finite amount of time. If a system is not controllable, no amount of control energy will ever be able to reach the uncontrolled states to move them.

A physical understanding of this concept can be attained if the system defined by Equation [2.1.14] is represented in an uncoupled diagonal form via a coordinate transformation. By defining a new state vector, z_x, by

$$x = T_x z_x \qquad [2.2.1]$$

where T_x is the matrix whose columns are the eigenvectors of matrix A, Equation [2.1.14] can be rewritten as

$$\dot{z}_x = \Lambda z_x + B^{@} u \qquad [2.2.2]$$

where

$$\Lambda = T_x^{-1} A T_x = diag(\lambda_1, \ldots, \lambda_{n_A}) \qquad [2.2.3]$$

$$B^{@} = T_x^{-1} B \qquad [2.2.4]$$

where the λ_k's are the eigenvalues of matrix A which is of order n_A. This produces a system of n_A *decoupled* differential equations for each state variable

$$(\dot{z}_x)_k = \lambda_k (z_x)_k + b^{@}_{kj} u_j \qquad k = 1, \ldots, n_A \qquad [2.2.5]$$

where from indicial notation, summation is implied for the repeated index j *only* but not for k.

If the $b_{kj}^{@}$'s are all zero for a given mode k, this mode does not see any inputs, and, as a result, this mode cannot be controlled

$$(\dot{z}_x)_k = \lambda_k (z_x)_k \qquad [2.2.6]$$

For example, if the system has three modes and two actuators with the following resultant diagonalized system representation

$$\frac{d}{dt}\begin{bmatrix}(z_x)_1\\(z_x)_2\\(z_x)_3\end{bmatrix} = \begin{bmatrix}\lambda_1 & 0 & 0\\0 & \lambda_2 & 0\\0 & 0 & \lambda_3\end{bmatrix}\begin{bmatrix}(z_x)_1\\(z_x)_2\\(z_x)_3\end{bmatrix} + \begin{bmatrix}b_{11}^{@} & b_{12}^{@}\\0 & 0\\b_{31}^{@} & b_{32}^{@}\end{bmatrix}\begin{bmatrix}u_1\\u_2\end{bmatrix} \qquad [2.2.7]$$

the second mode sees no input since $b_{21}^{@} = b_{22}^{@} = 0$, i.e., corresponding to a row of zeros in the $B^{@}$ matrix. Therefore, the second mode cannot be controlled, and, thus, the system is not completely controllable.

A simple test as to whether a system is controllable or not has been found [19, 29 – 32] to be as follows. By defining a controllability matrix, M_C, where

$$M_C = [B \quad AB \quad A^2B \quad \ldots \quad A^{n_A-1}B] \qquad [2.2.8]$$

where n_A is the order of the system, a linear, time-invariant system is viewed as completely controllable if

$$Rank[M_C] = n_A \qquad [2.2.9]$$

At this point, (A, B) is viewed as a controllable pair. If M_C is not of full rank, i.e., $Rank[M_C] = m_C < n_A$, then $n_A - m_C$ modes of the system are uncontrollable.

Observability, on the other hand, is viewed as the ability of the system to be able to determine its states by observing the output during a finite interval of time. If a system is not observable, there are some states which cannot be estimated since they do not influence $y(t)$, the output.

As before this can be viewed physically from the diagonal form of the state equation via the coordinate transformation presented earlier. This time, however, the coordinate transformation of Equation [2.2.1] will be substituted into the output Equation of [2.1.15] to produce

$$y = C^{@} z_x \qquad [2.2.10]$$

where

$$C^{@} = CT_x \qquad [2.2.11]$$

If there exists an entire column of zeros in the $C^{@}$ matrix, the mode corresponding to this column is not observed. As a result, the system is not completely observable. For example, if the system has three modes and two outputs with the following resultant coordinate transformation representation

$$\begin{bmatrix} y_1 \\ y_2 \end{bmatrix} = \begin{bmatrix} c_{11}^{@} & 0 & c_{13}^{@} \\ c_{21}^{@} & 0 & c_{23}^{@} \end{bmatrix} \begin{bmatrix} (z_x)_1 \\ (z_x)_2 \\ (z_x)_3 \end{bmatrix} \qquad [2.2.12]$$

the second mode is not observed (measured) by either of the outputs since $c_{12}^{@} = c_{22}^{@} = 0$. Therefore, the system is not completely observable.

As will be shown in Section 2.4.1.1, the observer problem is really a dual control problem. Therefore, from duality, the test for observability has been found [19, 29 – 31] to be as follows. By defining an observability matrix, M_O, where

$$M_O = [C^T \quad A^T C^T \quad (A^T)^2 C^T \quad \ldots \quad (A^T)^{n_A - 1} C^T] \qquad [2.2.13]$$

a linear, time-invariant system is viewed as completely observable if

$$Rank[M_O] = n_A \qquad [2.2.14]$$

At this point, (A, C) is viewed as an observable pair. If M_O is not of full rank, i.e., $Rank[M_O] = m_O < n_A$, then $n_A - m_O$ modes of the system are not observable.

2.3. LQR DESIGN

Linear state feedback regulators are designed to control the desired modes of vibration. The regulator is designed via the techniques of optimal control theory for the Linear Quadratic Regulator (LQR) which are discussed in many references, e.g., [25, 29, 33, 34].

2.3.1. Deterministic Regulator

For a system described by Equation [2.1.14], the deterministic LQR design minimizes the following performance index

$$J = \int_{t=0}^{\infty} (x^T Q x + u^T R u) dt \qquad [2.3.1]$$

where Q and R are weighting matrices. Q is a real symmetric positive semidefinite ($Q \geq 0$) matrix, and R is a real symmetric positive definite ($R > 0$) matrix. The structure of Q is related to the required performance of the output, while R is related to the cost of the control. The relative magnitudes of Q and R are adjusted to obtain the desired compromise between performance and control requirements.

In the LQR problem, perfect knowledge of the state, x, is assumed at all times. The minimization of J leads to a control law of the form

$$u = -G_c x = -R^{-1} B^T \overline{F} x \qquad [2.3.2]$$

where $\overline{F}$ is a real symmetric positive definite ($\overline{F} > 0$) matrix and is found by solving the following Riccati Equation

$$\overline{F}A + A^T\overline{F} - \overline{F}BR^{-1}B^T\overline{F} + Q = 0 \qquad [2.3.3]$$

which produces the minimum value of J as

$$J = x_o^T\overline{F}x_o \qquad [2.3.4]$$

where x_o is the initial state of the system.

The value of J can also be determined by representing the controlled system of Equation [2.1.14] in the following equivalent form

$$\dot{x} = \overline{A}_G x \qquad [2.3.5]$$

which is the differential equation governing the free response of the stable linear system. $\overline{A}_G$ is determined by substituting Equation [2.3.2] into [2.1.14] to produce

$$\overline{A}_G = (A - BG_c) \qquad [2.3.6]$$

The performance index for a free vibration system is represented by

$$J = \int_{t=0}^{\infty} (x^T\overline{Q}x)dt \qquad [2.3.7]$$

which can be shown to equal

$$J = x_o^T\overline{P}_L x_o \qquad [2.3.8]$$

where x_o is the initial state of the system, and $\overline{P}_L$ is a positive definite matrix which is the solution of the following Lyapunov Equation

$$\overline{A}_G^T\overline{P}_L + \overline{P}_L\overline{A}_G + \overline{Q} = 0 \qquad [2.3.9]$$

For the LQR problem, by substituting in Equation [2.3.2] into [2.3.1], this produces

$$\overline{Q} = Q + G_c^T R G_c \qquad [2.3.10]$$

It should be noted that the solutions of the Riccati Equation and the Lyapunov Equation produce the exact same result

$$\overline{F} = \overline{P}_L \qquad [2.3.11]$$

If one substitutes Equations [2.3.6], [2.3.10], and [2.3.2] into the Lyapunov Equation [2.3.9], the resulting equation will be the Riccati Equation [2.3.3].

The Lyapunov Equation free response formulation was presented here to demonstrate its equivalence to the Riccati Equation formulation. The Lyapunov form will be used exclusively when determining the performance index for the state feedback on the observed state case to be discussed in Section 2.4. Note that the Lyapunov formulation is more general because it applies also when G_c is not optimal.

2.3.1.1. Finite-time Deterministic Regulator - Time-Varying System

The above formulation was presented for a time-invariant system, i.e., all the system matrices are constant and not functions of time. The control law implemented a constant feedback gain matrix, G_c, which really is the steady-state solution of a more complex time-varying Riccati Equation. Therefore, the above solution is really a special subset of a much larger time-varying control problem [25, 35]. For completeness, this time-varying problem will be briefly presented.

For a system described by the following governing equation

$$\dot{x}(t) = A(t)x(t) + B(t)u(t) \qquad [2.3.12]$$

where now the system matrix, $A(t)$, and the control matrix, $B(t)$, are functions of time, the deterministic LQR design minimizes the following performance index

$$J = \int_{t=t_o}^{T} [x^T(t)Q(t)x(t) + u^T(t)R(t)u(t)]dt + x^T(T)Sx(T) \qquad [2.3.13]$$

where $Q(t)$ and $R(t)$ are now also functions of time. This regulator has a finite terminal time T. The additional quadratic expression, $x^T(T)Sx(T)$, in J is referred to as a terminal penalty term. S is a symmetric positive semidefinite ($S \geq 0$) matrix. The minimization of J leads to a control law of the form

$$u(t) = -G_c(t,T)x(t) = -R^{-1}(t)B^T(t)\bar{F}(t,T)x(t) \qquad [2.3.14]$$

where $\bar{F}(t,T)$ is found by solving the following Riccati Equation which is a differential equation

$$\bar{F}(t,T)A(t) + A^T(t)\bar{F}(t,T) - \bar{F}(t,T)B(t)R^{-1}(t)B^T(t)\bar{F}(t,T) + Q(t) = -\dot{\bar{F}}(t,T) \qquad [2.3.15]$$

with boundary condition $\bar{F}(T,T) = S$. The minimum value of J becomes

$$J = x^T(t_o)\bar{F}(t_o, T)x(t_o) \qquad [2.3.16]$$

This control law is valid for $t_o \leq t \leq T$.

2.3.1.2. Infinite-time Deterministic Regulator - Time-Varying System

For the time-varying system described in Equation [2.3.12], if the terminal time is allowed to go to infinity, $T \rightarrow \infty$, and $S = 0$, the deterministic LQR design minimizes the following performance index

$$J = \int_{t=t_o}^{\infty} [x^T(t)Q(t)x(t) + u^T(t)R(t)u(t)]dt \qquad [2.3.17]$$

The solution of this control problem exists and produces a finite value of J provided the system described by Equation [2.3.12] is completely controllable for all time. Therefore,

$$\bar{F}^{\times}(t) = \lim_{T \to \infty} \bar{F}(t,T) \qquad [2.3.18]$$

exists [35] and is a nonnegative-definite and symmetric matrix. $\bar{F}^{\times}(t)$ is referred to as the steady-state solution and turns out to be *independent* of S ($= 0$), the terminal condition of $\bar{F}(t,T)$ [25].

The control law becomes

$$\begin{aligned} u(t) &= -G_c(t)x(t) \\ &= -R^{-1}(t)B^T(t)\bar{F}^{\times}(t)x(t) \end{aligned} \qquad [2.3.19]$$

where $\bar{F}^{\times}(t)$ also satisfies the Riccati Equation [2.3.15]. The minimum value of J becomes

$$J = x^T(t_o)\bar{F}^{\times}(t_o)x(t_o) \qquad [2.3.20]$$

Some final comments on the time-invariant regulator problem presented earlier where all the system matrices were constant and not functions of time, $\bar{F}$ can be shown [35] to be represented as

$$\bar{F} = \lim_{T \to \infty} \bar{F}(t,T) = \lim_{t \to -\infty} \bar{F}(t,T) \qquad [2.3.21]$$

and is a constant, i.e., $\dot{\bar{F}} = 0$, to produce the *algebraic* Riccati Equation [2.3.3] and a constant control law [2.3.2]. Finally, the time reference frame, t_o, was set equal to 0 for this study.

2.3.2. Stochastic Regulator

In the presence of disturbances such as white noise, the system description can be represented as

$$\dot{x} = Ax + Bu + w_1 \qquad [2.3.22]$$

where w_1 is white noise of intensity W_1 and zero mean.

$$E[w_1] = 0 \qquad [2.3.23]$$

$$E[w_1 w_1^T] = W_1 \qquad [2.3.24]$$

The objective for the stochastic regulator is to minimize the following performance index

$$J = E[x^T Q x + u^T R u] \qquad [2.3.25]$$

where the symbol $E[.]$ represents the expected value of the function $[.]$. The expected value represents an integration over the range of all possible values the argument may assume as dictated by its probability density function [36].

The optimum solution of the stochastic LQR problem is the same as for the deterministic one. The minimization of J leads to the same control law of the form presented in Equation [2.3.2] and the same Riccati Equation [2.3.3]. But, the minimum value of J takes on another form as dictated by the presence of white noise as

$$J = tr[\bar{F} W_1] \qquad [2.3.26]$$

Similarly, the performance index can be determined by considering the equivalent form of the free response system where

$$J = E[x^T \bar{Q} x] \qquad [2.3.27]$$

where $\bar{Q}$ is defined from Equation [2.3.10] and satisfies the Lyapunov Equation [2.3.9] with $\bar{A}_G$ defined, as before, from Equation [2.3.6]. The minimization of J leads to

$$J = tr[\bar{P}_L W_1] \qquad [2.3.28]$$

with the understanding that $\bar{P}_L = \bar{F}$ to produce the same value of J. Again, note that the Lyapunov formulation is more general because it applies also when G_c is not optimal.

2.4. CONTROLLER DESIGN

2.4.1. Deterministic Controller

The objective is to design a controller for a system whose governing equations are defined by Equations [2.1.14] and [2.1.15]. The controller consists of two parts. The first is an observer. Since the state of the system is, in general, not fully known due to incomplete and noisy measurements and model uncertainties, it is reconstructed via a state estimator such as a Kalman-Bucy Filter (KBF) or a full state Luenberger Observer. The reconstructed state, $\hat{x}$, is obtained by integrating the general linear full state observer equation

$$\dot{\hat{x}} = A\hat{x} + Bu + K_e(y - C\hat{x}) \qquad [\hat{x}(0) = 0] \qquad [2.4.1]$$

where K_e is the observer gain matrix. If a KBF is used to estimate the state, the observer gain matrix is determined by treating the Kalman-Bucy Filter as a dual control problem. If a Luenberger Observer is used to estimate the state, the observer gain matrix is determined uniquely by pole-placement. The actual formulation of this problem and the evaluation of K_e will be presented shortly.

The second part of the controller consists of the regulator where G_c, the feedback gain matrix, is calculated by using the Linear Quadratic Regulator (LQR) design method where the control law is given as

$$u = -G_c\hat{x} \qquad [2.4.2]$$

The control law is implemented on the estimated state since the LQR no longer has the actual state available to it.

The state estimator error is defined as

$$e = \hat{x} - x \qquad [2.4.3]$$

The state vector of the composite system (regulator + observer) is selected to be $(x^T e^T)^T$. The corresponding governing equation for this system becomes .

$$\begin{bmatrix} \dot{x} \\ \dot{e} \end{bmatrix} = \begin{bmatrix} A - BG_c & -BG_c \\ 0 & A - K_c C \end{bmatrix} \begin{bmatrix} x \\ e \end{bmatrix} \qquad [2.4.4]$$

As can be readily seen from the block triangular form of the matrix, the poles (eigenvalues) of this system are those of the regulator, $(A - BG_c)$, and those of the observer, $(A - K_c C)$. This is known as the *separation principle* whereby the regulator and observer can be designed independently to produce the desired pole locations. As a result, the regulator gain matrix is determined exactly as it was for the deterministic regulator problem where the actual states were available. These pole locations will insure a stable system.

2.4.1.1. Kalman-Bucy Filter

The Kalman-Bucy Filter (KBF) is a state estimator which is optimal in the statistical sense [25, 29, 33, 34, 37]. Assuming plant noise w_1 and measurement noise w_2, the system equations are

$$\dot{x} = Ax + Bu + w_1 \qquad [2.4.5]$$

$$y = Cx + w_2 \qquad [2.4.6]$$

where w_1 and w_2 are uncorrelated white noise characterized by covariance matrices V_1 and V_2.

$$Cov(w_1, w_1^T) = V_1 \qquad [2.4.7]$$

$$Cov(w_2, w_2^T) = V_2 \qquad [2.4.8]$$

$$Cov(w_1, w_2^T) = 0 \qquad [2.4.9]$$

V_1 and V_2 are the plant noise intensity matrix and the measurement noise intensity matrix, respectively. V_1 is a real symmetric positive semidefinite ($V_1 \geq 0$) matrix, and V_2 is a real symmetric positive definite ($V_2 > 0$) matrix.

Many times the noise intensity matrices involved in the design of the Kalman-Bucy Filter are considered as free parameters which can be tuned to achieve desired properties in the control system. The KBF formulation is used merely as a design tool to develop a deterministic observer.

If W_1 and W_2 are defined as the actual plant noise intensity matrix and measurement noise intensity matrix, respectively, the KBF is truly optimal in the statistical sense when $V_1 = W_1$ and $V_2 = W_2$. The stochastic controller will result under these conditions and will be presented in Section 2.4.2.

When the noise matrices are used merely as a design tool as opposed to representing the actual noise statistics, the notation V_1 and V_2 will be used in place of W_1 and W_2.

The reconstructed state, $\hat{x}$, is obtained from

$$\dot{\hat{x}} = A\hat{x} + Bu + K_c(y - C\hat{x}) \qquad [\hat{x}(0) = 0] \qquad [2.4.10]$$

where

$$K_c = PC^T V_2^{-1} \qquad [2.4.11]$$

and P satisfies the observer Riccati Equation

$$AP + PA^T - PC^T V_2^{-1} CP + V_1 = 0 \qquad [2.4.12]$$

The objective is to have the observer state converge onto the actual state. By using Equation [2.4.4], it can be shown that $\hat{x}$ will converge towards x if $(A - K_c C)$ is stable. But to insure a good transient behavior and that $\hat{x}$ can follow x, the observer convergence rate is required to be faster than that of the regulator. Since the regulator control law is implemented on the estimated state,

$\hat{x}$, it is desired to have $\hat{x}$ converge onto x as fast as possible especially if the system dynamics are changing quickly. Therefore, the observer poles are generally selected to be to the left of the regulator poles in the complex plane, i.e., have a faster convergence speed.

A small V_2 implies that there is little measurement noise, i.e., very accurate measurement of the output. In general, this will result in a large K_e gain matrix. But, only the relative magnitudes of V_1 and V_2 are important and not their absolute values.

By tuning the relative magnitudes of V_1 and V_2, it may be possible to avoid having poles either too close to the imaginary axis or too far left in the complex plane. (The asymptotic behavior of the closed-loop poles will be discussed in Section 2.5.) The designer would like to insure that the observer poles follow the *rule-of-thumb* of being about 3 to 10 times faster than the regulator poles. The lower limit of 3 is placed so that the observer does not affect the dynamics of the closed-loop system. Whereas, the upper limit of 10 is placed in order that the system does not become overly sensitive to noise.

As stated before, the observer problem can also be treated as a dual control problem [23]. If one looks at the estimator error and rewrites the governing equations as

$$e = \hat{x} - x \qquad [2.4.13]$$

$$\dot{e} = (A - K_c C)e + K_c w_2 - w_1 \qquad [2.4.14]$$

Since the eigenvalues of $(A - K_c C)$ are the same as the eigenvalues of $(A^T - C^T K_c^T)$, a dual control problem can be formulated. By transposing the system matrices of the estimator and defining new state variables, z_i, to correspond to each of the e_i's, one obtains the dual system which is defined as

$$\dot{z} = (A^T - C^T K_c^T)z + \hat{v} \qquad [2.4.15]$$

This transposing of the system is performed in order to get the observer equation into the form of the regulator problem. It should be realized that the dual problem is a fictitious problem which produces the same closed-loop eigenvalues. By rearranging terms in the above expression and de-

fining new state variables, the system can be written as an optimal control problem that is defined by

$$\dot{z} = A^T z + C^T \hat{u} + \hat{v} \qquad [2.4.16]$$

where

$$\hat{u} = -K_c^T z \qquad [2.4.17]$$

and

$$K_c^T = V_2^{-1} CP \qquad [2.4.18]$$

The cost function can be defined as

$$J = \int_{t=0}^{\infty} (z^T V_1 z + \hat{u}^T V_2 \hat{u}) dt \qquad [2.4.19]$$

where the V_1 and V_2 matrices play the roles of the Q and R matrices, respectively, in the control problem. For an optimal control problem, the minimization of this cost function leads to the following Riccati Equation

$$PA^T + AP - PC^T V_2^{-1} CP + V_1 = 0 \qquad [2.4.20]$$

This is identical to the observer Riccati Equation as specified in Equation [2.4.12].

In terms of evaluating the performance index for the composite system of state feedback on the observed state, the Lyapunov free response formulation will be used. Let $e = \hat{x} - x$ be the estimator error and $\varepsilon = (x^T \ e^T)^T$ be the state vector of the composite system so that

$$\dot{\varepsilon} = \overline{A}_K \varepsilon \qquad [2.4.21]$$

where

$$\overline{A}_K = \begin{bmatrix} A - BG_c & -BG_c \\ 0 & A - K_cC \end{bmatrix} \qquad [2.4.22]$$

The deterministic performance index can be represented as

$$J = \int_{t=0}^{\infty} \varepsilon^T Q^{\times} \varepsilon dt \qquad [2.4.23]$$

where

$$Q^{\times} = \begin{bmatrix} Q + G_c^T R G_c & G_c^T R G_c \\ G_c^T R G_c & G_c^T R G_c \end{bmatrix} \qquad [2.4.24]$$

Therefore, the minimum value of J is

$$J = \varepsilon_o^T P_L^{\times} \varepsilon_o \qquad [2.4.25]$$

where $P_L^{\times}$ satisfies the following Lyapunov Equation

$$\overline{A}_K^T P_L^{\times} + P_L^{\times} \overline{A}_K + Q^{\times} = 0 \qquad [2.4.26]$$

and ε_o is the initial state.

2.4.1.2. Full State Luenberger Observer

Since an observer is basically defined by its gain matrix, K_e, there are other methods for designing an observer. A common technique is to use pole-placement [38, 39] where the observer poles of $(A - K_eC)$ can be arbitrarily designated, and then the corresponding K_e can be determined. The only condition on this is that the system be completely observable [25].

Given the observer poles, λ_i, we can write

$$\det[sI - (A - K_c C)] = \prod_{i=1}^{n_A}(s - \lambda_i) = s^{n_A} + a_{n_A - 1}s^{n_A - 1} + \cdots + a_1 s + a_0 \qquad [2.4.27]$$

By specifying the λ_i's, the designer can then evaluate the components of the observer gain matrix, K_c. This concept is implemented on the full-order Luenberger observer which satisfies Equation [2.4.1].

In addition to this, Luenberger also looked at the use of pole-placement for a reduced-order observer. He transformed the full-order observer into a reduced-order observer and then placed the observer poles of this reduced problem. The motivation for reducing the order of the observer lies with the fact that the full-order observer possesses some redundancy. The full-order observer tries to reconstruct the entire state of the system, yet, in actuality, part of the state is known from direct measurements of the output. As a result, Luenberger proposed that this redundancy be eliminated. The formulation of the reduced-order Luenberger observer will not be pursued here, but it can be found in References [25, 40 – 42]. Note that a benefit of redundancy is noise reduction. In the reduced-order case, the output noise is fed through to the output.

The determination of the performance index, J, for the composite system (observer + regulator) follows the same formulation as for the KBF problem with the exception that the K_c gain matrix is defined via pole-placement.

2.4.2. LQG Stochastic Controller

In the presence of disturbances such as white noise, the governing equations become

$$\dot{x} = Ax + Bu + w_1 \qquad [2.4.28]$$

$$y = Cx + w_2 \qquad [2.4.29]$$

where w_i is the actual white noise of intensity W_i and zero mean.

$$E[w_1] = 0 \qquad [2.4.30]$$

$$E[w_1 w_1^T] = W_1 \qquad [2.4.31]$$

$$E[w_2] = 0 \qquad [2.4.32]$$

$$E[w_2 w_2^T] = W_2 \qquad [2.4.33]$$

$$E[w_1 w_2^T] = 0 \qquad [2.4.34]$$

The optimum solution to the stochastic Linear Quadratic Gaussian (LQG) problem which combines the stochastic LQR with the stochastic KBF, is the same as for the deterministic controller problem. The same LQR control law is used (Equation [2.4.2]) along with the same observer relations and Riccati Equation (Equations [2.4.10] - [2.4.12]) except that now the K_c matrix is determined by the actual noise statistics, W_1 and W_2, rather than the designed statistics, V_1 and V_2.

In terms of evaluating the stochastic performance index for the compostie system, the Lyapunov free response formulation will be used. As before, let $e = \hat{x} - x$ be the estimator error and $\varepsilon = (x^T \; e^T)^T$ be the state vector of the composite system so that

$$\dot{\varepsilon} = \bar{A}_K \varepsilon + \bar{B}_w w \qquad [2.4.35]$$

where

$$\bar{A}_K = \begin{bmatrix} A - BG_c & -BG_c \\ 0 & A - K_c C \end{bmatrix} \qquad [2.4.36]$$

as before,

$$\bar{B}_w = \begin{bmatrix} I & 0 \\ -I & K_c \end{bmatrix} \qquad [2.4.37]$$

and

$$w = \begin{bmatrix} w_1 \\ w_2 \end{bmatrix} \qquad [2.4.38]$$

The stochastic performance index is again represented as

$$J = E[\varepsilon^T Q^{\times} \varepsilon] \qquad [2.4.39]$$

where

$$Q^{\times} = \begin{bmatrix} Q + G_c^T R G_c & G_c^T R G_c \\ G_c^T R G_c & G_c^T R G_c \end{bmatrix} \qquad [2.4.40]$$

But, the minimum value of J now becomes

$$J = tr[P_L^{\times} \bar{B}_w W \bar{B}_w^T] \qquad [2.4.41]$$

where $P_L^{\times}$ satisfies the following Lyapunov Equation

$$\bar{A}_K^T P_L^{\times} + P_L^{\times} \bar{A}_K + Q^{\times} = 0 \qquad [2.4.42]$$

and

$$W = E[ww^T] = \begin{bmatrix} W_1 & 0 \\ 0 & W_2 \end{bmatrix} \qquad [2.4.43]$$

J, in Equation [2.4.41], is a minimum when K_e is determined from $V_1 = W_1$ and $V_2 = W_2$. When K_e is determined from a KBF design which does not correspond to the actual noise statistics, i.e., $V_1 \neq W_1$ and $V_2 \neq W_2$, J will no longer attain the minimum value.

These Linear Quadratic Gaussian (LQG) techniques provide a systematic way of designing well conditioned linear state feedback controllers which are optimal with respect to the quadratic

performance index, J. They are well suited for small order systems, and their application to active damping of vibration requires the truncation of the system model to the most significant modes. This important step can be done in relation to the poles location relative to the bandwidth specification, or analyzing the magnitude of the residue matrices (modal gains which give a measure of the controllability of the modes by weighting the relative *energy* contribution to the impulse response of the system [43 – 46]), or with other techniques, e.g., modal cost analysis (modal costs which give a measure of the contribution of a mode to the quadratic performance index [47, 48]), eigenvalue, eigenvector, or controllability and observability criteria [49], etc. [50, 51]. The uncontrolled modes are ignored in the controller design although many of them are known with reasonable accuracy.

2.5. ASYMPTOTIC BEHAVIOR OF CLOSED-LOOP POLES

The performance index of Equation [2.3.1] can be rewritten as

$$J = \int_{t=0}^{\infty} (\chi^T \chi + u^T R u) dt \qquad [2.5.1]$$

where

$$\chi = Dx \qquad [2.5.2]$$

and D is the Cholesky factor of Q

$$Q = D^T D \qquad [2.5.3]$$

Since the solution of the regulator is unchanged if both Q and R are multiplied by the same scalar factor, it is convenient to let

$$R = \overline{\rho}\Xi \qquad [2.5.4]$$

where Ξ is a constant matrix, and $\overline{\rho}$ is a scalar scaling the relative weight of the control. The value of $\overline{\rho}$ is adjusted to achieve the desired compromise between performance and control cost. For $\overline{\rho} \to 0$, a small penalty is placed on the control, therefore, the amplitude of the input, u, is allowed to become very large, i.e., produces high regulator gains. For $\overline{\rho} \to \infty$, a heavy penalty is placed on the control, therefore, the amplitude of the input, u, is constrained to be very small, i.e., produces low regulator gains. This latter case is referred to as a *cheap* control. The asymptotic behavior of the closed-loop poles of the LQR, when $\overline{\rho} \to 0$ and $\overline{\rho} \to \infty$, has been studied [25].

Assuming that the open-loop transfer matrix (between u and χ) is square and is defined as

$$\mathscr{H}_1(s) = D(sI - A)^{-1}B \qquad [2.5.5]$$

then the open-loop characteristic polynomial, $\phi_{OL}(s)$, can be obtained from

$$\mathscr{H}_1(s) = \frac{\psi_{OL}(s)}{\phi_{OL}(s)} = \frac{h\prod_{i=1}^{m_A}(s - z_i)}{\prod_{j=1}^{n_A}(s - p_j)} \qquad [2.5.6]$$

for the SISO (scalar) case and

$$\det[\mathscr{H}_1(s)] = \frac{\psi_{OL}(s)}{\phi_{OL}(s)} = \frac{h\prod_{i=1}^{m_A}(s - z_i)}{\prod_{j=1}^{n_A}(s - p_j)} \qquad [2.5.7]$$

for the MIMO (multivariable) case. The z_i's are the open-loop zeros, and the p_j's are the open-loop poles.

It can be shown [25] that the asymptotic behavior of the closed-loop poles of the LQR, as $\overline{\rho} \to 0$, is as follows. m_A of the poles approach the open-loop zeros of $\mathscr{H}_1(s)$, z_i, if z_i is in the left half-plane or their mirror images, $-z_i^*$, if z_i is in the right half-plane. The remaining $n_A - m_A$ poles go to infinity in so-called Butterworth patterns. For a small penalty placed on the control, the regulator will place its poles at the *stable* mirror image position of the "unstable" open-loop zero locations or at the "stable" open-loop zero locations, i.e., the regulator poles are placed at the stable reflection of the open-loop (transmission) zeros.

The open-loop zeros of a system play a very significant role in the response of the system. For systems with only left half-plane zeros, the response to any initial condition is very fast since the response time is asymptotically completely determined by the closed-loop poles which are faraway. The nearby poles are effectively cancelled by the open-loop zeros, and their effect on the response of the controlled variables is not noticeable.

If the system has right half-plane open-loop zeros, the mirror image of the right half-plane zeros now acts as nearby closed-loop poles and no longer provides a pole-zero type cancellation. Their effect is limited only if they are located very far from the origin.

A system is known as a *minimum phase* system [19, 25] if all the zeros of the open-loop plant transfer function matrix (Section 2.7) are located in the left half-plane. Conversely, if there are some zeros located in the right half-plane, the system is a *nonminimum phase* system. Nonminimum phase systems may cause problems since they have a slower response. This slower response is attributed to the system's *initial* time response being negative (however, the *steady state* time response is positive) causing a faulty behavior at the beginning of the response, i.e., the state *initially* goes in the wrong direction than desired. This creates a performance problem and prevents one from achieving *"perfect"* control.

It should be noted that nonminimum phase systems are a result of modelling and can only be changed if the actuator and sensor positions are rearranged. If these positions are fixed to

produce a nonminimum phase system, the designer may be forced to accept the corresponding behavior.

As for the asymptotic behavior of the closed-loop poles of the LQR, as $\bar{\rho} \to \infty$, the n_A closed-loop poles approach the open-loop poles of $\mathscr{H}_1(s)$, p_j, if p_j is in the left half-plane, or their mirror images, $-p_j^*$, if p_j is in the right half-plane. Therefore, for a heavy penalty placed on the control, the regulator will place its poles at the *stable* mirror image position of the *unstable* open-loop pole locations or at the *stable* open-loop pole locations, i.e., the regulator poles are placed at the stable reflection of the open-loop poles.

Similarly, by duality of the KBF problem to that of the LQR, if V_2 is defined as

$$V_2 = \bar{v}\overline{Y} \qquad [2.5.8]$$

where $\overline{Y}$ is a constant matrix, $\bar{v}$ is a scalar parameter, and V_1 is defined as

$$V_1 = HH^T \qquad [2.5.9]$$

dual asymptotic properties are found.

As $\bar{v} \to 0$, the poles of the KBF behave as those of the dual LQR; some of them go to infinity in Butterworth patterns, and others move towards the zeros of the transfer matrix

$$\mathscr{H}_2(s) = C(sI - A)^{-1}H \qquad [2.5.10]$$

or their mirror images, if they are in the right half-plane. If the system has small observation noise, V_2, some of the observer poles will be located very far away from the origin. It is possible that some of the other poles will be located very close to the origin. These nearby poles produce a very slow recovery of the reconstruction error from certain initial conditions. However, in an exactly similar fashion to the LQR, if $\mathscr{H}_2(s)$ has no right half-plane zeros, the assumed noise cannot drive the reconstruction error in the subspace where it recovers slowly, and the nearby poles will not prevent an accurate reconstruction.

Finally, as $\bar{v} \to \infty$, the poles of the KBF approach the poles of $\mathscr{H}_2(s)$ or their mirror images if they are in the right half-plane.

Figure 1 presents an example of the asymptotic behavior of the closed-loop observer poles for the following configuration. The system is given six open-loop poles located on the imaginary axis plus four open-loop zeros. Two of the zeros are located in the left half-plane while the remaining two are located in the right half-plane. As a result, as $\bar{v} \to \infty$, the KBF poles approach the six poles of $\mathscr{H}_2(s)$. And, as $\bar{v} \to 0$, two KBF poles approach the left half-plane zeros of $\mathscr{H}_2(s)$, two KBF poles approach the mirror images of the right half-plane zeros of $\mathscr{H}_2(s)$, and two of the KBF poles go to infinity.

A similar type of example can, of course, be shown for the LQR.

According to the foregoing discussion, provided the noise statistics are known (and the open-loop transfer matrix has no right half-plane zeros), the nearby poles of the KBF do not restrict the reconstruction accuracy. However, in many practical applications, the noise statistics are not known accurately, and the values used in the design are chosen to provide a reasonable compromise between the speed of state reconstruction and the immunity to observation noise (giving respectively a lower and upper bound to the stability margin of the filter poles in the left half-plane). Frequently, the noise statistics are simply free parameters which are tuned to design a deterministic observer of appropriate dynamics (thus benefiting from the good properties of the KBF). In those cases, the actual noise statistics are likely to differ considerably from those assumed in the design, and the reconstruction error can be driven in the subspace where it recovers slowly which is unacceptable if the nearby poles are too close to the imaginary axis (a *rule-of-thumb* is that the observer should be between three to ten times faster than the regulator). A guaranteed minimum stability margin can be obtained by the procedure discussed in Section 2.6.

2.6. *ALPHA-SHIFTED PERFORMANCE INDEX*

The α - shifted performance index is a new cost function which insures a certain prescribed stability margin for the system. The α - shifted performance index will be presented in detail for

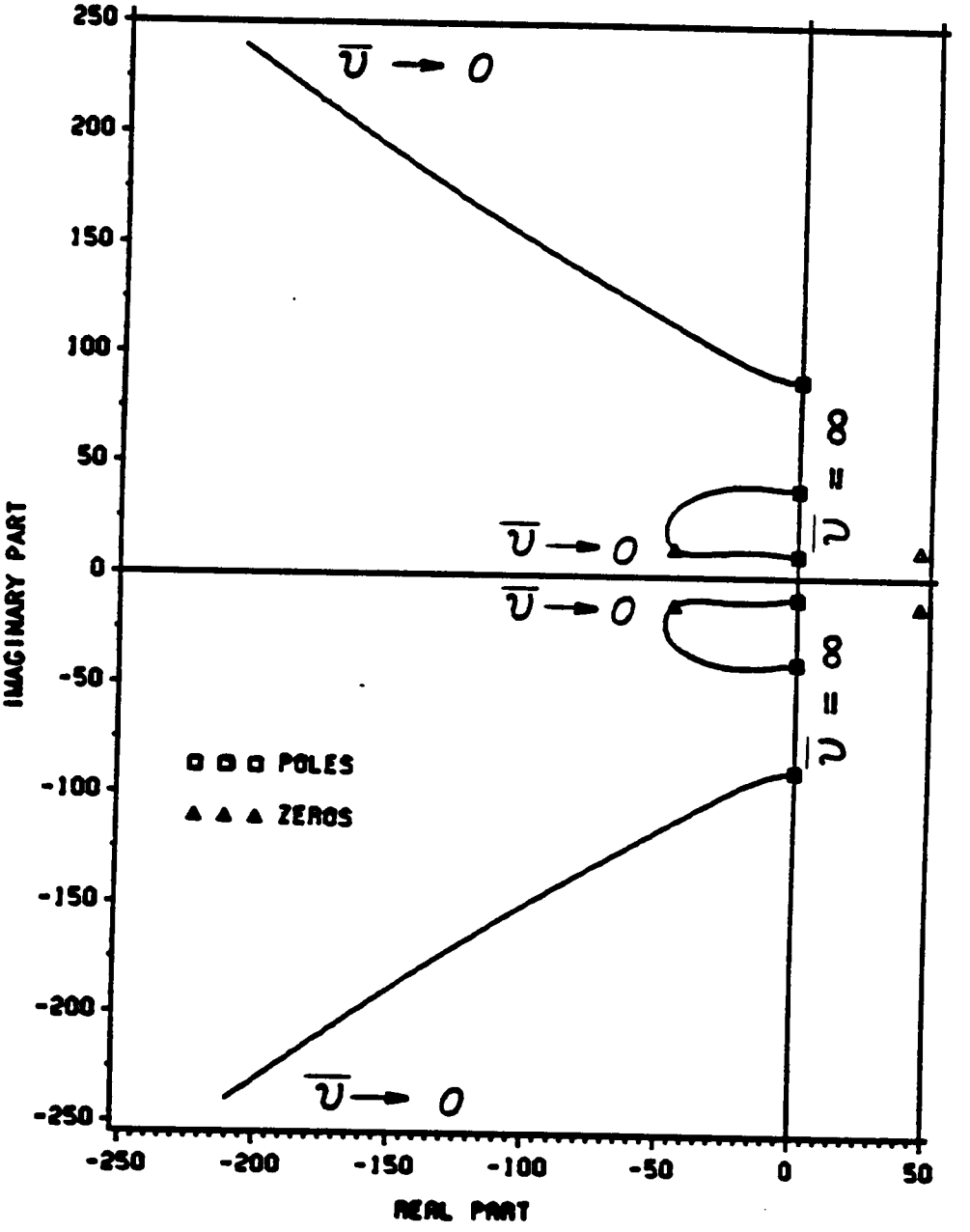

Figure 1. Asymptotic behavior of the observer poles.

the regulator problem. Its corresponding implementation to an observer will then be summarized based on the duality condition which exists between the observer and regulator problems [35].

As shown in Section 2.3, the regulator poles are found from the eigenvalues of the matrix $(A - BG_c)$. Since A and B are fixed for a given system, different pole locations arise from changing the gain matrix, G_c, which must be done via changes in the Q and R weighting matrices which appear in the performance index defined by Equation [2.3.1]. If a *certain* stability margin is desired, changing Q and R constantly by trial and error to get the required response can be rather tedious and inefficient if a solution is found at all (recall Section 2.5 about the discussion on the asymptotic behavior of the closed-loop poles).

A better way to achieve a required stability margin is to redefine the deterministic performance index as

$$J = \int_{t=0}^{\infty} e^{2\alpha t}(x^T Q x + u^T R u)dt \qquad [2.6.1]$$

Since the performance index is finite, this insures that the system response decays to zero at least as fast as $e^{-\alpha t}$.

Equation [2.6.1] can be rewritten as

$$J = \int_{t=0}^{\infty} [x^T \overline{Q}(t) x + u^T \overline{R}(t) u]dt \qquad [2.6.2]$$

where

$$\overline{Q}(t) = Qe^{2\alpha t} \qquad [2.6.3]$$

$$\overline{R}(t) = Re^{2\alpha t} \qquad [2.6.4]$$

which is the standard form for an optimal controller. Therefore, linear feedback control methodologies are still applicable. But now, $\overline{Q}(t)$ and $\overline{R}(t)$ are time dependent so the regulator problem formulation will have to be based on the time-varying system formulation presented in Section

2.3.1.2. Although not obvious, it turns out that the control law produces a constant gain matrix. To see how this happens, assume that $\overline{F}^{\times}(t)$ has the following form

$$\overline{F}^{\times}(t) = \overline{F}e^{2\alpha t} \qquad [2.6.5]$$

Since $\overline{F}^{\times}(t)$ satisfies the differential equation form of the Riccati Equation [2.3.15]

$$\overline{F}^{\times}(t)A + A^T\overline{F}^{\times}(t) - \overline{F}^{\times}(t)B\overline{R}^{-1}(t)B^T\overline{F}^{\times}(t) + \overline{Q}(t) = -\dot{\overline{F}}^{\times}(t) \qquad [2.6.6]$$

Substituting Equations [2.6.3] – [2.6.5] into Equation [2.6.6] produces

$$\overline{F}Ae^{2\alpha t} + A^T\overline{F}e^{2\alpha t} - e^{2\alpha t}\overline{F}BR^{-1}e^{-2\alpha t}B^T\overline{F}e^{2\alpha t} + Qe^{2\alpha t} = -2\alpha\overline{F}e^{2\alpha t} \qquad [2.6.7]$$

or

$$\overline{F}A + A^T\overline{F} - \overline{F}BR^{-1}B^T\overline{F} + Q = -2\alpha\overline{F} \qquad [2.6.8]$$

Representing

$$\begin{aligned} 2\alpha\overline{F} &= \alpha\overline{F} + \alpha\overline{F} \\ &= \overline{F}(\alpha I) + (\alpha I)^T\overline{F} \end{aligned} \qquad [2.6.9]$$

and substituting it into Equation [2.6.8] produces

$$\overline{F}(A + \alpha I) + (A + \alpha I)^T\overline{F} - \overline{F}BR^{-1}B^T\overline{F} + Q = 0 \qquad [2.6.10]$$

which looks very much like the algebraic Riccati Equation presented in Equation [2.3.3] except that A is substituted by $(A + \alpha I)$.

Finally, the control law is defined by Equation [2.3.19] to produce

$$u(t) = -\overline{R}^{-1}(t)B^T\overline{F}^{\times}(t)x(t) \qquad [2.6.11]$$

Substituting Equations [2.6.4] and [2.6.5] into Equation [2.6.11] produces

$$\begin{aligned} u(t) &= -e^{-2\alpha t}R^{-1}B^T\overline{F}e^{2\alpha t}x(t) \\ &= -R^{-1}B^T\overline{F}x(t) \end{aligned} \qquad [2.6.12]$$

or

$$u(t) = -G_c x(t) \qquad [2.6.13]$$

where

$$G_c = R^{-1}B^T\overline{F} \qquad [2.6.14]$$

The feedback gain matrix is constant!

The new performance index can also be justified by looking at a modified regulator problem. For the system

$$\dot{x} = Ax + Bu \qquad [2.6.15]$$

one can define the following variables

$$\bar{x} = e^{\alpha t}x \qquad [2.6.16]$$

$$\bar{u} = e^{\alpha t}u \qquad [2.6.17]$$

Therefore,

$$\begin{aligned}\dot{\bar{x}} &= d(e^{\alpha t}x)/dt \\ &= \alpha e^{\alpha t}x + e^{\alpha t}(Ax + Bu) \\ &= (A + I\alpha)e^{\alpha t}x + Be^{\alpha t}u \\ &= (A + I\alpha)\bar{x} + B\bar{u} \\ &= \bar{A}\bar{x} + B\bar{u}\end{aligned} \qquad [2.6.18]$$

The deterministic performance index becomes

$$\begin{aligned}J &= \int_{t=0}^{\infty}(\bar{x}^T Q\bar{x} + \bar{u}^T R\bar{u})dt \\ &= \int_{t=0}^{\infty}e^{2\alpha t}(x^T Qx + u^T Ru)dt\end{aligned} \qquad [2.6.19]$$

which is the modified cost function [2.6.1]. This is for a time-invariant problem since Q and R are constant, whereas, in Equations [2.6.2] to [2.6.4], the weighting matrices, $\overline{Q}(t)$ and $\overline{R}(t)$, were functions of time. The minimization of Equation [2.6.19] produces the following Riccati Equation

$$\overline{F}\overline{A} + \overline{A}^T\overline{F} - \overline{F}BR^{-1}B^T\overline{F} + Q = 0 \qquad [2.6.20]$$

Since $\overline{A} = A + \alpha I$, this becomes

$$\overline{F}(A + \alpha I) + (A + \alpha I)^T\overline{F} - \overline{F}BR^{-1}B^T\overline{F} + Q = 0 \qquad [2.6.21]$$

which is identical to Equation [2.6.10]. The optimal controller becomes

$$\overline{u}^{\times} = -R^{-1}B^T\overline{F}\overline{x} \qquad [2.6.22]$$

Substituting in the definitions for $\overline{u}$ and $\overline{x}$ from Equations [2.6.16] and [2.6.17] and cancelling out the common factor $e^{\alpha t}$ produces

$$u^{\times} = -R^{-1}B^T\overline{F}x \qquad [2.6.23]$$

which is identical to Equation [2.6.12].

A *non-rigorous proof* that the closed-loop poles of the system are to the left of $-\alpha$ (Figure 2) is presented in Appendix A.

Due to the duality between the regulator and observer, implementing this on the observer equations results in modifying the observer Riccati Equation from

$$AP + PA^T - PC^TV_2^{-1}CP + V_1 = 0 \qquad [2.6.24]$$

to the α - shifted version of

$$(A + \alpha I)P + P(A + \alpha I)^T - PC^TV_2^{-1}CP + V_1 = 0 \qquad [2.6.25]$$

Note that when $\alpha = 0$, one returns to the original performance index.

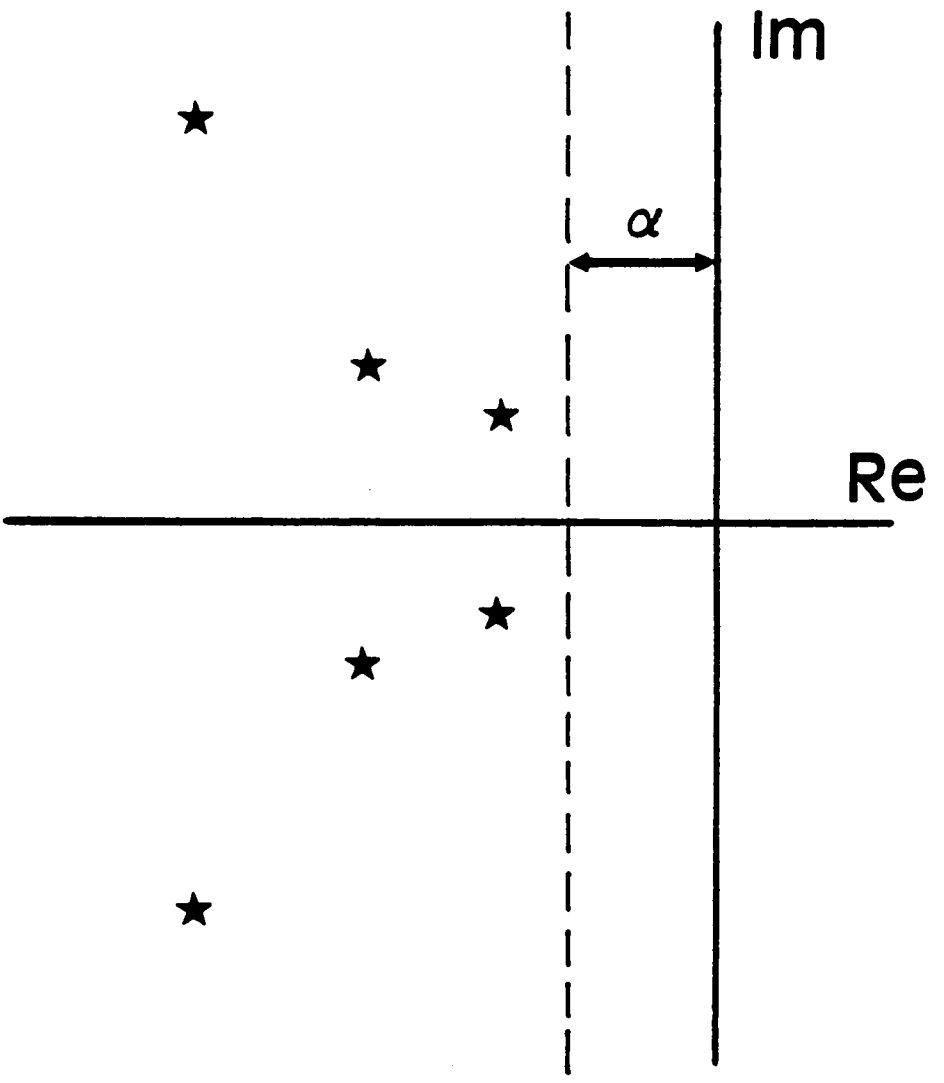

Figure 2. Prescribed stability margin.

It should be noted that whenever α is specified in any of the results presented in this dissertation, it is only used for the observer and not the regulator.

2.7. PLANTS AND COMPENSATORS

A plant is defined as any physical object or system which is to be controlled. A compensator, on the other hand, is any physical device (electrical, mechanical, etc.) which adjusts the system so as to satisfy certain required performance specifications. The typical SISO (single-input-single-output) block diagram of a compensated system is depicted in Figure 3, where $r(s)$ is the input command reference signal, $e(s)$ is the error signal, $u(s)$ is the control input signal, $y(s)$ is the output signal, $k(s)$ is the compensator transfer function, and $g(s)$ is the plant transfer function.

The plant transfer function is readily determined from the system's governing equations

$$\dot{x}(t) = Ax(t) + Bu(t) \qquad [2.7.1]$$

$$y(t) = Cx(t) \qquad [2.7.2]$$

The plant transfer function relates the control input signal, u, to the output signal, y. By taking the Laplace Transform of the above equations, one finds that

$$sx(s) = Ax(s) + Bu(s) \qquad [2.7.3]$$

$$(sI - A)x(s) = Bu(s) \qquad [2.7.4]$$

$$x(s) = (sI - A)^{-1}Bu(s) \qquad [2.7.5]$$

and

$$y(s) = Cx(s) \qquad [2.7.6]$$

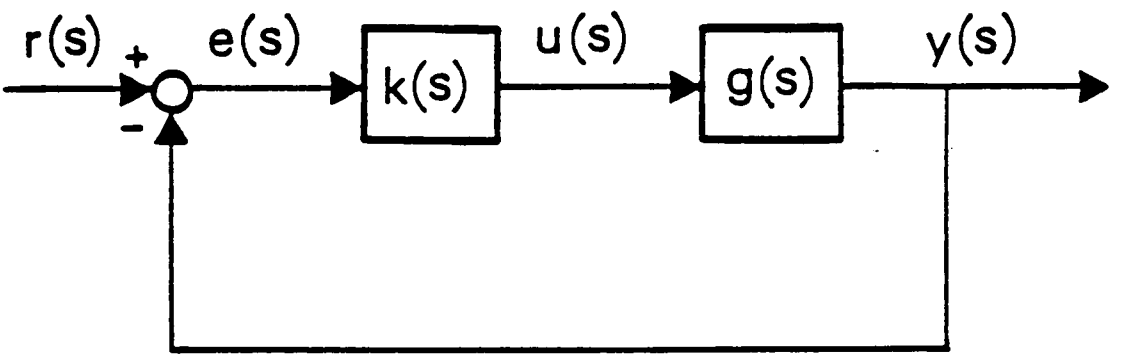

Figure 3. Block diagram of a compensated system.

Substituting Equation [2.7.5] into [2.7.6] produces

$$y(s) = C(sI - A)^{-1}Bu(s) \qquad [2.7.7]$$

or

$$y(s) = g(s)u(s) \qquad [2.7.8]$$

where

$$g(s) = C(sI - A)^{-1}B \qquad [2.7.9]$$

where $g(s)$ is the plant transfer function and is a ratio of polynomials.

The compensator transfer function, on the other hand, depends entirely on what performance specifications are to be satisfied. The compensator can be defined through various classical control techniques [30] or through modern control techniques [19]. Since only the LQG formulation is studied here, the compensator is determined from the LQR/KBF governing system equations.

Since the state of the system is reconstructed via a Kalman-Bucy Filter, whereby, the reconstructed state, $\hat{x}$, is obtained by integrating

$$\dot{\hat{x}}(t) = A\hat{x}(t) + Bu(t) + K_c[y(t) - C\hat{x}(t)] \qquad [\hat{x}(0) = 0] \qquad [2.7.10]$$

with the control law

$$u(t) = -G_c\hat{x}(t) \qquad [2.7.11]$$

the above equations produce a compensator transfer function which relates the output signal, y, to the control input signal, u. By taking the Laplace Transform of the above equations, one finds that

$$s\hat{x}(s) = A\hat{x}(s) + Bu(s) + K_c[y(s) - C\hat{x}(s)] \qquad [2.7.12]$$

and

$$u(s) = -G_c\hat{x}(s) \qquad [2.7.13]$$

Substituting Equation [2.7.13] into [2.7.12] produces

$$s\hat{x}(s) = A\hat{x}(s) - BG_c\hat{x}(s) - K_cC\hat{x}(s) + K_cy(s) \qquad [2.7.14]$$

$$(sI - A + BG_c + K_cC)\hat{x}(s) = K_cy(s) \qquad [2.7.15]$$

or

$$\hat{x}(s) = (sI - A + BG_c + K_cC)^{-1}K_cy(s) \qquad [2.7.16]$$

but $u(s)$ is related to $\hat{x}(s)$ through Equation [2.7.13] so

$$u(s) = -G_c(sI - A + BG_c + K_cC)^{-1}K_cy(s) \qquad [2.7.17]$$

or

$$u(s) = -k(s)y(s) \qquad [2.7.18]$$

where

$$k(s) = G_c(sI - A + BG_c + K_cC)^{-1}K_c \qquad [2.7.19]$$

where $k(s)$ is the compensator transfer function and is also a ratio of polynomials.

The system is being compensated by a feedback loop. The LQG block diagram of the compensated system corresponds to Figure 3 with $r(s) = 0$.

The stability of the compensated system can be determined from the block-diagram algebra [52] of Figure 3. The following relationships are readily apparent

$$y(s) = g(s)k(s)e(s) \qquad [2.7.20]$$

and

$$e(s) = r(s) - y(s) \qquad [2.7.21]$$

Combining the two above equations and rearranging terms produces

$$y(s) = \frac{g(s)k(s)}{1 + g(s)k(s)} r(s) \qquad [2.7.22]$$

where $[g(s)k(s)]/[1 + g(s)k(s)]$ is referred to as the closed-loop transfer function. The system is stable if the roots of the equation

$$1 + g(s)k(s) = 0 \qquad [2.7.23]$$

all lie in the left half-plane. It should be noted that the roots of Equation [2.7.23], when specialized to the LQG problem, are the same as the eigenvalues of Equation [2.4.4]. Since $g(s)$ and $k(s)$ are ratios of polynomials

$$g(s)k(s) = \frac{N_{gk}(s)}{D_{gk}(s)} \qquad [2.7.24]$$

Equation [2.7.23] becomes

$$\frac{D_{gk}(s) + N_{gk}(s)}{D_{gk}(s)} = 0 \qquad [2.7.25]$$

or

$$D_{gk}(s) + N_{gk}(s) = 0 \qquad [2.7.26]$$

$[D_{gk}(s) + N_{gk}(s)]$ is referred to as the closed-loop characteristic polynomial, $\phi_{CL}(s)$.

As a final comment, if one analyzes the open-loop system (no feedback), the governing equation becomes

$$y(s) = [g(s)k(s)]r(s) \qquad [2.7.27]$$

where $g(s)k(s)$ is referred to as the open-loop transfer function. The open-loop characteristic polynomial, $\phi_{OL}(s)$, is, therefore, defined by $D_{gk}(s)$.

As a result, $\phi_{CL}(s)$ and $\phi_{OL}(s)$ are related by

$$\phi_{CL}(s) = \phi_{OL}(s)[1 + g(s)k(s)] \qquad [2.7.28]$$

The above equation will be used in the development of the Nyquist Stability Criterion.

The above relationships for the plant and compensator transfer functions were shown for SISO systems. The same relationships apply for MIMO systems, i.e.,

$$G(s) = C(sI - A)^{-1}B \qquad [2.7.29]$$

$$K(s) = G_c(sI - A + BG_c + K_cC)^{-1}K_c \qquad [2.7.30]$$

except that now the transfer functions become transfer function matrices; $G(s)$ is the plant transfer function matrix, and $K(s)$ is the compensator transfer function matrix. It can also be shown that

$$\phi_{CL}(s) = \phi_{OL}(s)\det[I + G(s)K(s)] \qquad [2.7.31]$$

As an aside, it would also be interesting to look at a purely regulator compensated system alone when perfect knowledge of the state is known. For the system whose governing equation is

$$\dot{x}(t) = Ax(t) + Bu(t) \qquad [2.7.32]$$

it was shown in Equations [2.7.3] – [2.7.5] that by taking the Laplace Transform of the above equation, the control input signal, u, is related to the state vector, x, by

$$x(s) = (sI - A)^{-1}Bu(s) \qquad [2.7.33]$$

For the regulator problem, the control law is implemented on the actual state of the system as

$$u(t) = -G_c x(t) \qquad [2.7.34]$$

By taking the Laplace Transform of the above equation, it is seen that the state vector, x, is related to the control input signal, u, by

$$u(s) = -G_c x(s) \qquad [2.7.35]$$

Once again, the system is being *compensated* by a feedback loop. The LQR block diagram of the compensated system is presented in Figure 4. The open-loop transfer function for the regulator [19] is $G_c(sI - A)^{-1}B$.

2.8. NYQUIST STABILITY CRITERION

The Nyquist stability criterion for a SISO system [30, 52 – 55] is as follows:

For a feedback system to be stable, the Nyquist plot Γ_{gk} must encircle the point $-1 \pm j\,0$ exactly n_p times in a counterclockwise direction, where n_p is the number of poles of the system open-loop transfer function, $g(s)k(s)$, within the contour Γ_s as $r \to \infty$.

The Γ_s contour and a typical Γ_{gk} contour are found in Figure 5. Γ_s is the Nyquist contour which surrounds the entire right half-plane, and Γ_{gk} is the image of Γ_s under the mapping $g(s)k(s)$.

The above criterion will be presented in a more formal mathematical fashion so that the multivariable generalization of the Nyquist criterion will be an obvious and natural extension of the SISO case. For this formal description, a derivation of the Nyquist criterion follows.

The Nyquist criterion is based on the *principle of the argument* from *complex variable theory*. It states that as the contour, Γ_s, is mapped onto some new contour, $\overline{\Gamma}_s$, under the analytic con-

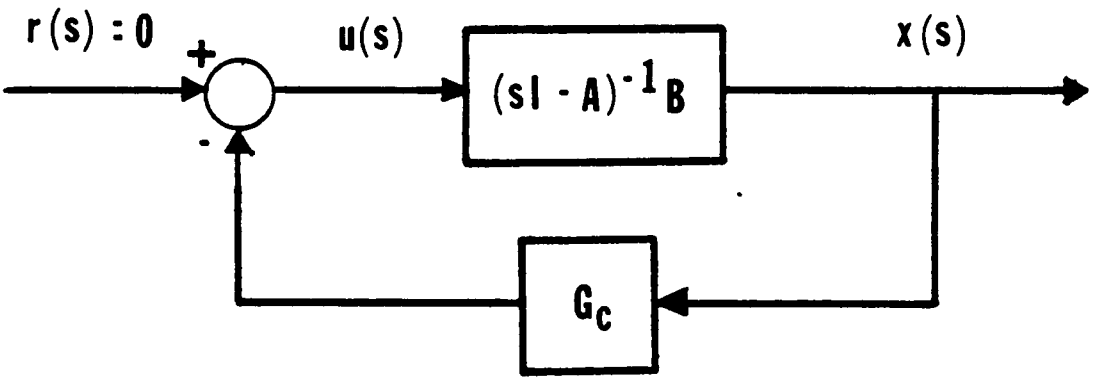

Figure 4. Block diagram for the Linear Quadratic Regulator.

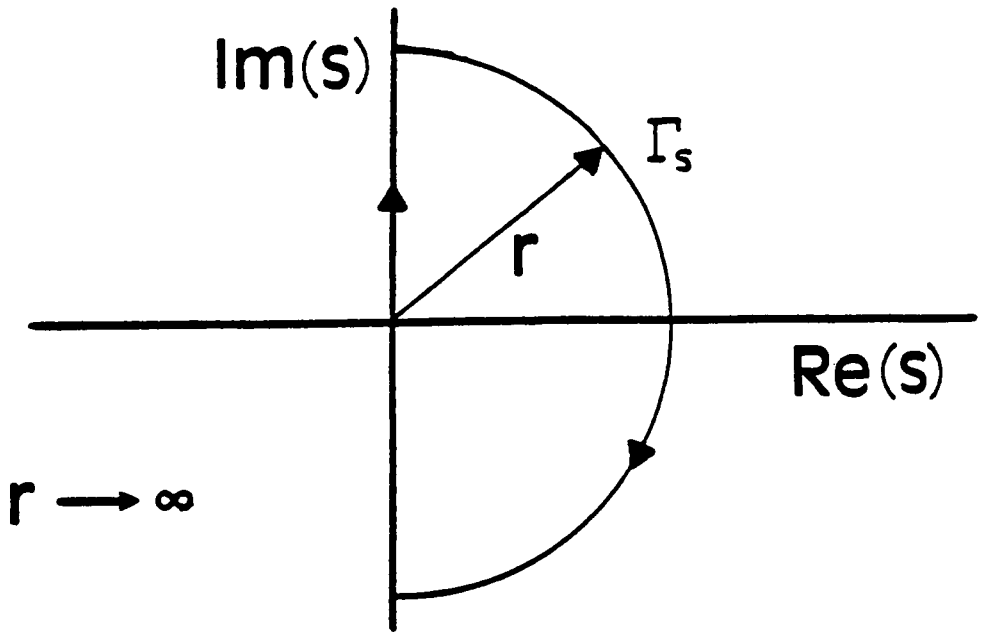

(a)

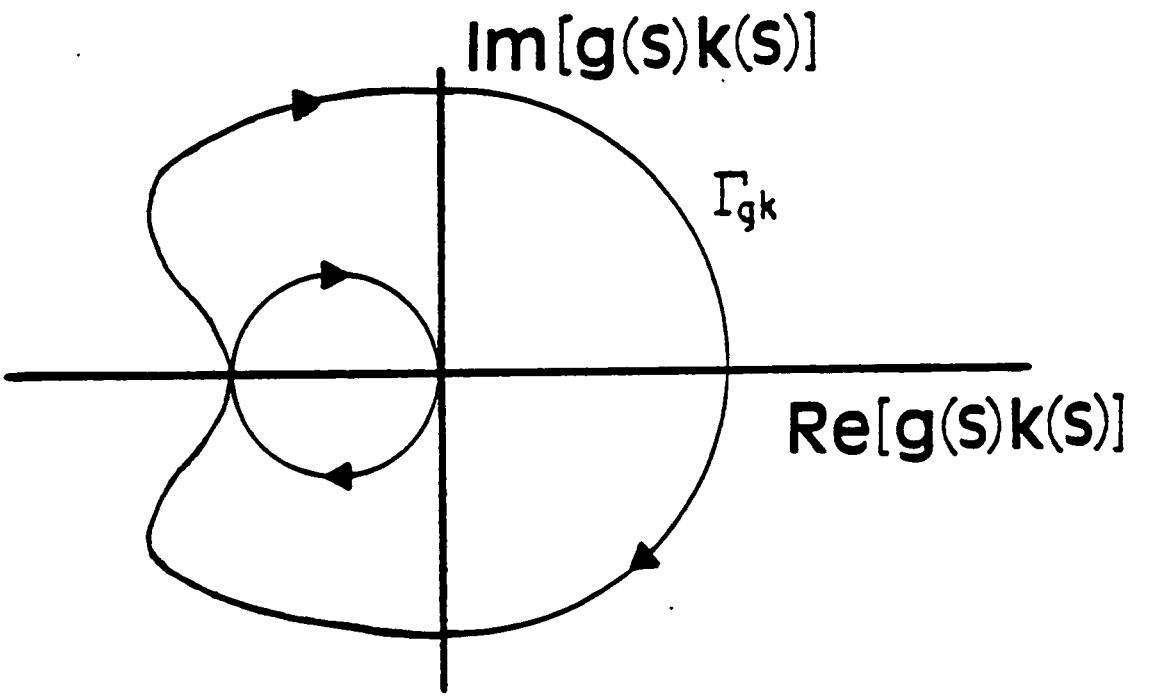

(b)

Figure 5. (a) Nyquist s-plane contour. (b) Nyquist plot.

formal map, $\Phi_c(s)$, $\overline{\Gamma}_s$ will encircle the origin $z_n - p_n$ times where z_n and p_n are the number of zeros and poles of $\Phi_c(s)$, respectively, in the right half-plane, i.e., in Γ_s.

Using this principle, $\Phi_c(s)$ will be selected as the feedback system's closed-loop characteristic polynomial, $\phi_{CL}(s)$. It can be shown [19, 56] that

$$\phi_{CL}(s) = \phi_{OL}(s)[1 + g(s)k(s)] \qquad [2.8.1]$$

where

$$\phi_{OL}(s) = \det(sI - A)\det(sI - A + BG_c + K_cC) \qquad [2.8.2]$$

for the LQG problem. In general, $\phi_{OL}(s)$ is the open-loop characteristic polynomial where $g(s)k(s)$ is the open-loop transfer function. $\phi_{CL}(s)$ plotted as $\overline{\Gamma}_s$ is comprised of evaluating $\phi_{CL}(s)$ at all the points on the Γ_s contour.

By introducing the notation $N(\overline{\beta}; \Phi_c(s); \Gamma)$ as the number of clockwise encirclements of the point $\overline{\beta}$ by the conformal mapping $\Phi_c(s)$ of contour Γ, the argument principle of $\phi_{CL}(s)$ can be stated as $\phi_{CL}(s)$ is analytic and

$$\lim_{r \to \infty} N(0; \phi_{CL}(s); \Gamma_s) = z_n - p_n \qquad [2.8.3]$$

where z_n and p_n are the number of zeros and poles of $\phi_{CL}(s)$ in the right half-plane, i.e., in Γ_s.

Recall that $\phi_{CL}(s)$ is the closed-loop characteristic polynomial, therefore, it has no poles, i.e., $p_n = 0$. It only has zeros; the zeros of $\phi_{CL}(s)$ are the poles of the closed-loop system. It should also be noted that for a stable closed-loop system, all roots of the characteristic polynomial must lie in the left hand side of the complex plane. This means that $\phi_{CL}(s)$ must have no zeros in the right half-plane, Γ_s, in order for the system to be stable, i.e., $z_n = 0$ for stability. As a result,

$$\lim_{r \to \infty} N(0; \phi_{CL}(s); \Gamma_s) = 0 \qquad [2.8.4]$$

From Equation [2.8.1], this becomes

$$\lim_{r \to \infty} N(0; \phi_{OL}(s)[1 + g(s)k(s)]; \Gamma_s) = 0 \qquad [2.8.5]$$

or

$$\lim_{r \to \infty} N(0; \phi_{OL}(s); \Gamma_s) + \lim_{r \to \infty} N(0; 1 + g(s)k(s); \Gamma_s) = 0 \qquad [2.8.6]$$

from the principle of the argument. If n_p is defined as the number of open-loop system poles in the right half-plane, Γ_s, then

$$\lim_{r \to \infty} N(0; \phi_{OL}(s); \Gamma_s) = n_p \qquad [2.8.7]$$

so Equation [2.8.6] becomes

$$\lim_{r \to \infty} N(0; 1 + g(s)k(s); \Gamma_s) = -n_p \qquad [2.8.8]$$

which becomes the general form of the Nyquist stability criterion, i.e., the closed-loop feedback system is stable if and only if $z_n = 0$ and Equation [2.8.8] applies where the encirclement is taken in the counterclockwise sense due to the negative sign in front of n_p.

To show how this is equivalent to the Nyquist stability criterion stated earlier, the point of encirclement can be moved from 0 to -1 to produce

$$\lim_{r \to \infty} N(-1; g(s)k(s); \Gamma_s) = -n_p \qquad [2.8.9]$$

which is identical to the Nyquist criterion stated. Under this translation, the resulting contour becomes Γ_{gk}.

As a result, the multivariable generalization follows in the same manner with only a few minor modifications. Equation [2.8.1] is replaced by the multivariable equivalent

$$\phi_{CL}(s) = \phi_{OL}(s) \det[I + G(s)K(s)] \qquad [2.8.10]$$

The derivation is identical except $[1 + g(s)k(s)]$ is being replaced by $\det[I + G(s)K(s)]$.

The multivariable generalization of the Nyquist stability criterion [19, 56 – 61] becomes

$$\lim_{r \to \infty} N(0; \det[I + G(s)K(s)]; \Gamma_s) = - N_p \qquad [2.8.11]$$

where the closed-loop system is stable if and only if the origin is encircled, under the mapping of Γ_s via $\det[I + G(s)K(s)]$, N_p times in a counterclockwise sense where N_p is the number of unstable open-loop poles of $G(s)K(s)$, the open-loop transfer matrix.

There are other variations [62] to the above generalized Nyquist criterion, but they will not be pursued here. Equation [2.8.11] will be used as the basis for the stability robustness tests which will be presented shortly.

2.9. *GAIN AND PHASE MARGINS*

Once a system's stability has been established, the designer may wish to know quantitatively by how much a system can be changed and yet still maintain its stability, i.e., its degree of stability. The concept of gain and phase margins is utilized to determine the system stability margins, i.e., characterize the system stability *robustness*. This information is important since the designer develops a compensator for some *model* of the actual system as opposed to the actual system itself.

The *gain margin* is defined as a multiplicative factor by which the system gain must be changed, i.e., the system must undergo a pure gain change, in order to produce instability:

$$g(s)k(s) = G_m[g(s)k(s)]_{model} \qquad [2.9.1]$$

$$GM^- < G_m < GM^+ \qquad [2.9.2]$$

where G_m is the allowable gain factor, and GM^- and GM^+ are the gain stability bounds. When G_m equals these bounds, instability occurs. These bounds represent the system gain margins. When G_m is defined anywhere within those bounds, the system still remains stable.

Similarly, the *phase margin* establishes how much pure phase change the system can undergo until it reaches instability:

$$g(s)k(s) = e^{j\theta_m}[g(s)k(s)]_{model} \qquad [2.9.3]$$

$$\mathrm{PM}^- < \theta_m < \mathrm{PM}^+ \qquad [2.9.4]$$

where θ_m is the allowable system phase change, and PM^- and PM^+ are the phase stability bounds. Again, when θ_m equals these bounds, instability occurs. These bounds represent the system phase margins. When θ_m is defined anywhere within those bounds, the system still remains stable.

In general, the system can be represented as

$$g(s)k(s) = G_m e^{j\theta_m}[g(s)k(s)]_{model} \qquad [2.9.5]$$

Therefore, the gain margins are determined at zero phase, i.e., $\theta_m = 0$, and the phase margins are determined at unity gain, i.e., $G_m = 1$.

For a stable system, the gain and phase margins can be determined by looking at the system's Nyquist plot. For a SISO system, if one looks at the positive and negative frequency portions of the Nyquist plot of $g(j\omega)k(j\omega)$, the gain and phase margins are indicated on Figure 6. The positive and negative frequency portions are mirror images of one another. As seen from Section 2.8, the $-1 \pm j0$ point establishes these margins. The gain margins are determined for zero phase as measured from the negative abscissa. They are the factors by which the gain needs to be multiplied by in order for the system to reach the $-1 \pm j0$ point. The phase margins, on the other hand, are determined for unity gain. They are the phase changes the system must undergo in order to reach the $-1 \pm j0$ point. Due to symmetry about the real axis, the PM^- and PM^+ bounds are typically related

as $PM^- = -PM^+$. A more detailed discussion on gain and phase margins can be found in References [19, 30, 52, 53].

Although the proof will not be presented here, the Linear Quadratic Regulator has been found to have the following *guaranteed* minimum gain and phase margins for both the SISO and MIMO cases [19, 51]:

$$\frac{1}{2} < G_m < \infty \qquad [2.9.6]$$

$$-60° < \theta_m < 60° \qquad [2.9.7]$$

where the loop transfer matrix for the regulator is represented as $G_c(sI - A)^{-1}B$. With the presence of an observer, the combined regulator and observer controller has been found to have *no guaranteed* margins [19, 63] .

2.10. DESIGNING ROBUST CONTROLLERS - STABILITY ROBUSTNESS TESTS

This section investigates how controllers should be designed in the presence of uncertainties. These uncertainties can take on several forms. Regarding system uncertainties, there are two broad classes: regular perturbations and singular perturbations. Regular perturbations are represented by uncertainties which preserve the order of the system, i.e., signal disturbances, sensor noise, parameter variations, system nonlinearities, and modelling errors. Singular perturbations, on the other hand, reflect changes in the order of the system, i.e., neglected dynamics, truncated modes, and modelling errors. These are only some of the factors which lead to system uncertainties. How some of these uncertainties enter and affect the system response will be investigated along with some of

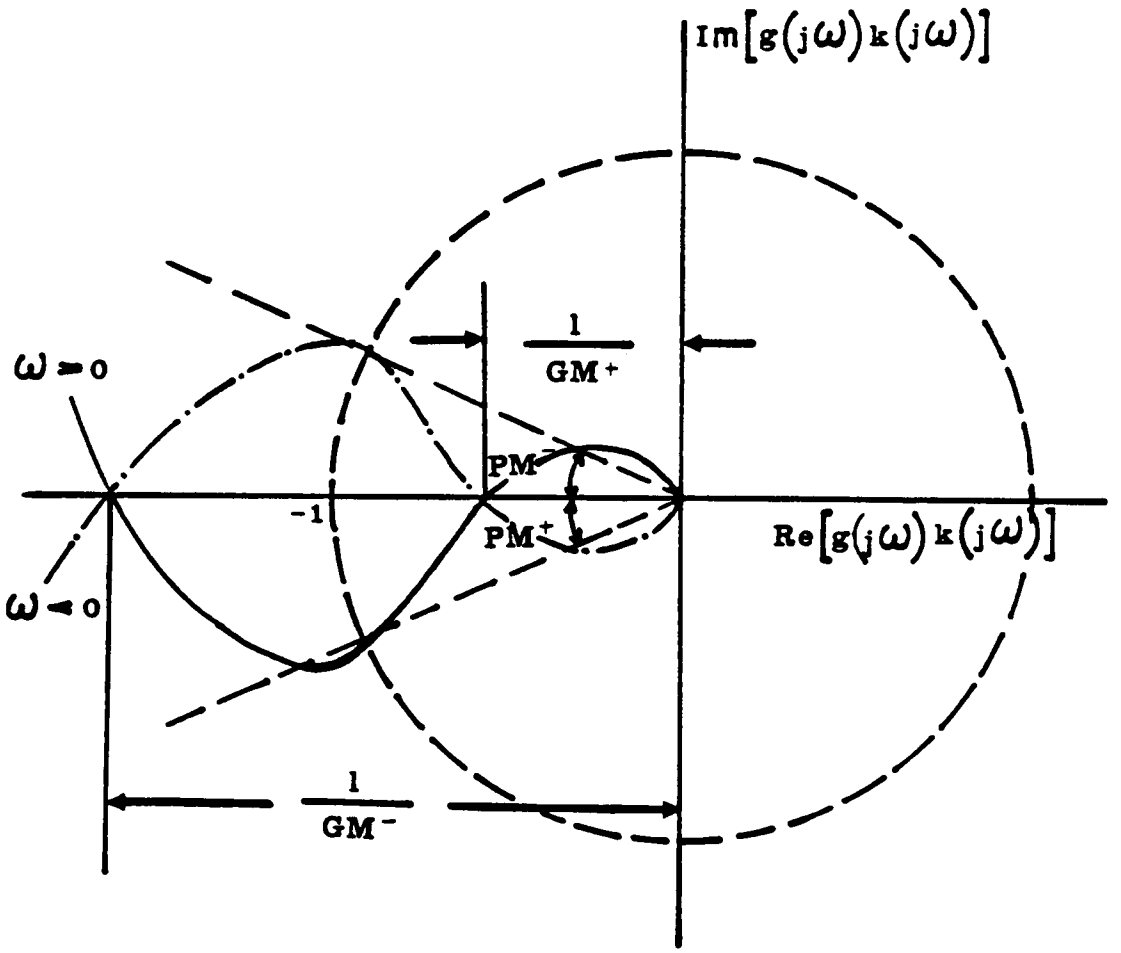

Figure 6. System stability margins.

the trade-offs involved in designing controllers in the presence of these uncertainties [19]. The entire framework in which these uncertainties operate will be explored.

There are also two classes of robustness considerations: stability robustness and performance robustness. Systems possess stability robustness if they remain stable in the presence of uncertainties. Systems possess performance robustness if they maintain a certain level of performance in the presence of uncertainties [7]. Although both types of robustness are important and will be presented in this section, only stability robustness will be considered in the course of the research analysis.

2.10.1. SISO Feedback Control Systems

A typical SISO (single-input-single-output) feedback control system loop is found in Figure 7, where $r(s)$ is the input command reference signal, $e(s)$ is the error signal, $u(s)$ is the control input signal, $d(s)$ is the (output) disturbance signal, $y(s)$ is the output signal, $n(s)$ is the sensor noise signal, $k(s)$ is the compensator transfer function [*where* $k(s) = G_c(sI - A + BG_c + K_cC)^{-1}K_c$], and $g(s)$ is the plant transfer function [*where* $g(s) = C(sI - A)^{-1}B$] .

From Figure 7, the following relationships are readily apparent

$$y(s) = d(s) + g(s)k(s)e(s) \qquad [2.10.1]$$

and

$$e(s) = r(s) - [n(s) + y(s)] \qquad [2.10.2]$$

Combining the two above equations and rearranging terms produces

$$y(s) = \frac{g(s)k(s)}{1 + g(s)k(s)}[r(s) - n(s)] + \frac{1}{1 + g(s)k(s)}d(s) \qquad [2.10.3]$$

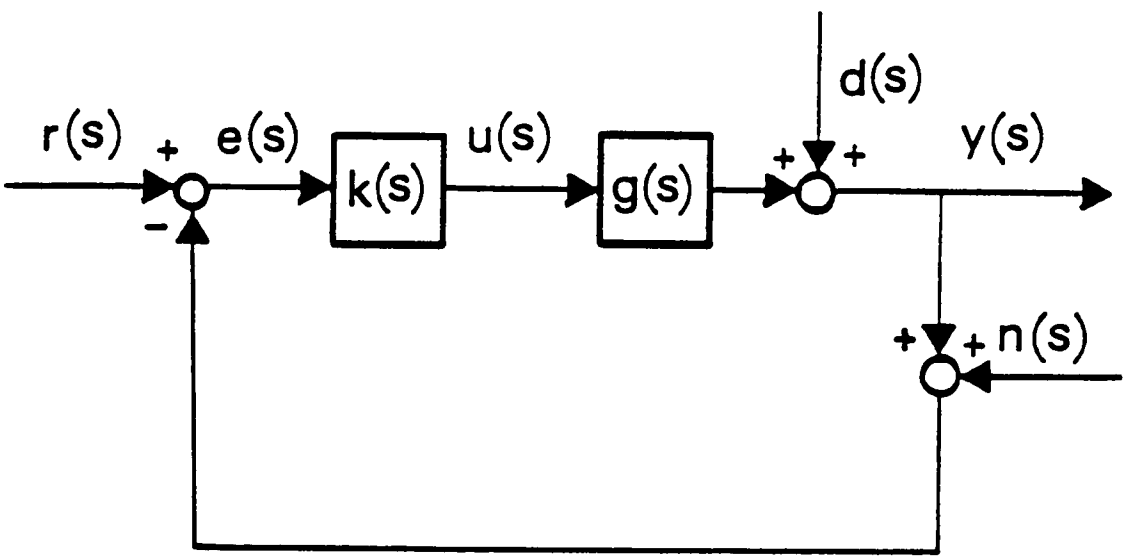

Figure 7. SISO feedback system.

which relates the output signal to the input command, sensor noise, and disturbance signals. In regards to terminology:

- $[g(s)k(s)]$ is the open-loop transfer function
- $[1 + g(s)k(s)]$ is the return difference transfer function
- $[g(s)k(s)]/[1 + g(s)k(s)]$ is the closed-loop transfer function (also known as the complementary sensitivity transfer function)
- $1/[1 + g(s)k(s)]$ is the sensitivity transfer function

A discussion will now be presented as to what qualitative properties a controller should possess in the presence of uncertainties.

2.10.2. Command Following, Disturbance Rejection, and Modelling Error Considerations

It will be assumed that the closed-loop system was designed to be stable, i.e., all the roots of $1 + g(s)k(s) = 0$ lie in the left half part of the complex plane. The actual compensator, $k(s)$, is designed to stabilize some nominal plant, $g^{\times}(s)$, therefore, the nominal closed-loop transfer function is defined as

$$T^{\times}_{CL}(s) = \frac{g^{\times}(s)k(s)}{1 + g^{\times}(s)k(s)} \qquad [2.10.4]$$

Due to modelling errors, the actual plant, $g(s)$, varies from the nominal plant as

$$g(s) = g^{\times}(s) + \delta g(s) \qquad [2.10.5]$$

to produce the actual closed-loop transfer function as

$$T_{CL}(s) = \frac{[g^{\times}(s) + \delta g(s)]k(s)}{1 + [g^{\times}(s) + \delta g(s)]k(s)} \qquad [2.10.6]$$

The objective then becomes to guarantee that the actual closed-loop transfer function is also stable. Any information available on $\delta g(s)$ should be used in the design of the compensator, $k(s)$.

Other considerations in the controller design involve performance characteristics. In terms of command following performance, the objective is generally to have the output follow the command input as closely as possible, i.e.,

$$y(s) \cong r(s) \qquad [2.10.7]$$

From Equation [2.10.3], by neglecting all noise and disturbances, this produces

$$y(s) = \frac{g(s)k(s)}{1 + g(s)k(s)} r(s) \qquad [2.10.8]$$

Equation [2.10.7] can be obtained from Equation [2.10.8] when $g(s)k(s)$ is large.

Also, in terms of disturbance rejection, from Equation [2.10.3], the disturbance, $d(s)$, affects the output, $y(s)$, by the factor $[1 + g(s)k(s)]^{-1}$. Therefore, for large $1 + g(s)k(s)$ and, thus, large $g(s)k(s)$, the system exhibits good disturbance rejection properties.

It should be noted that a large $g(s)k(s)$ function need not be large over the entire range of frequencies. For good command following, $g(s)k(s)$ need only be large in the frequency range of the reference command input signal, whereas, for good disturbance rejection properties, $g(s)k(s)$ need only be large in the frequency range of the disturbance's major energy frequency field.

And finally, in terms of modelling errors and their effect on reference command following performance, neglecting noise and disturbances, the nominal system can be represented from Equation [2.10.3] as

$$y^{\times}(s) = \frac{g^{\times}(s)k(s)}{1 + g^{\times}(s)k(s)} r(s) \qquad [2.10.9]$$

Since the actual plant is defined by Equation [2.10.5], the actual output becomes

$$y(s) = \frac{g(s)k(s)}{1 + g(s)k(s)} r(s) \qquad [2.10.10]$$

or

$$y(s) = \frac{[g^{\times}(s) + \delta g(s)]k(s)}{1 + [g^{\times}(s) + \delta g(s)]k(s)} r(s) \qquad [2.10.11]$$

which can be rewritten as

$$y(s) = y^{\times}(s) + \delta y(s) \qquad [2.10.12]$$

Combining Equations [2.10.11] and [2.10.12] and rearranging terms produces

$$\frac{\delta y(s)}{y^{\times}(s)} = \frac{1}{[1 + g(s)k(s)]} \frac{\delta g(s)}{g^{\times}(s)} \qquad [2.10.13]$$

Therefore, as can be seen from Equation [2.10.13], in order to produce small changes in the output, $\delta y(s)$, from the nominally expected $y^{\times}(s)$ in the presence of possibly large modelling errors, $\delta g(s)$, a large $1 + g(s)k(s)$ and, thus, a large $g(s)k(s)$ is needed. Therefore, for good command following under a nominal system, good command following under the actual system can be guaranteed with a large $g(s)k(s)$ transfer function.

Therefore, under the considerations of good command following performance, disturbance rejection, and modelling errors, a large $g(s)k(s)$ transfer function is desired. This translates into high loop gains to make the system insensitive to disturbances and modelling error sensitivities yet have good command following. Unfortunately, physical systems cannot achieve high loop gains in the high frequency region; $g(s)$ approaches zero in this frequency domain. There are also other performance considerations which make high loop gains totally unacceptable. These considerations stem from sensor noise response and stability robustness analysis for neglected and/or unmodelled dynamics. These factors will be presented next.

2.10.3. Sensor Noise and Stability Robustness Considerations

In terms of sensor noise response, from Equation [2.10.3], the noise enters the output by the factor $g(s)k(s)[1 + g(s)k(s)]^{-1}$. To eliminate this noise contribution, the ideal situation would be to have a small $g(s)k(s)$. But, from the command following objective, $g(s)k(s)$ was found to be needed large. These two conflicting objectives would be difficult to satisfy except that the command, $r(s)$, typically has most of its energy in the low frequency range, and the sensor noise, $n(s)$, typically has most of its energy in the high frequency range. As a result, under these two considerations, $g(s)k(s)$ should be made large in the low frequency region and small in the high frequency region.

Finally, in terms of neglected and/or unmodelled dynamics, high loop gains in the high frequency region are not desirable. The model is not properly represented in this region, therefore, high gains in the high frequency domain can cause an unstable system. As a result, a small $g(s)k(s)$ is desired in this region.

2.10.4. Design Trade-Offs

The different design objectives can be summarized by Figure 8, where the dB (decibels) indicated on the ordinate axis represents a logarithmic coordinate and is defined as

$$(.)dB = 20 \log_{10} |(.)|$$

There are restrictions placed on the magnitude of $g(s)k(s)$ in the different frequency regions. High loop gains are desirable in the low frequency range which is dominated by command following, disturbance rejection, and modelling error sensitivity considerations. On the other hand, low loop gains are desirable in the high frequency range which is dominated by sensor noise and unmodelled

dynamics considerations. The design objective is then to design a stable feedback controller subject to the constraints (barriers) placed on $g(s)k(s)$ as depicted in Figure 8.

Ideally, the designer would like high loop gains in the low frequency region for good performance and to extend this high loop gain region as much as possible to insure that the bandwidth of the controller is as large as the spectrum of the disturbance/excitation. After that, the gain should drop off quickly or, more ideally, suddenly change to a low value in the high frequency region for best robustness considerations. In this crossover region, a steep slope of the loop gain is desired at the crossover frequency point (0 dB). Without getting into the details, a steep slope produces small stability margins and poor performance and robustness characteristics near crossover [19]. As a result, the loop gain will have to reduce *gradually* from the low frequency region to the crossover region going into the high frequency region. Therefore, steep loop gain slopes should be avoided near crossover. This is especially critical for multivariable designs. Roughly speaking, this amounts to requesting that the bandwidth of the loop transfer matrix be smaller than the crossover frequency of the multiplicative uncertainty to be discussed in Section 2.10.6.

As a final comment, s was replaced by $j\omega$ in order to readily quantify the restrictions placed on $g(s)k(s)$. As a result, the analysis is done explicitly in the frequency domain.

2.10.5. MIMO Feedback Control Systems

MIMO (multi-input-multi-output) systems are very similar to SISO systems. Some of the major points will be highlighted, but the whole formulation, analysis, and conclusions are comparable to the SISO results.

A typical MIMO feedback control system loop is shown in Figure 9. The definitions of all the elements are the same as their SISO counterparts except that now the signals become vectors of signals and the transfer functions become transfer function matrices.

As before, from Figure 9, the following relationships are apparent

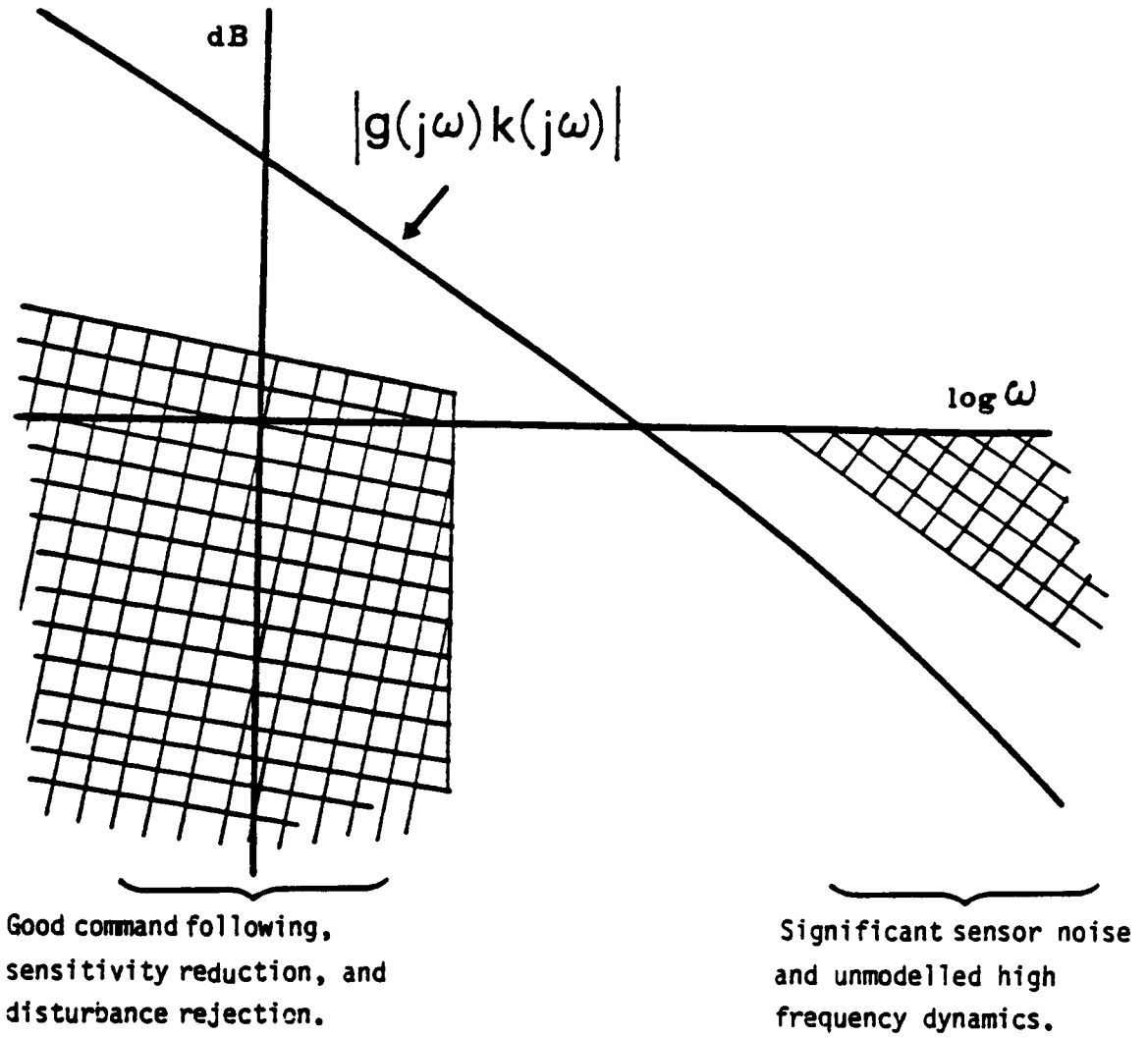

Figure 8. Bode plot of SISO performance and stability design considerations.

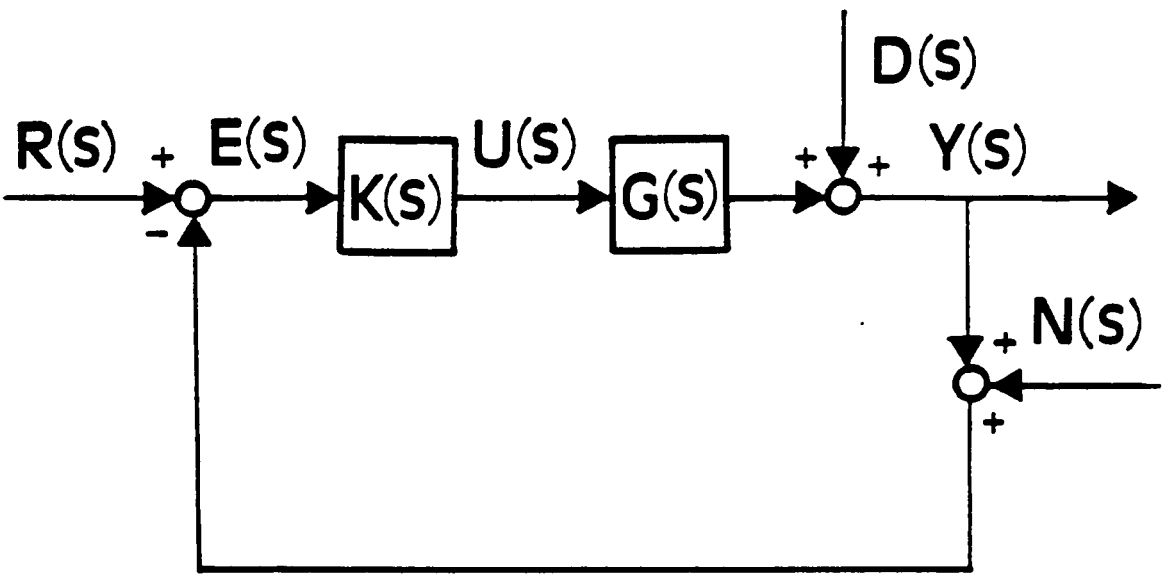

Figure 9. MIMO feedback system.

$$Y(s) = D(s) + G(s)K(s)E(s) \qquad [2.10.14]$$

and

$$E(s) = R(s) - [N(s) + Y(s)] \qquad [2.10.15]$$

Combining the two above equations and rearranging terms produces

$$Y(s) = [I + G(s)K(s)]^{-1}G(s)K(s)[R(s) - N(s)] + [I + G(s)K(s)]^{-1}D(s) \qquad [2.10.16]$$

which relates the output signal vector to the input command, sensor noise, and disturbance signal vectors. As before, the terminology becomes:

- $[G(s)K(s)]$ is the open-loop transfer matrix
- $[I + G(s)K(s)]$ is the return difference matrix
- $[I + G(s)K(s)]^{-1}$ is the inverse return difference matrix
- $[I + G(s)K(s)]^{-1}G(s)K(s)$ is the closed-loop transfer matrix

As for the SISO case, under performance, noise, disturbances, and modelling error sensitivity considerations, comparable restrictions on the size of $G(s)K(s)$ can be placed in the different frequency domain ranges. Singular values will be used in order to quantify these restrictions. A section on the properties and determination of singular values is found in Appendix B.

All the performance requirements have been explicitly treated for the SISO case except only qualitatively for unmodelled dynamics. As a result, this topic will presently be investigated rather thoroughly. It is the basis of the Doyle & Stein [19, 60] stability robustness tests.

2.10.6. Modelling Uncertainties - Stability Robustness Tests

Modelling errors result from truncated modes, parameter variations, system nonlinearities, and neglected dynamics. The objective is to try to estimate these errors in order that this information be used to design a compensator which is as little sensitive as possible to these modelling errors or at least stable in spite of them.

The stability robustness tests developed by Doyle & Stein [60] and Doyle [64] will be pursued. There are, of course, other robustness tests [17, 65 – 79]. The ones by Doyle and Stein are based on the Nyquist stability criterion. The formulation of these robustness tests follows.

Modelling errors are typically represented by additive unstructured uncertainties (see Figure 10), i.e.,

$$\tilde{G}(j\omega) = G(j\omega) + \Delta G(j\omega) \qquad [2.10.17]$$

where

$$\bar{\sigma}[\Delta G(j\omega)] < l_a(\omega) \qquad [2.10.18]$$

and (output) multiplicative unstructured uncertainties (see Figure 11), i.e.,

$$\tilde{G}(j\omega) = [I + L(j\omega)]G(j\omega) \qquad [2.10.19]$$

where

$$\bar{\sigma}[L(j\omega)] < l_m(\omega) \qquad [2.10.20]$$

(Input multiplicative unstructured uncertainties will be discussed later.) $\tilde{G}(j\omega)$ is the actual plant, and $G(j\omega)$ is the modelled plant. $\bar{\sigma}[.]$ is the maximum singular value of matrix [.] and is an indicator of the *size* of the complex matrix. It is a type of normalized eigenvalue which is a *real,* non-negative number. A discussion on the properties and determination of singular values is found in Appendix B. In the additive uncertainties, $\Delta G(j\omega)$ is the model error incurred with an upper bound

represented by $l_a(\omega)$. In the multiplicative uncertainties, $L(j\omega)$ is viewed as the relative error with an upper bound represented by $l_m(\omega)$. The errors are viewed as unstructured since it is assumed that no information is available about them except their upper bounds.

Note that an upper bound to the maximum singular value of the multiplicative uncertainty, $L(j\omega)$, can be obtained from that of the additive uncertainty, $\Delta G(j\omega)$, as follows:

$$[I + L(j\omega)]G(j\omega) = G(j\omega) + \Delta G(j\omega) \qquad [2.10.21]$$

$$L(j\omega) = \Delta G(j\omega)G^{-1}(j\omega) \qquad [2.10.22]$$

It follows that

$$\bar{\sigma}[L(j\omega)] \leq \bar{\sigma}[\Delta G(j\omega)]\bar{\sigma}[G^{-1}(j\omega)] \qquad [2.10.23]$$

or

$$\bar{\sigma}[L(j\omega)] \leq \frac{\bar{\sigma}[\Delta G(j\omega)]}{\underline{\sigma}[G(j\omega)]} \qquad [2.10.24]$$

where $\underline{\sigma}[.]$ is the minimum singular value of matrix $[.]$.

Since this dissertation assumes that the structural dynamicist will be able to predict more vibration modes than would be practical to include in the design of the controller, an approximation on the upper bounds of the additive and multiplicative uncertainties, $l_a(\omega)$ and $l_m(\omega)$, respectively, can be determined analytically.

The plants are, therefore, represented by

$$G(j\omega) = [C(sI - A)^{-1}B]_{controller\ model} \qquad [2.10.25]$$

$$\tilde{G}(j\omega) = [C(sI - A)^{-1}B]_{actual\ known\ system} \qquad [2.10.26]$$

As a result, the (output) multiplicative uncertainty becomes

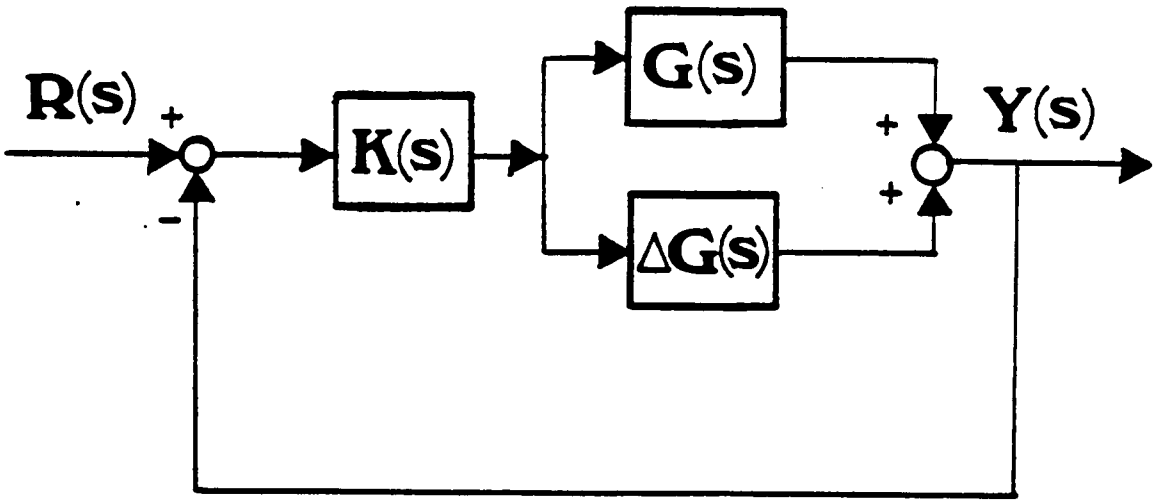

Figure 10. Unity feedback configuration with additive uncertainty.

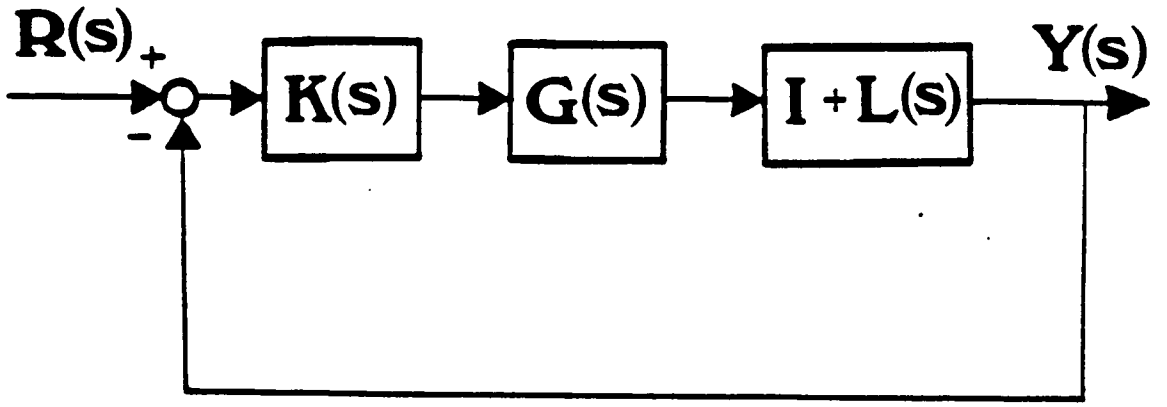

Figure 11. Unity feedback configuration with multiplicative uncertainty at the output.

$$L(j\omega) = \tilde{G}(j\omega)G^{-1}(j\omega) - I \qquad [2.10.27]$$

where it was assumed that the system has an equal number of actuators and sensors, i.e., the plants are square matrices.

Alternatively, from the spectral development of the transfer function [28], the actual and modelled plants are defined as (assuming the modal mass of the modes has been normalized to unity):

$$\tilde{G}(j\omega) = \sum_{i=1}^{m} \frac{\phi_i(s)\phi_i^T(a)}{(\omega_i^2 - \omega^2) + 2j\zeta_i\omega_i\omega} \qquad [2.10.28]$$

$$G(j\omega) = \sum_{i=1}^{n} \frac{\phi_i(s)\phi_i^T(a)}{(\omega_i^2 - \omega^2) + 2j\zeta_i\omega_i\omega} \qquad [2.10.29]$$

where the summation is taken over all the m known modes (controlled + residual) for the actual plant and over only the n controlled modes for the modelled plant. Equations [2.10.25] and [2.10.26] or their counterparts, Equations [2.10.28] and [2.10.29], yield the same results. However, the size of the matrices involved is very different with obvious consequences in terms of accuracy, CPU time, etc. The upper bound of the (output) multiplicative uncertainty can be defined by Equations [2.10.27] and [2.10.20] or by Equation [2.10.24] where the additive uncertainty is represented as

$$\Delta G(j\omega) = \sum_{i=n+1}^{m} \frac{\phi_i(s)\phi_i^T(a)}{(\omega_i^2 - \omega^2) + 2j\zeta_i\omega_i\omega} \qquad [2.10.30]$$

The upper bound of the additive uncertainty follows directly from Equations [2.10.30] and [2.10.18].

The multiplicative unstructured uncertainty is preferable to the additive one in terms of stability robustness tests. The reason for this is that the multiplicative uncertainty model for $G(j\omega)$ is identical to the multiplicative uncertainty model for $G(j\omega)K(j\omega)$, whereas, this is not the case under the additive uncertainty. As a result, the stability robustness test formulation here will only be pursued for the multiplicative uncertainty model. For the interested reader, the additive uncertainty formulation is presented in Reference [72].

The theory presented here is a general one which can be applied to arbitrary systems and is not specialized in any way to the systems studied in this dissertation. For ease of robustness formulation, it will be assumed that both $\tilde{G}(s)$ and $G(s)$ have the same number of unstable modes; the modes may be different though. It will also be assumed that $\tilde{G}(s)$ is finite-dimensional, time-invariant, linear, and strictly proper, i.e., the order of the numerator polynomial is less than the order of the denominator polynomial.

As a result, the design objectives of the controller become

- the nominal system defined by $G(j\omega)K(j\omega)[I + G(j\omega)K(j\omega)]^{-1}$ is stable. (NOTE: $[I + GK]^{-1}GK = GK[I + GK]^{-1}$)

- the actual system defined by $\tilde{G}(j\omega)K(j\omega)[I + \tilde{G}(j\omega)K(j\omega)]^{-1}$, under a multiplicative unstructured uncertainty, is also stable.

- the performance objectives dictated by command following and disturbance rejection are satisfied under $\tilde{G}(j\omega)$.

The first objective is satified by design using the standard Nyquist stability criterion for the SISO system and the multivariable generalization of the Nyquist criterion for the MIMO system.

For the second objective, since it was assumed that $G(j\omega)$ and $\tilde{G}(j\omega)$ both have the same number of unstable modes, this requirement simply reduces to requiring that the number of encirclements of the origin under the mapping $\det[I + \tilde{G}(s)K(s)]$ be identical to the number of encirclements of the origin under the mapping $\det[I + G(s)K(s)]$. This can be guaranteed if $\det[I + \tilde{G}(s)K(s)]$ does not become zero at any frequency. From a mathematical standpoint, a non-zero determinant of a matrix indicates that the matrix is nonsingular. This is equivalent to stating that the minimum singular value of this nonsingular matrix is also non-zero. Since singular values are already non-negative, this condition becomes

$$0 < \underline{\sigma}[I + \tilde{G}(s)K(s)] \qquad [2.10.31]$$

where $\tilde{G}(s)$ will be allowed to have a slightly less restrictive form as

$$\tilde{G}(s) = [I + \varepsilon_L L(s)]G(s) \qquad [2.10.32]$$

where $0 \leq \varepsilon_L \leq 1$. $\varepsilon_L = 1$ is the worst case scenerio since $L(s)$ represents the worst modelling error.

Since $\tilde{G}(s)$ goes to zero as the Nyquist contour goes to infinity, i.e., $\tilde{G}(s)$ is strictly proper, Equation [2.10.31] is reduced to considering only the imaginary axis, i.e.,

$$0 < \underline{\sigma}[I + \tilde{G}(j\omega)K(j\omega)] \qquad [2.10.33]$$

Substituting in Equation [2.10.32] produces

$$0 < \underline{\sigma}\{I + [I + \varepsilon_L L(j\omega)]G(j\omega)K(j\omega)\} \qquad [2.10.34]$$

which becomes

$$0 < \underline{\sigma}\{\{I + [G(j\omega)K(j\omega)]^{-1} + \varepsilon_L L(j\omega)\}G(j\omega)K(j\omega)\} \qquad [2.10.35]$$

From Equation [B.3.5], i.e., properties of singular values,

$$0 < \underline{\sigma}\{I + [G(j\omega)K(j\omega)]^{-1} + \varepsilon_L L(j\omega)\}\underline{\sigma}[G(j\omega)K(j\omega)] \qquad [2.10.36]$$

Since $\underline{\sigma}[G(j\omega)K(j\omega)]$ is positive and non-zero, this term can be divided out to produce

$$0 < \underline{\sigma}\{I + [G(j\omega)K(j\omega)]^{-1} + \varepsilon_L L(j\omega)\} \qquad [2.10.37]$$

From Equation [*B*.3.1], i.e., properties of singular values,

$$\underline{\sigma}\{I + [G(j\omega)K(j\omega)]^{-1}\} > \bar{\sigma}[\varepsilon_L L(j\omega)] \qquad [2.10.38]$$

From Equations [*B*.1.7] and [*B*.3.2], this produces

$$\frac{1}{\bar{\sigma}\{\{I + [G(j\omega)K(j\omega)]^{-1}\}^{-1}\}} > \frac{\varepsilon_L}{\underline{\sigma}[L^{-1}(j\omega)]} \qquad [2.10.39]$$

Using the identity

$$[I + (GK)^{-1}]^{-1} = \{[I + GK](GK)^{-1}\}^{-1} = GK[I + GK]^{-1} \qquad [2.10.40]$$

in Equation [2.10.39] gives

$$\frac{1}{\bar{\sigma}\{G(j\omega)K(j\omega)[I + G(j\omega)K(j\omega)]^{-1}\}} > \frac{\varepsilon_L}{\underline{\sigma}[L^{-1}(j\omega)]} \qquad [2.10.41]$$

From cross multiplication,

$$\frac{1}{\varepsilon_L}\underline{\sigma}[L^{-1}(j\omega)] > \bar{\sigma}\{G(j\omega)K(j\omega)[I + G(j\omega)K(j\omega)]^{-1}\} \qquad [2.10.42]$$

Recall Equation [2.10.20] and apply the singular value property of Equation [*B*.1.8] to show

$$\frac{1}{l_m(\omega)} < \underline{\sigma}[L^{-1}(j\omega)] \qquad [2.10.43]$$

Substituting Equation [2.10.43] into Equation [2.10.42] and assuming the worst case scenerio, i.e., $\varepsilon_L = 1$, produces

$$\bar{\sigma}\{G(j\omega)K(j\omega)[I + G(j\omega)K(j\omega)]^{-1}\} < \frac{1}{l_m(\omega)} \qquad [2.10.44]$$

as the MIMO stability robustness criterion for all $\omega \geq 0$. This criterion requires that for large magnitudes in the multiplicative uncertainty, the system loop gains be small. This was the same conclusion that was mentioned in the SISO discussion on unmodelled dynamics. Based on this argument, for $l_m(\omega) >> 1$ and small loop gains, the robustness criterion reduces to

$$\bar{\sigma}[G(j\omega)K(j\omega)] < \frac{1}{l_m(\omega)} \qquad [2.10.45]$$

for all frequencies, ω, whenever $l_m(\omega) >> 1$. Equation [2.10.45] will guarantee stability.

As a final note on stability robustness, the above formulation was for (output) multiplicative unstructured uncertainties. When the system uncertainty occurs at the plant input, the (input) multiplicative unstructured uncertainty becomes

$$\tilde{G}(j\omega) = G(j\omega)[I + L(j\omega)] \qquad [2.10.46]$$

The difference between this equation and that of [2.10.19] is that the matrix $G(j\omega)$ now appears to the left of $[I + L(j\omega)]$, whereas before, it appeared to the right of this expression. For uncertainties reflected at the input, the analogous stability condition from the Nyquist criterion under Equation [2.10.31] becomes

$$0 < \underline{\sigma}[I + K(s)\tilde{G}(s)] \qquad [2.10.47]$$

or

$$0 < \underline{\sigma}\{I + K(j\omega)G(j\omega)[I + L(j\omega)]\} \qquad [2.10.48]$$

A similar procedure is followed as before for the output case to produce new stability robustness tests. The results are of similar form. As a summary, for uncertainties at the output, $G(j\omega)K(j\omega)$ is used in the formulas, and for uncertainties at the input, $K(j\omega)G(j\omega)$ is used in the formulas. Therefore, for (input) multiplicative uncertainties, $K(j\omega)G(j\omega)$ replaces $G(j\omega)K(j\omega)$ in Equations [2.10.44] and [2.10.45]. It should also be noted that $l_m(\omega)$ has a different meaning in the input case as compared to the output case. It is still defined by Equation [2.10.20] except that $L(j\omega)$ now becomes

$$L(j\omega) = G^{-1}(j\omega)\tilde{G}(j\omega) - I \qquad [2.10.49]$$

as opposed to Equation [2.10.27]. As a result, MIMO systems have a concept of directionality associated with them, whereas, SISO systems do not. For a SISO system, input and output results are identical since $g(j\omega)k(j\omega) = k(j\omega)g(j\omega)$.

The concept of uncertainties at the output or input depends on where the analysis of testing robustness is being performed in terms of breaking the control loop (see Figure 12). Uncertainties are assumed to enter the system either at the input or output of the plant. The robustness analysis is performed where the uncertainty exists. The loop-breaking point (o) signifies robustness testing with respect to uncertainties at the plant output, while the loop-breaking point (i) signifies robustness testing with respect to uncertainties at the plant input.

Finally, the last design objective for the control designer was dictated by performance considerations in the low frequency region. Under the nominal system, the objective was to make $\bar{\sigma}\{[I + G(j\omega)K(j\omega)]^{-1}\}$ small, or, equivalently, from Equation [B.1.9],

$$ps(\omega) \leq \underline{\sigma}[I + G(j\omega)K(j\omega)] \qquad [2.10.50]$$

where $ps(\omega)$ is some performance specification.

Under the actual system which is governed by the (output) multiplicative unstructured uncertainty, this performance requirement becomes

$$ps(\omega) \leq \underline{\sigma}\{I + [I + L(j\omega)]G(j\omega)K(j\omega)\} \qquad [2.10.51]$$

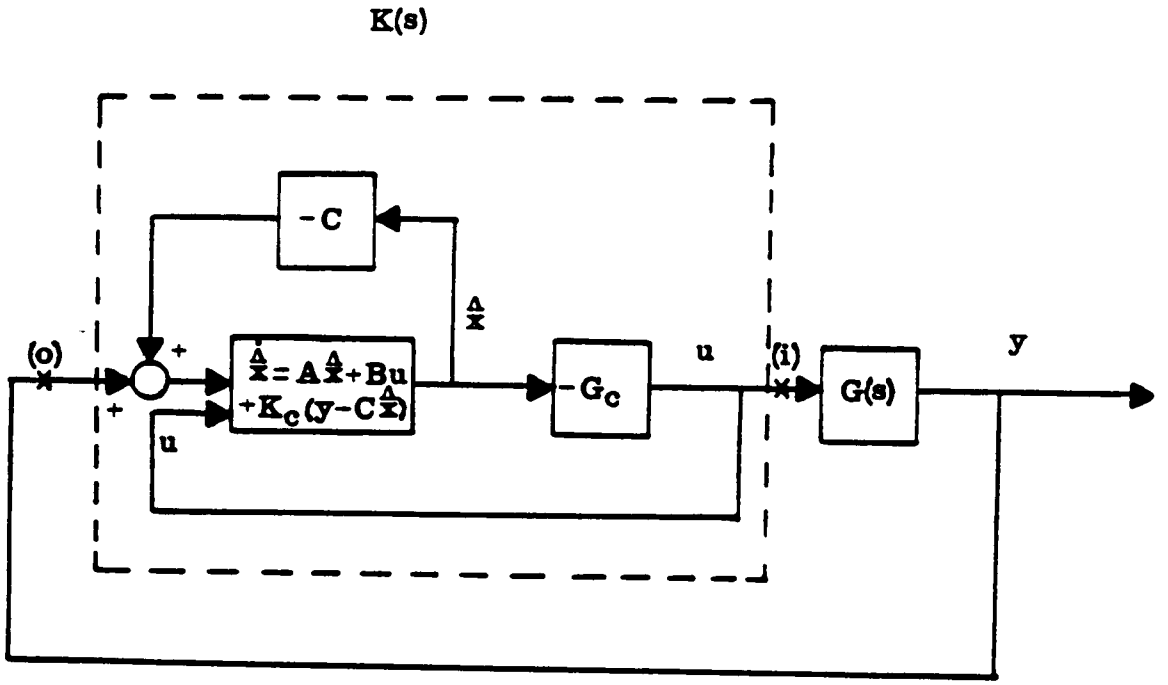

Figure 12. LQG loop.

It can be shown [19, 60] that this becomes

$$\frac{ps(\omega)}{1 - l_m(\omega)} \leq \underline{\sigma}[G(j\omega)K(j\omega)] \qquad [2.10.52]$$

in the frequency range, ω, where $l_m(\omega) < 1$ and $\underline{\sigma}[G(j\omega)K(j\omega)] >> 1$. Note that comparable results can be obtained for (input) multiplicative unstructured uncertainties.

As a result, as for the SISO case, the MIMO design objectives can be summarized by Figure 13. There are performance and stability robustness design restrictions placed on the maximum and minimum singular values of $G(j\omega)K(j\omega)$. Again, high loop gains are desirable in the low frequency range which is dominated by command following, disturbance rejection, and modelling error sensitivity considerations. On the other hand, low loop gains are desirable in the high frequency range which is dominated by sensor noise and stability robustness requirements. The design objective is then to design a stable feedback controller subject to the constraints placed on the maximum and minimum singular values of $G(j\omega)K(j\omega)$ as depicted in Figure 13. There is also an additional consideration for MIMO systems; it is desirable to have $\underline{\sigma}[.]$ as close as possible to $\bar{\sigma}[.]$, especially near crossover, so as to *balance* the multivariable loop [19, 60]. Therefore, the good properties are well distributed over the entire I/O (input/output) space.

As a final comment, the low frequency performance bound is desirable though not mandatory. The high frequency stability robustness bound, on the other hand, becomes *critical* to the designer since it is related to the stability of the system. It should be pointed out, though, that the robustness test is conservative. If the robustness test is violated, it does not mean that the system is going to be unstable, but rather that it may become unstable. The reason is that the structure of the uncertainty may not allow the instability to occur. In other words, the test does not take into account the structure of the system. It is dictated by the magnitude of the upper bound of the system error. No phase information is incorporated.

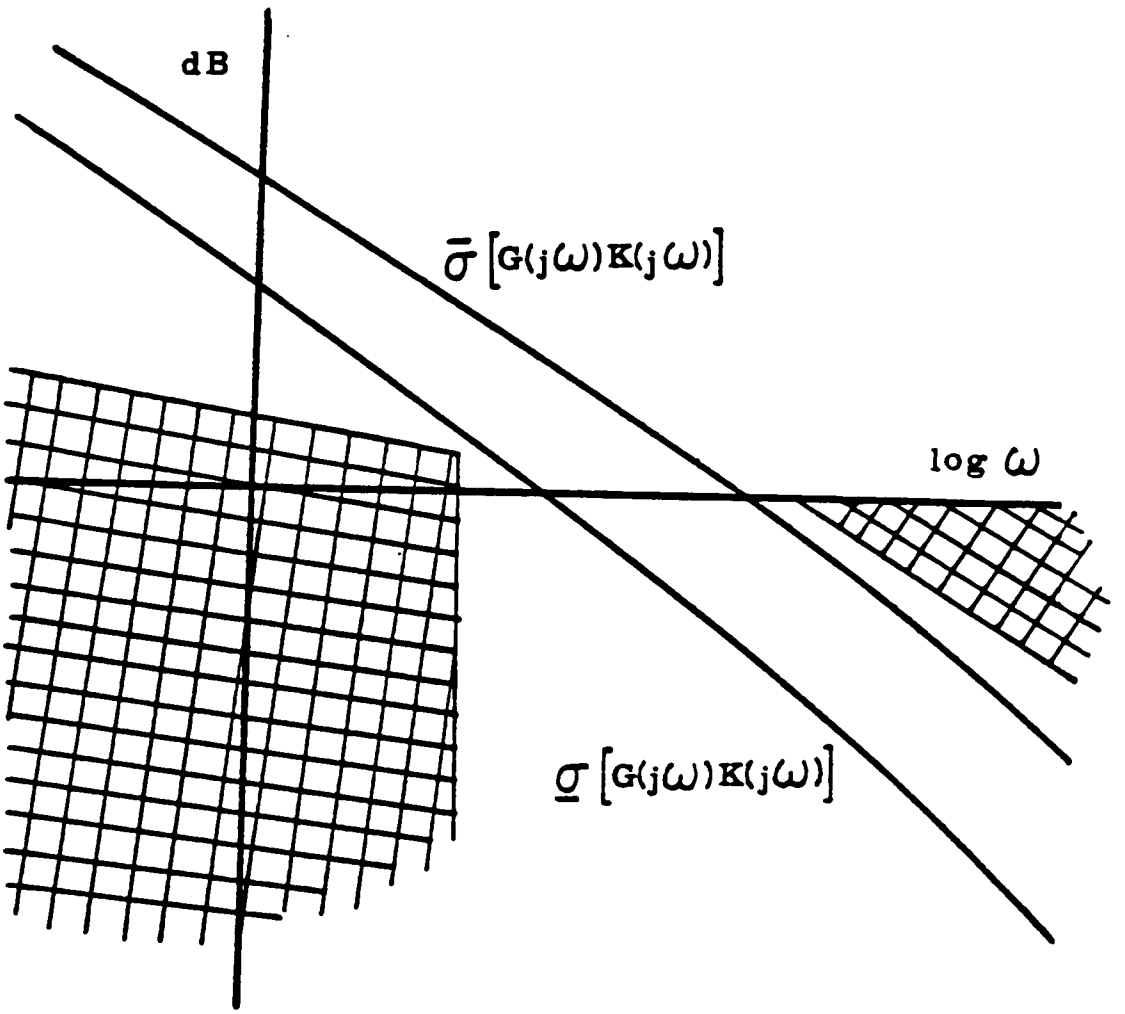

Figure 13. Bode plot of MIMO performance and stability design considerations.

2.11. LINEAR QUADRATIC GAUSSIAN WITH LOOP TRANSFER RECOVERY (LQG/LTR) METHOD

The Linear Quadratic Gaussian with Loop Transfer Recovery (LQG/LTR) Method is discussed extensively in References [7, 19, 80 – 84]. Only the highlights of its formulation will be presented here.

The LQG/LTR method is intended to design a regulator (LQR) which satisfies some robustness criterion, i.e., it has some guaranteed stability margins [78], and then to design an observer (KBF) so that the controller *recovers* the loop transfer matrix, and, thus, the stability margins, of the regulator. The reason for doing this is that an LQG controller has no guaranteed stability margins [63] since the state of the system must be estimated. The Linear Quadratic Regulator, however, has been shown to have guaranteed minimum stability margins (Section 2.9).

The formulation involves a modified Kalman-Bucy Filter. Given W_1 and W_2, the actual plant noise and measurement noise intensity matrices, respectively, the KBF noise matrices which are used in the design of the observer are

$$V_1 = W_1 + q^2 B Q_q B^T \qquad [2.11.1]$$

$$V_2 = W_2 \qquad [2.11.2]$$

where Q_q is any symmetric positive definite matrix, and q is a scalar.

When $q \to 0$, the result is the standard statistically optimum KBF. But, when $q \to \infty$, it can be shown [19] that the system *recovers* the loop transfer matrix of the regulator, i.e., it approaches the full-state feedback case, and, thus, approaches the stability margins of the regulator.

This is not accomplished without cost. The formulation artificially increases the assumed plant noise, and, as a result, the estimation of the state degrades appreciably as $q \rightarrow \infty$. However, the system becomes more robust against uncertainties since the original regulator was selected to have some guaranteed stability margins. Therefore, the LQG/LTR technique represents a trade-off between an accurate estimate of the state versus a stable (robust) plant.

The only condition on full recovery is that the system's open-loop plant be minimum phase. If it is not, *full* recovery is not possible. Depending on the location of the right-half plane transmission zeros of the plant relative to the crossover frequency of the uncertainty curve (whether they are above or below it), only partial recovery can be achieved, i.e., good performance recovery can be achieved at low frequencies but not robustness recovery at high frequencies, or visa versa [19].

It should be noted that this technique has not been found to work well with large lightly damped ($\zeta \rightarrow 0$), flexible space structures. Although the technique produces excellent stability margins, it does not directly utilize any information about parameter uncertainties which are inherently present. As a result, the LQG/LTR controller, for a lightly damped structure, can be very sensitive to modal frequency variations [85]. Another illustration of the problem associated with the LQG/LTR technique implemented on lightly damped structures will be discussed in Section 3.2.

CHAPTER 3. SPILLOVER INSTABILITY

As shown in Section 2.10.6, when $l_m(\omega) >> 1$, a closed-loop system is guaranteed to be stable in the presence of uncertainties if the maximum singular value of the loop transfer matrix satisfies Equation [2.10.45]. Since the robustness test is conservative, it is a sufficient but not a necessary condition for stability. A typical plot of $\bar{\sigma}[G(j\omega)K(j\omega)]$ and $1/l_m(\omega)$ is shown in Figure 14 for a low-damped vibrating structure which is represented by a model truncated to the low frequency modes (here three). The magnitude of the troughs in the uncertainty curve is governed by the damping ratio of the uncontrolled modes. Due to the low structural damping expected in large space structures and the relatively slow decay rate of $\bar{\sigma}[G(j\omega)K(j\omega)]$ at high frequencies, the robustness test cannot, in general, be satisfied by the uncontrolled modes in the transition region just outside the bandwidth of the controller (unless there is a *gap* in the natural frequencies of the structure). The modes which are in the transition region are candidates for destabilization and must be considered carefully. Amongst the uncontrolled modes, we distinguish

- the marginal *residual* modes which do not satisfy the robustness test or have only a small margin.

- the *control system robust residual* modes (called robust modes hereafter) which satisfy the stability robustness test and are guaranteed to be stable.

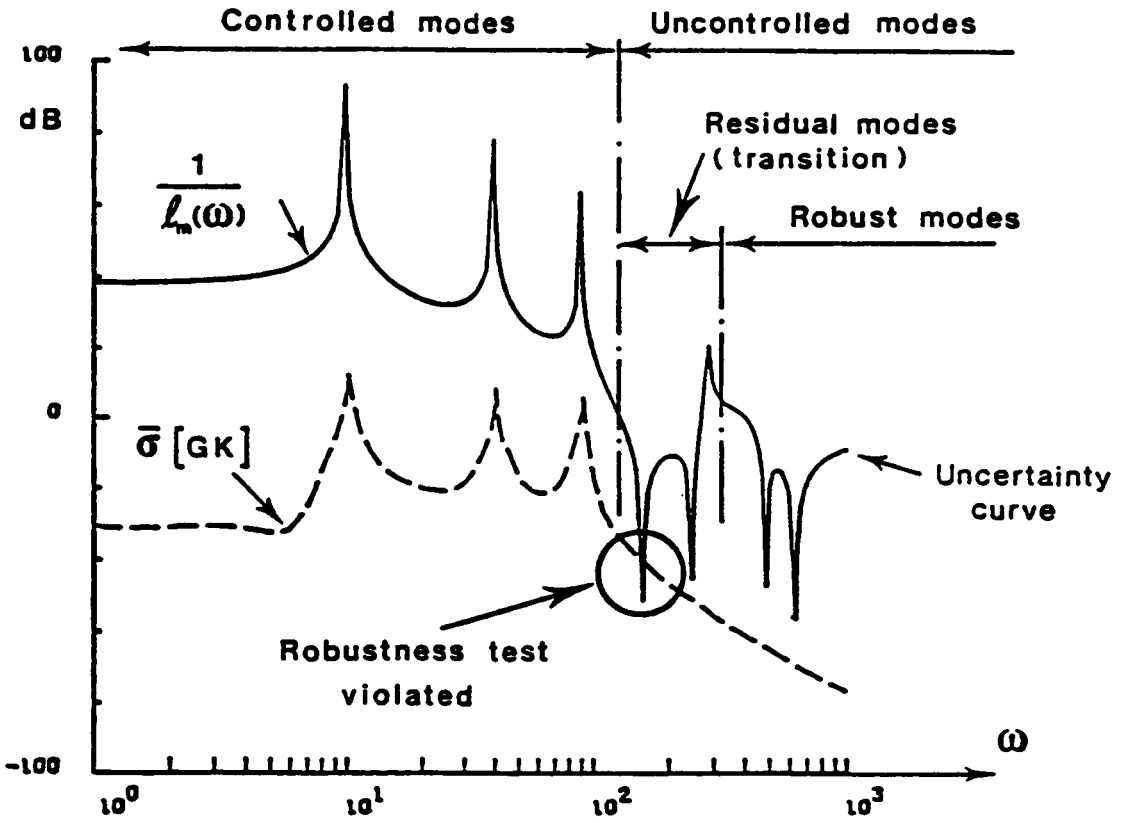

Figure 14. Typical robustness plot.

Only the controlled and the marginal residual modes will have to be considered in the remaining of this study; the latter will be called residual modes.

3.1. SPILLOVER PHENOMENON

The problem of spillover instability in a structure can be demonstrated in the following way. The equations of motion for a complete vibrating system are written in terms of modal amplitudes and reduced modal velocities. With subscripts c and r referring to the controlled and the residual modes, respectively, the equations of motion become

$$\dot{x}_c = A_c x_c + B_c u \qquad [3.1.1]$$

$$\dot{x}_r = A_r x_r + B_r u \qquad [3.1.2]$$

$$y = C_c x_c + C_r x_r \qquad [3.1.3]$$

where A_c and A_r are the system matrices, B_c and B_r are the control matrices, C_c and C_r are the output matrices, x_c and x_r are the state vectors, u is the control vector, and y is the output vector.

It is assumed that there is *perfect knowledge* of the dynamics of the n_c controlled modes. The residual modes are, of course, present in the system but are neglected in the design of the controller. As a result, the controller excites the residual modes.

The controller consists of two parts. The first is an observer. Since the state of the system is, in general, not fully known, it is reconstructed via either a Kalman-Bucy Filter (KBF) or a Luenberger observer. The reconstructed state, $\hat{x}_c$, is obtained by integrating

$$\dot{\hat{x}}_c = A_c \hat{x}_c + B_c u + K_c(y - C_c \hat{x}_c) \qquad [\hat{x}_c(0) = 0] \qquad [3.1.4]$$

where K_c is the observer gain matrix.

The second part of the controller is the regulator where its feedback gain matrix, G_c, is calculated here by using the Linear Quadratic Regulator (LQR) design method where the control law is given as $u = -G_c\hat{x}_c$.

The state estimator error is defined as $e_c = \hat{x}_c - x_c$. If the residual modes are ignored, the state vector is selected to be $(x_c^T\ e_c^T)^T$. The corresponding governing equation for this system becomes

$$\begin{bmatrix} \dot{x}_c \\ \dot{e}_c \end{bmatrix} = \begin{bmatrix} A_c - B_cG_c & -B_cG_c \\ 0 & A_c - K_cC_c \end{bmatrix} \begin{bmatrix} x_c \\ e_c \end{bmatrix} \qquad [3.1.5]$$

As can be readily seen from the block triangular form of the matrix, the poles (eigenvalues) of this system are those of the regulator, $(A_c - B_cG_c)$, and those of the observer, $(A_c - K_cC_c)$. This is known as the *separation principle* whereby the regulator and observer can be designed independently to produce the desired pole locations. These pole locations will insure a stable system.

The effect of the residual modes can be analyzed by considering the composite system where the state vector also includes the residual modes, i.e., $(x_c^T\ e_c^T\ x_r^T)^T$. The corresponding governing equation for this system becomes

$$\begin{bmatrix} \dot{x}_c \\ \dot{e}_c \\ \dot{x}_r \end{bmatrix} = \begin{bmatrix} A_c - B_cG_c & -B_cG_c & 0 \\ 0 & A_c - K_cC_c & K_cC_r \\ -B_rG_c & -B_rG_c & A_r \end{bmatrix} \begin{bmatrix} x_c \\ e_c \\ x_r \end{bmatrix} \qquad [3.1.6]$$

This equation is the starting point for analyzing spillover. The key terms in spillover are $-B_rG_c$ and K_cC_r. They arise from the sensor output being contaminated by the residual modes via the term C_rx_r (observation spillover) and the feedback control exciting the residual modes via the term B_ru (control spillover).

From the above equation, the following conclusions are readily apparent:

(1) If either $C_r = 0$ (no observation spillover) and/or $B_r = 0$ (no control spillover), the eigenvalues of the above system arise from $A_c - B_cG_c$, $A_c - K_cC_c$, and A_r. The result is that the system still remains stable. This means that spillover *cannot* destabilize this system.

(2) When both $C_r \neq 0$ and $B_r \neq 0$, i.e., both observation and control spillover are present, the eigenvalues of the system shift away from $A_c - B_c G_c$, $A_c - K_c C_c$, and A_r. The magnitude of this shift depends entirely on $-B_r G_c$ and $K_c C_r$. Since the poles of A_r will have small stability margin due to the low structural damping, they will lie near the imaginary axis. Even a slight shift from this position can bring the poles into the right half side of the complex plane and, thus, make the system unstable. This phenomenon is called spillover instability.

(3) The regulator poles from $A_c - B_c G_c$ and the observer poles from $A_c - K_c C_c$ will generally be designed with large stability margins. Therefore, instability is unlikely to arise from any shifting of these poles.

The spillover mechanism is illustrated in Figure 15. The flexible system reacts through the controlled modes; the residual modes are excited by the control (control spillover) and contribute to the output signal fed into the observer (observation spillover). When both control and observation spillover are present, they may lead to instability in the residual modes.

3.2. ROBUSTNESS

As stated in Section 2.10.6, if the robustness test is violated, it does not mean that the system is going to be unstable, but rather that it may become unstable. A typical example of a stable system which violates a stability robustness test is found for the Linear Quadratic Regulator with perfect knowledge of the controlled states. A typical robustness plot of the loop transfer matrix for the regulator of a flexible structure is shown in Figure 16. The robustness test is obviously violated, yet, in Section 2.9, it was discussed that the regulator has guaranteed stability margins as defined by its gain and phase margins. In addition to this, Section 3.1 showed that for control spillover alone, i.e., no observation spillover present, spillover *cannot* destabilize the system. The reason why the LQR problem typically fails the robustness test lies in the slow attenuation rate (like $1/\omega$) of the LQR's loop transfer function. As a result, it makes the robustness test very *difficult* to satisfy

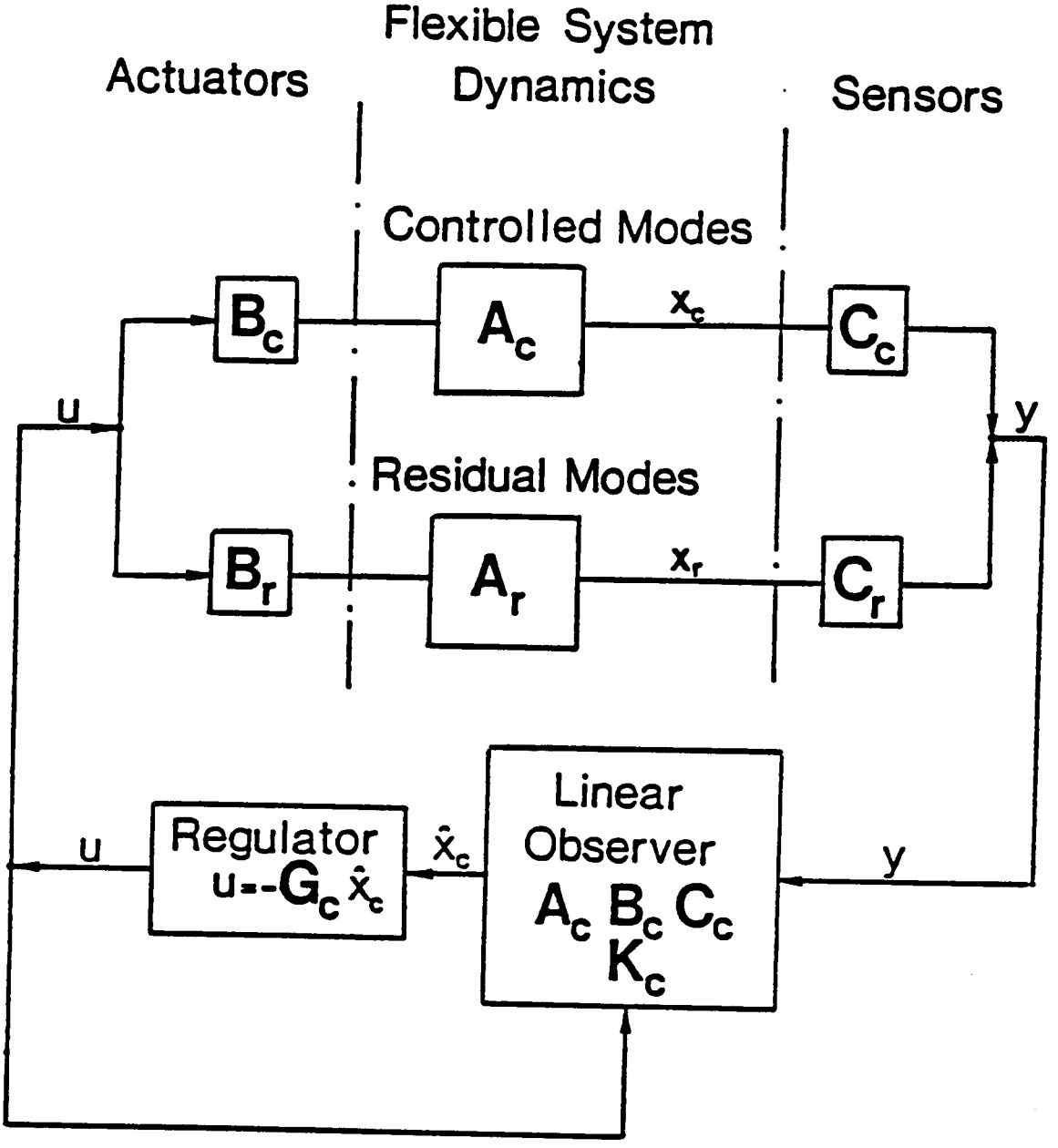

Figure 15. Spillover mechanism.

for this type of uncertainty (associated with the order of a lightly damped system). The design of the regulator must be subject to special frequency shaping in order to satisfy the robustness condition if it can be done at all.

This discussion then leads to an explanation of why the Linear Quadratic Gaussian with Loop Transfer Recovery (LQG/LTR) Method does not work well with large flexible space structures. This technique makes the controller *recover* the loop transfer matrix of the regulator assuming that the noise enters the plant at the input. But, it should be recalled that the LTR problem is a combined control and observation spillover problem, and, as such, can lead to spillover instability. In addition to this, the LQR margins that it is trying to recover are not designed for spillover considerations. They are enough to protect against some amount of regular perturbations, e.g., $\omega_i + \Delta\omega_i$ instead of ω_i, but they are not enough to protect against singular perturbations, e.g., neglected dynamics and truncated modes. As a result, the system regains some stability margins in the low frequency range at the expense of spillover robustness.

It is, therefore, desired that the designed controller have a faster high frequency decay rate than the $1/\omega$ rate of the LQR. This is done so as to facilitate the passing of the robustness stability test, since the model is completely false in the high frequency region.

3.3. MODEL ERROR SENSITIVITY SUPPRESSION (MESS) METHOD

The governing equations of the system are

$$\dot{x} = Ax + Bu + w_1 \qquad [3.3.1]$$

$$y = Cx + w_2 \qquad [3.3.2]$$

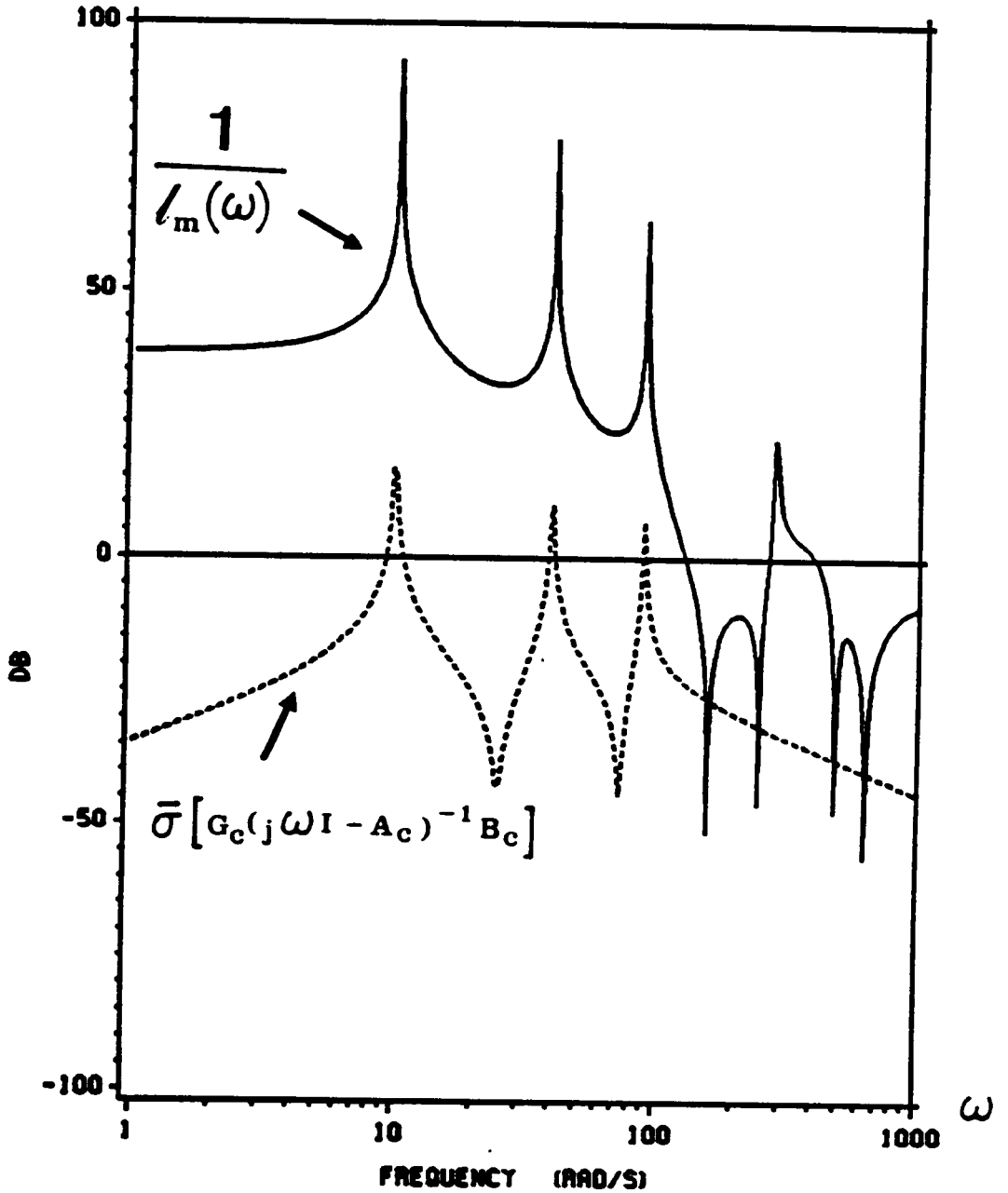

Figure 16. Typical robustness plot of the loop transfer matrix for the regulator. $\bar{\sigma}[G_c(j\omega I - A_c)^{-1}B_c]$

where w_1 and w_2 are noise matrices. In this system, there are two types of spillover which can occur: (1) control spillover and (2) observation spillover. A systematic technique has been developed to use the knowledge of known residual modes in designing a controller system. This technique is known as the Model Error Sensitivity Suppression (MESS) Method [23]. Its implementation will be shown for both control spillover and observation spillover alleviation.

3.3.1. Control Spillover

The governing system equations can be broken up into three parts:

$$\dot{x}_c = A_c x_c + B_c u \qquad [3.3.3]$$

$$\dot{x}_r = A_r x_r + B_r u \qquad [3.3.4]$$

$$\dot{x}_R = A_R x_R + B_R u \qquad [3.3.5]$$

where the subscripts represent: $c \equiv$ the controlled modes, $r \equiv$ the known residual (neglected) modes, and $R \equiv$ the unknown residual modes. Since nothing can be done about the unknown modes, one can only use the known residual modes with the controlled modes to aid in the design process.

In practice, regulators are designed to minimize the deterministic performance index defined by the controlled modes

$$J = \int_{t=0}^{\infty} (x_c^T Q_c x_c + u^T R u) dt \qquad [3.3.6]$$

One way of implementing the knowledge of the known residual modes is to construct a modified deterministic performance index for the modelled system as

$$J = \int_{t=0}^{\infty} (x_c^T Q_c x_c + x_r^T Q_r x_r + u^T R u) dt \qquad [3.3.7]$$

where

$$J_r = \int_{t=0}^{\infty} (x_r^T Q_r x_r) dt \qquad [3.3.8]$$

is the new term which penalizes the residual modes.

The objective behind including this term is to put a constraint on $B_r u$ in the system equations so as not to excite x_r. From singular perturbation theory, one can approximate x_r by simply setting $\dot{x}_r = 0$ in the governing equation and solving for x_r directly as:

$$x_r = -A_r^{-1} B_r u \qquad [3.3.9]$$

This singular perturbation relationship amounts to assuming that the residual modes respond purely statically. This expression for x_r can then be substituted into the expression for J_r producing

$$\begin{aligned} J_r &= \int_{t=0}^{\infty} u^T B_r^T (A_r^{-1})^T Q_r (A_r^{-1}) B_r u dt \\ &= \int_{t=0}^{\infty} u^T R_r u dt \end{aligned} \qquad [3.3.10]$$

where

$$R_r = B_r^T W_r B_r \qquad [3.3.11]$$

$$W_r = (A_r^{-1})^T Q_r (A_r^{-1}) \qquad [3.3.12]$$

where W_r is referred to as a control weighting matrix. Therefore, the overall deterministic performance index becomes

$$J = \int_{t=0}^{\infty} [x_c^T Q_c x_c + u^T (R + R_r) u] dt \qquad [3.3.13]$$

From a set of theorems in Reference [23], it can be shown that by minimizing J_r in J, x_r and $B_r u$ are constrained in such a way as to constrain the residual state control spillover and also the residual state response. This is, of course, only approximate because of the assumption embodied in Equation [3.3.9]. In practice, we only have a constraint on control spillover.

3.3.2. Observation Spillover

For the observer, a parallel type of methodology can be used. In Section [2.4.1.1], the observer problem was established as a dual control problem. The estimator dual problem can be expressed from Equation [2.4.16] as (for $\hat{v} = 0$)

$$\dot{z}_c = A_c^T z_c + C_c^T \hat{u} \qquad [3.3.14]$$

$$\dot{z}_r = A_r^T z_r + C_r^T \hat{u} \qquad [3.3.15]$$

$$\dot{z}_R = A_R^T z_R + C_R^T \hat{u} \qquad [3.3.16]$$

with the same subscript notation as for the control spillover problem. To parallel the previous method, the deterministic performance index can be written as:

$$J = \int_{t=0}^{\infty} (z_c^T V_{1_c} z_c + z_r^T V_{1_r} z_r + \hat{u}^T V_2 \hat{u}) dt \qquad [3.3.17]$$

As before, by setting $\dot{z}_r = 0$ in the governing equation and solving for z_r, the portion of the performance index relating to the residual modes can be rewritten as:

$$J_r = \int_{t=0}^{\infty} (z_r^T V_{1_r} z_r) dt$$
$$= \int_{t=0}^{\infty} (\hat{u}^T V_{2_r} \hat{u}) dt \qquad [3.3.18]$$

where

$$V_{2_r} = C_r A_r^{-1} V_{1_r} (A_r^{-1})^T C_r^T$$
$$= C_r W_{V_r} C_r^T \qquad [3.3.19]$$

The resulting deterministic performance index becomes

$$J = \int_{t=0}^{\infty} [z_c^T V_{1_c} z_c + \hat{u}^T (V_2 + V_{2_r}) \hat{u}] dt \qquad [3.3.20]$$

This amounts to assuming an increased noise intensity matrix in the sensor.

As before, it can be shown that this constrains the residual state observation spillover and also the residual state response. Since the Kalman-Bucy Filter design produces an observer blind to the measurement noise intensity matrix, by giving V_2 a ficititious contribution of the shape of the observation spillover, the resulting observer tends to be blind to the residual modes. As mentioned before, this is only approximate because of the assumption $\dot{z}_r = 0$. In practice, we only have a constraint on observation spillover.

It should be noted that MESS does not guarantee stability. It would if the singular perturbation assumptions were true. Also, MESS cannot be applied to SISO systems because the technique plays on the spatial space of the control and the observer.

CHAPTER 4. INFLUENCE OF THE PLANT NOISE INTENSITY MATRIX ON SPILLOVER

While V_1 represents the statistics of the plant noise, these are rarely known well. Therefore, it is an ideal candidate for tuning with the purpose of stabilizing spillover and improving robustness. To be effective, the choice of V_1 should have a significant effect on spillover and only a small effect on other properties of the system, i.e., performance. This section demonstrates these characteristics of V_1. Using a simply supported beam, it is shown that closed loop systems designed with different structures of V_1 have comparable performances in the controlled modes but are quite different vis-à-vis the spillover in the residual modes.

The beam (Figure 17) follows Balas' [1] configuration where the actuator is located at the 1/6 position and the displacement sensor is located at the 5/6 position. The state variables are the modal amplitudes and the reduced modal velocities. The first three modes are controlled by a Linear Quadratic Regulator (LQR) based on the reconstructed state obtained by the Kalman-Bucy Filter (KBF), while the fourth through eighth modes act as the known residual modes.

For this structure, the mass per unit length, $\overline{m}$, bending stiffness, EI, and length, L, are taken as unity. The natural frequencies and mode shapes (normalized to a unit modal mass) are:

$$\omega_k = (k\pi)^2 \qquad [4.1]$$

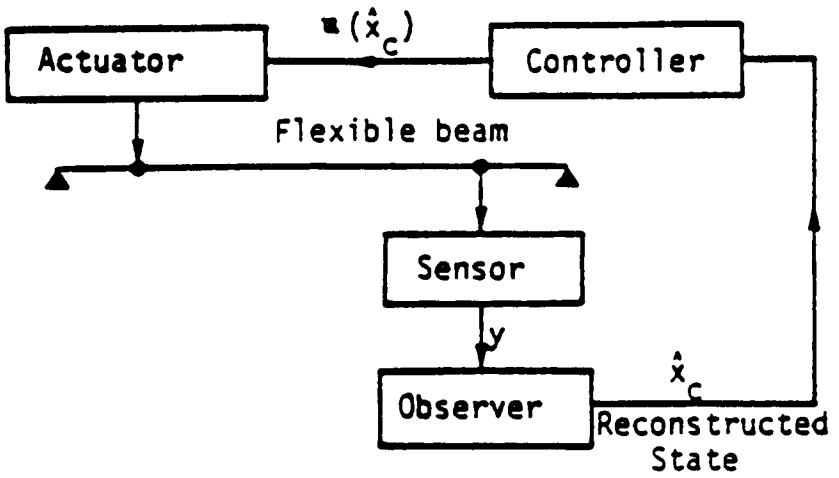

Figure 17. Balas beam example.

$$\phi_k(x) = \sqrt{2}\,\sin(k\pi x) \qquad [4.2]$$

The numerical values of the parameters involved in this problem are given in Tables 1 - 3 where no structural damping is assumed. The actuator and sensor locations in this problem produce a nonminimum phase system.

The LQR is the same as that of Balas [1]. Q_c was selected so that $x_c^T Q_c x_c$ represents the total energy (kinetic plus strain) in the controlled modes, i.e.,

$$Q_c = \frac{1}{2}\begin{bmatrix} \omega_1^2 & 0 & 0 & 0 & 0 & 0 \\ 0 & \omega_2^2 & 0 & 0 & 0 & 0 \\ 0 & 0 & \omega_3^2 & 0 & 0 & 0 \\ 0 & 0 & 0 & \omega_1^2 & 0 & 0 \\ 0 & 0 & 0 & 0 & \omega_2^2 & 0 \\ 0 & 0 & 0 & 0 & 0 & \omega_3^2 \end{bmatrix} \frac{\text{lb sec}^2}{in} \qquad [4.3]$$

R was set as $0.2\,\frac{\text{lb sec}^4}{in}$. The poles of the LQR are located in Table 4. As it turns out, for all the controller designs to be considered for the Balas beam, the regulator poles virtually do not move in the coupled system from their original design locations. As a result, they will not be tabulated further in any of the remaining tables.

To assess the effect of an observer on the performance of the system for different choices of V_1, V_2, and α, the quadratic performance index is calculated for unit initial amplitude and zero initial velocity in the first 3 modes.

$$x(0) = (1 \;\; 1 \;\; 1 \;\; 0 \;\; 0 \;\; 0)^T \qquad [4.4]$$

The optimum value of the performance index for the LQR alone (when the state is perfectly observed) is $J_{LQR} = 3139\,\frac{\text{lb sec}}{in}$.

Table 1. System matrices for the controlled and residual modes of the Balas beam.

$$A_c = \begin{bmatrix} 0 & 0 & 0 & 9.87 & 0 & 0 \\ 0 & 0 & 0 & 0 & 39.48 & 0 \\ 0 & 0 & 0 & 0 & 0 & 88.83 \\ -9.87 & 0 & 0 & 0 & 0 & 0 \\ 0 & -39.48 & 0 & 0 & 0 & 0 \\ 0 & 0 & -88.83 & 0 & 0 & 0 \end{bmatrix} \frac{1}{\text{sec}}$$

$$A_r = \begin{bmatrix} 0 & 0 & 0 & 0 & 0 & 157.91 & 0 & 0 & 0 & 0 \\ 0 & 0 & 0 & 0 & 0 & 0 & 246.74 & 0 & 0 & 0 \\ 0 & 0 & 0 & 0 & 0 & 0 & 0 & 355.31 & 0 & 0 \\ 0 & 0 & 0 & 0 & 0 & 0 & 0 & 0 & 483.61 & 0 \\ 0 & 0 & 0 & 0 & 0 & 0 & 0 & 0 & 0 & 631.65 \\ -157.91 & 0 & 0 & 0 & 0 & 0 & 0 & 0 & 0 & 0 \\ 0 & -246.74 & 0 & 0 & 0 & 0 & 0 & 0 & 0 & 0 \\ 0 & 0 & -355.31 & 0 & 0 & 0 & 0 & 0 & 0 & 0 \\ 0 & 0 & 0 & -483.61 & 0 & 0 & 0 & 0 & 0 & 0 \\ 0 & 0 & 0 & 0 & -631.65 & 0 & 0 & 0 & 0 & 0 \end{bmatrix} \frac{1}{\text{sec}}$$

Table 2. Control matrices for the controlled and residual modes of the Balas beam.

$$B_c = \begin{bmatrix} 0 \\ 0 \\ 0 \\ 0.07164 \\ 0.03102 \\ 0.01592 \end{bmatrix} \text{ sec}$$

$$B_r = \begin{bmatrix} 0 \\ 0 \\ 0 \\ 0 \\ 0 \\ 0.007756 \\ 0.002866 \\ 0 \\ -0.001462 \\ -0.001939 \end{bmatrix} \text{ sec}$$

Table 3. Output matrices for the controlled and residual modes of the Balas beam.

$$C_c = [0.7071 \quad -1.2247 \quad 1.4142 \quad 0 \quad 0 \quad 0]$$

$$C_r = [-1.2247 \quad 0.7071 \quad 0 \quad -0.7071 \quad 1.2247 \quad 0 \quad 0 \quad 0 \quad 0 \quad 0]$$

Table 4. Regulator poles for the Balas beam.

(System eigenvalues in 1/sec.)

Regulator poles	$-0.788 \pm j\,9.87$ $-1.368 \pm j\,39.48$ $-1.580 \pm j\,88.83$

4.1. SPILLOVER PROPERTIES

Next, several observers are considered. Special attention is placed on their effect on the performance index and the spillover of the fourth mode. Table 5 gives the pole locations of the Luenberger observer used by Balas [1], as well as the location of the residual mode poles as shifted by spillover. It is slightly unstable. Tables 6 and 7 give the corresponding poles for different steady-state KBF observers obtained with various choices of the noise intensity matrices V_1 and V_2. Also given in the tables are the ratios J/J_{LQR}, where J denotes the deterministic value of the performance index for the above initial conditions, including the cost increment incurred as a result of the estimation error. (All the results were obtained with the L-A-S computer program [86, 87].)

It can be observed from Table 6 that:

(a) For $V_1 = Q$, $\alpha = 0$ (the same as in the LQR design):

- reducing V_2 below 10^{-1} does not move four of the six poles of the observer. (This behavior is linked with the asymptotic properties associated with the closed-loop observer poles mentioned in Section 2.5.);

- the observer introduces only a slight degradation in performance, and the ratio J/J_{LQR} is not very sensitive to V_2;

- for small values of V_2, there is more spillover present than in the Luenberger design case. The amount of spillover depends strongly on V_2.

(b) For $V_1 = I$ (Identity matrix), $\alpha = 0$:

- the residual mode is stable (the spillover shifts the residual modes into the left half-plane);

Table 5. The Luenberger observer of Balas.

(System eigenvalues in 1/sec.)

Observer poles	-175.39 -20.92 $-24.40 \pm j\,50.87$ $-7.3 \pm j\,9.34$
Residual poles (4*th*)	$0.177 \pm j\,157.49$

Table 6. KBF poles of the Balas beam.

(System eigenvalues in 1/sec.)

(a) $V_1 = Q$, $\alpha = 0$ (same as in the LQR).

	$V_2 = 10^{-3}$	$V_2 = 10^{-1}$	$V_2 = 1$	$V_2 = 10$
Observer	$-2.49 \pm j9.93$ $-16.65 \pm j44.46$ -75.33 -3010.5	$-2.43 \pm j9.93$ $-16.47 \pm j44.06$ -91.99 -258.5	$-2.03 \pm j9.90$ $-14.33 \pm j41.62$ $-59.62 \pm j83.3$	$-1.01 \pm j9.87$ $-7.01 \pm j39.6$ $-19.56 \pm j88.7$
Residual	$0.561 \pm j157.42$	$0.363 \pm j157.34$	$0.056 \pm j157.48$	$-0.021 \pm j157.78$
J/J_{LQR}	1.066	1.067	1.08	1.10

(b) $V_1 = I$, $\alpha = 0$.

	$V_2 = 10^{-3}$	$V_2 = 10^{-2}$	$V_2 = 10^{-1}$
Observer	$-10.16 \pm j9.76$ $-22.54 \pm j38.9$ $-27.77 \pm j85.56$	$-4.58 \pm j9.86$ $-8.30 \pm j39.45$ $-9.8 \pm j88.76$	$-1.56 \pm j9.87$ $-2.73 \pm j39.48$ $-3.15 \pm j88.83$
Residual	$-0.052 \pm j157.7$	$-0.019 \pm j157.8$	$-0.003 \pm j157.9$
J/J_{LQR}	1.08	1.11	1.26

(c) $V_1 = I$, $\alpha = 2$.

	$V_2 = 10^{-2}$	$V_2 = 10^{-1}$	$V_2 = 1$	$V_2 = 10$
Observer	$-7.01 \pm j9.86$ $-10.54 \pm j39.45$ $-12.00 \pm j88.76$	$-4.54 \pm j9.87$ $-5.38 \pm j39.48$ $-5.74 \pm j88.83$	$-4.06 \pm j9.87$ $-4.18 \pm j39.48$ $-4.23 \pm j88.8$	$-4.01 \pm j9.87$ $-4.02 \pm j39.48$ $-4.02 \pm j88.83$
Residual	$-0.028 \pm j157.8$	$-0.0087 \pm j157.9$	$-0.0055 \pm j157.9$	$-0.0051 \pm j157.9$
J/J_{LQR}	1.10	1.15	1.19	1.20

(d) $V_1 = B_c B_c^T$ (Loop Transfer Recovery), $\alpha = 0$.

	$V_2 = 10^{-7}$	$V_2 = 10^{-6}$	$V_2 = 10^{-5}$	$V_2 = 10^{-4}$
Observer	$-23.24 \pm j11.42$ $-28.20 \pm j40.28$ $-24.83 \pm j98.72$	$-14.54 \pm j11.41$ $-14.69 \pm j41.01$ $-10.30 \pm j90.93$	$-6.90 \pm j10.58$ $-5.73 \pm j39.9$ $-3.52 \pm j89.09$	$-2.48 \pm j9.99$ $-1.89 \pm j39.53$ $-1.12 \pm j88.86$
Residual	$-0.151 \pm j157.71$	$-0.043 \pm j157.84$	$-0.0067 \pm j157.9$	$-0.00096 \pm j157.9$
J/J_{LQR}	1.077	1.103	1.216	1.632

Table 7. KBF poles of the Balas beam.

(System eigenvalues in 1/sec.)

(a) $V_2 = 10^{-7}$, $\alpha = 0$.

	$V_1 = B_c B_c^T$	$V_1 = I$	$V_1 = Q$
Observer	$-23.24 \pm j11.42$ $-28.20 \pm j40.28$ $-24.83 \pm j98.72$	$-16.77 \pm j11.64$ $-28.34 \pm j63.01$ -24.01 -6323.5	$-2.49 \pm j9.93$ $-16.65 \pm j44.46$ -75.20 $-301400.$
Residual	$-0.151 \pm j157.71$	$0.329 \pm j157.48$	$0.581 \pm j157.43$
J/J_{LQR}	1.077	1.064	1.066

(b) $V_2 = 10^{-3}$, $\alpha = 0$.

	$V_1 = B_c B_c^T$	$V_1 = I$	$V_1 = Q$
Observer	$-0.80 \pm j9.88$ $-0.60 \pm j39.49$ $-0.36 \pm j88.83$	$-10.16 \pm j9.76$ $-22.54 \pm j38.90$ $-27.77 \pm j85.56$	$-2.49 \pm j9.93$ $-16.65 \pm j44.46$ -75.33 -3010.5
Residual	$-0.000161 \pm j157.91$	$-0.052 \pm j157.7$	$0.561 \pm j157.42$
J/J_{LQR}	2.98	1.08	1.066

(c) $V_2 = 10^{-1}$, $\alpha = 0$.

	$V_1 = B_c B_c^T$	$V_1 = I$	$V_1 = Q$
Observer	$-0.08 \pm j9.87$ $-0.06 \pm j39.48$ $-0.04 \pm j88.83$	$-1.56 \pm j9.87$ $-2.73 \pm j39.48$ $-3.15 \pm j88.83$	$-2.43 \pm j9.93$ $-16.47 \pm j44.06$ -91.99 -258.5
Residual	$-0.00001 \pm j157.91$	$-0.003 \pm j157.9$	$0.363 \pm j157.34$
J/J_{LQR}	20.82	1.26	1.067

(d) $V_2 = 10^{-1}$, $\alpha = 2$.

	$V_1 = B_c B_c^T$	$V_1 = I$	$V_1 = Q$
Observer	$-4.00 \pm j9.87$ $-4.00 \pm j39.48$ $-4.00 \pm j88.83$	$-4.54 \pm j9.87$ $-5.38 \pm j39.48$ $-5.74 \pm j88.83$	$-5.15 \pm j9.93$ $-18.61 \pm j44.04$ -94.02 -260.48
Residual	$-0.005 \pm j157.89$	$-0.009 \pm j157.9$	$0.374 \pm j157.31$
J/J_{LQR}	1.20	1.15	1.06

(e) $V_2 = 10$, $\alpha = 2$.

	$V_1 = B_c B_c^T$	$V_1 = I$	$V_1 = Q$
Observer	$-4.00 \pm j9.87$ $-4.00 \pm j39.48$ $-4.00 \pm j88.83$	$-4.01 \pm j9.87$ $-4.02 \pm j39.48$ $-4.02 \pm j88.83$	$-4.24 \pm j9.87$ $-9.30 \pm j39.60$ $-21.66 \pm j88.66$
Residual	$-0.005 \pm j157.89$	$-0.005 \pm j157.9$	$-0.034 \pm j157.74$
J/J_{LQR}	1.20	1.20	1.085

- when the stability margin becomes small as compared to that of the LQR, there is a degradation in performance.

(c) For $V_1 = I$, $\alpha = 2$:

- the residual mode is stable;

- for large values of V_2, the observer poles line up on a vertical line corresponding to a real part of -2α. When this situation occurs, the pole locations become independent of the structure of V_2. (The stability margin of -2α rather than $-\alpha$ is associated with the structural damping of the system. A non-rigorous proof is presented in Appendix A.)

(d) For $V_1 = B_c B_c^T$ (Loop Transfer Recovery Form - Noise entering the plant at the input), $\alpha = 0$:

- same observations as in (b);

- The asymptotic behavior of the observer poles is readily obtainable and is presented in Figure 18.

It can be observed from Table 7 that:

(a) For $V_2 = 10^{-7}$, $\alpha = 0$:

- $V_1 = I$ and $V_1 = Q$ produce an unstable residual mode and extremely fast observer speeds. $V_1 = Q$ has much faster observer speeds than does $V_1 = I$.

- $V_1 = B_c B_c^T$ has much slower observer poles in comparison to I and Q and produces a stable *4th* residual mode.

- performance degradations are comparable, though $V_1 = B_c B_c^T$ experiences somewhat more performance deterioration than $V_1 = I$ or Q.

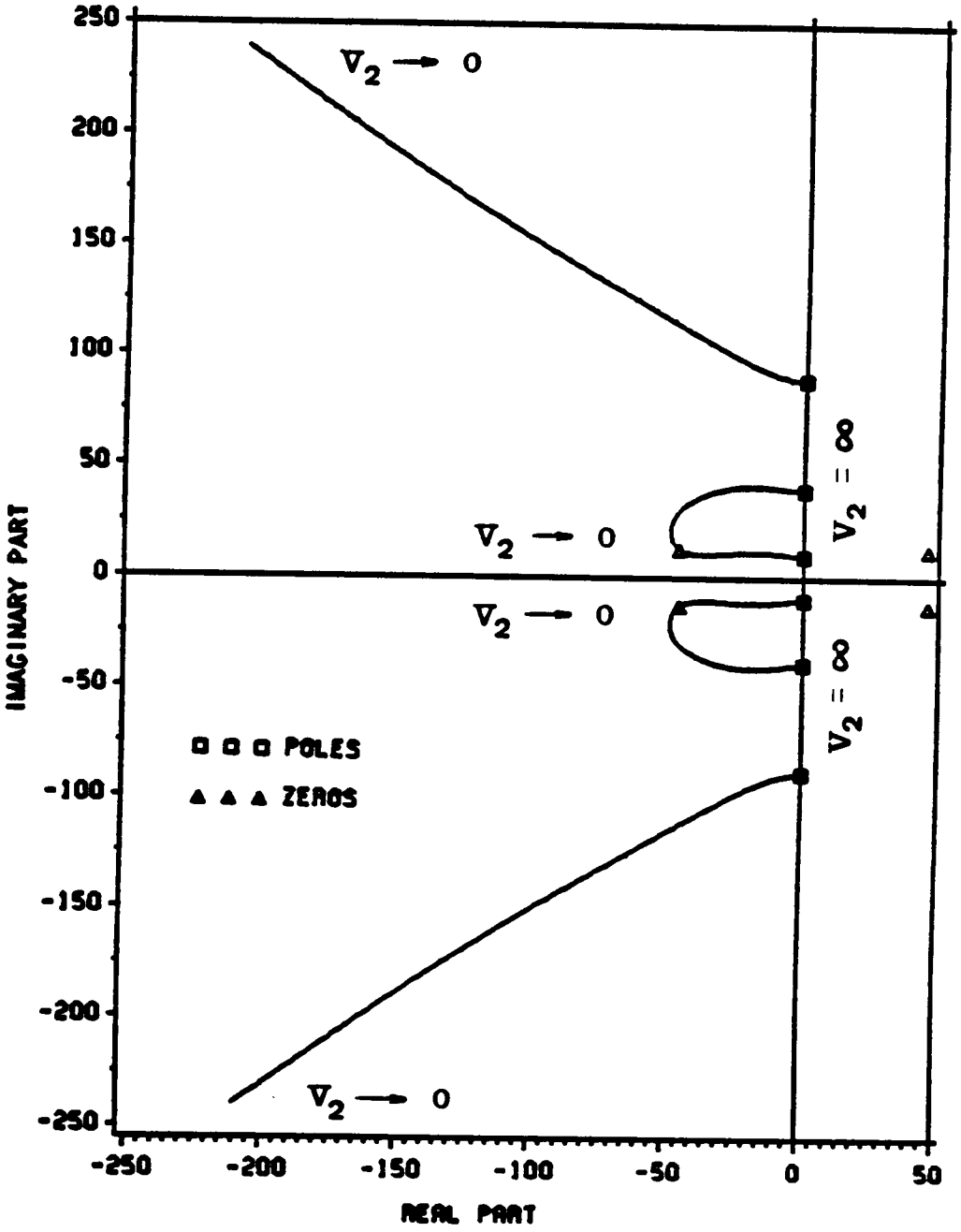

Figure 18. Asymptotic behavior of the KBF poles for the Balas beam. $[V_1 = B_c B_c^T.]$

(b) For $V_2 = 10^{-3}$, $\alpha = 0$:

- $V_1 = Q$ produces an unstable residual mode and extremely fast observer speeds.
- $V_1 = B_c B_c^T$ and I produce a stable residual mode with $V_1 = I$ having a much larger stability margin.
- four of the observer poles of $V_1 = B_c B_c^T$ lie to the right of the regulator poles, and the remaining two poles are located within the region of the regulator poles.
- $V_1 = B_c B_c^T$ experiences large deteriorations in performance.

(c) For $V_2 = 10^{-1}$, $\alpha = 0$:

- $V_1 = Q$ produces an unstable residual mode and very fast observer speeds.
- $V_1 = B_c B_c^T$ and I produce a stable residual mode with $V_1 = I$ having a somewhat larger stability margin.
- all of the observer poles for $V_1 = B_c B_c^T$ lie to the right of the regulator poles, and two of the observer poles for $V_1 = I$ lie within the speed region of the regulator poles.
- $V_1 = I$ experiences a noticeable performance degradation, while $V_1 = B_c B_c^T$ experiences enormous deterioration in performance.

(d) For $V_2 = 10^{-1}$, $\alpha = 2$:

- $V_1 = Q$ produces an unstable residual mode and very fast observer speeds.
- $V_1 = B_c B_c^T$ and I produce a stable residual mode with $V_1 = I$ having a slightly larger stability margin.

- all the observer poles of $V_1 = B_c B_c^T$ line up on a vertical line corresponding to a real part of -2α. The observer poles of $V_1 = I$ are somewhat to the left of this line.

- $V_1 = B_c B_c^T$ experiences the most performance degradation followed by $V_1 = I$. $V_1 = Q$ experiences a small amount of performance deterioration.

(e) For $V_2 = 10$, $\alpha = 2$:

- all V_1 designs produce a stable residual mode with $V_1 = Q$ producing the largest stability margin.

- the response of $V_1 = B_c B_c^T$ and I are practically identical in terms of observer speeds, stability margins, and performance degradation. All the observer poles line up on a vertical line corresponding to a real part of -2α. When this situation occurs, the pole locations become independent of the structure of V_1.

- $V_1 = Q$ produces the lowest deterioration in performance.

The foregoing results have also been illustrated in Figures 19 and 20. The notation is as follows. α_{RES} is the stability margin of the residual modes ($4th$ mode) and is defined as positive if the system is stable. α_{OBS} is the stability margin of the Kalman-Bucy Filter observer, and α_{LQR} is the stability margin of the Linear Quadratic Regulator. The ratio $\alpha_{OBS}/\alpha_{LQR}$ represents a type of relative stability margin of the observer (or relative observer speed). Therefore, the figures show, for given structures of V_1, as V_2 is allowed to vary, a measure of the degradation in performance due to the observer, J/J_{LQR}, and the stability margin of the residual mode, α_{RES}, as a function of the relative stability margin of the observer and the regulator, $\alpha_{OBS}/\alpha_{LQR}$.

In conclusion, the following statements can be made:

(1) The degradation in performance due to the observer, as reflected by the (deterministic) performance index for non-zero initial conditions, is not very sensitive to V_1, nor to the location of the poles in the complex plane, provided the observer is fast enough.

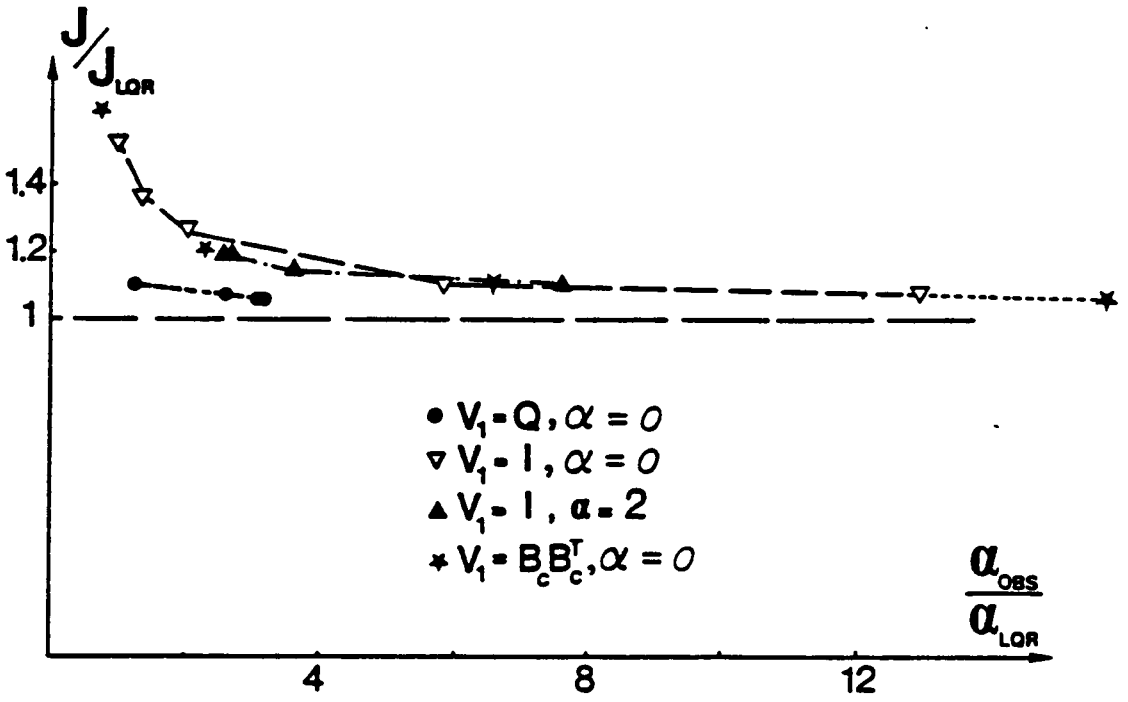

Figure 19. Relative performance of the closed-loop system as a function of the relative stability margin of the observer for the Balas beam.

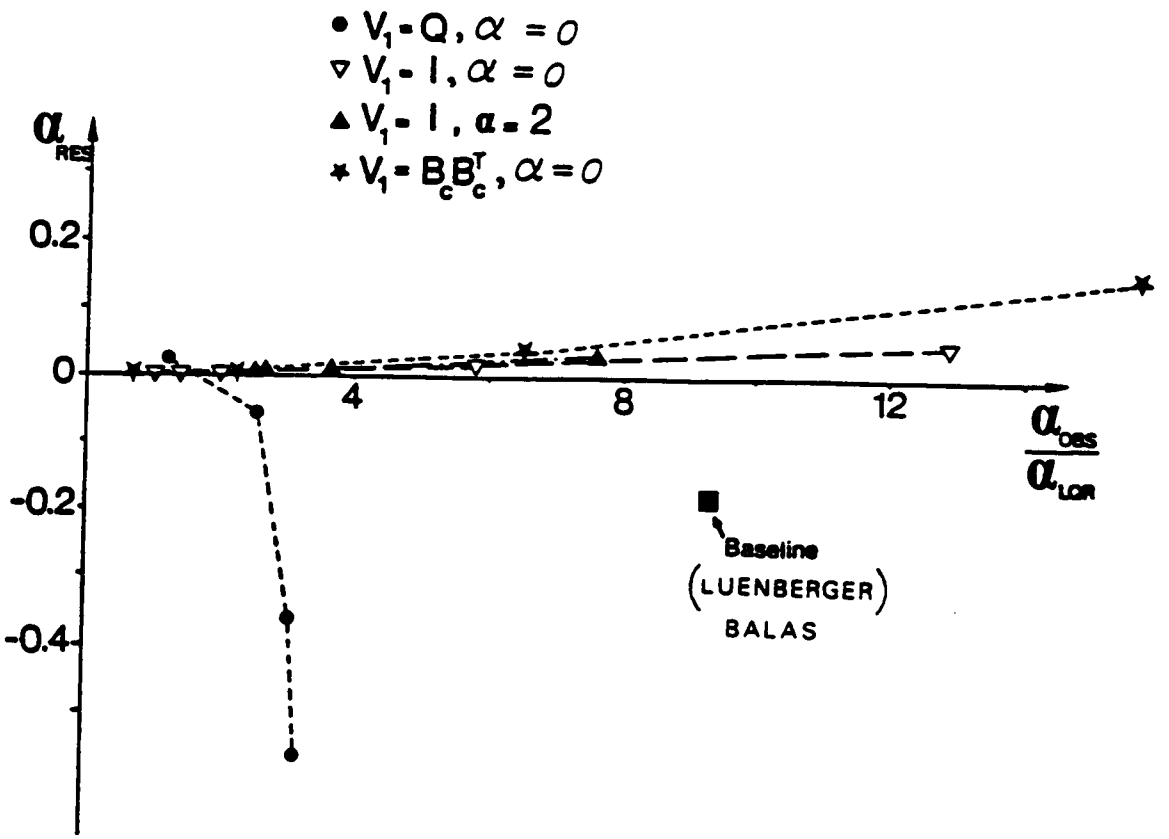

Figure 20. Stability margin of the residual mode as a function of the relative stability margin of the observer for the Balas beam.

(2) The spillover instability is strongly dependent on the structure of V_1. By changing V_1, one can make the spillover increase the stability margin of the residual modes, rather than decrease it.

(3) The parameter α can constrain the poles of the observer to have a stability margin within specified limits.

These results suggest that the structure of V_1 can be optimized, to maximize the stability margin of the residual modes. This topic is investigated in the next chapter.

4.2. STABILITY ROBUSTNESS TESTS

Stability robustness tests may provide some insight as to which residual modes are potentially critical from the point of view of spillover. In this section, the Bode plots of the loop transfer function of the various controllers considered in the previous section are analyzed. Their merits are compared on the basis of a stability robustness test based on singular values [19, 60, 64].

In Section 2.10.6, it was shown that the stability robustness of the control system is guaranteed if the maximum singular value of the loop transfer matrix satisfies the inequality

$$\bar{\sigma}[G(j\omega)K(j\omega)] < 1/l_m(\omega) \qquad [4.2.1]$$

in the frequency range where $l_m(\omega) >> 1$. l_m is an upper bound on the maximum singular value of the multiplicative uncertainty at the plant output. $G(j\omega)$ is the transfer function of the plant model of the open-loop system, and $K(j\omega)$ is the transfer function of the compensator. This is a sufficient but not a necessary condition for stability since the test does not take into account the structure of the uncertainty, i.e., phase angles. It is based on a worst case which is not necessarily allowed by the structure of the system. As a result, if the robustness test is violated, it does not mean that the system is going to be unstable but rather that it may become unstable.

A typical robustness plot for the kind of uncertainty we are interested in, i.e., the high frequency dynamics, was shown in Figure 14; the uncertainty curve, and particularly the negative

peaks, depend on the damping ratio of the neglected modes. Due to the relatively slow decay rate of $\bar{\sigma}[G(j\omega)K(j\omega)]$ outside the bandwidth of the controller and the low damping ratio, the robustness test cannot, in general, be satisfied by the uncontrolled modes directly outside the bandwidth of the controller unless there is a gap in the natural frequencies of the structure. The modes which are in the transition region (residuals) are candidates for destabilization and must be considered carefully. It should be mentioned that some damping must be assumed here or otherwise the transfer function of the plant model of the open-loop system, $G(j\omega)$, becomes infinite at the natural frequencies of the structure.

Figures 21 and 22 contain the robustness plots for a variety of controllers. For notational purposes, $V_1 = I$ corresponds to the case $V_1 = I$, $V_2 = 10$, and $\alpha = 2$ (see Table 6 (c)); $V_1 = B_c B_c^T$ corresponds to the case $V_1 = B_c B_c^T$, $V_2 = 10^{-7}$, and $\alpha = 0$ (see Table 6 (d)); $V_1 = Q(u)$ corresponds to the case $V_1 = Q$, $V_2 = 0.001$, and $\alpha = 0$ (see Table 6 (a)); and $V_1 = Q(s)$ corresponds to the case $V_1 = Q$, $V_2 = 10$, and $\alpha = 2$ (see Table 7 (e)). For all damping factors to be considered except $\zeta = 0.005$, $Q(s)$ produces a stable residual ($4th$) pole, whereas, $Q(u)$ produces an unstable residual ($4th$) pole for the same V_1 design. For $\zeta = 0.005$, both designs were stable. All the other controllers had a stable residual ($4th$) mode. The uncertainty plots consider the first eight modes of the Balas beam. All the plots are drawn for an assumed modal damping of $\zeta = 0.005$ in all the modes. Since the damping ratio affects significantly only the peaks, the peak values for $\zeta = 0.0025$ and 0.001 are indicated.

It should be noted that with this actuator and sensor location, the controlled system is controllable and observable. The composite system (controlled + residual) system, on the other hand, is controllable but not observable. The sixth mode is not observable, so no negative peak occurs at the frequency of the sixth mode.

Figure 21 shows the loop transfer function of the regulator alone for the three different damping ratios. As can be seen, the regulator fails the robustness test for all three damping ratios. The case $\zeta = 0.001$ produces the worst violation due to the large negative peaks in the high frequency range, whereas, the case $\zeta = 0.005$ produces the smallest amount of violation in the high

frequency range. This violation occurred even though the regulator has guaranteed stability margins and control spillover alone where destabilization cannot occur as was discussed in Section 3.2.

Figure 22 shows the loop transfer function of all four regulator/observer combinations considered for the three different damping ratios. As can be seen, in the high frequency region, the cases $V_1 = B_c B_c^T$ and $Q(s)$ as practically identical. For $\zeta = 0.001$, $V_1 = B_c B_c^T$ and $Q(s)$ just barely violate the robustness stability criterion by the fourth mode even though this mode was found to be stable with this controller design. This reinforces the concept that a robustness test violation does not mean that the system is going to be unstable but rather that it may become unstable. $V_1 = Q(u)$ produces the worst and most noticeable violation, and this controller produced an unstable residual ($4th$) mode, so this violation is expected. $V_1 = I$ satisfies the robustness stability test completely. $V_1 = I$ produces the largest roll-off in the high frequency range. For $\zeta = 0.0025$, the cases $V_1 = I$, $B_c B_c^T$, and $Q(s)$ all satisfy the robustness stability criterion, whereas, $V_1 = Q(u)$ violates it but not by such a degree as for the $\zeta = 0.001$ case. Finally, for $\zeta = 0.005$, all four LQG designs satisfy the robustness test.

It should be realized that the Balas beam is a simple example where the modes are well separated. This will not be the same in large space structures.

The following statements can now be made:

(1) At high frequency, the loop transfer function of the LQR decays very slowly (like $1/\omega$) which makes the regulator fail the test. From this observation, the LTR technique, which tries to *recover* the loop transfer matrix of the regulator, does not seem to be a good one for the kind of uncertainty associated with the neglected dynamics of lightly damped structures.

(2) At high frequency, the decay rate in the transition region for the loop transfer function of the LQG (LQR/KBF) appears to be strongly dependent on V_1; the unstable solution corresponding to $V_1 = Q(u)$ is also the one which has the slowest high frequency decay rate. (Recall that only the relative magnitudes of V_1 and V_2 are important and not their absolute magnitudes. V_1 and V_2 will produce a resulting K_c observer gain matrix which defines the speed of the observer. Whenever various observer designs produce the same K_c gain matrix, the corresponding robustness plots will also be the same.)

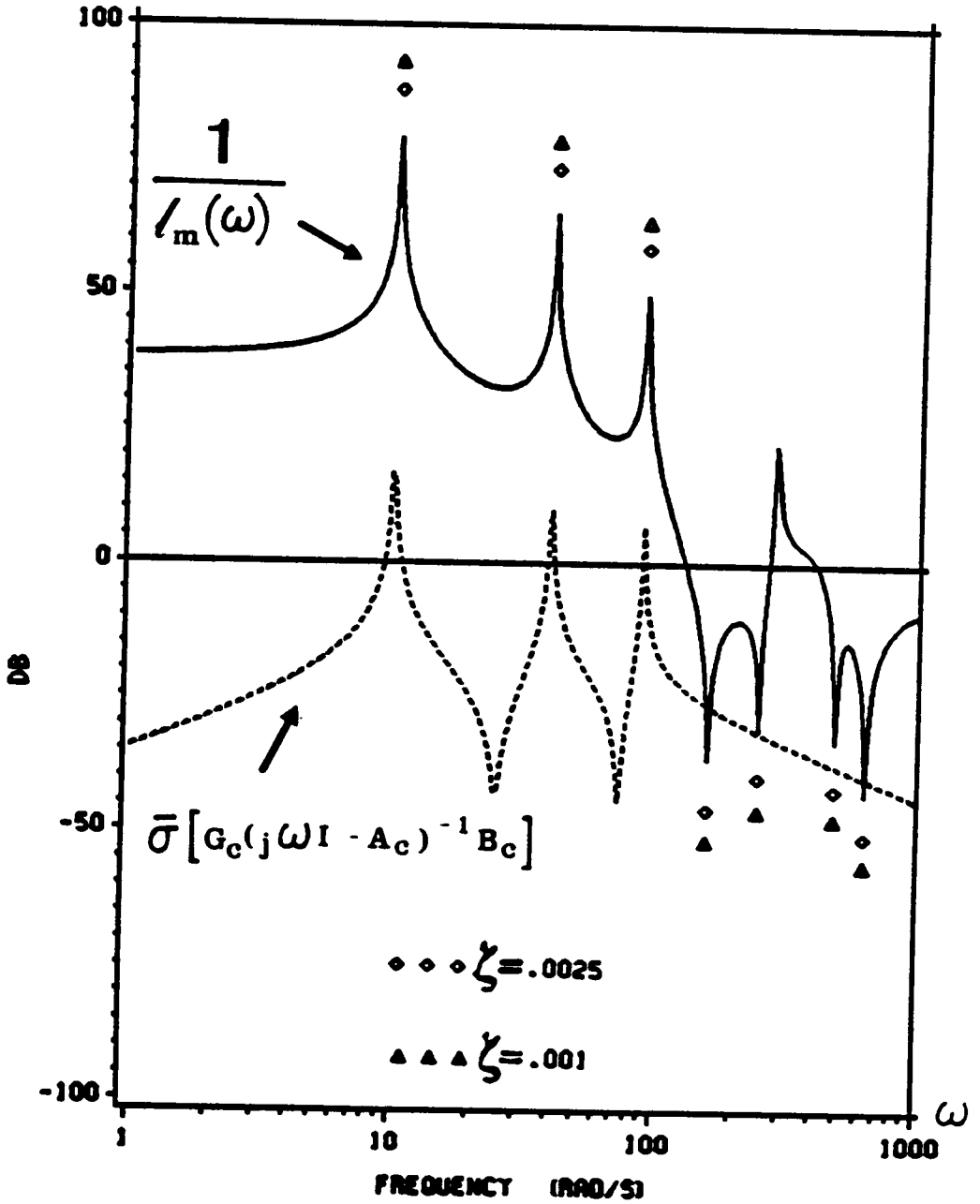

Figure 21. **Robustness plot of the loop transfer matrix for the regulator of the Balas beam.** $\bar{\sigma}[G_c(j\omega I - A_c)^{-1}B_c]$, $[\zeta = 0.005.]$

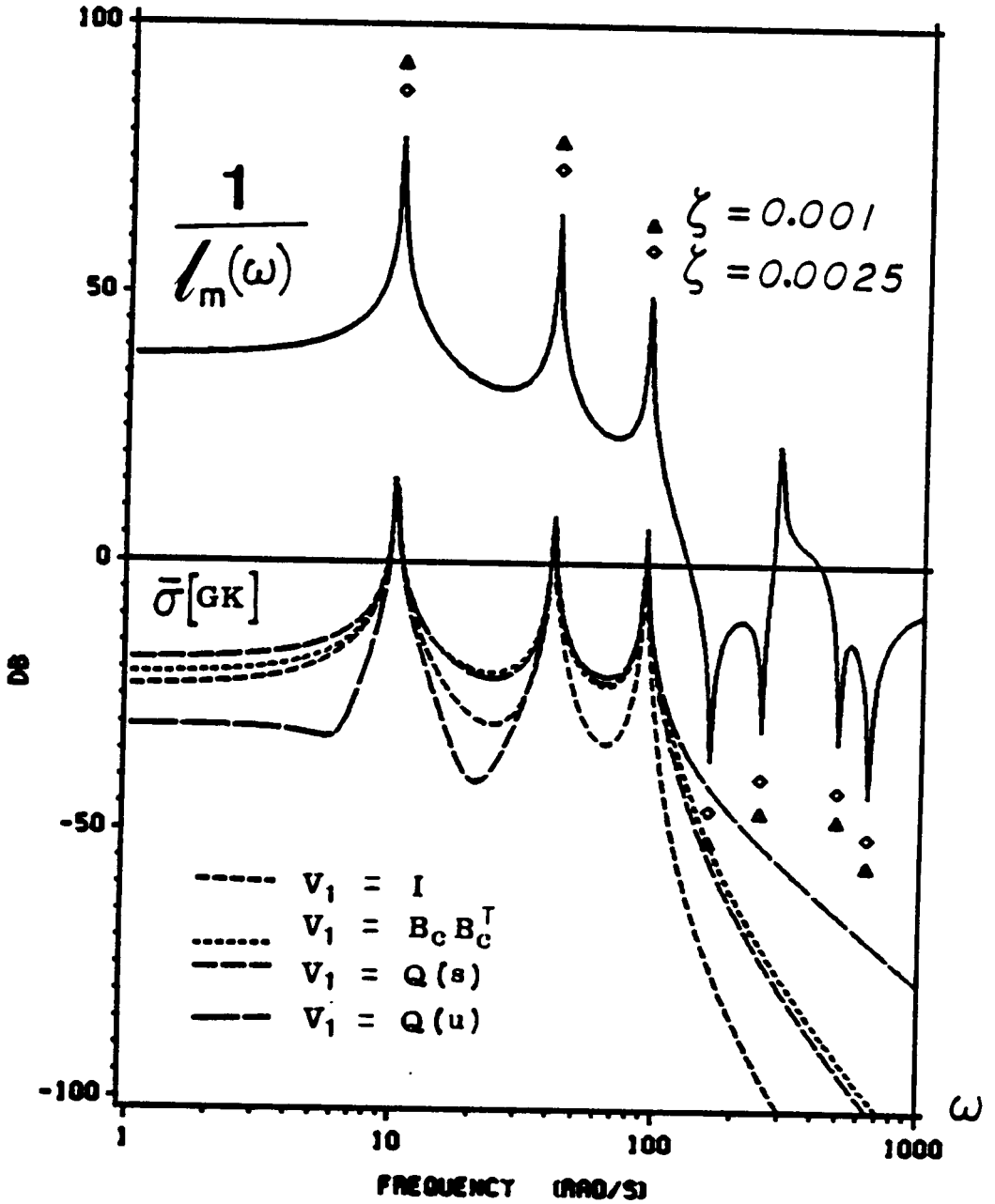

Figure 22. Robustness plot of the loop transfer matrix for selected LQG Balas beam designs. [$\zeta = 0.005$.]

(3) At high frequency, the decay rate in the transition region of the loop transfer function of the LQG (LQR/KBF) appears to be strongly related to the observer speeds; $V_1 = I$ produced the slowest observer and the largest roll-off in the high frequency range, whereas, $V_1 = Q(u)$ produced the fastest observer and the smallest roll-off in the high frequency range. This suggests that fast observers are dangerous for robustness.

(4) The fourth mode violates the robustness test for several of the LQG designs. It, thus, becomes a critical mode and must be checked explicitly. The robustness of modes five and above can be concluded from these curves and, thus, will not need to be considered further.

(5) The damping ratio of the residual modes is an essential design parameter which controls the high frequency robustness of the control system. (If the damping is increased from 0.001 to 0.005, the robustness test is satisfied for each of the LQG designs.)

These results suggest that the structure of V_1 can be optimized to produce an observer to maximize the stability margin explicitly of the fourth residual mode. This topic is investigated in the next chapter.

CHAPTER 5. OPTIMIZING THE PLANT NOISE INTENSITY MATRIX

An optimization procedure has been developed to maximize the stability margin of the residual modes by changing V_1. We take the point of view, similar to MESS and LQG/LTR, that the noise statistics are free parameters that can be adjusted to obtain desired system properties. The regulator is assumed to be known as well as the measurement noise intensity matrix, V_2, via MESS. The elements of V_1, the plant noise intensity matrix, are the design variables.

The objective function is defined as

$$\min \; f = \sum_{i=1}^{\bar{n}} [Re(\lambda_i) - t_i]_{(+)}^2 \qquad [5.1]$$

where $[a]_{(+)} = \max(a,0)$, therefore, terms in the summation contribute only when $Re(\lambda_i) > t_i$. The summation is taken over all the eigenvalues, λ_i, of the closed-loop system (see Figure 23).

Since the observer and the regulator poles have large stability margins, t_i is selected to be to the right of the controller poles so they do not contribute to the objective function, but also far enough to the left of the imaginary axis so as to place a penalty on the residual modes. This drives

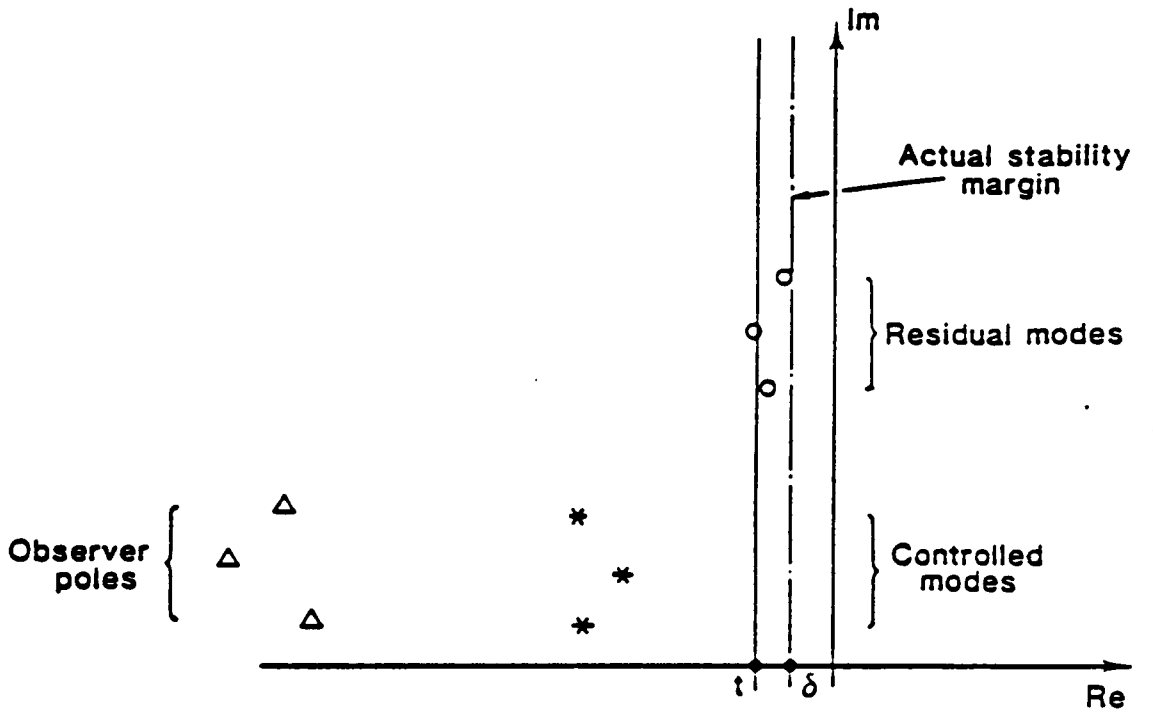

Figure 23. Location of closed-loop poles (only the upper part of the complex plane is shown).

the residual modes, and only them, as far left in the complex plane as possible. This procedure is demonstrated for the Balas beam example.

For this analysis, the fourth mode will be the only residual mode considered since it was the only mode found to be critical in the stability robustness test analysis. As a result, matrices A_r, B_r, and C_r will be reduced in size to reflect the contribution of only this one mode (see Table 8).

The design variables were selected to specify the matrix V_1. Three different forms of V_1 were selected which insure that V_1 is symmetric and positive semidefinite. They include:

$$V_1 = diag(v_i^2), \quad i = 1, \ldots, 6$$

$$V_1 = aa^T \qquad (a = 6 \times 1 \text{ vector})$$

$$V_1 = HH^T \qquad (H = 6 \times 6 \text{ matrix})$$

As a first step, no additional constraints were placed on the optimization problem. The procedure was implemented on a general purpose optimization program, NEWSUMT-A [88, 89]. The results are given in Table 9 (a). It can be seen, that excellent stability margins were obtained for the residual modes, but that the designed observers are more than 10 times faster than the regulator poles (Table 4).

To rectify this problem, an additional constraint was added to the optimization procedure of Equation [5.1] of the form

$$Re(\lambda_i) + \lambda_{max} \geq 0 \qquad [5.2]$$

where λ_{max} was selected to be 16/sec.

The results of this analysis are found in Table 9 (b). The optimum values of the design parameters for the three different structures of V_1 as generated by NEWSUMT-A are found in Tables 10 and 11.

It is interesting to note that the $V_1 = aa^T$ design is much more effective than the $V_1 = diag(v_i^2)$ design, even though both have six design variables. The HH^T design with 36 design variables is

Table 8. System, control, and output matrices for the residual modes of the Balas beam.

$$A_r = \begin{bmatrix} 0 & 157.91 \\ -157.91 & 0 \end{bmatrix} \frac{1}{\text{sec}}$$

$$B_r = \begin{bmatrix} 0 \\ 0.007756 \end{bmatrix} \text{ sec}$$

$$C_r = [\,-1.2247 \quad 0\,]$$

Table 9. Optimization results for the Balas beam example.

(System eigenvalues in 1/sec.)

(a) Unconstrained ($\lambda_{max} = \infty$)

	$V_1 = diag(v_i^2)$	$V_1 = aa^T$	$V_1 = HH^T$
Observer	-42.45 -2881.4 $-5.43 \pm j11.96$ $-5.82 \pm j88.38$	-7.86 -16.67 -68.13 -167.29 $-30.07 \pm j139.63$	-5.50 -15.82 -56.09 -216.73 $-26.65 \pm j143.78$
Residual	$-0.204 \pm j158.11$	$-4.013 \pm j158.17$	$-5.423 \pm j157.74$
J/J_{LQR}	1.253	1.195	1.224

(b) Constrained ($\lambda_{max} = 16$)

	$V_1 = diag(v_i^2)$	$V_1 = aa^T$	$V_1 = HH^T$
Observer	$-8.73 \pm j8.41$ $-15.20 \pm j37.12$ $-15.97 \pm j88.60$	$-16.05 \pm j20.46$ $-5.63 \pm j35.10$ $-11.12 \pm j91.15$	$-9.66 \pm j4.85$ $-16.05 \pm j35.55$ $-14.89 \pm j93.41$
Residual	$-0.048 \pm j157.79$	$-0.101 \pm j157.79$	$-0.102 \pm j157.78$
J/J_{LQR}	1.087	1.112	1.089

Table 10. Design parameters for the plant noise intensity matrix - Unconstrained problem, Balas beam.

$(V_2 = 0.02.)$

V_1	*Design*
$diag(v_i^2)$	$V_1 = diag(9.241\ 110800.\ 1.029\ 51290.\ 122400.\ 2720.)$
aa^T	$a^T = (49.55\ 91.04\ 41.88\ 89.09\ 106.6\ 32.54)$
HH^T	$H = \begin{bmatrix} 25.25 & 25.25 & 25.25 & 25.25 & 25.25 & 25.25 \\ 48.93 & 48.93 & 48.93 & 48.93 & 48.93 & 48.93 \\ 22.73 & 22.73 & 22.73 & 22.73 & 22.73 & 22.73 \\ 31.35 & 31.35 & 31.35 & 31.35 & 31.35 & 31.35 \\ 44.14 & 44.14 & 44.14 & 44.14 & 44.14 & 44.14 \\ 13.25 & 13.25 & 13.25 & 13.25 & 13.25 & 13.25 \end{bmatrix}$

Table 11. Design parameters for the plant noise intensity matrix - Constrained problem, Balas beam.

$(V_2 = 0.02.)$

V_1	*Design*
$diag(v_i^2)$	$V_1 = diag(10.45 \;\; 12.67 \;\; 4.082 \;\; 5.061 \;\; 3.155 \;\; 8.203)$
aa^T	$a^T = (0.1207 \;\; -0.1686 \;\; -0.01756 \;\; -11.47 \;\; 1.796 \;\; 2.429)$
HH^T	$H = \begin{bmatrix} -2.968 & 0.9709 & 0.9709 & 0.9709 & 0.9709 & 0.9709 \\ 1.193 & 1.644 & 1.644 & 1.644 & 1.644 & 1.644 \\ 1.054 & 0.9778 & 0.9778 & 0.9778 & 0.9778 & 0.9778 \\ 0.9925 & 0.9916 & 0.9916 & 0.9916 & 0.9916 & 0.9916 \\ 1.223 & 1.223 & 1.223 & 1.223 & 1.223 & 1.223 \\ 1.090 & 1.090 & 1.090 & 1.090 & 1.090 & 1.090 \end{bmatrix}$

more effective in the unconstrained case, but in the constrained case the improvement is marginal. The fact that almost all the improvement can be obtained with the 6-variable aa^T design is important because, for larger problems, the HH^T problem can be very expensive computationally.

Also, in the unconstrained case, the H matrix has identical columns, i.e.,

$$H = [b \;\; b \;\; b \;\; b \;\; b \;\; b] \qquad [5.3]$$

where b is a column vector. As a result, V_1 can be written as

$$V_1 = HH^T = n_b bb^T \qquad [5.4]$$

where n_b is the number of columns of H. As a result, V_1 takes on the vector times vector transpose form of $V_1 = aa^T$ where

$$a = \sqrt{n_b}\, b \qquad [5.5]$$

The optimizer did not find this solution for the unconstrained $V_1 = aa^T$ problem, and, thus, produced a solution with a residual mode stability margin to be much lower than that produced by the $V_1 = HH^T$ problem. Initial conditions were found to be important in this optimal design formulation, indicating a number of local optima.

The computational costs, as demonstrated by the length of execution time involved on an IBM 3084 computer, are given in Table 12. As expected, the cost increases with the number of design variables. The constrained case is much cheaper than the unconstrained case. This may be due to the optimizer limiting its search to a much smaller domain.

Also, for all the constrained designs, the ratio J/J_{LQR} is close to one which indicates that little performance degradation has taken place. For the unconstrained designs, the performance degradation is somewhat more appreciable.

Stability robustness tests developed by Doyle & Stein [60] and Doyle [64] were also applied for three different damping ratios, i.e., $\zeta = 0.001$, 0.0025, and 0.005 (see Figures 24 and 25). The robustness tests were performed using the knowledge of the first eight modes of the beam in order to insure that the optimum controllers do not have any problems with the higher frequency modes

Table 12. Computational costs for the Balas beam example.

(CPU time in minutes; IBM 3084)

(a) Unconstrained ($\lambda_{max} = \infty$)

Design	*Time*
$V_1 = diag(v_i^2)$	3.45
$V_1 = aa^T$	7.53
$V_1 = HH^T$	12.58

(b) Constrained ($\lambda_{max} = 16$)

Design	*Time*
$V_1 = diag(v_i^2)$	1.35
$V_1 = aa^T$	1.29
$V_1 = HH^T$	1.99

which were not taken into account in the analysis. The constrained optimized designs were found to be robust (see Figure 25). For the unconstrained designs, the results were mixed (see Figure 24). In general, the unconstrained designs were found to be considerably less robust than the constrained ones.

The unconstrained $V_1 = aa^T$ and $V_1 = HH^T$ designs failed the robustness test for all three damping ratios (Figure 24). These two designs are virtually one on top of the other on the frequency domain Bode plots. They not only ran into trouble with the fourth mode but also the fifth mode which was not explicitly taken into account in the optimization routine. Although the unconstrained $V_1 = diag(v_i^2)$ design satisfied the robustness test for the higher damping ratios (Figure 24), it exhibited an unexpected response at the $\omega = 3$ rad/ sec area.

For the constrained designs, the frequency response for all three designs are comparable. They all lie virtually one on top of the other on the Bode plots. For $\zeta = 0.001$ (Figure 25), the robustness test is borderline, but for $\zeta = 0.0025$ and $\zeta = 0.005$ (Figure 25), the robustness test is satisfied.

The constrained optimized solutions ($\lambda_{max} = 16$/ sec) behaved better in the high frequency range than the unconstrained solutions. In general, the designs with very fast observers produced systems which were less robust, whereas, the ones with the slower observers preserved robustness vis-à-vis the unknown dynamics. This, in turn, gives an additional justification for applying an upper bound on the *speed* of the observer. The speed of the observer is dictated by its gain. Low gain observers produce slower speeds whereas high gain observers produce faster speeds.

Finally, it should be emphasized that this procedure does not aim at designing *robust* controllers but rather *stable* ones. The difference lies in the fact that the structure of the uncertainty is taken into account explicitly. The robustness tests are conservative, and, as such, a robustness test violation does not mean that the system is going to be unstable, but rather that it may become unstable. Designing controllers, based purely on robustness considerations, can result in overly conservative designs at the expense of overall system performance [85], i.e., controller effectiveness.

An easy way to satisfy a robustness test is to lower all the controller gains, i.e., regulator gains and observer gains. This lowers the loop transfer matrix curve and, thus, moves it away from the uncertainty curve.

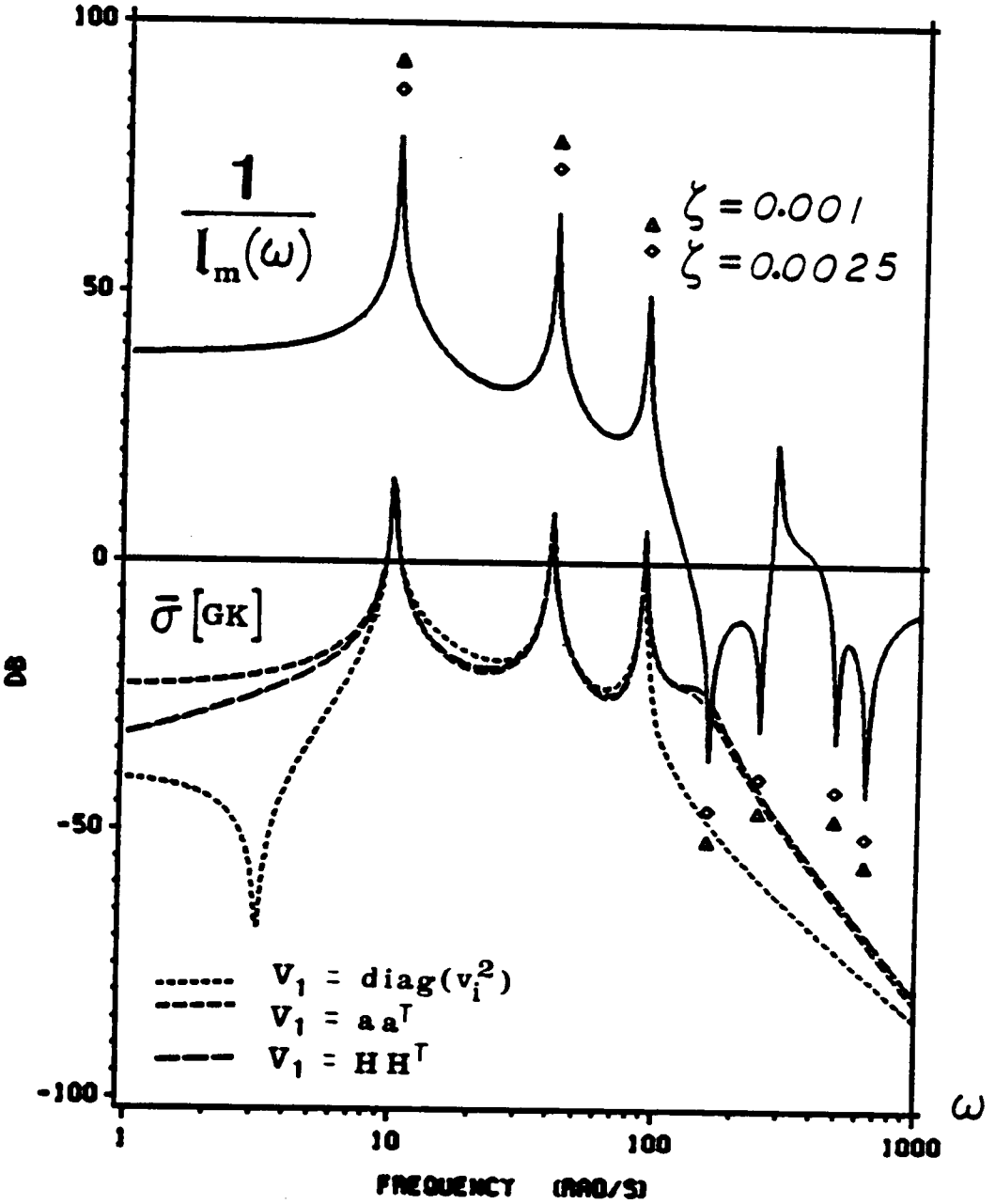

Figure 24. Robustness plot of the loop transfer matrix for the unconstrained optimized designs, Balas beam example. [$\zeta = 0.005$.]

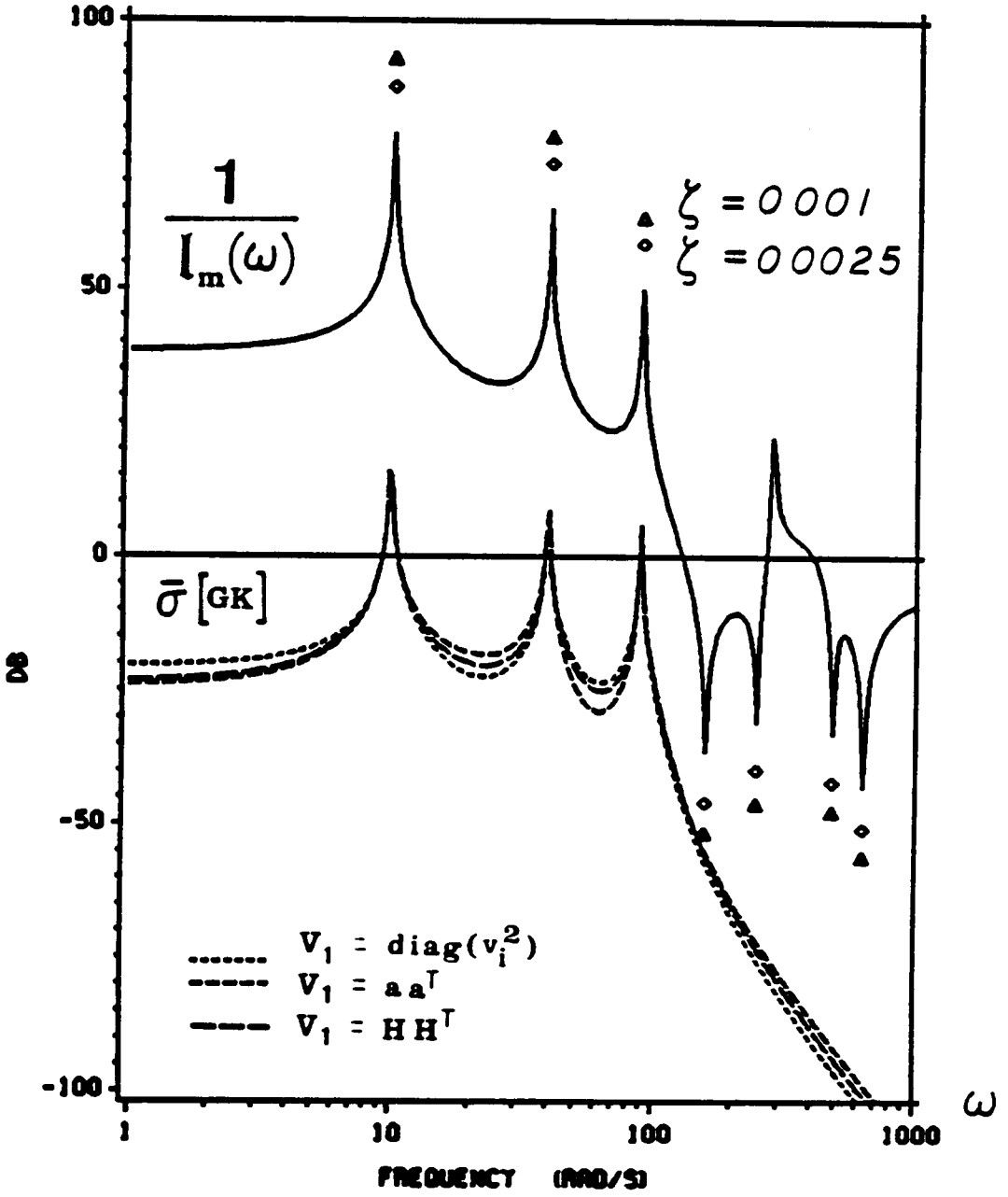

Figure 25. Robustness plot of the loop transfer matrix for the constrained optimized designs, Balas beam example. [$\zeta = 0.005$.]

This is not accomplished without cost. Lowering the observer gains by too much can bring the observer poles towards the imaginary axis and into the speed regime of the regulator poles. This can produce a very slow recovery of the reconstruction error from certain initial conditions, and it also effects the dynamics of the closed-loop system (control system/regulator). Finally, if the regulator gains are lowered considerably, the regulator may not be able to produce the needed or necessary force required of it. The system ends up with effectively no control.

CHAPTER 6. DECENTRALIZED MODAL CONTROL AND SPILLOVER ALLEVIATION

6.1. THEORY

The basic idea of decentralized modal control [24, 90 – 104] is that separate controllers are designed to independently control various sets of modes which are locally dominant. In the absence of control reconfiguration, independence implies that if one of the controllers is turned off (following a failure or for any other reason) the closed-loop system remains stable. When a local controller does not operate, the corresponding set of modes has a small stability margin and is a candidate for destabilization, i.e., the controlled modes of one controller become the residual modes of the other controller. This implies that each individual modal controller provides the set of modes it does not control with a positive stability margin. This is designated as the reliability condition [90], and it is in this context that spillover alleviation is analyzed. It must remain stable in spite of its interaction with the other subsystems.

When controllers operate together, the system must be globally stable. However, no destabilizing effect is expected from the controller interaction because the sets of controlled modes are

designed with substantial stability margins so global stability may not be difficult to satisfy. Therefore, the reliability condition will have the major impact on the design of the controller, since it is the more difficult of the two stability requirements to maintain. Along with these two stability conditions and other performance requirements, the development of the proper design of decentralized modal control is based on the following theory. For simplicity, it will be assumed that only two sets of modes will be controlled. The methodology can be easily extended to control more sets of modes. The governing system of equations to control two sets of modes is:

$$\dot{x}_1 = A_1 x_1 + B_1 u_1 + \beta_1 u_2 \qquad [6.1.1]$$

$$\dot{x}_2 = A_2 x_2 + \beta_2 u_1 + B_2 u_2 \qquad [6.1.2]$$

$$y_1 = C_1 x_1 + \gamma_1 x_2 \qquad [6.1.3]$$

$$y_2 = \gamma_2 x_1 + C_2 x_2 \qquad [6.1.4]$$

which governs the system dynamics and output. The standard definitions apply here with the addition of the Greek letters. $\beta_i u_j$ and $\gamma_i x_j$ represent the coupling of the two systems whereby system i excites system j and visa versa. In a sense, these terms can be viewed as contributions from residual type modes. $\beta_i u_j$ represents the excitation of subsystem i due to the control force aimed at controlling subsystem j, and $\gamma_i x_j$ is the contribution of subsystem j to the output y_i, on which the state reconstruction of subsystem i is based. When truly locally dominant modes exist, β_i and γ_i are small in magnitude. In practice, this is the desired situation.

Since the state of the system is, in general, not fully known, it is reconstructed via a Kalman-Bucy Filter (KBF). The reconstructed states, $\hat{x}_1$ and $\hat{x}_2$, are obtained by integrating

$$\dot{\hat{x}}_1 = A_1 \hat{x}_1 + B_1 u_1 + \beta_1 u_2 + K_{c_1}(y_1 - C_1 \hat{x}_1) \qquad [\hat{x}_1(0) = 0] \qquad [6.1.5]$$

$$\dot{\hat{x}}_2 = A_2 \hat{x}_2 + \beta_2 u_1 + B_2 u_2 + K_{c_2}(y_2 - C_2 \hat{x}_2) \qquad [\hat{x}_2(0) = 0] \qquad [6.1.6]$$

where K_{c_1} and K_{c_2} are the observer gain matrices.

In the above equations, it is assumed that the control vectors, u_1 and u_2, are made available simultaneously to both observers. In truly decentralized modal control, this is not the case; the $\beta_i u_j$ terms are not present in the observer equations. The observer of one controller knows absolutely nothing about what is happening at the other controller. The effect of removing this assumption in the example to be presented here is negligibly small due to the diagonally dominant characteristics of the matrices to be presented (see Appendix C).

The control vectors, u_1 and u_2, are given as

$$u_1 = -G_{c_1}\hat{x}_1 \qquad [6.1.7]$$

$$u_2 = -G_{c_2}\hat{x}_2 \qquad [6.1.8]$$

where G_{c_1} and G_{c_2}, the feedback gain matrices, are calculated from the Linear Quadratic Regulator (LQR) design methodology.

The two regulators are designed independently of one another and also independently of the two observers. Similarly, the two observers are also designed independently of one another and of the regulators. Each individual regulator is determined from the LQR design methodology, and each individual observer is determined from the KBF design methodology. Both neglect the presence of the coupling terms, $\beta_i u_j$ and $\gamma_i x_j$.

The state estimator error is defined as $e_i = \hat{x}_i - x_i$, and the state vector is selected to be $(x_1^T\ x_2^T\ e_1^T\ e_2^T)^T$. The corresponding system matrix for this defined state becomes

$$A_D = \begin{bmatrix} A_1 - B_1G_{c_1} & -\beta_1 G_{c_2} & -B_1G_{c_1} & -\beta_1 G_{c_2} \\ -\beta_2 G_{c_1} & A_2 - B_2G_{c_2} & -\beta_2 G_{c_1} & -B_2G_{c_2} \\ 0 & K_{c_1}\gamma_1 & A_1 - K_{c_1}C_1 & 0 \\ K_{c_2}\gamma_2 & 0 & 0 & A_2 - K_{c_2}C_2 \end{bmatrix} \qquad [6.1.9]$$

which can be written as

$$A_D = A_D^{\times} + A_D^{s} \qquad [6.1.10]$$

where

$$A_D^{\times} = \begin{bmatrix} A_1 - B_1 G_{c_1} & 0 & -B_1 G_{c_1} & 0 \\ 0 & A_2 - B_2 G_{c_2} & 0 & -B_2 G_{c_2} \\ 0 & 0 & A_1 - K_{c_1} C_1 & 0 \\ 0 & 0 & 0 & A_2 - K_{c_2} C_2 \end{bmatrix} \qquad [6.1.11]$$

and

$$A_D^{s} = \begin{bmatrix} 0 & -\beta_1 G_{c_2} & 0 & -\beta_1 G_{c_2} \\ -\beta_2 G_{c_1} & 0 & -\beta_2 G_{c_1} & 0 \\ 0 & K_{c_1} \gamma_1 & 0 & 0 \\ K_{c_2} \gamma_2 & 0 & 0 & 0 \end{bmatrix} \qquad [6.1.12]$$

$A_D^{\times}$ contains the contributions of the individual regulators and observers and is the dominant part of the matrix A_D. From its block triangular form, it has the same poles as the individual regulators and observers. A_D^{s} contains the control spillover terms ($\beta_i G_{c_j}$) and the observation spillover terms ($K_{c_i} \gamma_i$). When the β_i and γ_i terms are small, the condition of locally dominant modes exists. This implies that the actuators and sensors have been properly located to take advantage of the local nature of the system dynamics. When this is the case and the Gershgorin Theorem [105, 106] applies, A_D^{s} can be treated as a perturbation term which causes a slight deviation of the system poles from the design controller locations. This is desirable since, in general, the global system will be stable because $A_D^{\times}$ has been designed to have poles with large stability margins.

In treating the above as a perturbation problem, the smallness of the spillover terms is not enough to insure that the poles of the composite system will vary only slightly from the poles of the designed system. The conditions of the Gershgorin theorem must also be satisfied. This theorem maintains that provided the matrix is diagonally dominant and the diagonal entries are suffi-

ciently far apart, the system can sustain small off-diagonal terms and produce eigenvalues which are only slight deviations from the original eigenvalues.

In this problem, A_b^* is block triangular rather than diagonal. An appropriate transformation can produce A_b^* into diagonal form with its elements defined by the eigenvalues of the individual regulators and observers. At this point, A_b^* has also been transformed accordingly and, only then, is the Gershgorin theorem applied.

In terms of evaluating the deterministic performance index for the composite decentralized Linear Quadratic Regulator problem, perfect knowledge of the states, x_1 and x_2, is assumed. By applying the control laws

$$u_1 = -G_{c_1}x_1 \qquad [6.1.13]$$

$$u_2 = -G_{c_2}x_2 \qquad [6.1.14]$$

into Equations [6.1.1] and [6.1.2], one obtains

$$\dot{\varepsilon}_x = \bar{A}_{LQR}^D \varepsilon_x \qquad [6.1.15]$$

where $\varepsilon_x = (x_1^T \;\; x_2^T)^T$ is the state vector, and

$$\bar{A}_{LQR}^D = \begin{bmatrix} (A_1 - B_1 G_{c_1}) & -\beta_1 G_{c_2} \\ -\beta_2 G_{c_1} & (A_2 - B_2 G_{c_2}) \end{bmatrix} \qquad [6.1.16]$$

The performance index can be represented as

$$J = \int_{t=0}^{\infty} \varepsilon_x^T \bar{Q}_{LQR}^D \varepsilon_x dt \qquad [6.1.17]$$

where

$$\bar{Q}_{LQR}^D = \begin{bmatrix} Q_1 + G_{c_1}^T R_1 G_{c_1} & 0 \\ 0 & Q_2 + G_{c_2}^T R_2 G_{c_2} \end{bmatrix} \qquad [6.1.18]$$

Therefore, the minimum value of J is

$$J = \varepsilon_{x_o}^T P_{LQR}^D \varepsilon_{x_o} \qquad [6.1.19]$$

where P_{LQR}^D satisfies the following Lyapunov Equation

$$(\overline{A}_{LQR}^D)^T P_{LQR}^D + P_{LQR}^D \overline{A}_{LQR}^D + \overline{Q}_{LQR}^D = 0 \qquad [6.1.20]$$

and ε_{x_o} is the initial state.

In terms of evaluating the deterministic performance index for the state feedback on the observed state for decentralized modal control, the governing equations presented in Equation [6.1.1] to [6.1.8] are used. Let $e_i = \hat{x}_i - x_i$ be the state estimator, therefore,

$$u_i = -G_{c_i}(e_i + x_i) \qquad [6.1.21]$$

Define the state vector of the composite system as $\varepsilon = (x_1^T \; x_2^T \; e_1^T \; e_2^T)^T$ so that

$$\dot{\varepsilon} = \overline{A}_D \varepsilon \qquad [6.1.22]$$

where

$$\overline{A}_D = \begin{bmatrix} A_1 - B_1 G_{c_1} & -\beta_1 G_{c_2} & -B_1 G_{c_1} & -\beta_1 G_{c_2} \\ -\beta_2 G_{c_1} & A_2 - B_2 G_{c_2} & -\beta_2 G_{c_1} & -B_2 G_{c_2} \\ 0 & K_{c_1}\gamma_1 & A_1 - K_{c_1} C_1 & 0 \\ K_{c_2}\gamma_2 & 0 & 0 & A_2 - K_{c_2} C_2 \end{bmatrix} \qquad [6.1.23]$$

The performance index can be represented as

$$J = \int_{t=0}^{\infty} \varepsilon^T \overline{Q}^{\times} \varepsilon dt \qquad [6.1.24]$$

where

$$\overline{Q}^{\times} = \begin{bmatrix} Q_1 + G_{c_1}^T R_1 G_{c_1} & 0 & G_{c_1}^T R_1 G_{c_1} & 0 \\ 0 & Q_2 + G_{c_2}^T R_2 G_{c_2} & 0 & G_{c_2}^T R_2 G_{c_2} \\ G_{c_1}^T R_1 G_{c_1} & 0 & G_{c_1}^T R_1 G_{c_1} & 0 \\ 0 & G_{c_2}^T R_2 G_{c_2} & 0 & G_{c_2}^T R_2 G_{c_2} \end{bmatrix} \qquad [6.1.25]$$

Therefore, the minimum value of J is

$$J = \varepsilon_o^T \overline{P}_L^{\times} \varepsilon_o \qquad [6.1.26]$$

where $\overline{P}_L^{\times}$ satisfies the following Lyapunov Equation

$$\overline{A}_D^T \overline{P}_L^{\times} + \overline{P}_L^{\times} \overline{A}_D + \overline{Q}^{\times} = 0 \qquad [6.1.27]$$

and ε_o is the initial state.

With the global stability requirement being satisfied, the next condition to be investigated is that of reliability, i.e., the stability of the disabled control system. This condition requires that the system remain stable even if one of the controllers becomes inoperational.

Consider first the case of subsystem 2 being disabled, and define the state vector as $(x_1^T x_2^T e_1^T)^T$. It can be shown that the reduced system matrix is found by setting $G_{c_2} = 0$ in the submatrix corresponding to the new state. Denoting the system matrix as $\overline{A}_1^D$, we have

$$\overline{A}_1^D = \begin{bmatrix} A_1 - B_1 G_{c_1} & 0 & -B_1 G_{c_1} \\ -\beta_2 G_{c_1} & A_2 & -\beta_2 G_{c_1} \\ 0 & K_{c_1} \gamma_1 & A_1 - K_{c_1} C_1 \end{bmatrix} \qquad [6.1.28]$$

which can be written as

$$\overline{A}_1^D = \overline{A}_1^{\times} + \overline{A}_1^s \qquad [6.1.29]$$

where

$$\overline{A}_1^{\times} = \begin{bmatrix} A_1 - B_1 G_{c_1} & 0 & -B_1 G_{c_1} \\ 0 & A_2 & 0 \\ 0 & 0 & A_1 - K_{c_1} C_1 \end{bmatrix} \qquad [6.1.30]$$

and

$$\overline{A}_1^{s} = \begin{bmatrix} 0 & 0 & 0 \\ -\beta_2 G_{c_1} & 0 & -\beta_2 G_{c_1} \\ 0 & K_{c_1}\gamma_1 & 0 \end{bmatrix} \qquad [6.1.31]$$

The term A_2 in $\overline{A}_1^{\times}$ has only small stability margin provided by structural damping alone. Therefore, any slight perturbations, $\overline{A}_1^{s}$, can lead to an unstable system.

Similarly, if subsystem 1 is disabled, the state vector becomes $(x_1^T\, x_2^T\, e_2^T)^T$. The corresponding system matrix is

$$\overline{A}_2^{D} = \begin{bmatrix} A_1 & -\beta_1 G_{c_2} & -\beta_1 G_{c_2} \\ 0 & A_2 - B_2 G_{c_2} & -B_2 G_{c_2} \\ K_{c_2}\gamma_2 & 0 & A_2 - K_{c_2} C_2 \end{bmatrix} \qquad [6.1.32]$$

which can be written as

$$\overline{A}_2^{D} = \overline{A}_2^{\times} + \overline{A}_2^{s} \qquad [6.1.33]$$

where

$$\overline{A}_2^{\times} = \begin{bmatrix} A_1 & 0 & 0 \\ 0 & A_2 - B_2 G_{c_2} & -B_2 G_{c_2} \\ 0 & 0 & A_2 - K_{c_2} C_2 \end{bmatrix} \qquad [6.1.34]$$

and

$$\overline{A}_2^x = \begin{bmatrix} 0 & -\beta_1 G_{c_2} & -\beta_1 G_{c_2} \\ 0 & 0 & 0 \\ K_{c_2}\gamma_2 & 0 & 0 \end{bmatrix} \qquad [6.1.35]$$

Once again, $\overline{A}_2^x$ has small stability margin, therefore, any perturbations can lead to an unstable system.

In summary, for decentralized modal control to satisfy the reliability conditions, each controller must guarantee a positive stability margin for the other subsystem which can be treated as its residual modes. The optimization procedure discussed in the centralized beam example suggests a method for designing a reasonable KBF which, for a given regulator, maximizes the stability margins of the residual modes as defined by the reliability conditions.

6.2. CONTROLLER DESIGN

The two regulators are designed independently of one another and also independently of the two observers. In other words, the design of the regulator follows the form of the Linear Quadratic Regulator (LQR) which assumes the following form of the system dynamics

$$\dot{x}_i = A_i x_i + B_i u_i \qquad [6.2.1]$$

$$u_i = -G_{c_i} x_i = -R_i^{-1} B_i^T \overline{F}_i x_i \qquad [6.2.2]$$

which minimizes the performance index

$$J_i = \int_{t=0}^{\infty} (x_i^T Q_i x_i + u_i^T R_i u_i) dt \qquad [6.2.3]$$

where Q_i and R_i are weighting matrices. In the example to be discussed later, Q_i was selected so that $x_i^T Q_i x_i$ is the total energy of system i,

$$Q_i = \frac{1}{2}\begin{bmatrix} diag(\omega_i^2) & 0 \\ 0 & diag(\omega_i^2) \end{bmatrix} \qquad [6.2.4]$$

while R_i is defined via the Model Error Sensitivity Suppression (MESS) Method [23, 24] as

$$R_i = R_{o_i} + B_{r_i}^T W_i B_{r_i} \qquad [6.2.5]$$

$$R_i = \rho_{1_i}(I + \rho_{2_i} B_{r_i}^T B_{r_i}) \qquad [6.2.6]$$

with $\rho_{1_i} > 0$ and $\rho_{2_i} \geq 0$. B_r refers to the control matrix of the known residual modes. For the decentralized problem, β corresponds to B_r. The particular form of R_i was chosen such that R_i is positive definite. The minimization of J_i leads to the following Riccati Equation

$$\bar{F}_i A_i + A_i^T \bar{F}_i - \bar{F}_i B_i R_i^{-1} B_i^T \bar{F}_i + Q_i = 0 \qquad [6.2.7]$$

The two observers are also designed independently of one another and of the regulators. Each observer follows the equations of

$$\dot{x}_i = A_i x_i + B_i u_i + w_{1_i} \qquad [6.2.8]$$

$$y_i = C_i x_i + w_{2_i} \qquad [6.2.9]$$

where

$$Cov(w_{1_i}, w_{1_i}^T) = V_{1_i} \qquad [6.2.10]$$

$$Cov(w_{2_i}, w_{2_i}^T) = V_{2_i} \qquad [6.2.11]$$

$$Cov(w_{1_i}, w_{2_i}^T) = 0 \qquad [6.2.12]$$

where w_{1_i} and w_{2_i} are uncorrelated white noise. V_{1_i} and V_{2_i} are the plant noise intensity matrices and the measurement noise intensity matrices, respectively.

In the reconstructed state, the governing equation is

$$\dot{\hat{x}}_i = A_i\hat{x}_i + B_iu_i + K_{c_i}(y_i - C_i\hat{x}_i) \qquad [6.2.13]$$

where

$$K_{c_i} = P_iC_i^TV_{2_i}^{-1} \qquad [6.2.14]$$

Here V_{2_i} is selected using the MESS method [23, 24]

$$\begin{aligned} V_{2_i} &= V_{o_i} + C_{r_i}V_iC_{r_i}^T \\ &= v_{1_i}(I + v_{2_i}C_{r_i}C_{r_i}^T) \end{aligned} \qquad [6.2.15]$$

with $v_{1_i} > 0$ and $v_{2_i} \geq 0$. C_r refers to the output matrix of the known residual modes. For the decentralized problem, γ corresponds to C_r. The particular form of V_{2_i} was chosen such that V_{2_i} is positive definite.

Applying the $\alpha-$ shift procedure, P_i is found by solving the following observer Riccati Equation

$$(A_i + \alpha_iI)P_i + P_i(A_i + \alpha_iI)^T - P_iC_i^TV_{2_i}^{-1}C_iP_i + V_{1_i} = 0 \qquad [6.2.16]$$

6.3. GRID STRUCTURE EXAMPLE

A numerical study of decentralized modal control was performed on a grid structure (Figure 26) which is representative of Large Space Structures [107]. This structure is part of a research facility at Virginia Tech. The plane grid structure was represented as a finite element model [108, 109] . The results of this model were incorporated in this theoretical study.

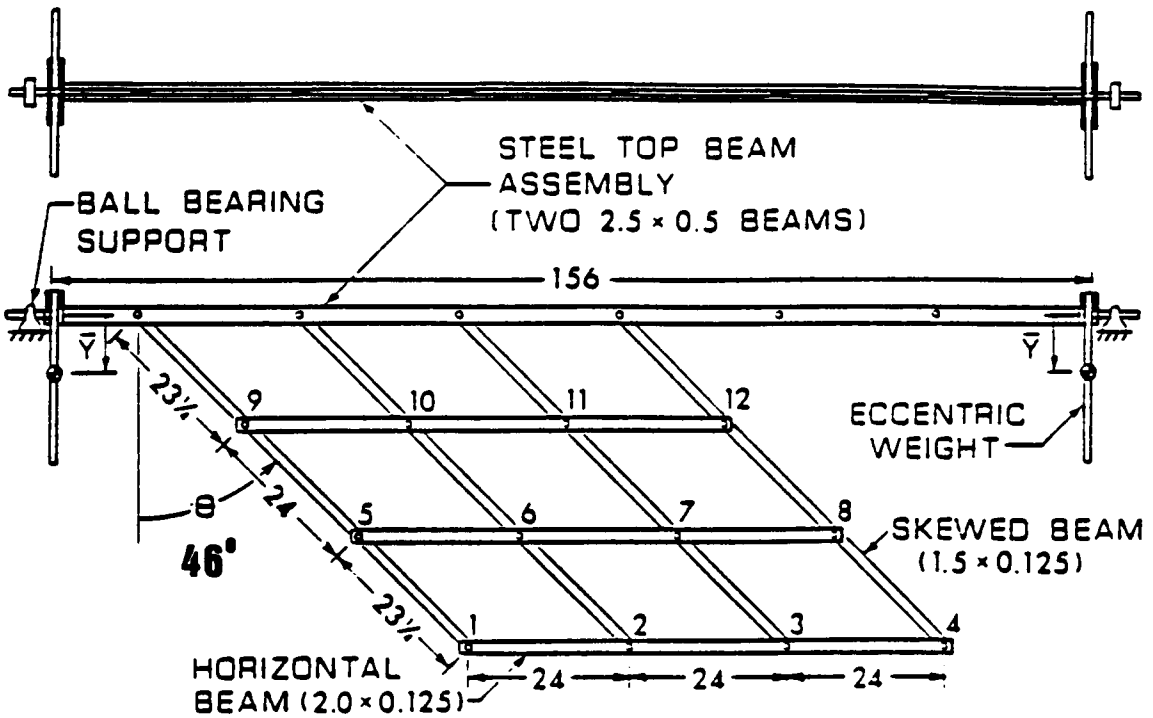

Figure 26. Grid structure. (All dimensions in inches.)

Two colocated actuator-and-sensor pairs were positioned at locations 4 and 8 to control Modes 1, 2, and 3, while two other colocated actuator-and-sensor pairs were positioned at locations 11 and 12 to control Modes 4, 5, and 6. The residual modes of one controller are the controlled modes of the other controller. The colocation property was not used in that the full state is reconstructed in the controller design.

The locations of the actuators and sensors selected for this numerical study do not represent the actual experimental configuration of sensors and actuators. The locations were selected to achieve the smallest possible coupling between the controllers, because the modes of the grid structure are not local in nature.

The modal amplitudes at the nodes are given in Table 13. The terms in the diagonal boxes of the table correspond to the B_i and C_i matrices, while the off-diagonal boxes correspond to the β_i and γ_i matrices. Note that the magnitude of the terms involved in β_1 and γ_1 is comparable to that of those involved in B_1 and C_1, indicating strong coupling between the two systems.

For this example, the Q_i matrices are defined so that $x_i^T Q_i x_i$, $i = 1,2$, represents the total energy of each set of modes (see Equation [6.2.4]). As mentioned before, R_i and V_{2_i} follow the MESS methodology as defined in the previous section (Equations [6.2.6] and [6.2.15], respectively). The two subsystems are controllable and observable.

There are a number of design parameters involved, i.e., ρ_1, ρ_2, ν_1, ν_2, α, ζ, and V_1 for each of the controllers. To demonstrate the effect of V_1 on spillover, Table 14 contains the results of two cases where the only difference is in the choice of V_1 . In one case, $V_1 = Q$ for observer 1 and $V_1 = I$ for observer 2. For the second case, the forms of V_1 are exchanged.

From Table 14, it is seen that despite the large coupling between the two subsystems, the interaction between the controllers does not destabilize the system when they work together. Indeed, for both cases, the coupled system poles are very close to the original controller poles designed independently of one another.

When one controller is disabled, for the first case of $V_1 = Q$ for observer 1 and $V_1 = I$ for observer 2, the disabled system remains stable, though with only small stability margins. On the other hand, for the second case where $V_1 = I$ for observer 1 and $V_1 = Q$ for observer 2, the disabled sub-

Table 13. Normalized modal amplitudes at actuator and sensor locations for the decentralized grid structure.

		Controller 1		*Controller* 2	
	Frequency (*Hz*)	*Node* 4	*Node* 8	*Node* 11	*Node* 12
Modes Set 1	0.584	−7.40	−4.68	−1.72	−2.05
	0.890	11.27	6.05	−0.44	1.61
	1.373	−9.18	−5.00	1.03	−1.76
		(B_1, C_1)		(β_2, γ_2)	
Modes Set 2	3.279	11.68	−3.20	−4.88	−5.25
	3.593	2.21	5.81	4.20	4.70
	4.957	−5.70	10.33	−2.44	8.67
		(β_1, γ_1)		(B_2, C_2)	

Table 14. Comparison of two KBF designs for the decentralized grid structure.

(For both systems, $\zeta = 0$, $\rho_1 = 30$, $\rho_2 = 30$, $\nu_1 = 0.01$, $\nu_2 = 5$, and $\alpha = 0.5$ for controller 1 and $\zeta = 0$, $\rho_1 = 20$, $\rho_2 = 10$, $\nu_1 = 1$, $\nu_2 = 1$, and $\alpha = 3$ for controller 2.)
(System eigenvalues in 1/sec.)

(A)
Observer 1 designed with $V_1 = Q$
Observer 2 designed with $V_1 = I$

Poles	*Individual*	*Coupled*	*2 – disabled*	*1 – disabled*
Regulator 1	$-0.23 \pm j3.67$ $-0.36 \pm j5.59$ $-0.30 \pm j8.63$	$-0.29 \pm j3.57$ $-0.35 \pm j5.54$ $-0.29 \pm j8.58$	$-0.23 \pm j3.67$ $-0.36 \pm j5.59$ $-0.30 \pm j8.63$	$-0.033 \pm j3.57$ $-0.007 \pm j5.54$ $-0.007 \pm j8.58$
Observer 1	$-1.43 \pm j3.90$ $-2.16 \pm j6.78$ -7.42 -39.30	$-1.43 \pm j3.88$ $-2.14 \pm j6.80$ -7.20 -39.48	$-1.42 \pm j3.88$ $-2.14 \pm j6.80$ -7.20 -39.48	↑ *STABLE*
Regulator 2	$-0.50 \pm j20.61$ $-0.44 \pm j22.57$ $-0.56 \pm j31.15$	$-0.56 \pm j20.76$ $-0.41 \pm j22.58$ $-0.57 \pm j31.13$	$-0.034 \pm j20.75$ $-0.002 \pm j22.59$ $-0.005 \pm j31.12$	$-0.50 \pm j20.60$ $-0.44 \pm j22.57$ $-0.56 \pm j31.14$
Observer 2	$-6.47 \pm j20.68$ $-6.35 \pm j22.50$ $-6.67 \pm j31.15$	$-6.58 \pm j20.58$ $-6.20 \pm j22.60$ $-6.66 \pm j31.17$	↑ *STABLE*	$-6.58 \pm j20.59$ $-6.20 \pm j22.59$ $-6.65 \pm j31.17$

(B)
Observer 1 designed with $V_1 = I$
Observer 2 designed with $V_1 = Q$

Poles	*Individual*	*Coupled*	*2 – disabled*	*1 – disabled*
Regulator 1	$-0.23 \pm j3.67$ $-0.36 \pm j5.59$ $-0.30 \pm j8.63$	$-0.23 \pm j3.83$ $-0.40 \pm j5.45$ $-0.32 \pm j8.51$	$-0.23 \pm j3.67$ $-0.36 \pm j5.59$ $-0.30 \pm j8.63$	$0.049 \pm j3.81$ $-0.047 \pm j5.47$ $-0.056 \pm j8.53$
Observer 1	$-1.62 \pm j4.18$ $-5.48 \pm j5.33$ $-2.31 \pm j7.79$	$-1.62 \pm j4.19$ $-5.58 \pm j5.11$ $-2.24 \pm j7.80$	$-1.62 \pm j4.19$ $-5.58 \pm j5.12$ $-2.24 \pm j7.80$	↑ *UNSTABLE*
Regulator 2	$-0.50 \pm j20.61$ $-0.44 \pm j22.57$ $-0.56 \pm j31.15$	$-0.48 \pm j20.69$ $-0.43 \pm j22.56$ $-0.57 \pm j31.14$	$0.032 \pm j20.67$ $0.003 \pm j22.58$ $-0.007 \pm j31.14$	$-0.50 \pm j20.60$ $-0.44 \pm j22.56$ $-0.56 \pm j31.14$
Observer 2	$-35.08 \pm j14.64$ $-6.17 \pm j21.64$ $-44.11 \pm j21.72$	$-35.23 \pm j14.60$ $-6.15 \pm j21.71$ $-43.90 \pm j21.58$	↑ *UNSTABLE*	$-35.23 \pm j14.60$ $-6.15 \pm j21.71$ $-43.91 \pm j21.58$

systems are unstable. Therefore, the reliability condition for the second case is not satisfied which makes this an unacceptable design.

The value of the deterministic performance indices based on zero initial velocity and initial amplitudes corresponding to a uniform strain energy in all the modes were compared. The following performance indices are computed: (1) individual regulator J^1_{LQR}, J^2_{LQR}, (2) individual controllers $J^1_{LQR+KBF}$, $J^2_{LQR+KBF}$, and (3) coupled control system $J^{1+2}_{LQR+KBF}$. The results given in Table 15 indicate that, in the stable case (A), the increment in the performance index resulting from the interaction between the subsystems is small, while in the unstable case (B), it is substantial.

The foregoing results show that a change of the structure of the plant noise intensity matrix, V_1, can drastically change the stability of the disabled system (reliability condition). This makes the grid structure a candidate for the optimization procedure presented earlier. This is the subject of the following section.

6.4. OPTIMIZING THE PLANT NOISE FOR THE DECENTRALIZED PROBLEM

The optimization procedure used to maximize the stability margin of the disabled systems is similar to the procedure employed for the centralized problem. Since now there will be more than one residual mode, the optimization problem is modified slightly and is written as

$$\min \; f = k_s(\delta - t)^2 \qquad [6.4.1]$$

subject to

$$Re(\lambda_i) < \delta \qquad [6.4.2]$$

$$\delta < 0 \qquad [6.4.3]$$

Table 15. Deterministic performance indices for the decentralized grid structure.

(Indices in lb-sec/in.)

PERFORMANCE INDICES		*Case A* *Observer* 1: $V_1 = Q$ *Observer* 2: $V_1 = I$	*Case B* *Observer* 1: $V_1 = I$ *Observer* 2: $V_1 = Q$
Individual	J^1_{LQR}	5.423	5.423
regulators	J^2_{LQR}	3.395	3.395
Including state	$J^1_{LQR+KBF}$	5.587	5.610
estimation	$J^2_{LQR+KBF}$	3.427	3.412
Including	$J^{1+2}_{LQR+KBF}$	9.123	12.111
coupling			
Increment due	$\dfrac{J^{1+2}_{LQR+KBF} - J^1_{LQR+KBF} - J^2_{LQR+KBF}}{J^1_{LQR+KBF} + J^2_{LQR+KBF}}$	0.012	0.342
to *coupling*			

The elements of V_1, the plant noise intensity matrices, and δ are the design variables, t is a negative number which drives the system to a desired stability margin (t was selected to be -0.05/sec.), and the λ_i's are all the eigenvalues from the reliability condition when one of the controllers becomes inoperational. t can be viewed as the minimum stability margin that one wishes to achieve, and the final value of δ is the actual stability margin. The constant k_r is used for scaling, and for the grid example, it was set at 100. As for the beam example, three forms of V_1 were selected:

$$V_1 = diag(v_i^2), \qquad i = 1, \ldots, 6$$

$$V_1 = aa^T \qquad (a = 6\,x\,1 \text{ vector})$$

$$V_1 = HH^T \qquad (H = 6\,x\,6 \text{ matrix})$$

Since in this problem, both V_1 matrices are to be designed, the number of design variables involved is 13 for the first two choices and 73 for the third choice.

The results of the optimization of the stability margins are found in Table 16. The actual values of the design parameters for the three different structures of V_1 as generated by NEWSUMT-A are found in Table 17. It should be noted that the design conditions of Tables 16 and 17 are *not* the same as those of Table 14.

As can be seen, for all the cases, the stability margins are small. The reliability condition is very difficult to satisfy, and, when it is satisfied, the stability margins are small. The results are acceptable, though, since the goal was to avoid destabilization. The stability margins of all the uncontrolled modes, in general, increase as V_1 increases in complexity, which is to be expected, though the difference between $diag(v_i^2)$ and HH^T is negligible. In both cases, the stability margins are approximately twice as large as that for $V_1 = aa^T$.

HH^T resembles the diagonal case very closely in terms of the elements of HH^T and in terms of performance, i.e., coupled and disabled systems. The diagonal elements of H are approximately the square root of the diagonal elements for the design $V_1 = diag(v_i^2)$. The off-diagonal terms of H are very close to zero. The difference in the system stability margin under the reliability condition

Table 16. Optimization results for the decentralized grid structure.

(For all systems, $\zeta = 0$, $\rho_1 = 30$, $\rho_2 = 30$, $\nu_1 = 0.0001$, $\nu_2 = 7$, and $\alpha = 0.5$ for controller 1 and $\zeta = 0$, $\rho_1 = 20$, $\rho_2 = 10$, $\nu_1 = 0.1$, $\nu_2 = 1$, and $\alpha = 0.75$ for controller 2.)
(System eigenvalues in 1/sec.)

(a) $V_1 = diag(v_1^2)$

Poles	*Individual*	*Coupled*	2 – *disabled*	1 – *disabled*
Regulator 1	$-0.23 \pm j3.67$ $-0.36 \pm j5.59$ $-0.30 \pm j8.63$	$-0.28 \pm j3.45$ $-0.34 \pm j5.56$ $-0.29 \pm j8.60$	$-0.23 \pm j3.68$ $-0.36 \pm j5.60$ $-0.30 \pm j8.63$	$-0.03444 \pm j3.45$ $-0.00341 \pm j5.56$ $-0.00225 \pm j8.60$
Observer 1	-157.05 -4.26 $-2.03 \pm j7.99$ $-1.82 \pm j3.93$	-157.08 -4.14 $-2.02 \pm j8.04$ $-1.84 \pm j3.88$	-157.08 -4.13 $-2.02 \pm j8.04$ $-1.83 \pm j3.87$	↑
Regulator 2	$-0.50 \pm j20.61$ $-0.44 \pm j22.57$ $-0.56 \pm j31.15$	$-0.58 \pm j20.71$ $-0.42 \pm j22.58$ $-0.56 \pm j31.13$	$-0.05510 \pm j20.70$ $-0.00227 \pm j22.59$ $-0.00214 \pm j31.13$	$-0.50 \pm j20.61$ $-0.44 \pm j22.57$ $-0.56 \pm j31.15$
Observer 2	$-5.66 \pm j20.57$ $-1.94 \pm j22.18$ $-3.92 \pm j31.14$	$-5.63 \pm j20.59$ $-1.94 \pm j22.19$ $-3.92 \pm j31.16$	↑	$-5.62 \pm j20.58$ $-1.94 \pm j22.19$ $-3.92 \pm j31.16$

(b) $V_1 = aa^T$

Poles	*Individual*	*Coupled*	2 – *disabled*	1 – *disabled*
Regulator 1	$-0.23 \pm j3.67$ $-0.36 \pm j5.59$ $-0.30 \pm j8.63$	$-0.28 \pm j3.53$ $-0.36 \pm j5.53$ $-0.30 \pm j8.58$	$-0.23 \pm j3.67$ $-0.36 \pm j5.59$ $-0.30 \pm j8.63$	$-0.02268 \pm j3.53$ $-0.01105 \pm j5.54$ $-0.01399 \pm j8.58$
Observer 1	$-14.43 \pm j16.16$ $-2.90 \pm j4.66$ $-3.66 \pm j4.39$	$-14.35 \pm j15.83$ $-2.95 \pm j4.65$ $-3.65 \pm j4.46$	$-14.36 \pm j15.83$ $-2.94 \pm j4.65$ $-3.66 \pm j4.45$	↑
Regulator 2	$-0.50 \pm j20.61$ $-0.44 \pm j22.57$ $-0.56 \pm j31.15$	$-0.59 \pm j20.85$ $-0.40 \pm j22.59$ $-0.56 \pm j31.12$	$-0.03140 \pm j20.84$ $-0.00285 \pm j22.59$ $-0.00106 \pm j31.11$	$-0.50 \pm j20.61$ $-0.44 \pm j22.57$ $-0.56 \pm j31.15$
Observer 2	$-3.33 \pm j19.24$ $-2.26 \pm j23.93$ $-9.93 \pm j32.44$	$-3.34 \pm j19.25$ $-2.25 \pm j23.94$ $-9.89 \pm j32.47$	↑	$-3.34 \pm j19.25$ $-2.25 \pm j23.94$ $-9.89 \pm j32.47$

(c) $V_1 = HH^T$

Poles	*Individual*	*Coupled*	2 – *disabled*	1 – *disabled*
Regulator 1	$-0.23 \pm j3.67$ $-0.36 \pm j5.59$ $-0.30 \pm j8.63$	$-0.28 \pm j3.45$ $-0.34 \pm j5.56$ $-0.29 \pm j8.60$	$-0.23 \pm j3.68$ $-0.36 \pm j5.60$ $-0.30 \pm j8.63$	$-0.03445 \pm j3.45$ $-0.00341 \pm j5.56$ $-0.00225 \pm j8.60$
Observer 1	-156.91 -4.27 $-2.03 \pm j7.99$ $-1.82 \pm j3.93$	-156.93 -4.15 $-2.02 \pm j8.04$ $-1.84 \pm j3.88$	-156.93 -4.14 $-2.02 \pm j8.04$ $-1.83 \pm j3.87$	↑
Regulator 2	$-0.50 \pm j20.61$ $-0.44 \pm j22.57$ $-0.56 \pm j31.15$	$-0.58 \pm j20.71$ $-0.42 \pm j22.58$ $-0.56 \pm j31.13$	$-0.05518 \pm j20.70$ $-0.00227 \pm j22.59$ $-0.00215 \pm j31.13$	$-0.50 \pm j20.61$ $-0.44 \pm j22.57$ $-0.56 \pm j31.15$
Observer 2	$-5.67 \pm j20.57$ $-1.94 \pm j22.18$ $-3.92 \pm j31.14$	$-5.63 \pm j20.59$ $-1.94 \pm j22.19$ $-3.92 \pm j31.16$	↑	$-5.63 \pm j20.58$ $-1.94 \pm j22.19$ $-3.92 \pm j31.16$

Table 17. Design parameters for the plant noise intensity matrices for the decentralized grid structure.

(a) $V_1 = diag(v_i^2)$

Observer	*Design*
1	$V_1 = diag(0.9026\ 7.800\ 1.142\ 1.480\ 1.367\ 4.454)$
2	$V_1 = diag(1.211\ 0.2572\ 0.2148\ 0.02918\ 0.2969\ 0.2138)$

(b) $V_1 = aa^T$

Observer	*Design*
1	$a^T = (-2.278x10^{-8}\ \ -3.023x10^{-3}\ 0.1651\ 2.006\ 1.981\ 2.064)$
2	$a^T = (-7.127x10^{-2}\ 1.574x10^{-3}\ \ -3.471x10^{-3}\ 2.001\ 2.013\ 1.987)$

(c) $V_1 = HH^T$

$$H = \begin{bmatrix} 0.9500 & -5.988x10^{-4} & -1.375x10^{-4} & -3.014x10^{-6} & -1.952x10^{-4} & 1.246x10^{-4} \\ 1.979x10^{-3} & 2.790 & 2.083x10^{-3} & 2.135x10^{-4} & 3.155x10^{-4} & -1.338x10^{-3} \\ -9.129x10^{-4} & -6.818x10^{-4} & 1.069 & -4.669x10^{-4} & -2.235x10^{-5} & -1.026x10^{-4} \\ 1.861x10^{-3} & 9.933x10^{-4} & 2.616x10^{-5} & 1.217 & 2.261x10^{-5} & -5.661x10^{-6} \\ 1.801x10^{-4} & -1.068x10^{-3} & 3.126x10^{-4} & -1.643x10^{-3} & 1.170 & -3.320x10^{-4} \\ 2.637x10^{-4} & -5.720x10^{-5} & 1.973x10^{-5} & 1.375x10^{-3} & 2.629x10^{-4} & 2.111 \end{bmatrix}$$

for observer 1 and

$$H = \begin{bmatrix} 1.100 & 1.519x10^{-4} & -2.339x10^{-4} & 3.898x10^{-5} & 1.446x10^{-4} & -4.756x10^{-4} \\ -5.756x10^{-4} & 0.5075 & 3.634x10^{-4} & 5.702x10^{-6} & -5.593x10^{-5} & 6.128x10^{-5} \\ 7.072x10^{-4} & -4.282x10^{-4} & 0.4631 & 1.448x10^{-5} & 1.813x10^{-5} & -2.198x10^{-4} \\ 8.655x10^{-4} & -4.234x10^{-4} & -9.545x10^{-4} & 0.1708 & 2.249x10^{-4} & 3.771x10^{-5} \\ 2.198x10^{-5} & 3.297x10^{-5} & -5.381x10^{-5} & -8.164x10^{-5} & 0.5452 & 3.607x10^{-4} \\ -1.142x10^{-4} & 1.637x10^{-5} & 1.860x10^{-4} & 1.008x10^{-4} & -4.100x10^{-4} & 0.4619 \end{bmatrix}$$

for observer 2.

is negligible. Therefore, there seems to be no advantage to complicate the optimization problem by providing so many design variables.

As a final comment, the initial conditions for $V_1 = diag(v_i^2)$ were $V_1 = I$ for each controller; for $V_1 = aa^T$, a was set to B_e of the corresponding controller; and for $V_1 = HH^T$, H was set to produce the optimum result of $V_1 = diag(v_i^2)$.

When comparing the centralized and decentralized cases, one reaches the conclusion that designing V_1 as $diag(v_i^2)$ and aa^T and then selecting the better of the two results is more than sufficient in the optimization procedure. Complicating the problem by introducing many design variables via HH^T has been shown as unnecessary. The fact that almost all the improvement in terms of stability margins can be obtained with a 6-variable design of V_1 is important because, for larger problems, the HH^T problem can be very expensive computationally.

The computational cost times on an IBM 3084 computer are given in Table 18. As expected, the length of time involved increases as the number of design variables increases.

As seen in Table 19, the performance indices are quite comparable. There is a slight improvement as V_1 becomes fully populated, i.e., $V_1 = aa^T$. Since $V_1 = HH^T$ is very similar to $V_1 = diag(v_i^2)$, the performance indices are practically identical.

As a final note, the results produced by the optimization procedure provide the V_1 matrices with certain relative magnitudes. What needs to be established is that not only is the net magnitude of the matrix important, but also that the distribution of the elements of the matrices must be as specified by the optimization routine, i.e., certain V_1 element locations must possess large numbers while others small. This is illustrated in Table 20, where V_1 is defined as some constant times the identity matrix. This constant was taken as the average of the diagonal elements of each optimized diagonal V_1 matrix. What can be seen is that, although the performance indices are comparable (Table 21) and the V_1 matrices are of the same order of magnitude, the averaged V_1 produces unstable poles that do not satisfy the reliability condition. We can conclude that obtaining the correct magnitude of V_1 is not enough. The correct positioning of the various elements of different magnitudes must be made. An averaging process is not acceptable.

Table 18. Computational costs for the decentralized grid structure.

(CPU time in minutes; IBM 3084)

Design	*Time*
$V_1 = diag(v_i^2)$	6.93
$V_1 = aa^T$	9.59
$V_1 = HH^T$	27.90

Table 19. Performance indices for the optimum cases of the decentralized grid structure.

(Indices in lb-sec/in.)

PERFORMANCE INDICES		$V_1 = diag(v_i^2)$	$V_1 = aa^T$	$V_1 = HH^T$
Individual	J^1_{LQR}	5.423	5.423	5.423
regulators	J^2_{LQR}	3.395	3.395	3.395
Including state	$J^1_{LQR+KBF}$	5.578	5.636	5.577
estimation	$J^2_{LQR+KBF}$	3.455	3.422	3.455
Including	$J^{1+2}_{LQR+KBF}$	9.773	9.480	9.773
coupling				
Increment due	$\dfrac{J^{1+2}_{LQR+KBF} - J^1_{LQR+KBF} - J^2_{LQR+KBF}}{J^1_{LQR+KBF} + J^2_{LQR+KBF}}$	0.082	0.047	0.082
to *coupling*				

Table 20. Results from the averaged optimum plant noise intensity matrices for the decentralized grid structure.

(System eigenvalues in 1/sec.)

Observer 1: $V_1 = 2.858I$
Observer 2: $V_1 = 0.370I$

Poles	*Individual*	*Coupled*	2 – *disabled*	1 – *disabled*
Regulator 1	$-0.23 \pm j3.67$ $-0.36 \pm j5.59$ $-0.30 \pm j8.63$	$-0.29 \pm j3.46$ $-0.35 \pm j5.55$ $-0.29 \pm j8.60$	$-0.23 \pm j3.67$ $-0.36 \pm j5.59$ $-0.30 \pm j8.63$	$-0.034 \pm j3.46$ $-0.004 \pm j5.55$ $-0.004 \pm j8.60$
Observer 1	-129.72 -5.77 $-2.14 \pm j7.56$ $-2.43 \pm j4.24$	-129.75 -5.80 $-2.05 \pm j7.56$ $-2.46 \pm j4.14$	-129.75 -5.81 $-2.06 \pm j7.57$ $-2.44 \pm j4.14$	↑ *STABLE*
Regulator 2	$-0.50 \pm j20.61$ $-0.44 \pm j22.57$ $-0.56 \pm j31.15$	$-0.56 \pm j20.76$ $-0.42 \pm j22.58$ $-0.55 \pm j31.14$	$-0.042 \pm j20.75$ $-0.004 \pm j22.59$ $0.012 \pm j31.13$	$-0.50 \pm j20.61$ $-0.44 \pm j22.57$ $-0.56 \pm j31.15$
Observer 2	$-2.12 \pm j21.76$ $-4.94 \pm j21.42$ $-4.87 \pm j31.14$	$-2.13 \pm j21.77$ $-4.90 \pm j21.44$ $-4.87 \pm j31.16$	↑ *UNSTABLE*	$-2.13 \pm j21.77$ $-4.90 \pm j21.44$ $-4.87 \pm j31.16$

Table 21. Performance indices for the averaged case of the decentralized grid structure.

(Indices in lb-sec/in.)

PERFORMANCE INDICES		*Observer* 1: $V_1 = 2.858I$ *Observer* 2: $V_1 = 0.370I$
Individual	J^1_{LQR}	5.423
regulators	J^2_{LQR}	3.395
Including state	$J^1_{LQR+KBF}$	5.583
estimation	$J^2_{LQR+KBF}$	3.444
Including	$J^{1+2}_{LQR+KBF}$	9.703
coupling		
Increment due	$\dfrac{J^{1+2}_{LQR+KBF} - J^1_{LQR+KBF} - J^2_{LQR+KBF}}{J^1_{LQR+KBF} + J^2_{LQR+KBF}}$	0.075
to *coupling*		

CHAPTER 7. OBSERVER DESIGN IN THE PRESENCE OF KNOWN NOISE STATISTICS

In the previous chapters, it was assumed that the actual noise environment of the system was not known. The plant and measurement noise intensity matrices, V_1 and V_2, respectively, were fictitious and were used as design tools in order to develop an observer. In this chapter, a design procedure will again be developed for the observer, but, in this case, the actual noise environment will be assumed as known to the designer.

The actual noise environment is defined by the noise intensity matrices W_1 and W_2. For given (W_1, W_2), the optimum observer is the Kalman-Bucy Filter (KBF). It may be advantageous to use different noise matrices in the design of the observer. Let V_1 and V_2 be, respectively, the plant noise and measurement noise intensity matrices used in the design of the KBF. When V_1 and V_2 are different from W_1 and W_2, the resulting KBF is no longer statistically optimum with respect to the given noise environment. However, typically the stochastic performance index

$$J = E[x^T Q x + u^T R u] \qquad [7.1]$$

is not overly sensitive to the choice of (V_1, V_2) for a wide range of values, i.e., the optimum is rather flat. Therefore, it is reasonable to select V_1 and V_2 so as to suppress spillover instability, as long as the performance of the KBF is not overly compromised.

There are some reasons for possibly not wanting to operate at the statistical optimum, i.e., $V_1 = W_1$ and $V_2 = W_2$. The statistical optimum may produce unstable residual modes, or it may produce stable ones but with stability margins which are not deemed to be acceptable. There is also a chance that the optimal observer poles may not follow the *rule-of-thumb* of being between 3 to 10 times faster than the regulator poles. (This may be of concern if W_1 and W_2 are not known accurately.) These are all matters which must be considered. It should also be noted that the farther away V_1 and V_2 go from the statistical optimum, the greater the penalty to be paid in terms of deterioration in performance of the KBF.

In Chapter 5, an optimization procedure was developed which used information on the residual modes to minimize spillover (i.e., maximize the stability margin) of known residual modes while preserving robustness vis-à-vis the unknown dynamics. It incorporated the performance implicitly by imposing a maximum stability margin on the observer. The design method offered no way to include the actual noise statistics, (W_1, W_2), in the design, even if they are known with some accuracy. Therefore, the current objective is to expand the optimization procedure to include the performance explicitly, based on the actual plant and measurement noise statistics.

7.1. OBSERVER PERFORMANCE

The performance index of the stochastic linear quadratic regulator, J_{LQR}, in Equation [7.1] can be evaluated from the solution of an $n_A \times n_A$ Lyapunov Equation (Equations [2.3.9] and [2.3.28]) where n_A is the order of the controlled system. When the LQR is implemented on the reconstructed state from an observer, there is an additional penalty resulting from the imperfect knowledge of the state. The new value of the performance index, J, can be evaluated by solving a

$2n_A \times 2n_A$ Lyapunov Equation (Equations [2.4.41] and [2.4.42]). The following ratio can be taken as a measure of how well the observer works

$$F_{performance} = \frac{J - J_{LQR}}{J_{LQR}} \geq 0 \qquad [7.1.1]$$

J and J_{LQR} are evaluated with the actual noise statistics (W_1, W_2), and not those, (V_1, V_2), taken in the design of the KBF, so that $F_{performance}$ represents the performance deterioration for the actual noise statistics.

7.2. OPTIMIZATION OF NOISE INTENSITY MATRICES

The observer is obtained as the KBF whose plant noise intensity matrix, V_1, is the solution of the following optimization problem.

Find V_1, δ such that

$$\min \quad F = k_s[(\delta - t)_+^2 + \mu F_{performance}] \qquad [7.2.1]$$

subject to the constraints

$$Re(\lambda_i) < \delta \qquad [7.2.2]$$

$$\delta < 0 \qquad [7.2.3]$$

The parameter μ is used to weight the objectives of spillover stability and performance. t is the minimum desired stability margin, the final value of δ is the actual stability margin (Figure 23), the

λ_i's are all the composite (controlled + residual) eigenvalues, and $[a]_+ = \max(a, 0)$. The spillover part does not contribute to the objective function if the real parts of all the poles are smaller than t. In that case, the design is based on performance only. The constant k_s is used for scaling.

In the above procedure, the measurement noise intensity matrix, V_2, can be taken either according to the MESS (Model Error Sensitivity Suppression) Method [23, 24], so as to minimize the observation spillover, or set equal to W_2, the actual noise.

Note that if t is set to a large value so that the spillover part does not contribute to the objective function, and if $V_2 = W_2$, then the optimal solution will correspond to $V_1 = W_1$, the actual plant noise intensity matrix. This means that the optimum observer will be the KBF corresponding to (W_1, W_2) which minimizes J in Equation [7.1.1]. The same conclusion holds for extremely large μ causing the performance term to be dominant in Equation [7.2.1] and the spillover term to be negligible.

In this formulation, the number of design variables is equal to $n_A^2 + 1$. To reduce the number of design variables, V_1 was assumed to be either diagonal

$$V_1 = diag(v_i^2) \qquad [7.2.4]$$

or of the form

$$V_1 = aa^T \qquad [7.2.5]$$

where a is a vector. This reduces the number of design variables in the optimization to $n_A + 1$. In Chapters 5 and 6, it was shown that these special forms of V_1 produced virtually the same improvements in spillover alleviation as the full V_1.

7.3. DIRECT DESIGN OF OBSERVER GAIN MATRIX

In the foregoing formulation, the observer gain matrix is obtained as a KBF with noise intensity matrices, V_1 and V_2. It requires the solution of a nonlinear matrix Riccati Equation which may become difficult if the dimension of the system becomes large. An alternative formulation for the observer design, which does not require multiple solutions of the Riccati Equation, is to take the elements of the observer gain matrix, K_e, as design variables instead of the elements of V_1.

The KBF corresponding to the actual noise statistics, (W_1, W_2), is taken as a starting point. If all the residual modes satisfy the condition

$$Re(\lambda_i) < t \qquad [7.3.1]$$

an optimum solution has been found. If condition [7.3.1] is not satisfied, the observer gain matrix, K_e, is obtained as the solution of the following optimization problem.

Find K_e, δ such that

$$\min \quad F = k_s[(\delta - t)_+^2 + \mu F_{performance}] \qquad [7.3.2]$$

subject to the constraints

$$Re(\lambda_i) < \delta \qquad [7.3.3]$$

$$\delta < 0 \qquad [7.3.4]$$

The objective function and constraints are the same as before, but the design variables are now the elements of the gain matrix, K_e, rather than those of the plant noise intensity matrix, V_1. The resulting observer will no longer be a KBF (unless condition [7.3.1] is satisfied) and will not enjoy its properties.

The benefit of the foregoing formulation is that the solution of the Riccati Equation is not required anymore within the optimization process. The evaluation of the objective function requires only the solution of the linear matrix Lyapunov Equation. The number of design variables is now $n_A n_z + 1$, where n_z is the number of outputs of the system. It cannot be reduced by making assumptions on the structure of the matrix as in the previous formulation.

Again, a stable solution cannot be guaranteed, but the optimal value of δ, if positive, gives the minimum amount of passive damping which is necessary to achieve stability. If it is judged too large, the value of μ may be reduced in the objective function, to put less emphasis on performance and more on spillover. This is shown in Figure 27. Part (a) of the figure shows the individual contributions to the objective function, F, i.e., the performance contribution, $F_{performance}$, and the stability contribution, $(\delta - t)_+^2$. Part (b) of the figure shows the summation of the two contributions subject to the weighting parameter, μ, on $F_{performance}$. For a given μ_1, a minimum can be found, i.e., δ_{OPT}. If μ is lowered to the value $\mu_2 < \mu_1$, less emphasis is placed on the performance and more on the stability margin, so δ_{OPT} would move leftward in the negative direction.

The NEWSUMT-A program [88, 89] was used for optimization where the derivatives of the constraints and the objective function were calculated by finite difference. The L-A-S program [86, 87] was used for control calculations.

7.4. BEAM EXAMPLE

Once again, the Balas [1] beam example (Figure 17) is used to demonstrate the proposed method. The beam is controlled by one actuator located at the 1/6 position and a displacement sensor located at the 5/6 position. The state variables in the problem are modal amplitudes and reduced modal velocities. The first three modes are controlled by a Linear Quadratic Regulator (LQR) based on the reconstructed state obtained by the Kalman-Bucy Filter (KBF), while the

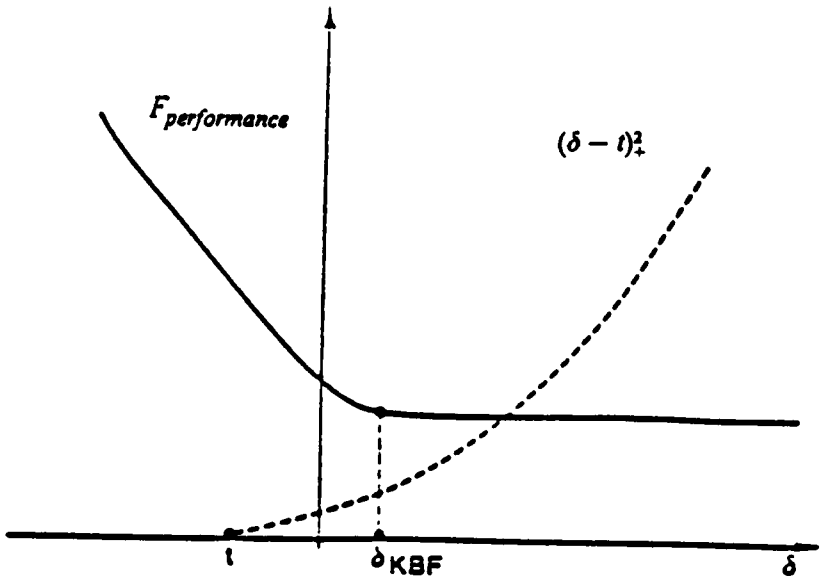

(a)

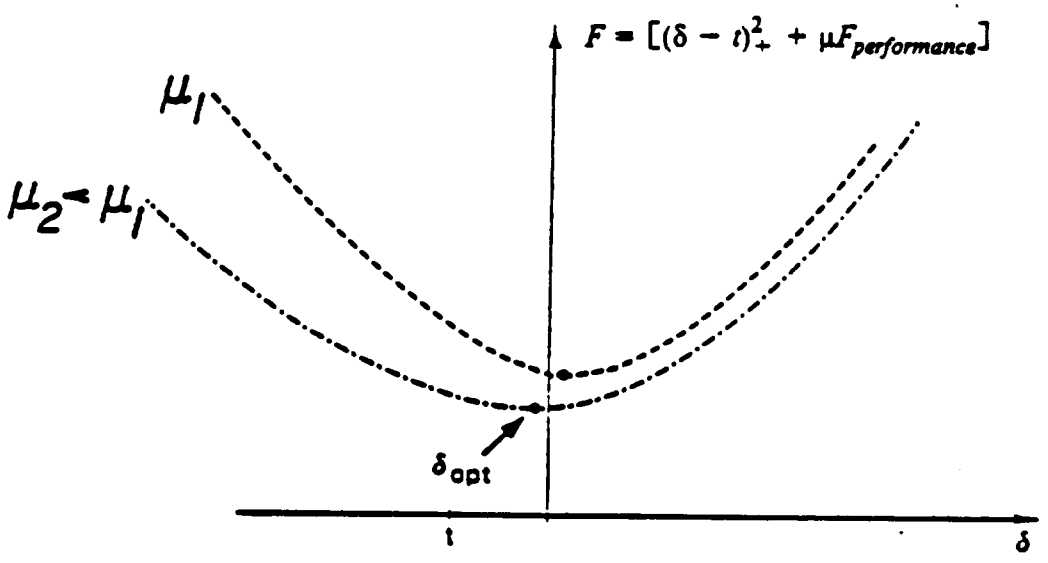

(b)

Figure 27. (a) Contributions of performance and stability to the objective function as functions of the stability margin. (b) Effect of the weighting parameter on the objective function.

fourth mode acts as the known residual mode. The value of the stochastic performance index based on perfect knowledge of the state is denoted J_{LQR}.

The actual noise statistics were assumed to be $W_1 = I$ and $W_2 = 0.02$. The statistically optimum KBF corresponds to the case when $V_1 = W_1$ and $V_2 = W_2$, and its properties are given in Table 22.

For the optimization, t was taken to equal $-0.100\ \text{sec}^{-1}$, k_r was set at 100, and V_2 was taken as equal to W_2, the actual measurement noise. A tracing method was used for each of the designs, i.e., the optimum V_1 (or K_c) for one value of μ was used as the initial solution for the next value of μ.

It should be mentioned that there were difficulties in using NEWSUMT-A and the tracing approach. For different initial design conditions, different optima were produced. These optima varied appreciably in terms of controller speeds and performance degradation. Yet, in terms of the objective function [7.2.1], the difference was typically between 1% and 4%. (One example of this occurring will be presented.) NEWSUMT-A is not sensitive enough to pick up such small differences. Because of this, several initial design conditions were used. Only the best results obtained will be presented here.

The results for the observer design based on optimizing the matrices V_1 and K_c based on spillover and performance considerations are given in Figures 28 - 31 and Tables 23 - 28 as a function of the weighting parameter, μ. Figures 28 - 30 show the individual δ vs. J plots for each of the designs considered, i.e., $V_1 = diag(v_i^2)$, $V_1 = aa^T$, and K_c. Figure 31 overlaps these three plots in order to readily compare them. Tables 23 - 28 list the observer poles, the residual poles, the performance degradation, the actual designs, and their corresponding observer gain matrices, K_c. It should be noted that for each design, μ was allowed to vary from $\mu = 10000.$ to $\mu = 0.001$. Eight different μ's were considered in each design.

It is shown that substantial gains in the stability of the residual mode can be obtained without a great loss of performance. For example, for $\mu = 0.001$, the $V_1 = diag(v_i^2)$ design produces $\delta = -0.08104\ \text{sec}^{-1}$ and $J = 8686.\ \text{lb} - \text{sec}/in$; the $V_1 = aa^T$ design produces $\delta = -0.10006\ \text{sec}^{-1}$

Table 22. Statistical optimum KBF for the Balas beam.

$(V_1 = W_1 = I \text{ and } V_2 = W_2 = 0.02.)$

(System poles in 1/sec.)

(Performance indices in lb-sec/in.)

Observer poles	$-3.372 \pm j9.866$ $-5.988 \pm j39.472$ $-6.996 \pm j88.813$
Residual poles (4th)	$-0.010958 \pm j157.87$
$J_{OPT} = J$	7760.0
J_{LQR}	6267.6
K_c^T	(9.974 −9.857 9.608 0.716 −1.687 2.774)

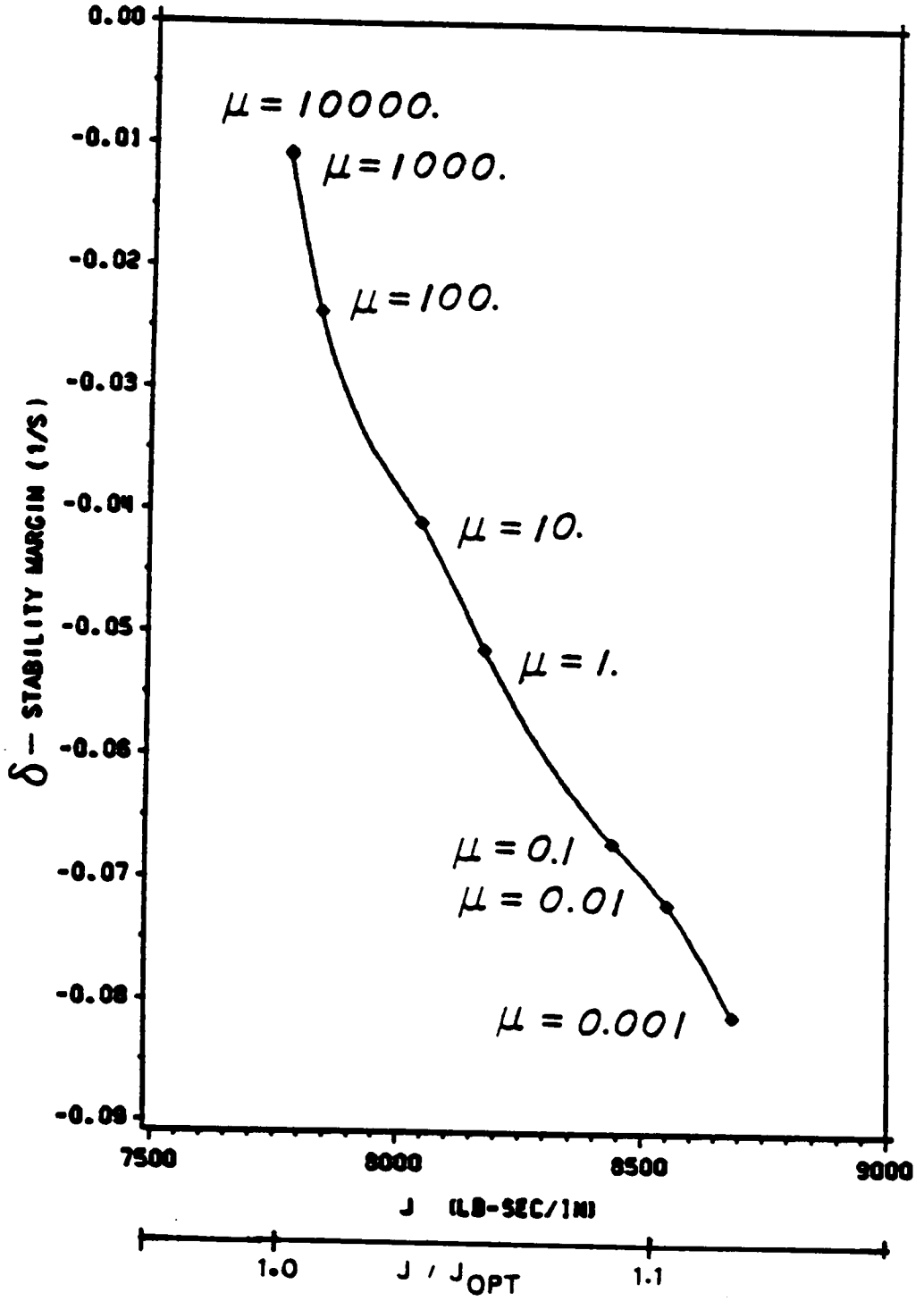

Figure 28. Stability margin vs. performance index for the Balas beam. [$V_1 = diag(v_i^2)$.]

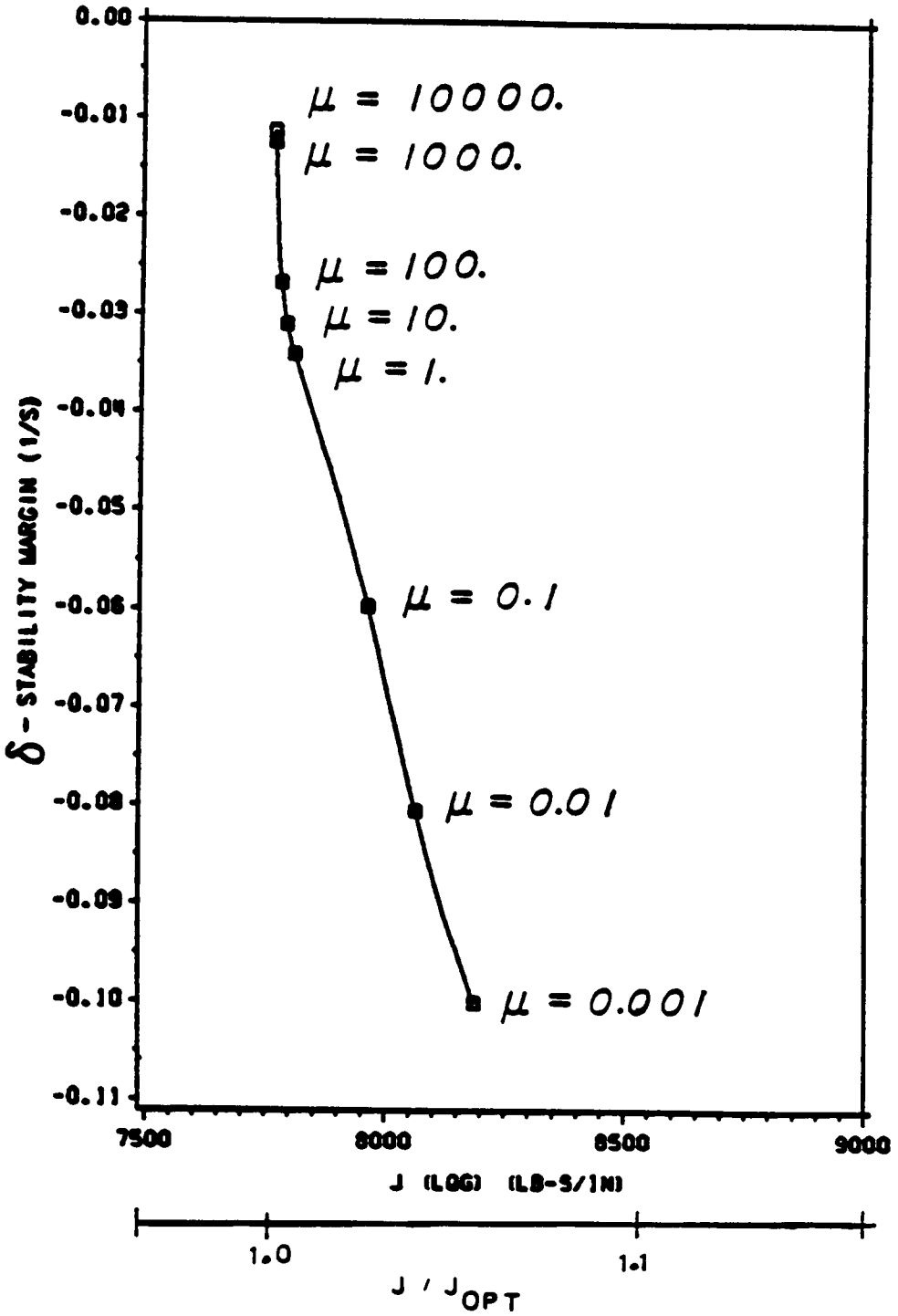

Figure 29. Stability margin vs. performance index for the Balas beam. $[V_1 = aa^T.]$

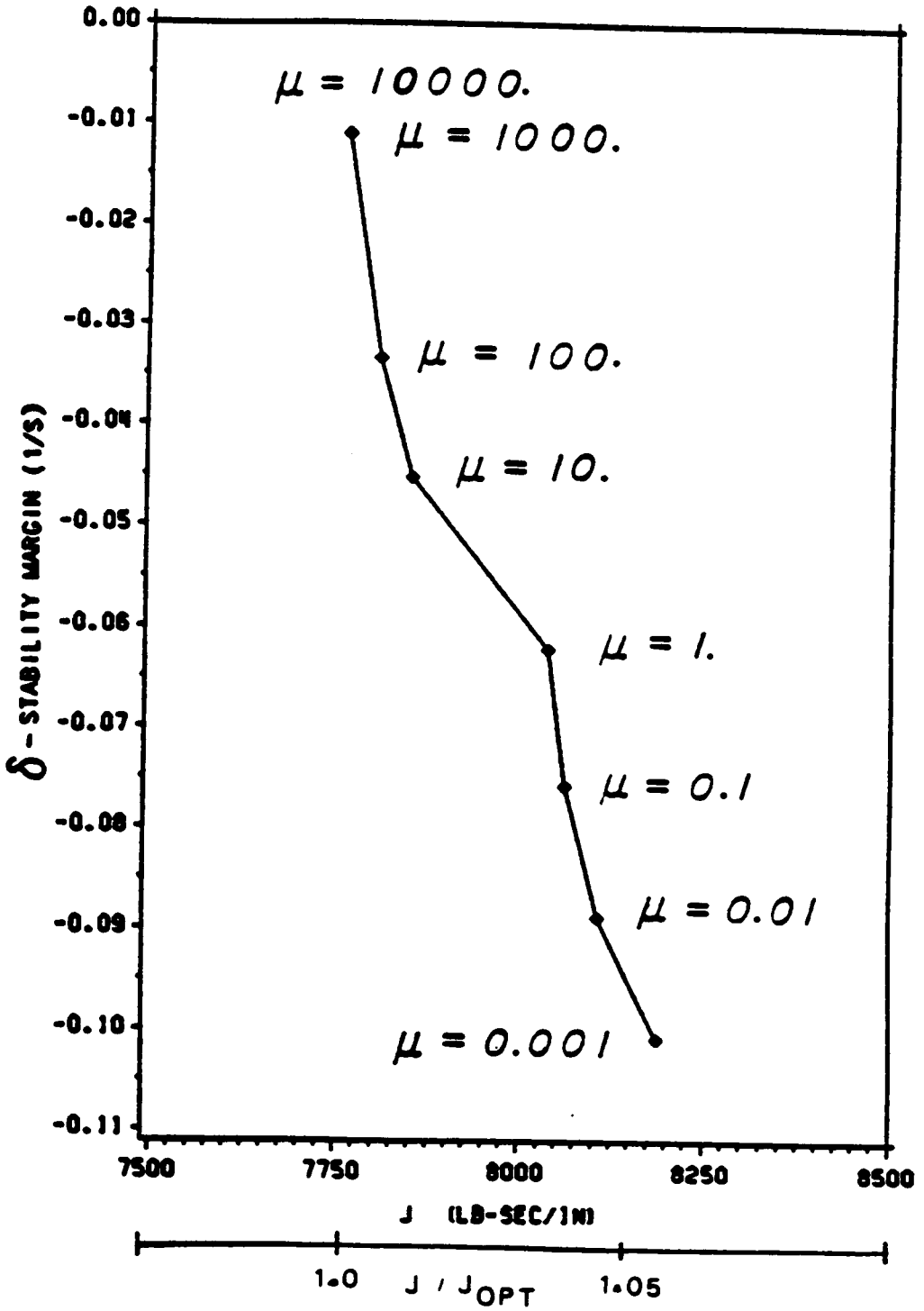

Figure 30. Stability margin vs. performance index for the Balas beam. $[K_c]$

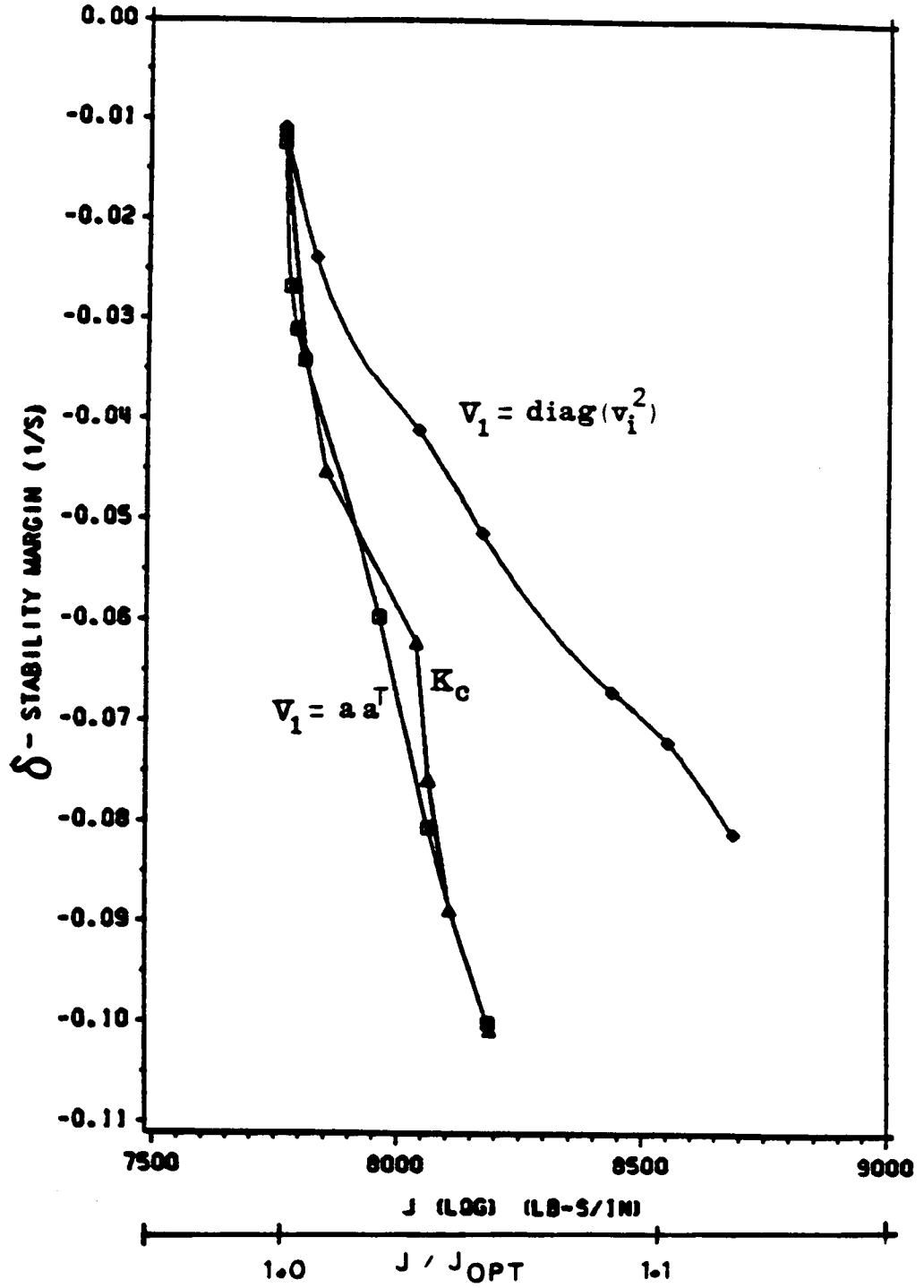

Figure 31. Stability margin vs. performance index for various designs of the Balas beam.

Table 23. Optimization results for the Balas beam. $[V_1 = diag(v_i^2).]$

(System eigenvalues in 1/sec.)

Weight	$\mu = 10000.$	$\mu = 1000.$	$\mu = 100.$	$\mu = 10.$
Observer	$-3.40 \pm j\,9.87$ $-5.85 \pm j\,39.48$ $-6.92 \pm j\,88.81$	$-3.27 \pm j\,9.78$ $-5.83 \pm j\,39.54$ $-7.26 \pm j\,88.82$	$-3.88 \pm j\,9.50$ $-8.19 \pm j\,39.12$ $-9.92 \pm j\,89.12$	$-4.87 \pm j\,9.71$ $-8.83 \pm j\,39.23$ $-14.49 \pm j\,89.77$
Residual (4th)	$-0.011 \pm j\,157.87$	$-0.011 \pm j\,157.86$	$-0.024 \pm j\,157.84$	$-0.041 \pm j\,157.80$
J/J_{OPT}	1.00001	1.0001	1.0086	1.0359

Weight	$\mu = 1.$	$\mu = 0.1$	$\mu = 0.01$	$\mu = 0.001$
Observer	$-8.09 \pm j\,11.73$ $-11.21 \pm j\,40.91$ $-16.49 \pm j\,90.08$	$-10.21 \pm j\,11.70$ $-11.02 \pm j\,40.57$ $-20.95 \pm j\,90.73$	$-10.83 \pm j\,11.71$ $-11.47 \pm j\,40.61$ $-22.68 \pm j\,91.00$	-10.12 -45.60 $-13.43 \pm j\,33.47$ $-23.12 \pm j\,88.72$
Residual (4th)	$-0.051 \pm j\,157.78$	$-0.067 \pm j\,157.73$	$-0.072 \pm j\,157.71$	$-0.081 \pm j\,157.67$
J/J_{OPT}	1.0529	1.0872	1.1017	1.1193

Table 24. Optimum designs for the Balas beam. $[V_1 = diag(v_i^2).]$

(With corresponding K_c values)

μ	$V_1 = diag(v_i^2)$
10000.	$V_1 = diag(1.006\ \ 0.946\ \ 0.979\ \ 1.019\ \ 0.963\ \ 0.975)$ $K_c^T = (10.033\ \ -9.628\ \ 9.506\ \ 0.759\ \ -1.659\ \ 2.707)$
1000.	$V_1 = diag(1.098\ \ 0.797\ \ 1.038\ \ 0.775\ \ 1.106\ \ 1.112)$ $K_c^T = (9.667\ \ -9.613\ \ 9.969\ \ 0.400\ \ -1.656\ \ 2.839)$
100.	$V_1 = diag(2.013\ \ 2.772\ \ 0.711\ \ 0.689\ \ 1.166\ \ 3.434)$ $K_c^T = (11.619\ \ -13.881\ \ 13.260\ \ -0.328\ \ -2.064\ \ 5.607)$
10.	$V_1 = diag(2.704\ \ 3.245\ \ 0.219\ \ 2.086\ \ 1.789\ \ 8.797)$ $K_c^T = (15.445\ \ -15.622\ \ 18.616\ \ 0.949\ \ -2.766\ \ 10.210)$
1.	$V_1 = diag(4.118\ \ 0.504\ \ 0.272\ \ 19.441\ \ 8.610\ \ 11.262)$ $K_c^T = (31.393\ \ -18.548\ \ 18.848\ \ 13.870\ \ -10.567\ \ 14.881)$
0.1	$V_1 = diag(9.980\ \ 1.224\ \ 0.502\ \ 30.535\ \ 8.959\ \ 18.717)$ $K_c^T = (40.697\ \ -19.163\ \ 22.703\ \ 19.223\ \ -11.913\ \ 21.108)$
0.01	$V_1 = diag(12.540\ \ 1.539\ \ 0.593\ \ 36.169\ \ 10.204\ \ 22.246)$ $K_c^T = (44.475\ \ -20.297\ \ 23.801\ \ 21.388\ \ -13.234\ \ 23.989)$
0.001	$V_1 = diag(81.400\ \ 35.599\ \ 0.173\ \ 63.364\ \ 0.507\ \ 34.743)$ $K_c^T = (80.949\ \ -34.851\ \ 20.437\ \ 26.182\ \ -24.305\ \ 36.444)$

Table 25. Optimization results for the Balas beam. $[V_1 = aa^T.]$

(System eigenvalues in 1/sec.)

Weight	$\mu = 10000.$	$\mu = 1000.$	$\mu = 100.$	$\mu = 10.$
Observer	$-3.32 \pm j\,9.83$ $-6.03 \pm j\,39.49$ $-6.99 \pm j\,88.86$	$-3.08 \pm j\,9.54$ $-6.12 \pm j\,39.55$ $-7.00 \pm j\,89.01$	$-3.51 \pm j\,10.51$ $-5.94 \pm j\,38.67$ $-7.79 \pm j\,89.61$	$-3.62 \pm j\,10.81$ $-5.91 \pm j\,38.31$ $-8.33 \pm j\,89.70$
Residual (4*th*)	$-0.011 \pm j\,157.87$	$-0.012 \pm j\,157.87$	$-0.027 \pm j\,157.86$	$-0.031 \pm j\,157.85$
J/J_{OPT}	1.0000	1.0001	1.0020	1.0036

Weight	$\mu = 1.$	$\mu = 0.1$	$\mu = 0.01$	$\mu = 0.001$
Observer	$-3.98 \pm j\,10.92$ $-5.72 \pm j\,38.14$ $-8.91 \pm j\,89.80$	$-3.11 \pm j\,12.25$ $-13.78 \pm j\,37.48$ $-9.33 \pm j\,90.80$	$-9.36 \pm j\,18.19$ $-10.94 \pm j\,35.00$ $-10.28 \pm j\,91.05$	$-15.82 \pm j\,20.60$ $-5.94 \pm j\,34.92$ $-11.03 \pm j\,91.15$
Residual (4*th*)	$-0.034 \pm j\,157.84$	$-0.060 \pm j\,157.84$	$-0.081 \pm j\,157.82$	$-0.100 \pm j\,157.79$
J/J_{OPT}	1.0057	1.0259	1.0389	1.0549

Table 26. Optimum designs for the Balas beam. $[V_1 = aa^T.]$

(With corresponding K_c values)

μ	$V_1 = aa^T$
10000.	$a^T = (-0.873 \quad -1.285 \quad 0.676 \quad -1.086 \quad 0.622 \quad 1.241)$ $K_c^T = (9.832 \quad -9.945 \quad 9.580 \quad 0.576 \quad -1.718 \quad 2.830)$
1000.	$a^T = (-1.076 \quad -1.242 \quad 0.612 \quad -0.708 \quad 0.768 \quad 1.279)$ $K_c^T = (9.099 \quad -10.178 \quad 9.560 \quad -0.428 \quad -1.723 \quad 3.018)$
100.	$a^T = (-0.561 \quad -0.845 \quad 0.179 \quad -1.402 \quad 1.146 \quad 1.593)$ $K_c^T = (10.344 \quad -10.063 \quad 10.494 \quad 2.650 \quad -0.372 \quad 4.283)$
10.	$a^T = (-0.048 \quad -0.800 \quad 0.147 \quad -1.580 \quad 1.181 \quad 1.715)$ $K_c^T = (10.593 \quad -10.086 \quad 11.228 \quad 3.562 \quad 0.226 \quad 4.703)$
1.	$a^T = (0.137 \quad -0.745 \quad 0.135 \quad -1.733 \quad 1.181 \quad 1.842)$ $K_c^T = (11.574 \quad -9.863 \quad 11.990 \quad 4.146 \quad 0.446 \quad 5.168)$
0.1	$a^T = (0.184 \quad -0.807 \quad 0.032 \quad -1.940 \quad 3.231 \quad 2.049)$ $K_c^T = (11.448 \quad -23.437 \quad 11.063 \quad 7.673 \quad -2.314 \quad 9.361)$
0.01	$a^T = (0.149 \quad -0.617 \quad -0.082 \quad -6.923 \quad 2.558 \quad 2.258)$ $K_c^T = (32.211 \quad -18.182 \quad 11.390 \quad 36.880 \quad -3.944 \quad 11.206)$
0.001	$a^T = (0.127 \quad -0.251 \quad -0.044 \quad -11.323 \quad 1.857 \quad 2.412)$ $K_c^T = (46.721 \quad -12.821 \quad 11.915 \quad 65.027 \quad -3.329 \quad 12.205)$

Table 27. Optimization results for the Balas beam. $[K_c.]$

(System eigenvalues in 1/sec.)

Weight	$\mu = 10000.$	$\mu = 1000.$	$\mu = 100.$	$\mu = 10.$
Observer	$-3.47 \pm j\,9.89$ $-6.00 \pm j\,39.49$ $-6.99 \pm j\,88.82$	$-3.74 \pm j\,9.85$ $-6.10 \pm j\,39.70$ $-6.99 \pm j\,88.90$	$-5.39 \pm j\,8.23$ $-8.41 \pm j\,39.14$ $-7.92 \pm j\,90.48$	$-6.70 \pm j\,8.45$ $-9.30 \pm j\,37.18$ $-9.02 \pm j\,90.41$
Residual (4th)	$-0.011 \pm j\,157.87$	$-0.011 \pm j\,157.87$	$-0.033 \pm j\,157.86$	$-0.045 \pm j\,157.84$
J/J_{OPT}	1.0000	1.00004	1.0060	1.0117

Weight	$\mu = 1.$	$\mu = 0.1$	$\mu = 0.01$	$\mu = 0.001$
Observer	$-10.82 \pm j\,19.60$ $-10.67 \pm j\,41.65$ $-11.90 \pm j\,89.86$	$-11.95 \pm j\,20.11$ $-9.36 \pm j\,39.47$ $-11.76 \pm j\,90.43$	$-14.30 \pm j\,20.40$ $-7.12 \pm j\,36.90$ $-11.50 \pm j\,90.73$	$-16.05 \pm j\,20.45$ $-5.63 \pm j\,35.10$ $-11.12 \pm j\,91.15$
Residual (4th)	$-0.062 \pm j\,157.81$	$-0.076 \pm j\,157.80$	$-0.089 \pm j\,157.80$	$-0.101 \pm j\,157.79$
J/J_{OPT}	1.0358	1.0390	1.0448	1.0554

Table 28. Optimum designs for the Balas beam. $[K_c.]$

μ	K_c
10000.	$K_c^T = (10.274 \quad -9.861 \quad 9.591 \quad 0.847 \quad -1.774 \quad 2.799)$
1000.	$K_c^T = (11.245 \quad -10.012 \quad 9.520 \quad 0.973 \quad -2.315 \quad 2.997)$
100.	$K_c^T = (16.370 \quad -14.728 \quad 9.777 \quad -2.219 \quad -3.850 \quad 6.756)$
10.	$K_c^T = (18.972 \quad -16.976 \quad 11.198 \quad -0.244 \quad -2.115 \quad 8.112)$
1.	$K_c^T = (48.852 \quad -11.736 \quad 12.640 \quad 66.258 \quad -13.917 \quad 10.901)$
0.1	$K_c^T = (48.250 \quad -11.682 \quad 12.517 \quad 66.174 \quad -10.468 \quad 11.484)$
0.01	$K_c^T = (48.107 \quad -11.543 \quad 12.503 \quad 66.145 \quad -6.164 \quad 11.805)$
0.001	$K_c^T = (47.260 \quad -12.359 \quad 12.054 \quad 65.876 \quad -3.152 \quad 12.240)$

and $J = 8186.4$ lb $-$ sec $/in$; and the K_c design produces $\delta = -0.10076$ sec^{-1} and $J = 8189.6$ lb $-$ sec $/in$.

As expected, as μ decreases in value, the performance index, J, increases in magnitude. This indicates a deterioration in performance. At the same time, the system stability margin increases since the optimizer places more emphasis on a stable system at the cost of performance.

One also sees that the design $V_1 = aa^T$ is more effective than $V_1 = diag(v_i^2)$ even though both have six design variables. The case $V_1 = aa^T$ fully populates the V_1 matrix, and, for a given δ, produces designs which give J's which are appreciably lower than those of the $V_1 = diag(v_i^2)$ design. The $V_1 = aa^T$ design also gives much slower observers than the $V_1 = diag(v_i^2)$ design. These differences are most obvious when μ is small.

Before proceeding further, it was mentioned before that there were difficulties in using NEWSUMT-A and the tracing approach. Some of the difficulties can be illustrated by Figure 32 which presents the optimum δ vs. J curves for $V_1 = diag(v_i^2)$ (same as Figure 28) and for two $V_1 = aa^T$ curves. The two $V_1 = aa^T$ curves are the result of different initial conditions. The first $V_1 = aa^T$ curve (Case #1) is the same as that shown in Figure 29. The initial conditions for a were the results found from the deterministic constrained study (Tables 9 and 11). The second $V_1 = aa^T$ curve (Case #2) had the initial conditions of

$$a^T = (1 \quad 1 \quad 1 \quad 1 \quad 1 \quad 1)$$

(For completeness, the initial condition for $V_1 = diag(v_i^2)$ was $V_1 = I$.) These initial conditions were set at one value of μ, and the tracing method was applied for subsequent μ's. Although the Case #1 $V_1 = aa^T$ curve is appreciably better than the Case #2 $V_1 = aa^T$ curve, NEWSUMT-A was unable to find the Case #1 curve based on the initial condition $a^T = (1 \ 1 \ 1 \ 1 \ 1 \ 1)$. As it turns out, for a given μ, the objective function, F, from Equation [7.2.1] is smaller for the Case #1 curve than for the Case #2 curve, but the difference between the two curves is typically between 1 - 4%. NEWSUMT-A is not sensitive enough to pick up this small difference, or possibly the two are local optima. Initial design conditions played a significant role in the design process.

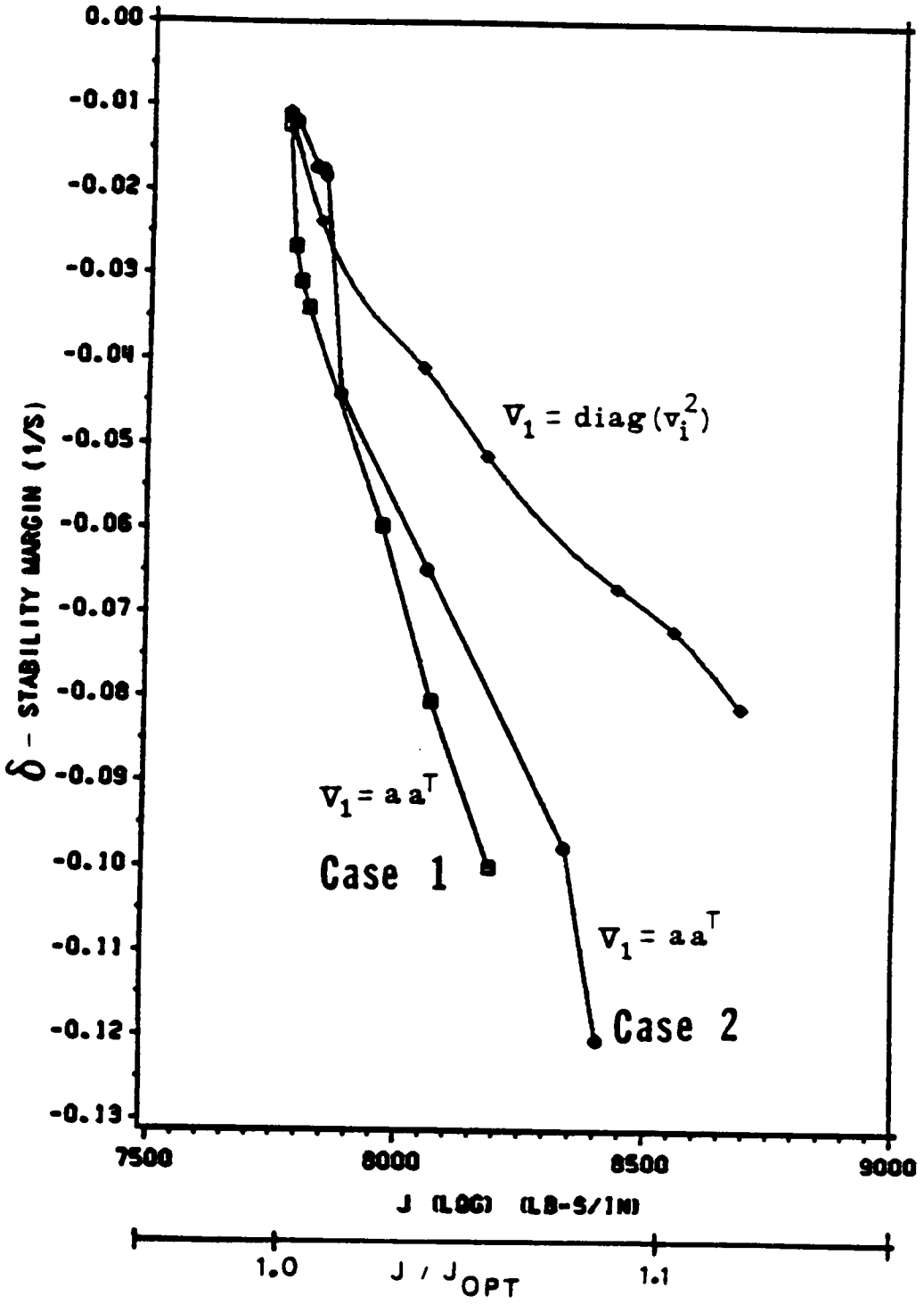

Figure 32. Comparison of the stability margin vs. performance index for various designs of the Balas beam.

Another comment about the Case #2 $V_1 = aa^T$ curve lies with its comparison to the $V_1 = diag(v_i^2)$ curve. For medium and large values of μ, the $V_1 = aa^T$ curve lies to the right of the $V_1 = diag(v_i^2)$ curve indicating that it is a somewhat worse design even though $V_1 = aa^T$ fully populates the V_1 matrix, and $V_1 = diag(v_i^2)$ does not.

As a final comment, although the designs of the Case #2 $V_1 = aa^T$ curve will not be presented here, they produced extremely fast observer speeds, whereas, the Case #1 curve was much slower, and, as a result, more realistic.

The case $V_1 = HH^T$ was not investigated since, from the deterministic studies, it was found to have negligible benefits at a great cost in computer time and in complicating the optimization problem by introducing many design variables. This sentiment is further reinforced when one analyzes the direct K_c designs which represent the most general case. The K_c designs (δ vs. J) are comparable to those of the $V_1 = aa^T$ designs. The resulting observer speeds are also comparable. The δ vs. J curve obtained by optimizing K_c should be to the left of the $V_1 = aa^T$ curve because any design obtained by optimizing V_1 can also be obtained by optimizing K_c. This holds for only part of the curve. The differences between the curves amount to less than 1% in the objective function [7.3.2], and NEWSUMT-A is not that sensitive. The $V_1 = aa^T$ case picks up most of the stability margin with low performance deterioration. The only advantage of the K_c formulation is that it does not require the solution of the nonlinear matrix Riccati Equation. However, this is not important for this low-order problem.

Also, although not apparent from Figures 28 - 31, the KBF design noise matrices correspond to the actual noise matrices (Table 22) for extremely large values of μ, i.e., a heavy penalty is placed on performance in the optimization process. For example, when $\mu = 10000.$, the optimum V_1 matrix for $V_1 = diag(v_i^2)$ becomes (see Table 24)

$$V_1 = diag(1.0061 \;\; 0.9458 \;\; 0.9791 \;\; 1.0187 \;\; 0.9633 \;\; 0.9749)$$

For the direct K_c design, the optimum K_c matrix becomes (see Table 28)

$$K_c^T = (10.274 \;\; -9.861 \;\; 9.591 \;\; 0.847 \;\; -1.774 \;\; 2.799)$$

which, again, is extremely close to the statistical optimum gain matrix (Table 22). Even for $V_1 = aa^T$, the results are surprisingly good. Even though $V_1 = aa^T$ can never take on the form of a diagonal matrix, i.e., the identity matrix - the form of W_1 in this problem, it still produces a gain matrix which is close to that attained for the statistical optimum (see Table 26), i.e., for $\mu = 10000.$,

$$a^T = (-0.873 \quad -1.285 \quad 0.676 \quad -1.086 \quad 0.622 \quad 1.241)$$

the corresponding K_c becomes

$$K_c^T = (9.832 \quad -9.945 \quad 9.580 \quad 0.576 \quad -1.718 \quad 2.830)$$

Figures 33 - 35 illustrate the root-locus plots of the optimum designs. They show the evolution of the closed-loop system poles (regulator + observer) for the different values of μ. As can be seen, as μ decreases in value (i.e., the stability margin of the residual poles increases), the observer poles (or at least one set) significantly increase their speed. For the $V_1 = diag(v_i^2)$ case, all three sets of observer poles essentially increase their speed. For the $V_1 = aa^T$ case, two of the three sets increase their speed, whereas, one set loops back on itself. And, for the K_c case, one set increases its speed, whereas, two sets loop back on themselves. The regulator poles are essentially fixed.

Stability robustness tests were also applied for three different damping ratios, i.e., $\zeta = 0.001$, 0.0025, and 0.005. Once again, the robustness tests were performed using the knowledge of the first eight modes of the beam in order to insure that the optimum controllers do not have any problems with the higher frequency modes which were not taken into account in this analysis.

The robustness test was satisfied for all the designs except for a few of the $V_1 = diag(v_i^2)$ designs, which produced the fast observer speeds (low μ and high K_c) at $\zeta = 0.001$ only. The case $\mu = 0.001$ and $\zeta = 0.001$ for $V_1 = diag(v_i^2)$ is shown in Figure 36. The violation involved only the fourth mode yet this mode was taken into account explicitly in the spillover analysis and was stable. For $\mu = 0.001$ and $\zeta = 0.001$, the $V_1 = aa^T$ (Figure 37) and K_c (Figure 38) designs are borderline. What is typically seen is that low emphasis on performance (low μ) produces higher observer gain

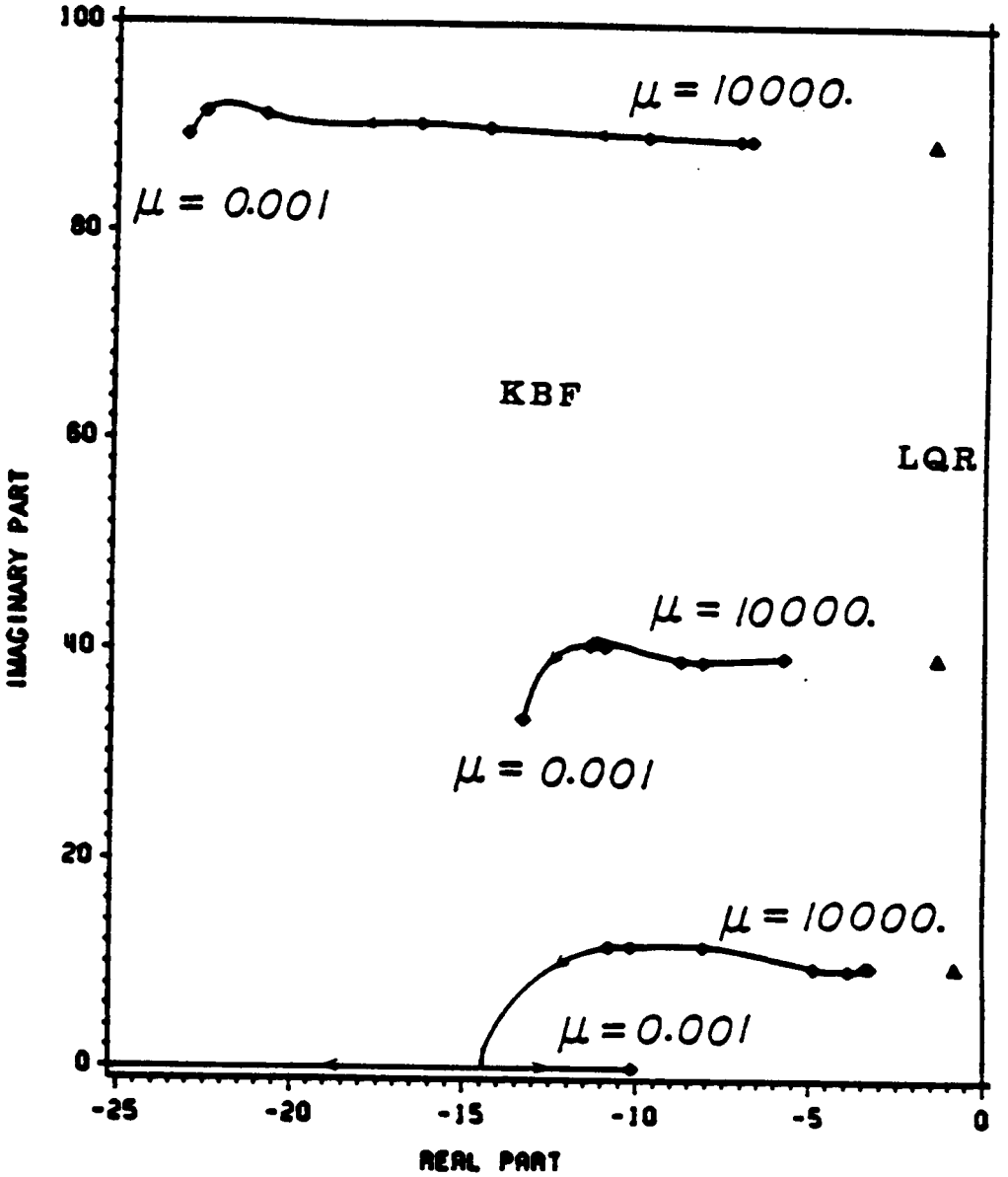

Figure 33. Evolution of the closed-loop poles as a function of the weighting parameter for the Balas beam. [$V_1 = diag(v_i^2)$.]

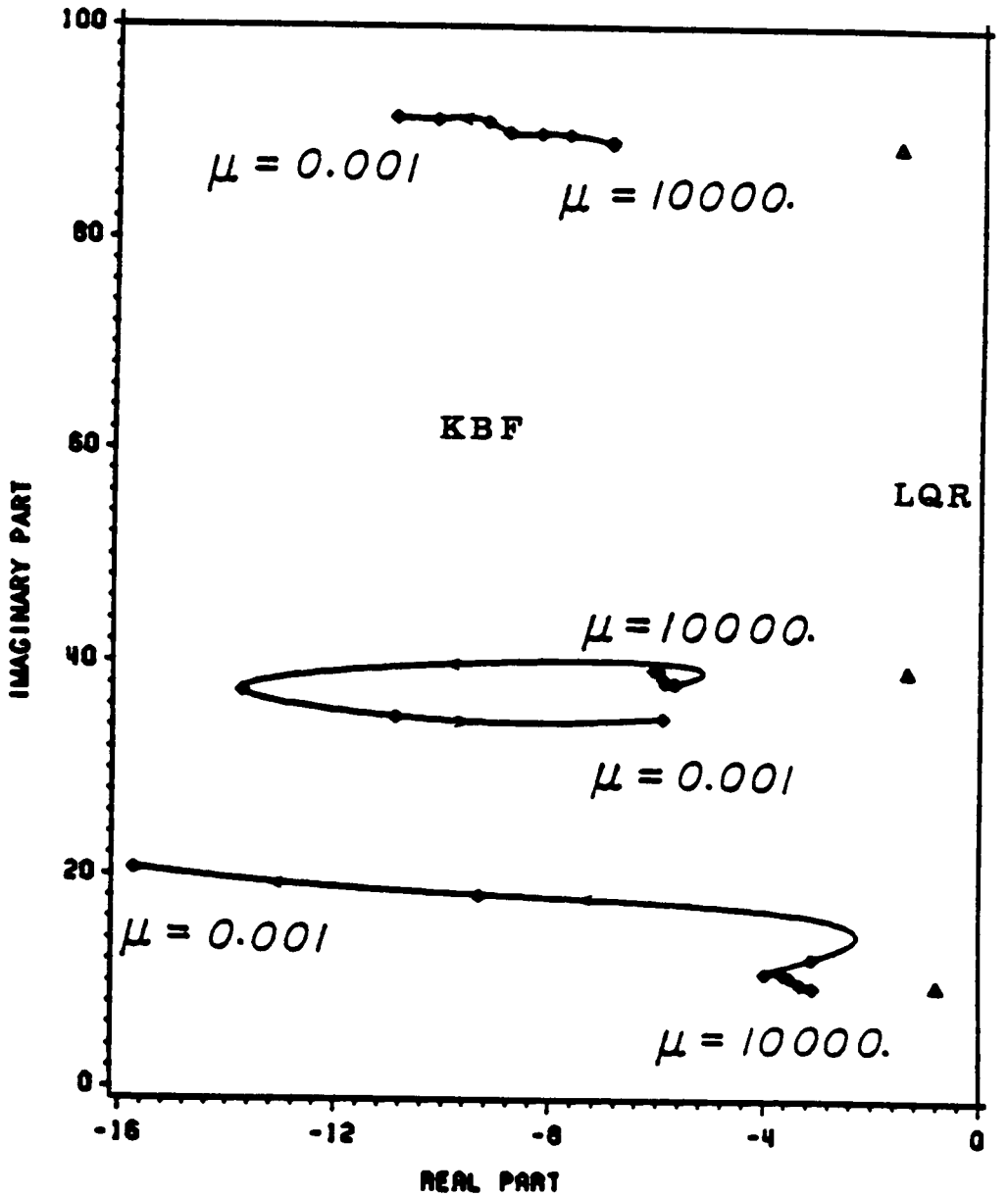

Figure 34. Evolution of the closed-loop poles as a function of the weighting parameter for the Balas beam. [$V_1 = aa^T$.]

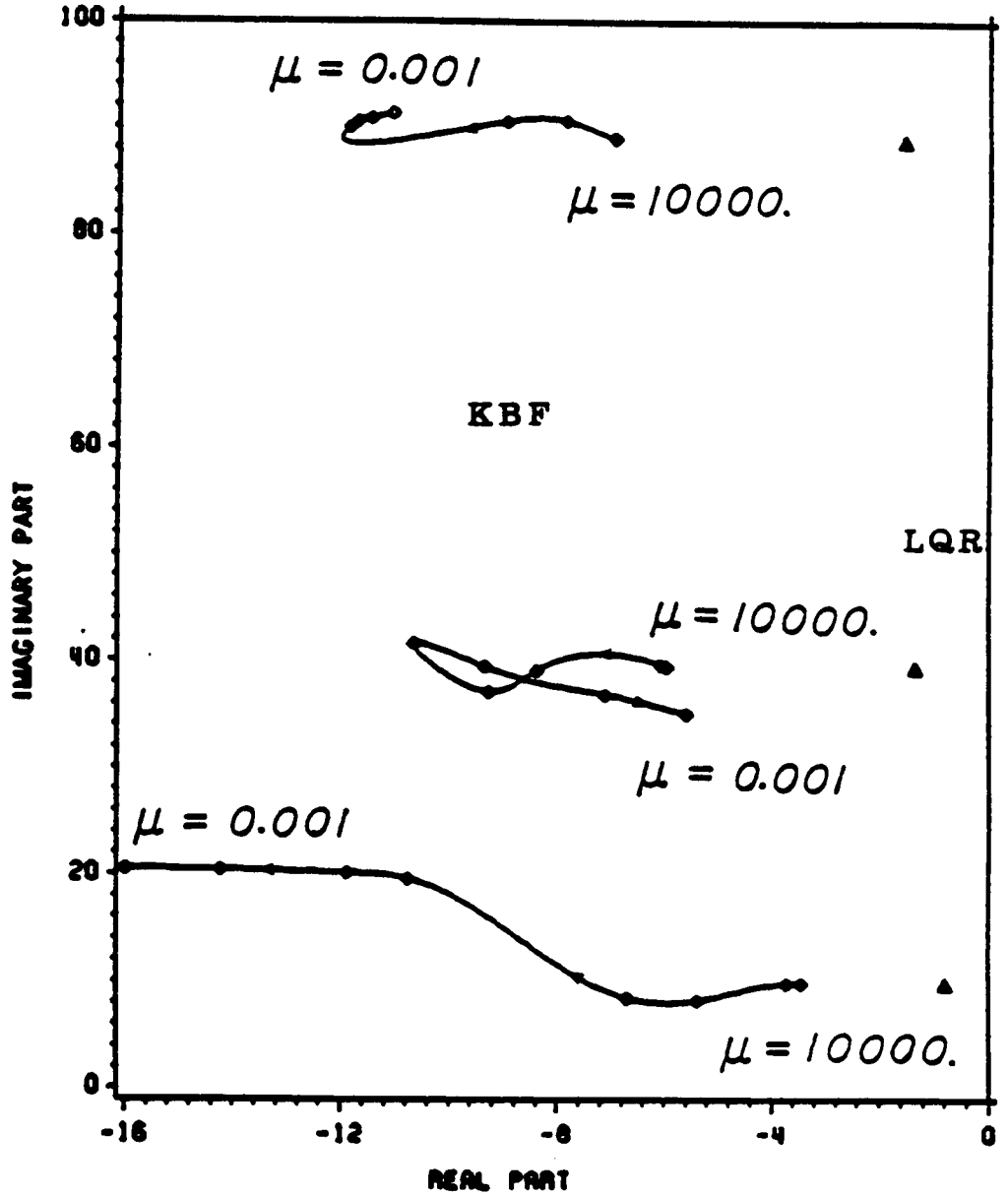

Figure 35. Evolution of the closed-loop poles as a function of the weighting parameter for the Balas beam. $[K_c.]$

matrices and faster observers (see Tables 23 - 28), and, therefore, the $\bar{\sigma}[G(j\omega)K(j\omega)]$ curve goes up in magnitude and, thus, has a potential of causing a robustness test violation in the high frequency domain response of low-damping structures. Low damped structures produce more appreciable peaks which cause this problem. As a result, low gain systems are generally recommended for large flexible space structures since they lower the $\bar{\sigma}[G(j\omega)K(j\omega)]$ curve. The designer is faced with the trade-off between spillover stabilization and performance degradation/stability robustness considerations.

All the designs have essentially the same number of design variables, and the computational costs, as demonstrated by the length of execution time involved on an IBM 3084 computer, for all eight μ designs combined are given in Table 29. The computer costs are comparable. The K_c design did not require the solution of a Riccati Equation, but the solution of the nonlinear matrix Riccati Equation is not the primary computational cost in the optimization procedure for this low-order problem.

7.5. GRID STRUCTURE EXAMPLE - MIMO CASE

The two observer design procedures were also applied to the grid structure (Figure 26) which is representative of Large Space Structures [107]. The plane grid structure was represented as a finite element model [108, 109]. The results of this model were incorporated in this numerical study. The design followed a centralized formulation of three inputs and three outputs (MIMO).

Three colocated actuator-and-sensor pairs were positioned at locations 1, 4, and 11 to control Modes 1 - 9 of the grid structure. Modes 10 - 20 act as the known residual modes. The colocation property was not used in that the full state is reconstructed in the controller design. Once again, the locations of the actuators and sensors for this numerical study do not represent the actual experimental configuration of sensors and actuators. With these actuator and sensor locations, both

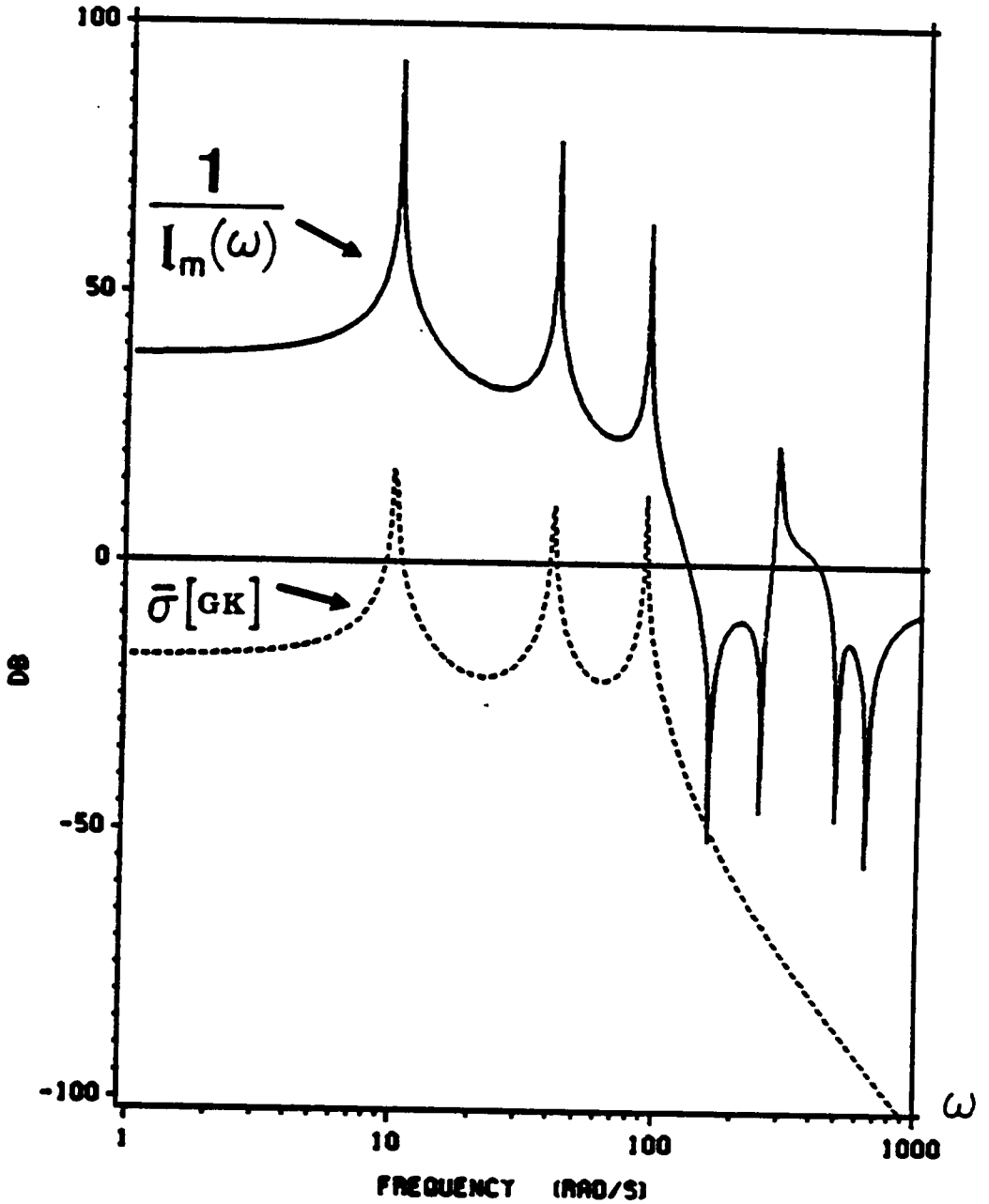

Figure 36. Robustness plot of the loop transfer matrix for the optimized LQG Balas beam design. [$V_1 = diag(v_i^2)$, $\mu = 0.001$, $\zeta = 0.001$.]

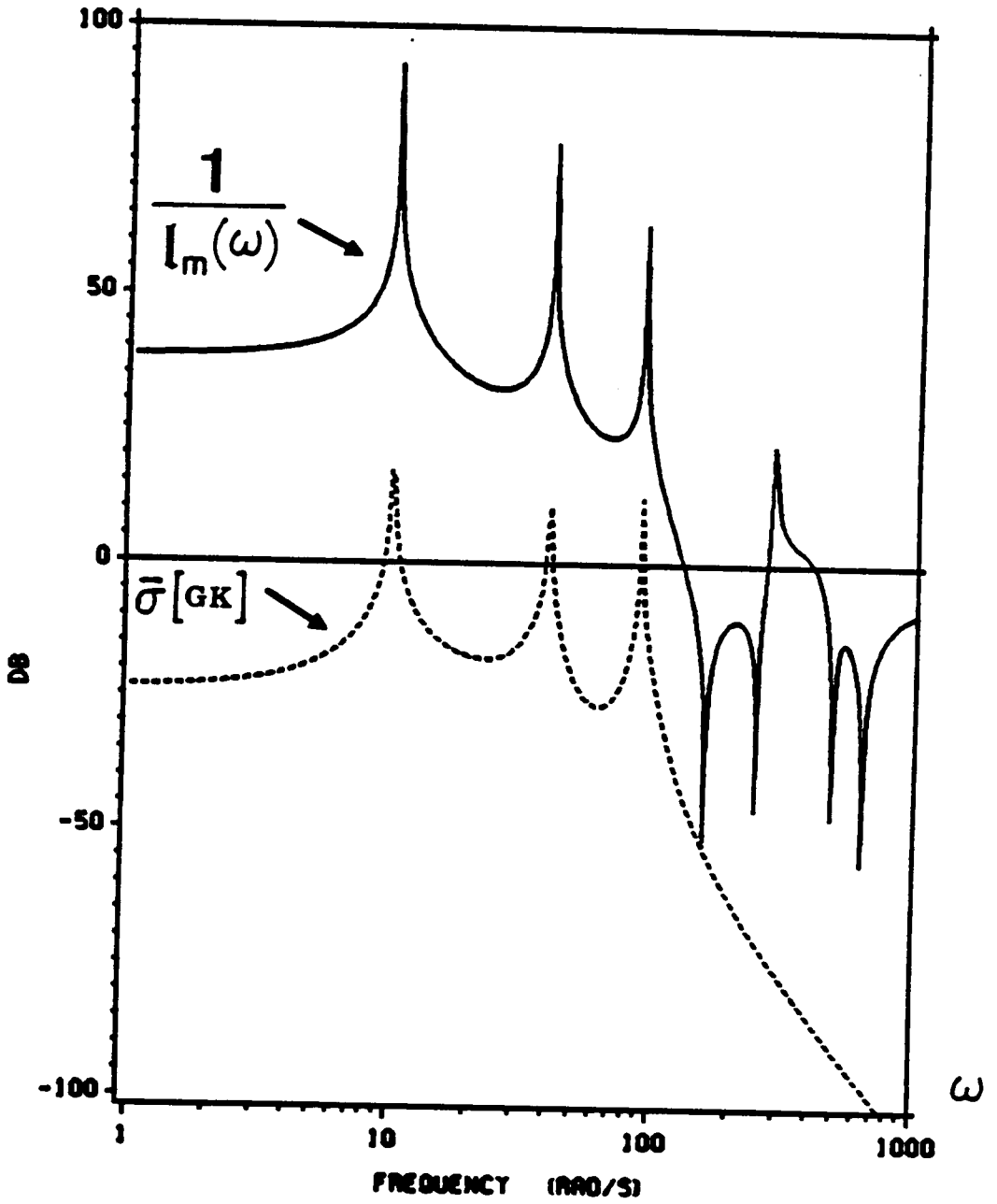

Figure 37. Robustness plot of the loop transfer matrix for the optimized LQG Balas beam design. [$V_1 = aa^T$, $\mu = 0.001$, $\zeta = 0.001$.]

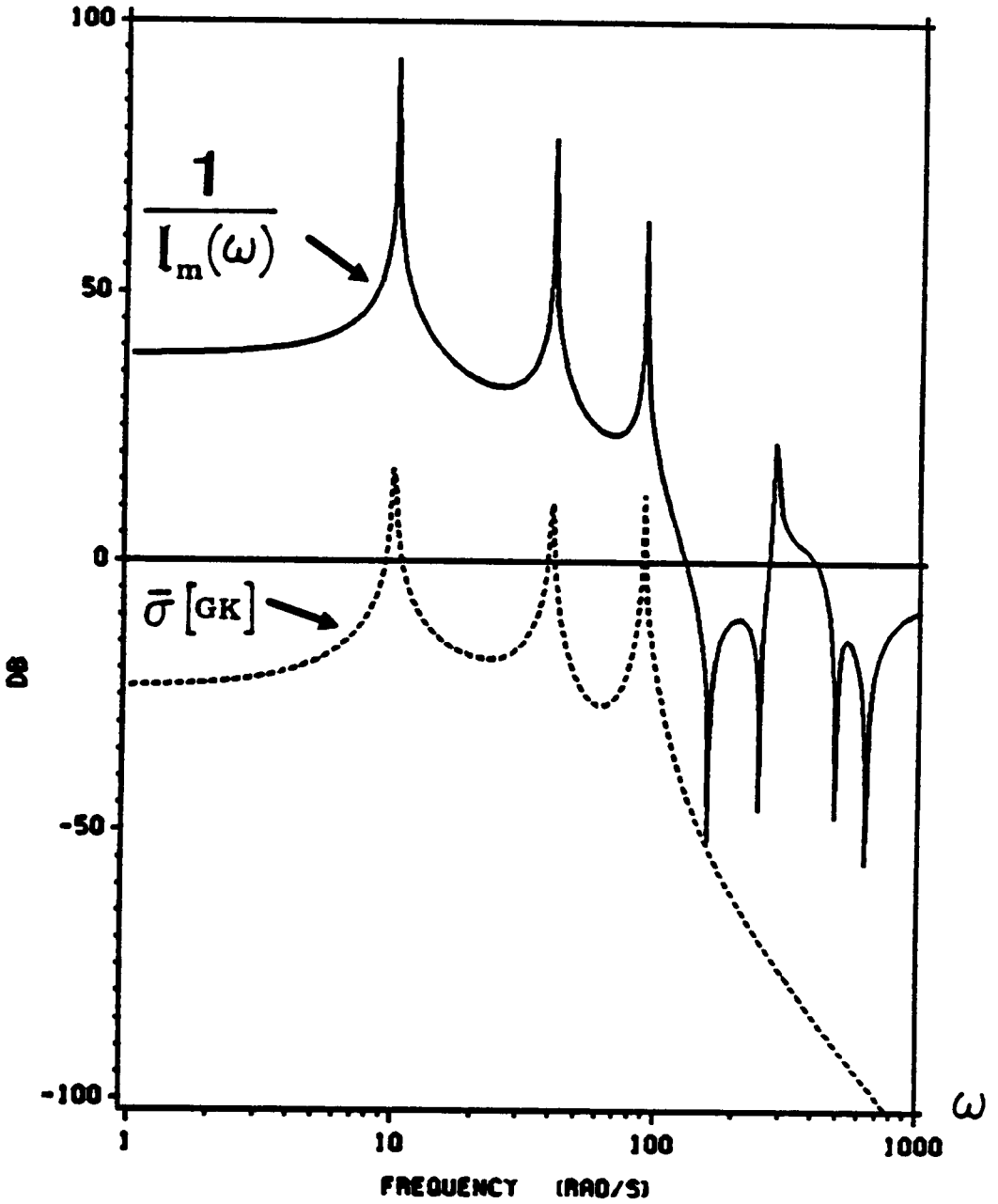

Figure 38. Robustness plot of the loop transfer matrix for the optimized LQG Balas beam design. [K_c, $\mu = 0.001$, $\zeta = 0.001$.]

Table 29. Computational costs for the Balas beam.

(CPU time in minutes; IBM 3084)

Design	*Time*
$V_1 = diag(v_i^2)$	79.37
$V_1 = aa^T$	23.79
K_c	28.85

the controlled and composite (controlled + residual) systems were found to be controllable and observable. The controlled system's plant was also found to be minimum phase.

The numerical values of the system matrices will not be presented here due to the large sizes involved, but the controlled and residual matrices follow the form of Equation [2.1.16] where

$$A_c = \begin{bmatrix} 0 & diag(\omega_1, \ldots, \omega_9) \\ -diag(\omega_1, \ldots, \omega_9) & -2diag(\zeta_1\omega_1, \ldots, \zeta_9\omega_9) \end{bmatrix} \qquad [7.5.1]$$

and

$$A_r = \begin{bmatrix} 0 & diag(\omega_{10}, \ldots, \omega_{20}) \\ -diag(\omega_{10}, \ldots, \omega_{20}) & -2diag(\zeta_{10}\omega_{10}, \ldots, \zeta_{20}\omega_{20}) \end{bmatrix} \qquad [7.5.2]$$

as the system matrices for the controlled and residual modes, respectively. No structural damping is assumed here, and the values of the natural frequencies of the grid structure are found in Table 30. The numerical values of the control matrices for the controlled and residual modes are given in Table 31 and of the output matrices for the controlled and residual modes are given in Table 32.

The LQR was defined by a similar form as before. Q_c was selected so that $x_c^T Q_c x_c$ represents the total energy (kinetic plus strain) in the controlled modes, i.e.,

$$Q_c = \frac{1}{2}\begin{bmatrix} diag(\omega_1^2, \ldots, \omega_9^2) & 0 \\ 0 & diag(\omega_1^2, \ldots, \omega_9^2) \end{bmatrix} \quad \frac{lb - sec^2}{in} \qquad [7.5.3]$$

R was defined by MESS as

$$R = \rho_1[I + \rho_2 B_r^T B_r] \qquad [7.5.4]$$

where ρ_1 was set as 100, and ρ_2 was set as 50. The designed locations of the regulator poles are tabulated in Table 33. For all the controller designs to be considered for the grid structure, the

Table 30. Natural frequencies of the grid structure.

ω_i	(rad/ sec)
ω_1	3.668
ω_2	5.591
ω_3	8.627
ω_4	20.604
ω_5	22.576
ω_6	31.147
ω_7	34.462
ω_8	35.522
ω_9	38.919
ω_{10}	50.244
ω_{11}	52.771
ω_{12}	59.018
ω_{13}	61.616
ω_{14}	73.100
ω_{15}	83.397
ω_{16}	129.160
ω_{17}	155.384
ω_{18}	169.387
ω_{19}	181.304
ω_{20}	193.193

Table 31. Control matrices for the controlled and residual modes of the MIMO grid structure.

$$B_c = \begin{bmatrix} 0 & 0 & 0 \\ 0 & 0 & 0 \\ 0 & 0 & 0 \\ 0 & 0 & 0 \\ 0 & 0 & 0 \\ 0 & 0 & 0 \\ 0 & 0 & 0 \\ 0 & 0 & 0 \\ 0 & 0 & 0 \\ -5.807/\omega_1 & -7.405/\omega_1 & -1.723/\omega_1 \\ 0.321/\omega_2 & 11.267/\omega_2 & -0.438/\omega_2 \\ 10.208/\omega_3 & -9.177/\omega_3 & 1.032/\omega_3 \\ 7.299/\omega_4 & 11.676/\omega_4 & -4.879/\omega_4 \\ -3.161/\omega_5 & 2.215/\omega_5 & 4.198/\omega_5 \\ 9.472/\omega_6 & -5.698/\omega_6 & -2.445/\omega_6 \\ -2.079/\omega_7 & -0.671/\omega_7 & -0.867/\omega_7 \\ -0.0053/\omega_8 & 1.598/\omega_8 & 0.757/\omega_8 \\ 5.324/\omega_9 & 9.041/\omega_9 & 5.871/\omega_9 \end{bmatrix} \text{ sec} \qquad B_r = \begin{bmatrix} 0 & 0 & 0 \\ 0 & 0 & 0 \\ 0 & 0 & 0 \\ 0 & 0 & 0 \\ 0 & 0 & 0 \\ 0 & 0 & 0 \\ 0 & 0 & 0 \\ 0 & 0 & 0 \\ 0 & 0 & 0 \\ -4.446/\omega_{10} & 0.472/\omega_{10} & -8.383/\omega_{10} \\ -4.586/\omega_{11} & 0.052/\omega_{11} & -7.319/\omega_{11} \\ 4.901/\omega_{12} & -7.587/\omega_{12} & -3.743/\omega_{12} \\ -4.216/\omega_{13} & -3.259/\omega_{13} & 1.695/\omega_{13} \\ 4.979/\omega_{14} & 0.576/\omega_{14} & -9.162/\omega_{14} \\ 2.295/\omega_{15} & -5.726/\omega_{15} & 8.086/\omega_{15} \\ -0.083/\omega_{16} & 0.103/\omega_{16} & -0.039/\omega_{16} \\ 2.494/\omega_{17} & 6.420/\omega_{17} & 0.908/\omega_{17} \\ 2.210/\omega_{18} & -1.771/\omega_{18} & -1.293/\omega_{18} \\ -2.145/\omega_{19} & -1.623/\omega_{19} & 0.696/\omega_{19} \\ 3.389/\omega_{20} & 3.711/\omega_{20} & 0.437/\omega_{20} \end{bmatrix} \text{ sec}$$

Table 32. Output matrices for the controlled and residual modes of the MIMO grid structure.

$$C_c^T = \begin{bmatrix} -5.807 & -7.405 & -1.723 \\ 0.321 & 11.267 & -0.438 \\ 10.208 & -9.177 & 1.032 \\ 7.299 & 11.676 & -4.879 \\ -3.161 & 2.215 & 4.198 \\ 9.472 & -5.698 & -2.445 \\ -2.079 & -0.671 & -0.867 \\ -0.0053 & 1.598 & 0.757 \\ 5.324 & 9.041 & 5.871 \\ 0 & 0 & 0 \\ 0 & 0 & 0 \\ 0 & 0 & 0 \\ 0 & 0 & 0 \\ 0 & 0 & 0 \\ 0 & 0 & 0 \\ 0 & 0 & 0 \\ 0 & 0 & 0 \\ 0 & 0 & 0 \end{bmatrix}$$

$$C_r^T = \begin{bmatrix} -4.446 & 0.472 & -8.383 \\ -4.586 & 0.052 & -7.319 \\ 4.901 & -7.587 & -3.743 \\ -4.216 & -3.259 & 1.695 \\ 4.979 & 0.576 & -9.162 \\ 2.295 & -5.726 & 8.086 \\ -0.083 & 0.103 & -0.039 \\ 2.494 & 6.420 & 0.908 \\ 2.210 & -1.771 & -1.293 \\ -2.145 & -1.623 & 0.696 \\ 3.389 & 3.711 & 0.437 \\ 0 & 0 & 0 \\ 0 & 0 & 0 \\ 0 & 0 & 0 \\ 0 & 0 & 0 \\ 0 & 0 & 0 \\ 0 & 0 & 0 \\ 0 & 0 & 0 \\ 0 & 0 & 0 \\ 0 & 0 & 0 \\ 0 & 0 & 0 \end{bmatrix}$$

regulator poles of the coupled system virtually do not move from their original design locations. Therefore, they are not tabulated further in any of the remaining tables.

The actual noise environment was selected as $W_1 = I$ and $W_2 = I$. The corresponding optimum value of the stochastic performance index for the LQR alone (when the state is perfectly observed) is $J_{LQR} = 50445. \frac{lb - sec}{in}$.

7.5.1. Spillover Properties

Next, several observers are considered. Special attention is placed on their effect on the performance index and the spillover of the tenth and eleventh modes. From the robustness results to be presented shortly, it will be demonstrated that only these two residual modes are critical.

Table 34 gives the corresponding poles for different steady-state KBF observers obtained with various choices of the noise intensity matrices V_1 and V_2 including the actual noise statistics, $V_1 = W_1 = I$ and $V_2 = W_2 = I$. (Table 35 presents the corresponding statistical optimum gain matrix, K_c.) One of the KBF observers imposes a minimum stability margin by means of Anderson and Moore's α - shift procedure [35]. Also given in the table are the various stochastic performance indices. J denotes the stochastic value of the performance index which includes the cost increment incurred as a result of the estimation error. The ratios J/J_{OPT} are also provided where J_{OPT} is the statistically optimum stochastic performance index of the actual noise environment.

It can be observed from Table 34 that:

(a) For $V_1 = W_1 = I$, $V_2 = W_2 = I$, $\alpha = 0$ (actual noise statistics):

- the residual modes are stable;

- some of the observer poles violate the rule-of-thumb of being between 3 to 10 times faster than the regulator poles of Table 33. Some of the poles lie in the speed range of the regulator poles, whereas, others are faster than the 10 time limit.

Table 33. Designed regulator poles for the MIMO grid structure.

(Eigenvalues in 1/sec.)

Regulator poles	$-0.324 \pm j3.67$ $-0.372 \pm j5.59$ $-0.402 \pm j8.63$ $-0.506 \pm j20.60$ $-0.161 \pm j22.58$ $-0.342 \pm j31.15$ $-0.072 \pm j34.46$ $-0.056 \pm j35.52$ $-0.381 \pm j38.92$

Table 34. KBF poles of the MIMO grid structure.

(System eigenvalues in 1/sec and performance indices in lb-sec/in.)

	Actual Noise $V_1 = W_1 = I$, $V_2 = W_2 = I$, $\alpha = 0$	*Kalman – Bucy Filters* $V_1 = I$, $V_2 = \nu_1[I + \nu_2 C_r C_r^T]$, $\nu_1 = 0.040$, $\nu_2 = 1.0$	
		$\alpha = 0$	$\alpha = 0.75$
Observer poles	$-7.209 \pm j2.92$ $-1.875 \pm j5.14$ $-8.611 \pm j6.38$ $-8.883 \pm j19.95$ $-3.010 \pm j22.68$ $-7.134 \pm j30.52$ $-0.754 \pm j34.46$ $-0.474 \pm j35.54$ $-7.701 \pm j38.36$	$-2.691 \pm j4.61$ $-1.930 \pm j4.75$ $-3.686 \pm j8.33$ $-3.901 \pm j20.57$ $-1.363 \pm j22.58$ $-3.196 \pm j31.12$ $-0.513 \pm j34.44$ $-0.350 \pm j35.53$ $-3.213 \pm j38.85$	$-3.412 \pm j4.54$ $-3.030 \pm j4.81$ $-4.513 \pm j8.34$ $-4.726 \pm j20.57$ $-2.310 \pm j22.58$ $-4.041 \pm j31.12$ $-1.673 \pm j34.39$ $-1.583 \pm j35.52$ $-3.994 \pm j38.88$
Residual poles (*10th and 11th*)	$-0.032 \pm j50.28$ $-0.025 \pm j52.80$	$-0.006 \pm j50.26$ $-0.004 \pm j52.78$	$-0.020 \pm j50.27$ $-0.016 \pm j52.79$
J	54582.	55281.	56831.
J/J_{OPT}	1.0000	1.0128	1.0412

Table 35. Statistical optimum gain matrix for the MIMO grid structure.

$(V_1 = W_1 = I,\ V_2 = W_2 = I,\ \textit{and}\ \alpha = 0.)$

$$K_c = \begin{bmatrix} -0.978 & -0.618 & -0.773 \\ -0.084 & 1.119 & -0.497 \\ 1.109 & -0.494 & 0.034 \\ 0.551 & 0.867 & -0.572 \\ -0.352 & 0.780 & 1.115 \\ 0.921 & -0.533 & -0.246 \\ -0.437 & -0.801 & -0.714 \\ 0.437 & 0.756 & 0.246 \\ 0.476 & 0.457 & 0.717 \\ -0.049 & -0.183 & -0.168 \\ 0.518 & 0.410 & 0.242 \\ 0.573 & -0.237 & 0.374 \\ 0.180 & 0.748 & -0.161 \\ -0.052 & 0.104 & -0.107 \\ 0.732 & -0.491 & -0.172 \\ -0.455 & 0.497 & 0.451 \\ -0.815 & 0.658 & -0.280 \\ 0.460 & 0.861 & 0.313 \end{bmatrix}$$

(b) For $V_1 = I$, $V_2 = v_1[I + v_2 C_r C_r^T]$, $\alpha = 0$ (MESS formulation):

- the residual poles are barely stable;
- the performance degradation is small;
- the observer poles do not violate the 10 time speed limit of the regulator poles, but the 3 time limit is violated. Some of the poles are stuck in the LQR regime. (This behavior is linked with the asymptotic properties associated with the closed-loop observer poles discussed in Section 2.5.)

(c) For $V_1 = I$, $V_2 = v_1[I + v_2 C_r C_r^T]$, $\alpha = 0.75$ (MESS and α – shift formulations):

- the performance degradation is small but is larger than that for case (b);
- the observer poles are within the 3 to 10 time rule-of-thumb speed regime of the regulator poles;
- the residual modes are stable but not as stable as those of case (a) based on the actual noise statistics. They are more stable than those without the α – shift formulation.

7.5.2. Stability Robustness Tests

In this section, the Bode plots of the loop transfer function of the various controllers considered in the previous section are analyzed. Their merits are compared on the basis of the stability robustness tests based on singular values [19, 60, 64].

In Section 2.10.6, it was shown that for an (output) multiplicative uncertainty, the stability robustness of the control system is guaranteed if the maximum singular value of the loop transfer matrix satisfies the inequality

$$\bar{\sigma}\{G(j\omega)K(j\omega)[I + G(j\omega)K(j\omega)]^{-1}\} < 1/l_m(\omega) \qquad [7.5.5]$$

whereas, for the (input) multiplicative uncertainty

$$\bar{\sigma}\{K(j\omega)G(j\omega)[I + K(j\omega)G(j\omega)]^{-1}\} < 1/l_m(\omega) \qquad [7.5.6]$$

is the MIMO stability criterion for all $\omega \geq 0$. This more exact form is used here instead of the simplified criterion used for the Balas beam. Again, it should be reminded that this is a sufficient but not a necessary condition for stability since the test does not take into account the structure of the uncertainty, i.e., phase angles. It is based on a worst case which is not necessarily allowed by the structure of the system. As a result, if the robustness test is violated, it does not mean that the system is going to be unstable but rather that it may become unstable.

Figures 39 - 44 contain the robustness plots for a variety of controllers. The plots are drawn for $\zeta = 0.005$. $l_m(\omega)$ was computed by two methods where the corresponding plants were represented by the controls method of Equations [2.10.25] and [2.10.26] and by the spectral development method of Equations [2.10.28] and [2.10.29]. As expected, both methods produced the same $1/l_m(\omega)$ curve.

Figures 39 and 40 show the loop transfer function for the actual noise statistics for the (input) and (output) multiplicative uncertainties, respectively. As can be seen in the high frequency residual mode regime, the robustness test is violated by the tenth and eleventh modes which were identified by their frequencies, i.e., $\omega_{10} = 50.24$ rad/ sec and $\omega_{11} = 52.77$ rad/ sec.

Figures 41 and 42 show the loop transfer function for the MESS and $\alpha -$ shift KBF observer for the (input) and (output) multiplicative uncertainties, respectively. Again, the tenth and eleventh modes violate the robustness test in the high frequency regime.

Finally, Figures 43 and 44 show the loop transfer function of the regulator alone for the (input) and (output) multiplicative uncertainties, respectively. As can be seen, the regulator greatly fails the robustness test all the way out to the $15th$ mode.

The following statements can now be made:

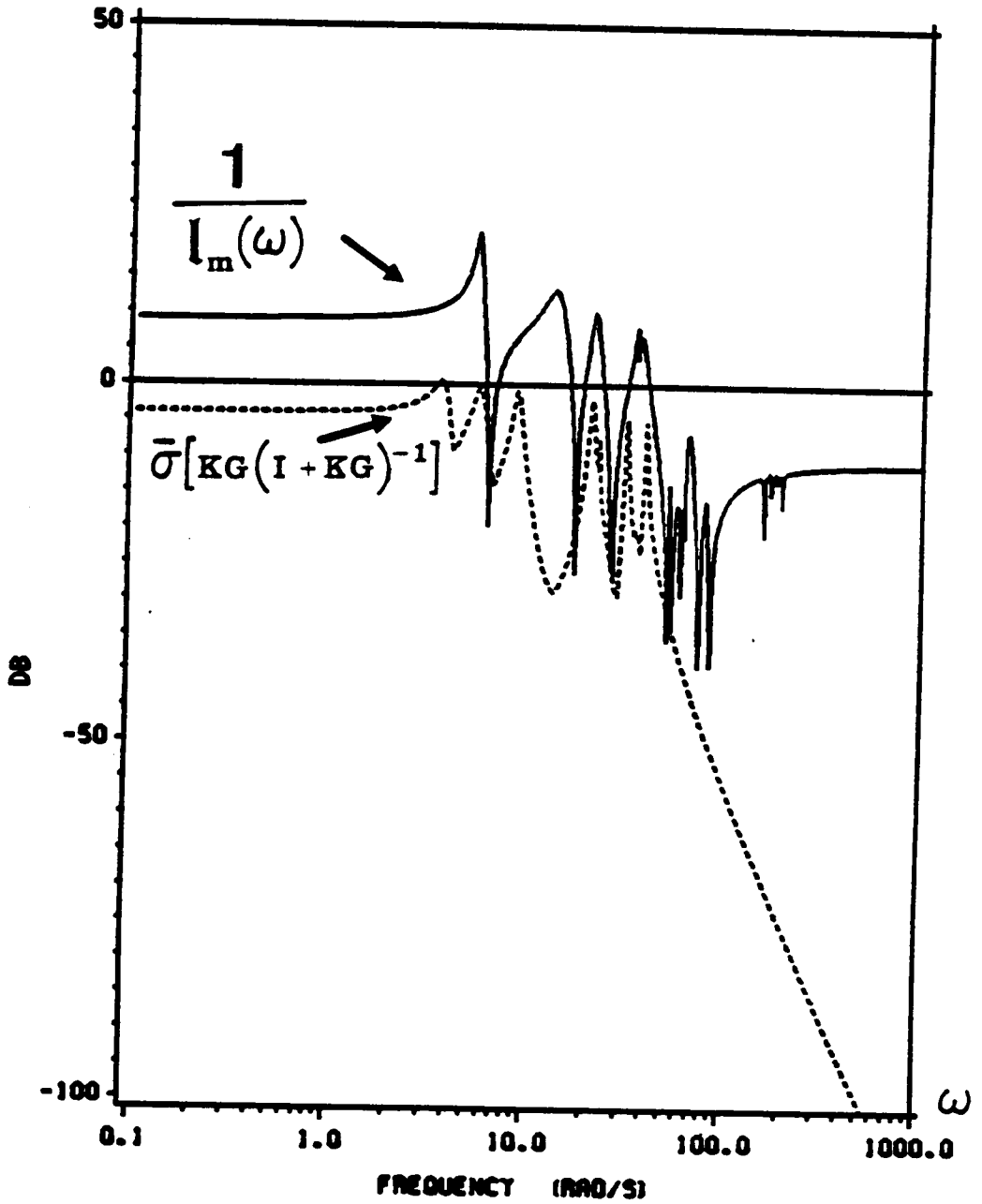

Figure 39. Robustness plot of the MIMO grid's loop transfer matrix for the actual noise statistics for (input) multiplicative uncertainty. [$\zeta = 0.005$.]

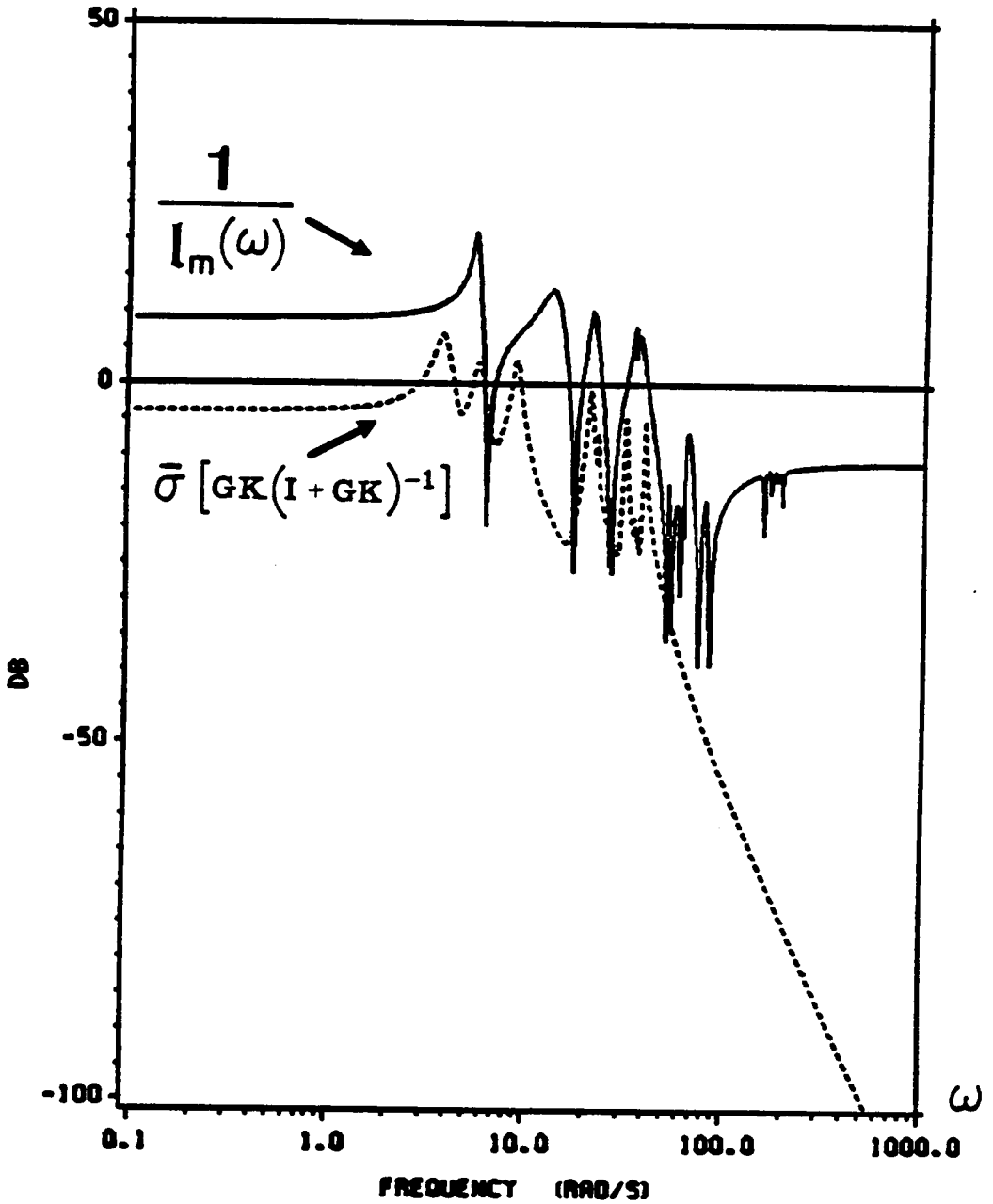

Figure 40. Robustness plot of the MIMO grid's loop transfer matrix for the actual noise statistics for (output) multiplicative uncertainty. [$\zeta = 0.005$.]

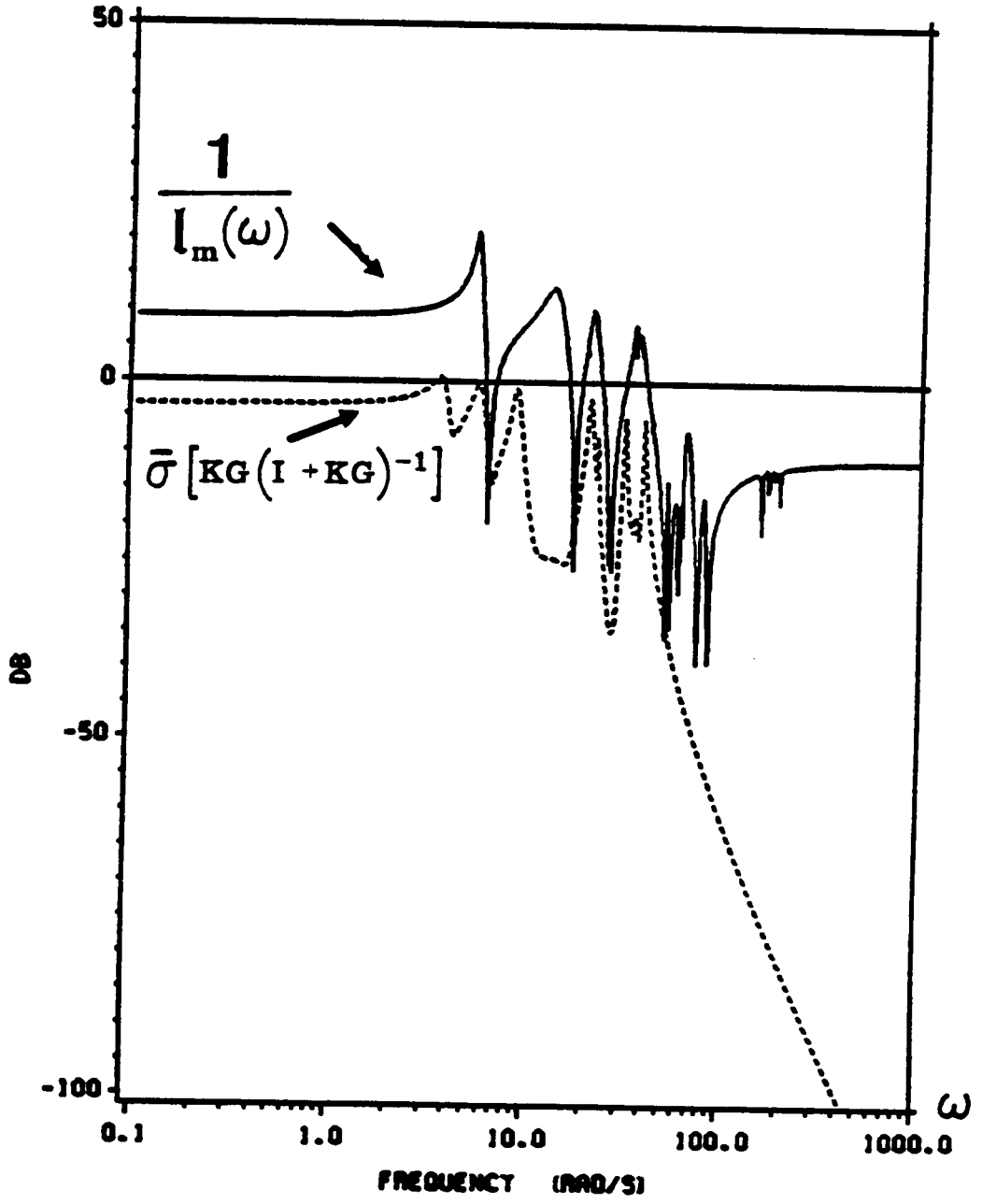

Figure 41. Robustness plot of the MIMO grid's loop transfer matrix for the KBF for (input) multiplicative uncertainty. [$\zeta = 0.005$.]

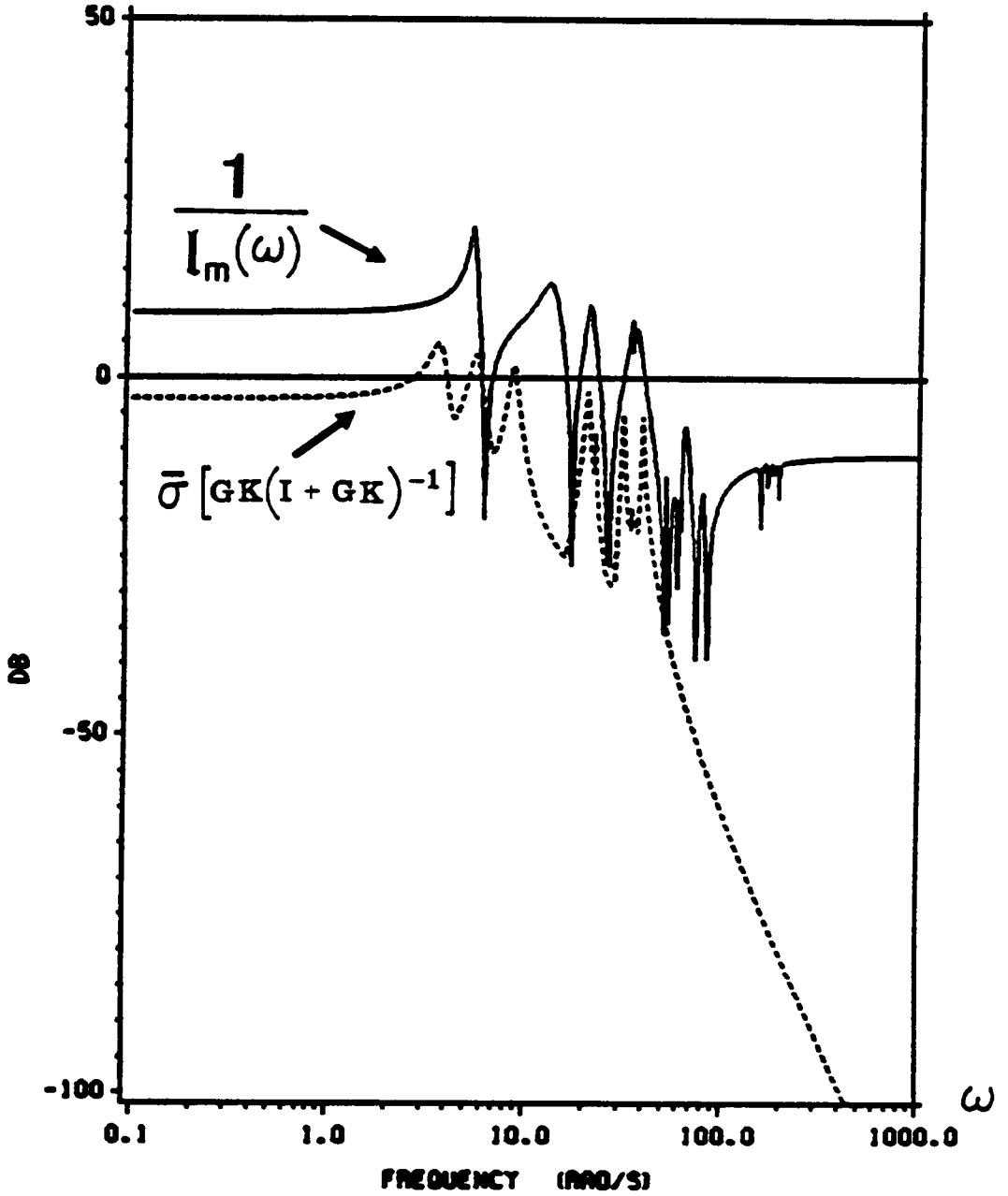

Figure 42. Robustness plot of the MIMO grid's loop transfer matrix for the KBF for (output) multiplicative uncertainty. [$\zeta = 0.005$.]

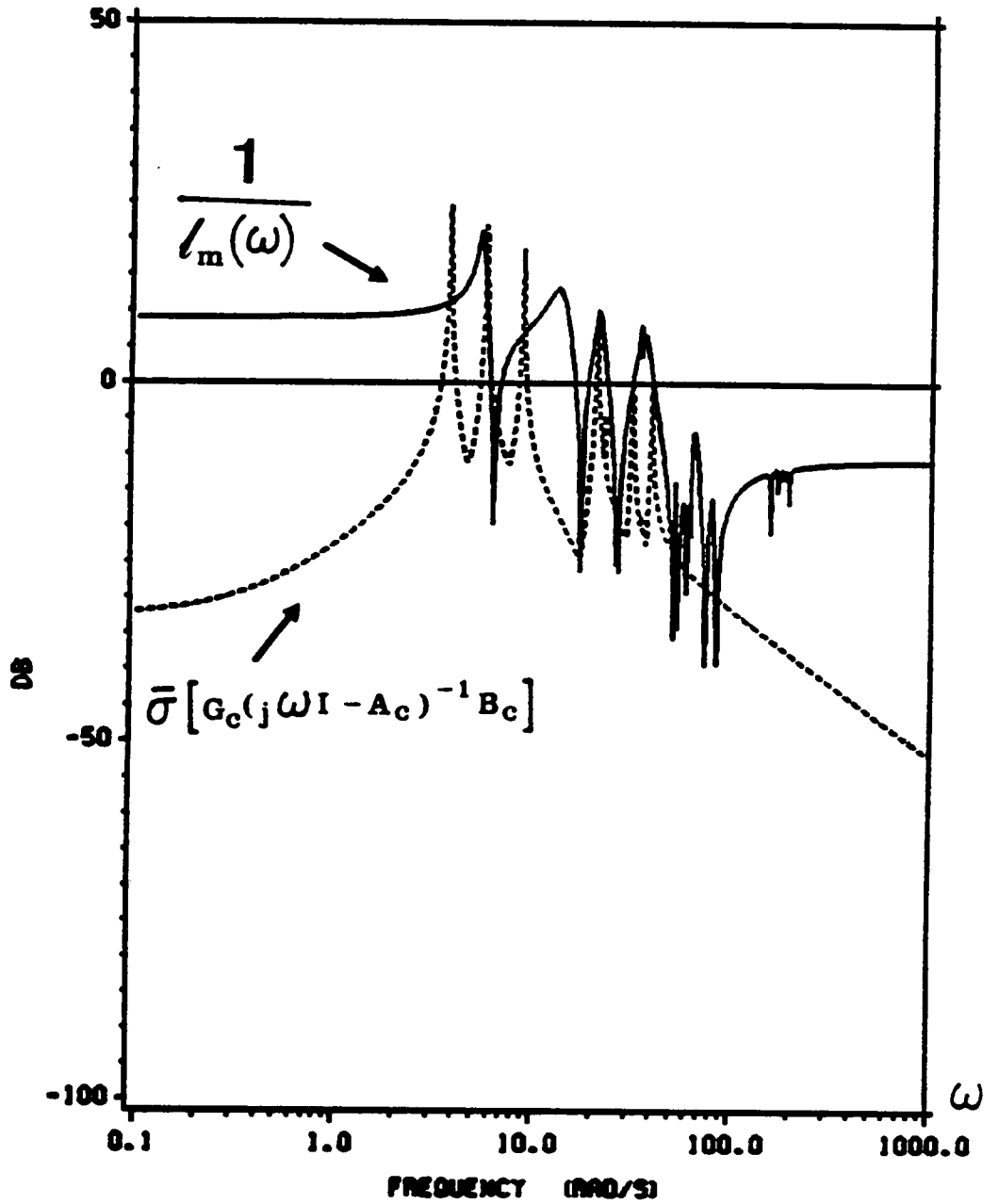

Figure 43. Robustness plot of the MIMO grid's loop transfer matrix for the regulator for (input) multiplicative uncertainty. [$\zeta = 0.005$.]

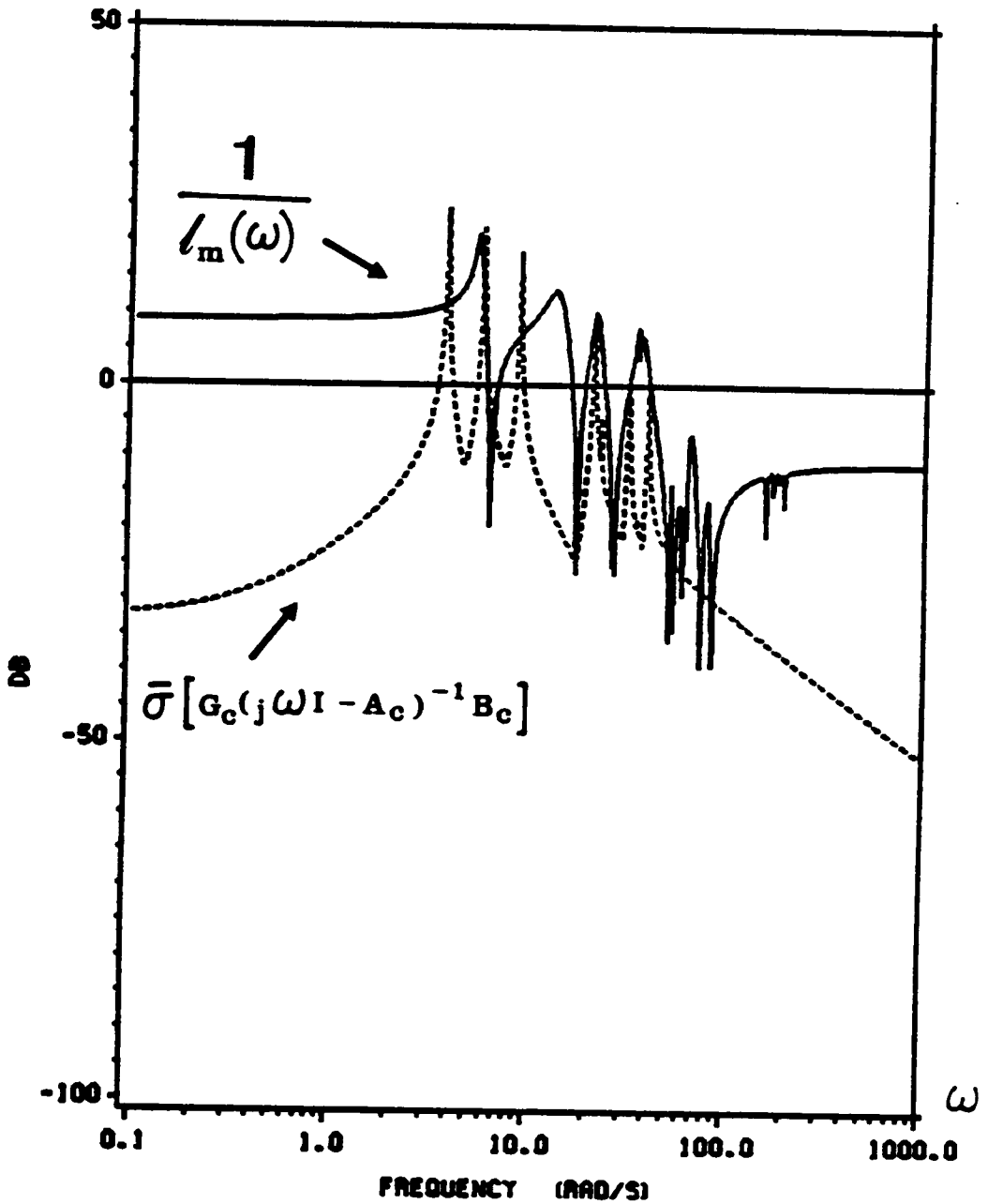

Figure 44. Robustness plot of the MIMO grid's loop transfer matrix for the regulator for (output) multiplicative uncertainty. [$\zeta = 0.005$.]

(1) At high frequency, the loop transfer function of the LQR decays very slowly (like $1/\omega$) which makes the regulator fail the test. From this observation, the LTR technique, which tries to *recover* the loop transfer matrix of the regulator, does not seem to be a good one for the kind of uncertainty associated with the neglected dynamics of lightly damped structures.

(2) The tenth and eleventh modes violate the robustness test for all the LQG designs. They, thus, become critical modes and must be checked explicitly. The robustness of modes twelve and above can be concluded from the robustness curves and, thus, are not considered further. Recall that the tenth and eleventh modes were found to be stable (Table 34). This again reinforces the concept that a robustness test violation does not mean that the system is going to be unstable.

These results will be used to optimize the structures of V_1 and K_c to maximize the stability margins explicitly for the tenth and eleventh modes. This topic is investigated in the next section.

From the above results, matrices A_r, B_r, and C_r will be reduced in size to reflect the contributions of only the tenth and eleventh modes.

Another indicator of the conservative nature of the robustness tests is demonstrated by the violation of the test in the bandwidth of the controller. From linear optimal control theory, this region is guaranteed to be stable, yet the robustness criterion shows several appreciable negative peaks in this regime which violate the criterion.

In the bandwidth of the controller, the uncertainty, $l_m(\omega)$, should be small since the difference in the actual plant, $\tilde{G}(j\omega)$, from the modelled plant, $G(j\omega)$, is only in the truncated residual modes frequency regime. This regime is, by definition, outside of the bandwidth of the controller. (For $1/l_m(\omega)$ to be very small for some frequencies, it means that $l_m(\omega)$ is very large.) From Equation [2.10.24],

$$\bar{\sigma}[L(j\omega)] \leq \frac{\bar{\sigma}[\Delta G(j\omega)]}{\underline{\sigma}[G(j\omega)]} \equiv l_m(\omega)$$

Since $\bar{\sigma}[\Delta G(j\omega)]$ is small throughout the frequency range of the controlled modes, it means that $\underline{\sigma}[G(j\omega)]$ becomes close to zero for some frequencies. For the minimum singular value to approach zero, the matrix must become singular. Therefore, the modelled plant, $G(j\omega)$, becomes close

to singular for some frequencies. This looks like an *anti-resonance* type behavior since the plant is a ratio of the system output to its input. What this means is that for some frequencies and some modes of excitation, the response of the system is very close to zero. This is also the definition of a transmission zero.

Figure 45 is a plot of $\underline{\sigma}[G(j\omega)]$ as a function of frequency, ω. The negative peaks shown coincide with those of $\frac{1}{l_m(\omega)}$. Since $\bar{\sigma}[\Delta G(j\omega)]$ is small throughout the frequency range of the controlled modes, it just *scales* the $\underline{\sigma}[G(j\omega)]$ curve upwards.

Table 36 lists the transmission zeros of the plant for the MIMO grid structure at $\zeta = 0.005$. For low-damped systems with colocated actuator and sensor pairs, the transmission zeros are effectively imaginary. (For $\zeta = 0$, the transmission zeros are purely imaginary.) As a result, when the robustness plots are drawn in the frequency domain, the transmission zeros are picked up exactly to cause this anti-resonance problem. As can be seen, the transmission zeros of the plant coincide with the negative peaks shown for $1/l_m(\omega)$ and $\underline{\sigma}[G(j\omega)]$.

As a final check that this is indeed an anti-resonance behavior, a structural analysis was performed on this grid structure. Using the finite element representation of this structure, the anti-resonance frequencies can be computed by blocking the translation degrees of freedom (leaving the rotation free) at the nodes 1, 4, and 11 of the grid structure. These nodes are the locations of the actuators and produced effectively no response. Computing the natural frequencies of this modified grid structure produces the anti-resonance frequencies. When this analysis was performed, the anti-resonance frequencies corresponded to the transmission zeros and the negative peaks shown in $1/l_m(\omega)$ and $\underline{\sigma}[G(j\omega)]$.

7.5.3. Optimizing the Observer Design

Recall that the actual noise statistics were assumed to be $W_1 = I$ and $W_2 = I$. The statistically optimum KBF corresponds to the case when $V_1 = W_1$ and $V_2 = W_2$ and $\alpha = 0$. The properties associated with the statistical optimum are given in Tables 34 and 35.

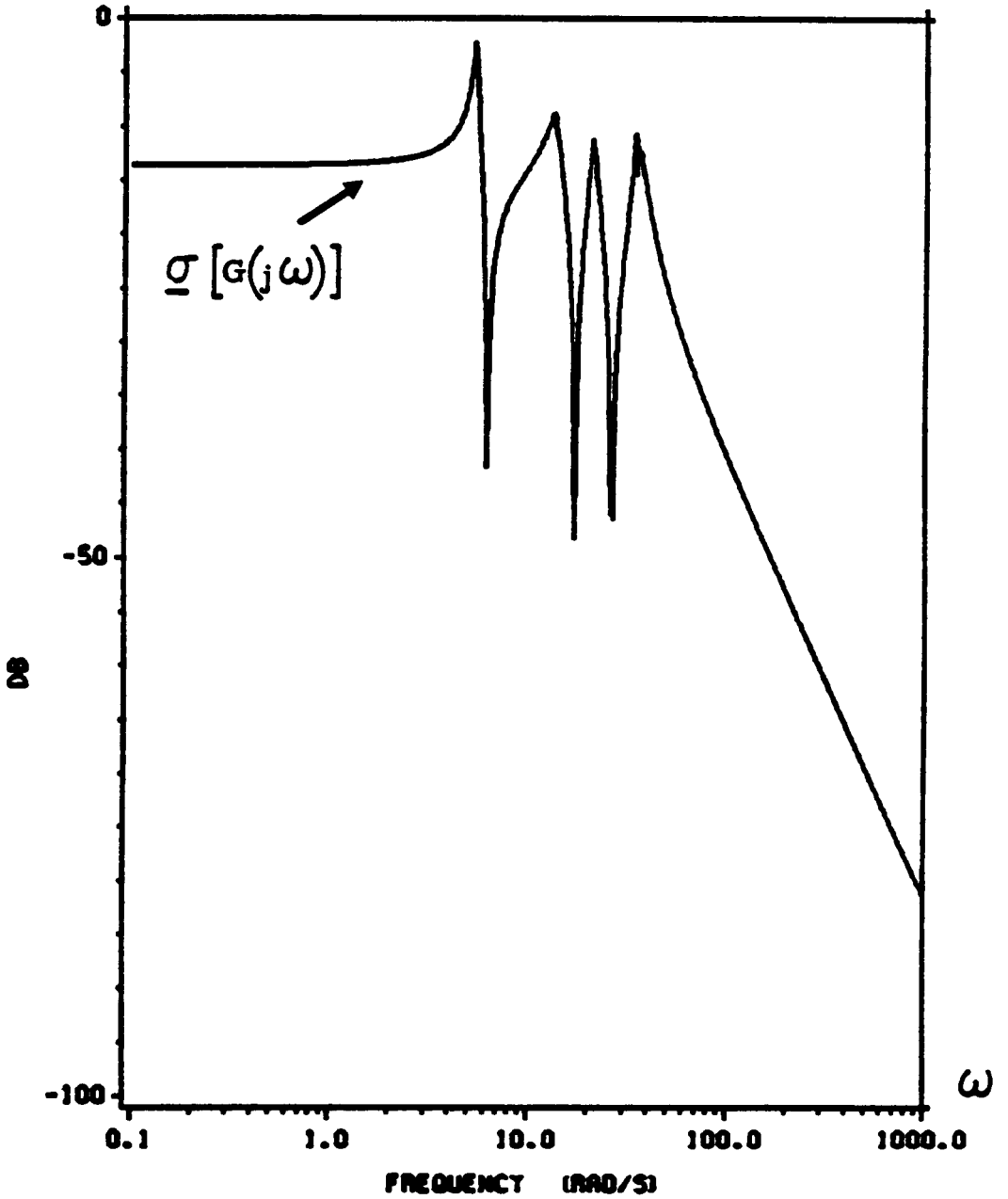

Figure 45. Plot of the minimum singular value of the plant vs. frequency for the MIMO grid structure.

Table 36. Transmission zeros of the plant for the MIMO grid structure. [$\zeta = 0.005$.]

(Eigenvalues in 1/sec.)

Transmission zeros	$-0.028 \pm j6.17$ $-0.069 \pm j17.07$ $-0.114 \pm j25.80$ $-0.124 \pm j26.58$ $-0.173 \pm j34.59$ $-0.178 \pm j35.57$

Due to the large order of the system involved, the computer costs required a reduction in the number of design variables. The problem formulation was also slightly modified. For the optimization of the noise intensity matrix, the problem becomes

Find V_1, δ such that

$$\min F = k_s[(\delta - t)_+^2 + \mu F_{performance}] \qquad [7.5.7]$$

subject to the constraints

$$Re(\lambda_i^{R+}) < \delta \qquad [7.5.8]$$

$$\delta < 0 \qquad [7.5.9]$$

where λ_i^{R+} are the eigenvalues of the residual modes. Since there is symmetry about the real axis, only those in the upper portion of the complex plane need to be considered. These modes are identified by their frequencies. For Equation [7.5.8] to be satisfied, the more general constraint of Equation [7.2.2] is also satisfied since the regulator and observer are designed with large stability margins. This modification is performed in order to cut down the number of constraints from 22 to 3.

In addition to this, since NEWSUMT-A [88, 89] takes first derivatives of the constraints and second derivatives of the objective function with respect to the design variables, a reduction in the number of design variables also seems warranted since the derivatives are not analytic but rather are performed by finite difference. This has an appreciable cost in terms of computer execution time. As a result, for the diagonal case, V_1 was selected to be of the form

$$V_1 = diag(a_v^2\ a_v^2\ a_v^2\ b_v^2\ b_v^2\ b_v^2\ c_v^2\ c_v^2\ c_v^2\ d_v^2\ d_v^2\ d_v^2\ e_v^2\ e_v^2\ e_v^2\ f_v^2\ f_v^2\ f_v^2) \qquad [7.5.10]$$

This reduces the number of design variables from 19 to 7. This number proved to be effective for the Balas beam.

An alternative approach to reducing the number of design variables is to select V_1 to possess a form comparable to the Loop Transfer Recovery (LTR) Method of Equation [2.11.1]. This assumes that the noise enters the plant at the input.

$$V_1 = B_c Q_q B_c^T \qquad [7.5.11]$$

where Q_q is any 3×3 symmetric positive semidefinite matrix. Q_q can be further restricted and was selected to be of the aa^T form.

$$\begin{aligned} Q_q &= a_Q a_Q^T \\ &= \begin{bmatrix} a_q \\ b_q \\ c_q \end{bmatrix} [a_q \;\; b_q \;\; c_q] \end{aligned} \qquad [7.5.12]$$

This reduces the number of design variables to 4.

Of course, by assuming that the noise enters the plant at the input, we restrict the domain, where NEWSUMT-A searches for a solution, to the corresponding subspace. A stable solution is not guaranteed, but the most stable one in the subspace will be found. In addition to this, recovery of the regulator's loop transfer matrix can become a *major* concern as was discussed in Sections 2.11 and 3.2.

However, the benefits of this procedure are as follows:

- It drastically reduces the number of design variables.
- The procedure suggests a rationale for the choice of Q_q when the noise is assumed of the form [7.5.11]. (Usually, control designers take $Q_q = I$ for lack of anything else.)
- A side benefit is that assuming that the noise enters at the input has been observed to improve robustness (though not necessarily with respect to spillover which is the major concern here).

Similarly, for the direct design of the observer gain matrix, the optimization problem becomes

Find K_c, δ such that

$$\min F = k_s[(\delta - t)_+^2 + \mu F_{performance}] \qquad [7.5.13]$$

subject to the constraints

$$Re(\lambda_i^{R+}) < \delta \qquad [7.5.14]$$

$$\delta < 0 \qquad [7.5.15]$$

The constraint modifications are identical to the optimization problem of the noise intensity matrix. Since K_c is an 18×3 matrix, the original optimization problem would dictate 55 design parameters for K_c and δ combined. Again, due to large computer costs, K_c was constrained to the following form

$$K_c = \begin{bmatrix} a_k \begin{bmatrix} -0.978 \\ -0.084 \\ 1.109 \\ 0.551 \\ -0.352 \\ 0.921 \\ -0.437 \\ 0.437 \\ 0.476 \end{bmatrix} & c_k \begin{bmatrix} -0.618 \\ 1.119 \\ -0.494 \\ 0.867 \\ 0.780 \\ -0.533 \\ -0.801 \\ 0.756 \\ 0.457 \end{bmatrix} & e_k \begin{bmatrix} -0.773 \\ -0.497 \\ 0.034 \\ -0.572 \\ 1.115 \\ -0.246 \\ -0.714 \\ 0.246 \\ 0.717 \end{bmatrix} \\ b_k \begin{bmatrix} -0.049 \\ 0.518 \\ 0.573 \\ 0.180 \\ -0.052 \\ 0.732 \\ -0.455 \\ -0.815 \\ 0.460 \end{bmatrix} & d_k \begin{bmatrix} -0.183 \\ 0.410 \\ -0.237 \\ 0.748 \\ 0.104 \\ -0.491 \\ 0.497 \\ 0.658 \\ 0.861 \end{bmatrix} & f_k \begin{bmatrix} -0.168 \\ 0.242 \\ 0.374 \\ -0.161 \\ -0.107 \\ -0.172 \\ 0.451 \\ -0.280 \\ 0.313 \end{bmatrix} \end{bmatrix} \qquad [7.5.16]$$

where, when $a_k = b_k = c_k = d_k = e_k = f_k = 1$, the statistical optimum gain matrix emerges.

For the optimization, t was taken to equal $-0.100\,\text{sec}^{-1}$, k_s was set at 100, and $V_2 = v_1[I + v_2 C_r C_r^T]$ where $v_1 = 0.040$ and $v_2 = 1.0$. Therefore, $V_2 \neq W_2$ in this problem formulation. No α – shift was used, i.e., $\alpha = 0$, so that the optimizer would be influenced by the actual

noise environment and not be overly subject to the α – shift effect. A tracing method was used for each of the designs, i.e., the optimum V_1 (or K_c) for one value of μ was used as the initial solution for the next value of μ.

The results for the observer design based on optimizing the matrices V_1 and K_c based on spillover and performance considerations are given in Figures 46 - 50 and Tables 37 - 42 as a function of the weighting parameter, μ. Figures 46 - 48 show the individual δ vs. J plots for each of the designs considered, i.e., $V_1 = diag(v_i^2)$, $V_1 = B_c Q_q B_c^T$, and K_c. Figures 49 and 50 overlap these three plots in order to readily compare them. Tables 37 - 42 list the observer poles, the residual poles, the performance degradation, the actual designs, and their corresponding observer gain matrices, K_c. It should be noted that for each design, μ was allowed to vary from $\mu = 1000.$ to $\mu = 10.$ Three different μ's were considered in each design.

For two of the designs, it is shown that substantial gains in the stability of the residual modes can be obtained without a great loss of performance. For example, for $\mu = 10.$, the $V_1 = diag(v_i^2)$ design produces $\delta = -0.08067$ sec^{-1} and $J = 55726.$ lb – sec /*in*; and the K_c design produces $\delta = -0.03950$ sec^{-1} and $J = 54713.$ lb – sec /*in*. The LTR technique, on the other hand, produces substantial performance degradation and small stability margins. For example, for $\mu = 10.$, the $V_1 = B_c Q_q B_c^T$ design produces $\delta = -0.01748$ sec^{-1} and $J = 67196.$ lb – sec /*in*.

As expected, as μ decreases in value, the performance index, J, increases in magnitude. This indicates a deterioration in performance. At the same time, the system stability margin increases since the optimizer places more emphasis on a stable system at the cost of performance.

The design K_c is more effective than $V_1 = diag(v_i^2)$ even though both have the same number of design variables. For a given δ, the case K_c produces designs which give J's which are appreciably lower than those of the very constrained form of the $V_1 = diag(v_i^2)$ design. The K_c design also gives slower observers than the $V_1 = diag(v_i^2)$ design.

The designs K_c and $V_1 = diag(v_i^2)$ are both appreciably more effective than $V_1 = B_c Q_q B_c^T$. It should be recalled that K_c and $V_1 = diag(v_i^2)$ also have twice as many design variables. Therefore, the reduction in terms of the number of design variables certainly involved a major cost in terms of performance and stability margins. In addition to this, the special form of $V_1 = B_c Q_q B_c^T$ produced

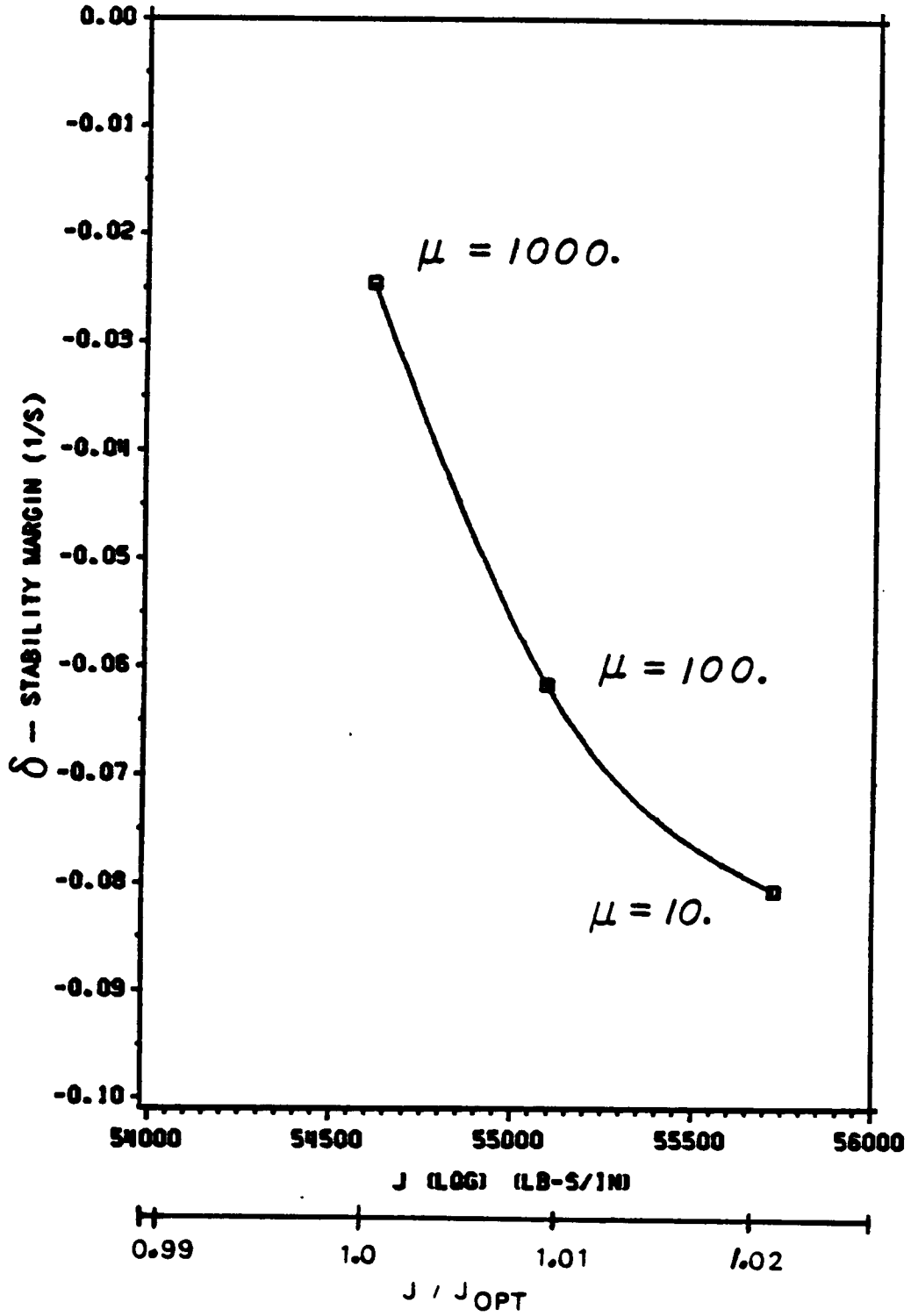

Figure 46. Stability margin vs. performance index for the MIMO grid struncture. [$V_1 = diag(v_i^2)$.]

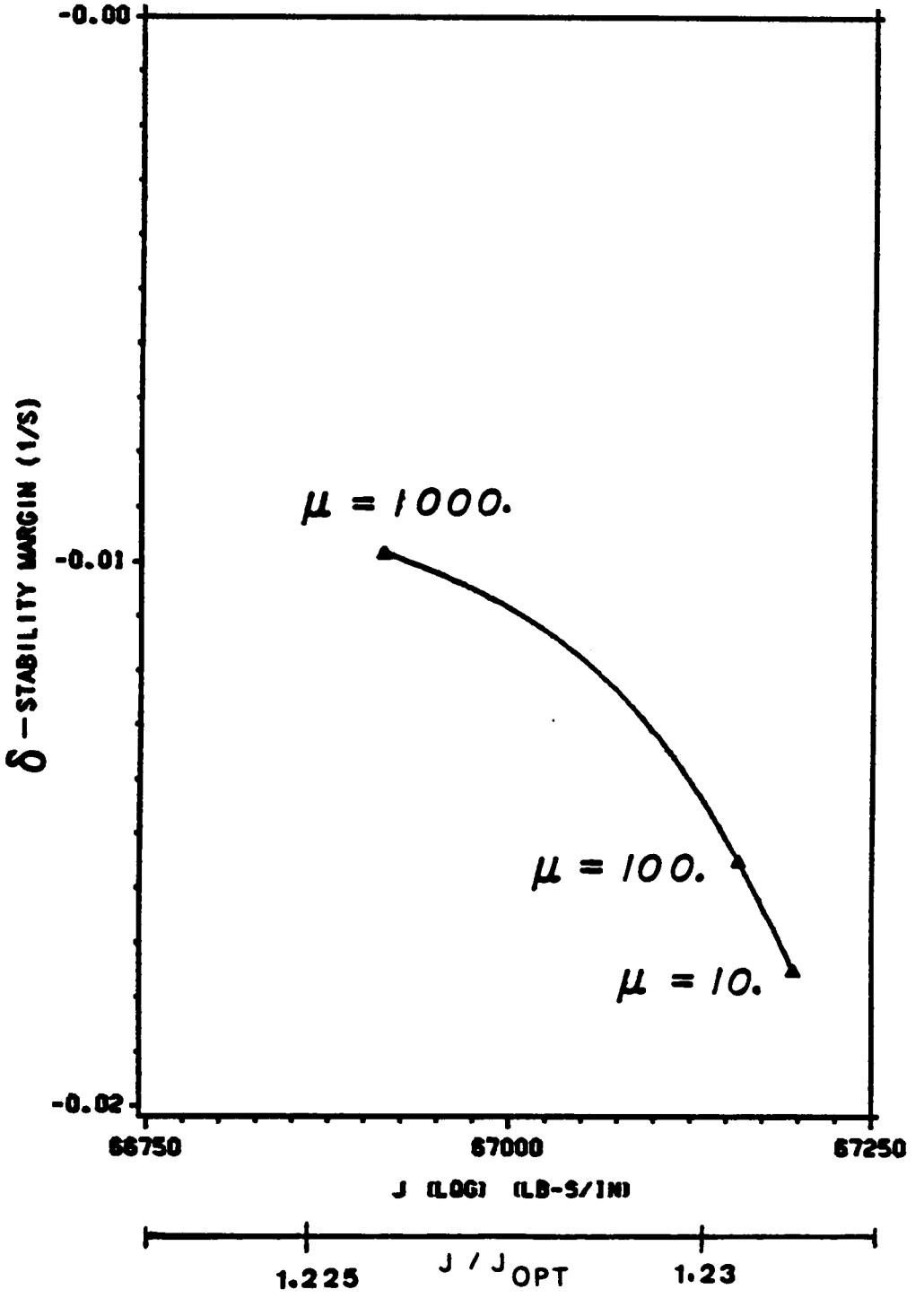

Figure 47. Stability margin vs. performance index for the MIMO grid structure. [$V_1 = B_c Q_q B_c^T$.]

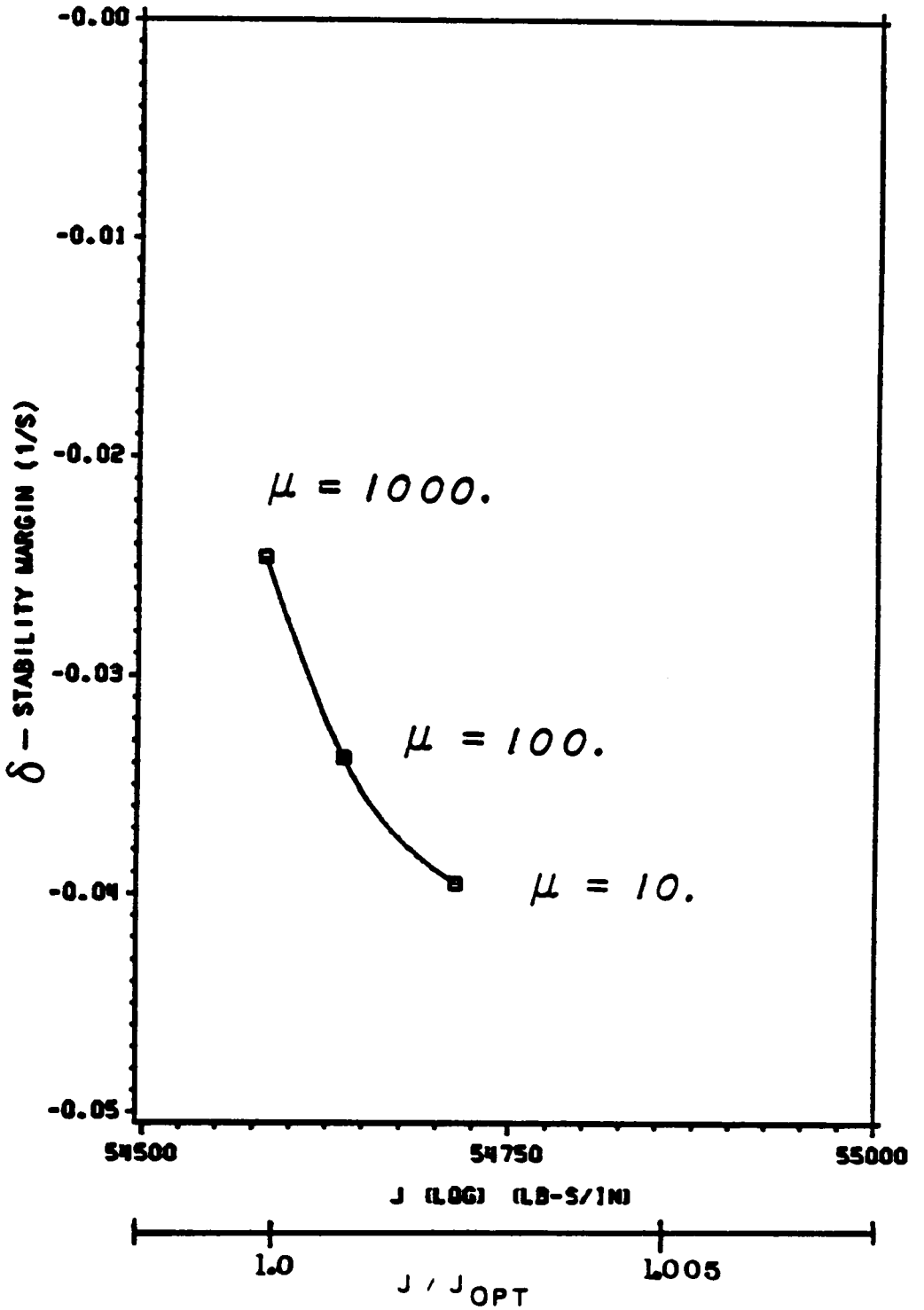

Figure 48. Stability margin vs. performance index for the MIMO grid structure. $[K_c]$

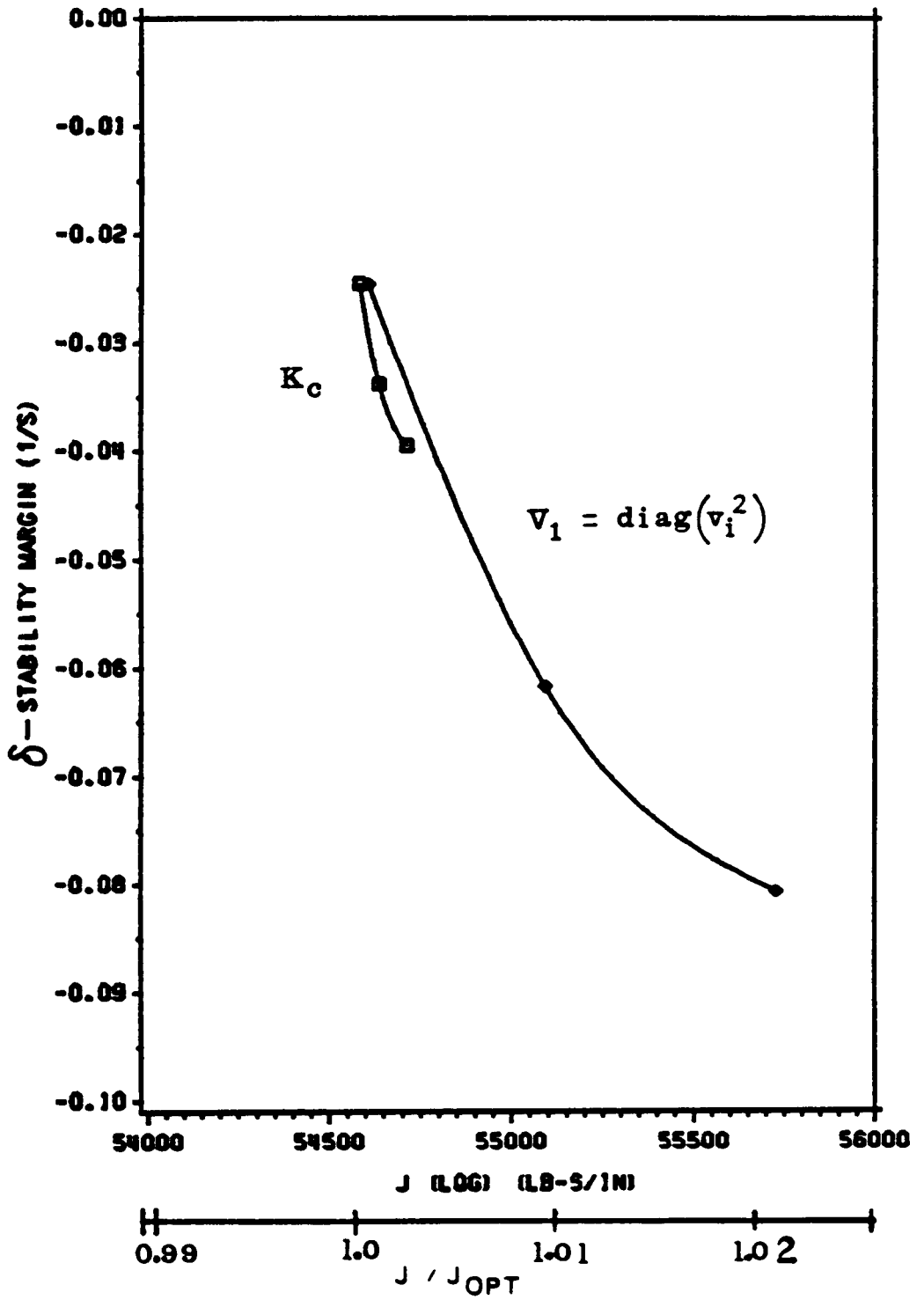

Figure 49. Stability margin vs. performance index for various optimized controller designs of the MIMO grid structure.

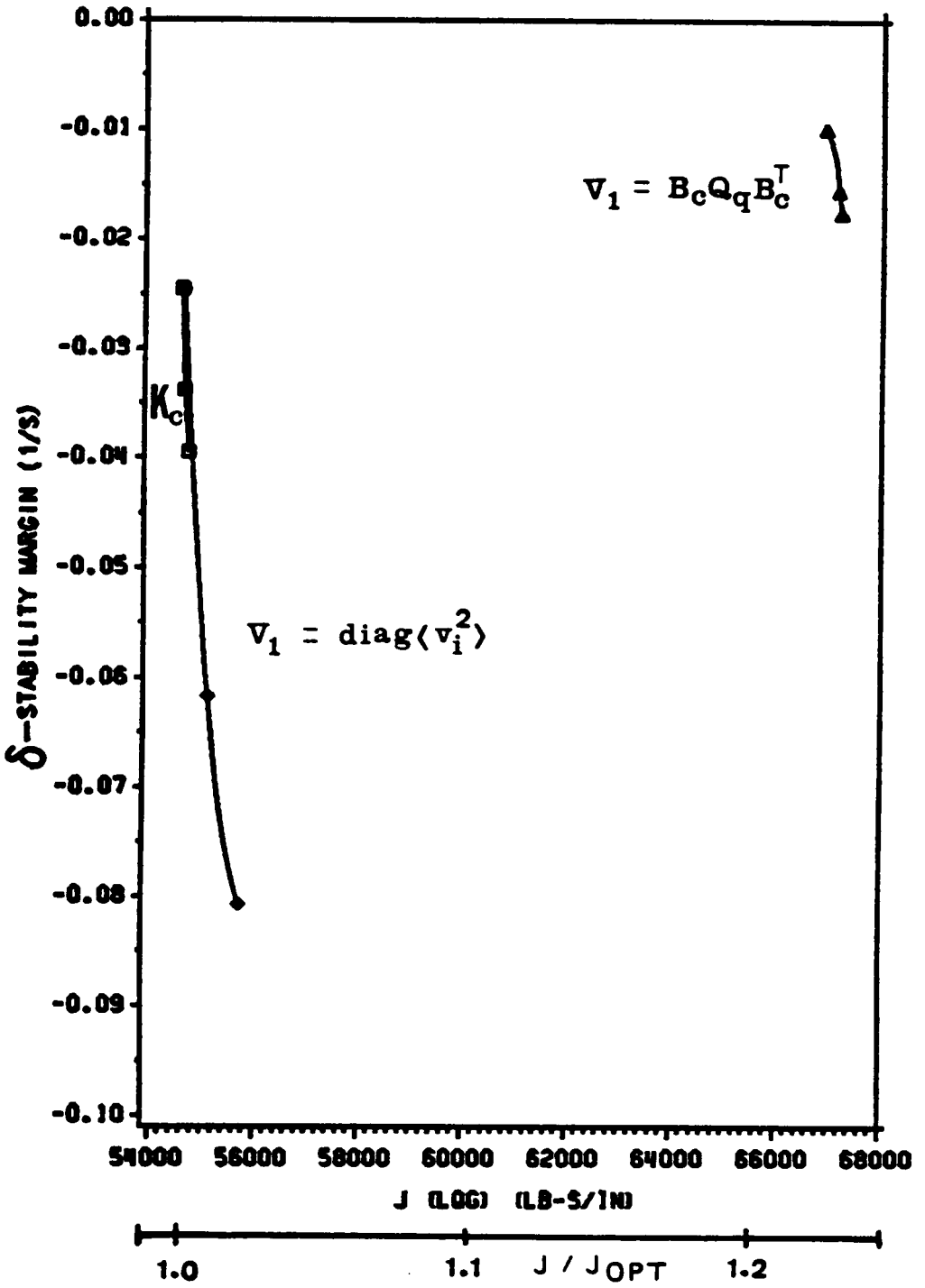

Figure 50. Stability margin vs. performance index for various optimized controller designs of the MIMO grid structure.

Table 37. Optimization results for the MIMO grid structure. $[V_1 = diag(v_i^2).]$

(System eigenvalues in 1/sec.)

Weight	$\mu = 1000.$	$\mu = 100.$	$\mu = 10.$
Observer poles	-3.955 -22.296 $-10.979 \pm j3.18$ $-1.826 \pm j5.20$ $-9.141 \pm j17.35$ $-3.163 \pm j22.52$ $-7.821 \pm j28.90$ $-0.740 \pm j34.46$ $-0.469 \pm j35.54$ $-8.181 \pm j38.17$	-0.930 -155.873 -1.719 -121.571 $-3.530 \pm j5.15$ $-12.629 \pm j17.26$ $-3.194 \pm j21.74$ $-5.576 \pm j28.99$ $-0.859 \pm j34.48$ $-0.488 \pm j35.54$ $-11.497 \pm j34.91$	-0.819 -259.587 -1.501 -209.333 $-3.804 \pm j5.49$ -17.031 -38.878 $-4.158 \pm j21.39$ $-6.255 \pm j27.96$ $-0.854 \pm j34.50$ $-0.467 \pm j35.53$ $-12.002 \pm j32.32$
Residual poles (10*th and* 11*th*)	$-0.031 \pm j50.28$ $-0.025 \pm j52.80$	$-0.072 \pm j50.28$ $-0.062 \pm j52.81$	$-0.090 \pm j50.29$ $-0.081 \pm j52.81$
J/J_{OPT}	1.0004	1.0093	1.0210

Table 38. Optimum designs for the MIMO grid structure. $[V_1 = diag(v_i^2).]$

(With corresponding K_c values.)

μ	$(a_v\ b_v\ c_v\ d_v\ e_v\ f_v)^T$	K_c
1000.	−3.579 4.076 2.657 −2.896 1.713 3.442	−1.398 −0.874 −0.672 −0.066 1.406 −0.400 1.535 −0.617 −0.113 0.824 1.073 −0.491 −0.573 0.988 1.059 1.116 −0.614 −0.287 −0.475 −1.114 −0.651 0.744 0.887 0.187 0.476 0.445 0.592 0.034 −0.208 −0.141 0.760 0.497 0.210 0.743 −0.220 0.304 0.310 0.881 −0.022 −0.114 0.205 −0.137 1.070 −0.623 −0.251 −0.696 0.440 0.463 −0.911 0.873 −0.136 0.743 1.198 0.276
100.	21.862 10.736 −11.408 5.017 −4.660 6.525	−4.278 −4.751 −4.848 1.644 6.740 −3.231 8.143 −3.153 −0.989 1.699 1.313 −1.832 −0.225 2.346 2.908 1.428 −0.906 −1.037 −0.949 −3.252 −2.544 3.309 1.330 1.087 0.608 0.102 1.558 0.489 −0.297 0.403 1.419 0.506 1.491 1.258 −0.375 1.834 0.916 3.229 −0.022 0.324 1.490 0.312 3.784 −1.771 −1.137 −2.145 0.870 0.887 −1.924 3.081 0.065 2.661 3.133 1.998

μ	$(a_v\ b_v\ c_v\ d_v\ e_v f_v)^T$	K_c
10.	35.017 21.486 −18.859 7.023 −11.171 12.283	$\begin{bmatrix} -6.250 & -7.085 & -8.132 \\ 2.775 & 11.175 & -4.494 \\ 12.971 & -4.886 & -1.271 \\ 3.540 & 2.879 & -3.551 \\ -0.575 & 4.602 & 6.019 \\ 2.788 & -1.396 & -1.515 \\ -1.367 & -5.781 & -4.745 \\ 5.837 & 1.302 & 2.137 \\ 0.534 & -0.521 & 1.760 \\ 0.674 & -0.365 & 1.044 \\ 1.939 & 0.070 & 2.758 \\ 1.543 & -0.668 & 3.191 \\ 1.868 & 6.773 & -0.406 \\ 1.145 & 3.031 & 1.214 \\ 8.048 & -3.981 & -2.404 \\ -3.127 & 0.965 & 0.339 \\ -2.313 & 5.644 & 0.453 \\ 4.471 & 4.943 & 4.320 \end{bmatrix}$

Table 39. Optimization results for the MIMO grid structure. $[V_1 = B_e Q_v B_e^T.]$

(System eigenvalues in 1/sec.)

Weight	$\mu = 1000.$	$\mu = 100.$	$\mu = 10.$
Observer poles	$-0.297 \pm j4.79$ $-0.238 \pm j8.70$ $-1.264 \pm j15.11$ $-0.129 \pm j22.59$ $-0.443 \pm j31.11$ $-2.965 \pm j33.56$ $-0.220 \pm j34.57$ $-0.063 \pm j35.60$ $-26.845 \pm j36.35$	$-0.292 \pm j4.80$ $-0.322 \pm j8.72$ $-1.018 \pm j15.14$ $-0.143 \pm j22.59$ $-0.577 \pm j31.07$ $-2.443 \pm j33.02$ $-0.226 \pm j34.60$ $-0.055 \pm j35.52$ $-33.99 \pm j42.27$	$-0.303 \pm j4.77$ $-0.141 \pm j8.68$ $-1.055 \pm j15.04$ $-0.111 \pm j22.59$ $-0.497 \pm j31.08$ $-2.064 \pm j33.27$ $-0.243 \pm j34.62$ $-0.062 \pm j35.61$ $-41.788 \pm j48.59$
Residual poles (10*th and* 11*th*)	$-0.011 \pm j50.26$ $-0.010 \pm j52.79$	$-0.016 \pm j50.26$ $-0.015 \pm j52.79$	$-0.017 \pm j50.26$ $-0.019 \pm j52.79$
J/J_{OPT}	1.2259	1.2304	1.2311

Table 40. Optimum designs for the MIMO grid structure. $[V_1 = B_c Q_q B_c^T.]$

(With corresponding K_e values.)

μ	$(a_q\ b_q\ c_q)^T$	K_c
1000.	7.566 8.075 7.151	$\begin{bmatrix} -0.870 & -1.476 & -0.233 \\ 0.536 & 1.242 & 0.175 \\ 0.103 & 0.132 & 0.025 \\ 0.768 & 0.949 & -0.233 \\ 0.128 & 0.242 & -0.015 \\ 0.098 & 0.010 & -0.021 \\ -0.221 & -0.010 & -0.054 \\ 0.017 & 0.150 & 0.047 \\ 0.668 & 1.017 & 0.377 \\ -6.948 & -10.775 & -0.940 \\ 3.519 & 5.418 & 0.465 \\ 0.263 & 0.389 & 0.033 \\ 1.056 & 1.569 & 0.160 \\ 0.185 & 0.277 & 0.036 \\ 0.019 & 0.018 & 0.027 \\ -0.093 & -0.179 & -0.047 \\ 0.029 & 0.122 & 0.030 \\ 0.449 & 0.863 & 0.122 \end{bmatrix}$
100.	10.867 11.181 10.888	$\begin{bmatrix} -1.050 & -1.670 & -0.285 \\ 0.661 & 1.360 & 0.211 \\ 0.158 & 0.193 & 0.040 \\ 0.907 & 1.156 & -0.266 \\ 0.173 & 0.313 & -0.023 \\ 0.138 & 0.026 & -0.026 \\ -0.277 & -0.156 & -0.075 \\ 0.037 & 0.198 & 0.058 \\ 0.914 & 1.379 & 0.476 \\ -10.236 & -15.130 & -1.472 \\ 5.068 & 7.442 & 0.716 \\ 0.512 & 0.733 & 0.069 \\ 1.556 & 2.228 & 0.248 \\ 0.313 & 0.445 & 0.058 \\ 0.046 & 0.054 & 0.043 \\ -0.155 & -0.287 & -0.071 \\ 0.057 & 0.190 & 0.046 \\ 0.745 & 1.345 & 0.201 \end{bmatrix}$

μ	$(a_q\ b_q\ c_q)^T$	K_c
10.	14.226 15.840 12.103	$\begin{bmatrix} -0.998 & -1.860 & -0.280 \\ 0.650 & 1.593 & 0.220 \\ 0.067 & 0.102 & 0.019 \\ 1.242 & 1.501 & -0.269 \\ 0.184 & 0.301 & -0.019 \\ 0.141 & 0.053 & -0.028 \\ -0.323 & -0.212 & -0.083 \\ 0.057 & 0.244 & 0.063 \\ 1.111 & 1.698 & 0.531 \\ -13.186 & -20.652 & -1.876 \\ 6.946 & 10.844 & 0.974 \\ 0.312 & 0.479 & 0.043 \\ 2.272 & 3.423 & 0.347 \\ 0.357 & 0.542 & 0.062 \\ 0.070 & 0.092 & 0.043 \\ -0.214 & -0.390 & -0.083 \\ 0.099 & 0.267 & 0.057 \\ 1.051 & 1.892 & 0.250 \end{bmatrix}$

Table 41. Optimization results for the MIMO grid structure. $[K_c.]$

(System eigenvalues in 1/sec.)

Weight	$\mu = 1000.$	$\mu = 100.$	$\mu = 10.$
Observer poles	$-7.231 \pm j2.90$ $-1.875 \pm j5.14$ $-8.601 \pm j6.37$ $-8.883 \pm j19.94$ $-3.010 \pm j22.68$ $-7.134 \pm j30.52$ $-0.754 \pm j34.46$ $-0.474 \pm j35.54$ $-7.701 \pm j38.36$	$-12.025 \pm j1.55$ $-1.811 \pm j5.24$ -4.885 -23.398 $-10.930 \pm j16.94$ $-3.692 \pm j22.82$ $-8.322 \pm j27.66$ $-0.769 \pm j34.44$ $-0.504 \pm j35.52$ $-9.251 \pm j36.40$	-7.833 -28.196 $-1.800 \pm j5.27$ -4.260 -38.432 $-9.870 \pm j14.90$ $-4.338 \pm j23.00$ $-7.678 \pm j25.68$ $-0.779 \pm j34.44$ $-0.521 \pm j35.51$ $-9.578 \pm j35.02$
Residual poles (*10th and 11th*)	$-0.032 \pm j50.28$ $-0.025 \pm j52.80$	$-0.041 \pm j50.27$ $-0.034 \pm j52.80$	$-0.047 \pm j50.27$ $-0.039 \pm j52.80$
J/J_{OPT}	1.0000	1.0010	1.0024

Table 42. Optimum designs for the MIMO grid structure. $[K_c]$

μ	$(a_k\ b_k\ c_k\ d_k\ e_k\ f_k)^T$
1000.	1.0003 1.0002 1.0001 1.0002 0.9999 1.0000
100.	1.395 1.429 1.349 1.448 1.224 1.382
10.	1.695 1.761 1.635 1.796 1.397 1.684

a V_1 matrix with many zeros. If V_1 is partitioned into four 9×9 blocks, three of those blocks contain only zeros. Only the lower diagonal block is non-zero. The result is appreciable performance degradation and small stability margins.

The initial condition for $V_1 = diag(v_i^2)$ was set as I (see Table 34 for properties), and K_c was initially set at the statistical optimum (see Table 35). $V_1 = B_c Q_q B_c^T$ had $a_Q = (5\ 5\ 5)^T$. For extremely large μ 's, i.e., a heavy penalty is placed on performance in the optimization procedure, the fact that K_c produced the statistical optimum is not surprising, but for $V_1 = diag(v_i^2)$, even though $V_2 \neq W_2$ but rather was defined by MESS, NEWSUMT-A was still able to produce an effective δ and J which were comparable to the statistical optimum, i.e., $\delta = -0.02454$ sec^{-1} and $J = 54606.\,\text{lb} - \text{sec}/in$ for $V_1 = diag(v_i^2)$ versus $\delta = -0.02564$ sec^{-1} and $J = 54582.\,\text{lb} - \text{sec}/in$ for the stochastic statistical optimum. The case $V_1 = B_c Q_q B_c^T$ could not produce the statistical optimum.

Figures 51 - 54 illustrate the root-locus plots of the optimum designs. They show the evolution of the closed-loop system poles (regulator + observer) for the different values of μ. As can be seen, as μ decreases in value (i.e., the stability margin of the residual poles increases), some of the observer poles significantly increase their speed. Some of the others vary in terms of increasing and decreasing their speed. And the remainder remain virtually stuck in their locations; these poles are the ones closest to the regulator poles. The regulator poles are essentially fixed.

Finally, stability robustness tests were also applied for $\zeta = 0.005$. The robustness tests were performed using the knowledge of the first 20 modes of the grid in order to insure that the optimum controllers do not have any problems with the higher frequency modes which were not taken into account in this analysis.

All the robustness tests were violated by the tenth and eleventh modes, yet it should be emphasized that these two modes were taken into account explicitly by the optimization routine and were stable. It should also be recalled that the original KBF design based on the actual statistical environment also produced a violation for these two modes. The plots for the lowest emphasis on performance - - fastest observer speeds (low μ and high K_c) are presented for each of the design formulations. The case $\mu = 10.$ for $V_1 = diag(v_i^2)$ is shown in Figures 55 and 56 for the (input) and

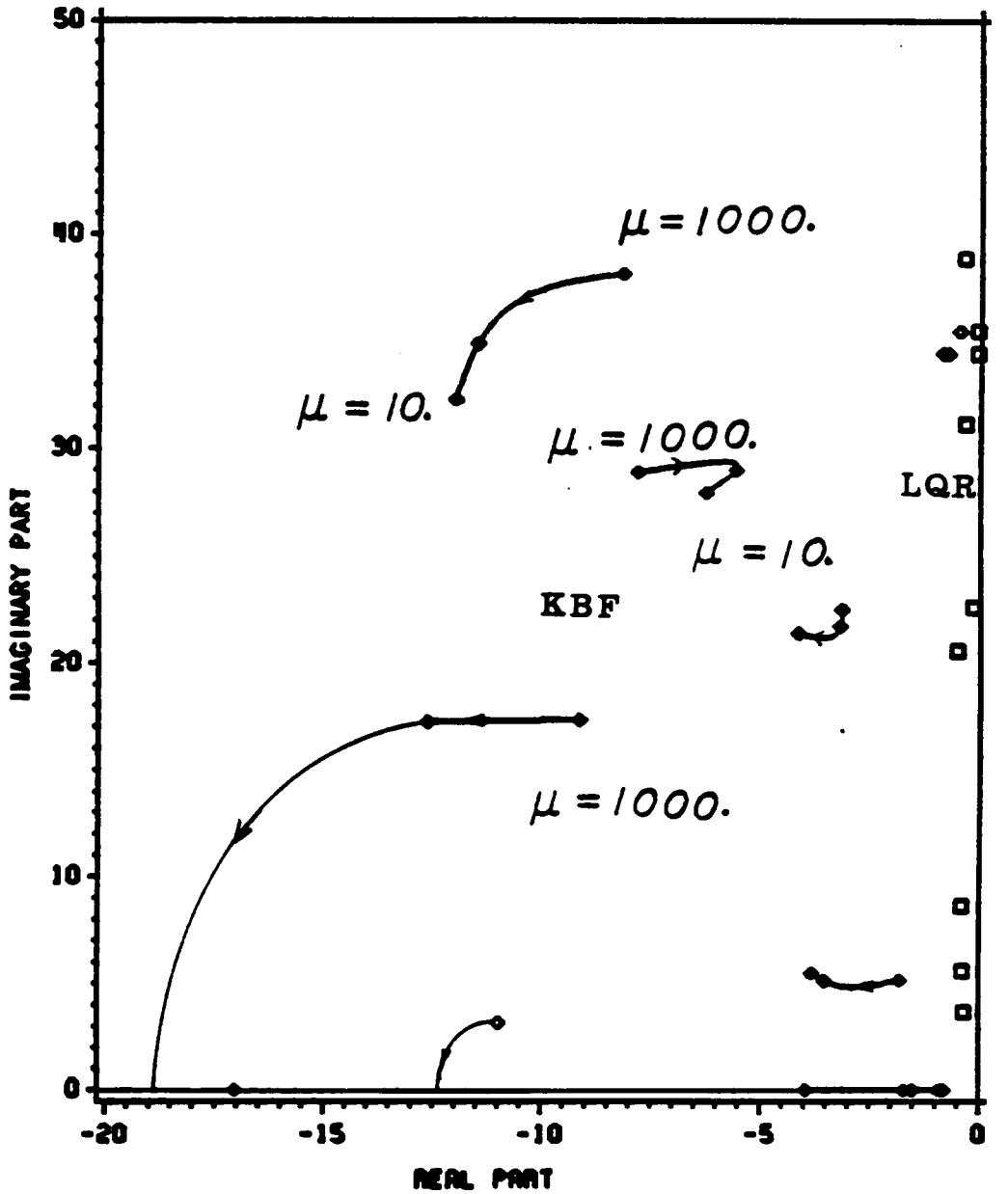

Figure 51. Evolution of the closed-loop poles as a function of the weighting parameter for the MIMO grid structure. [$V_1 = diag(v_i^2)$.]

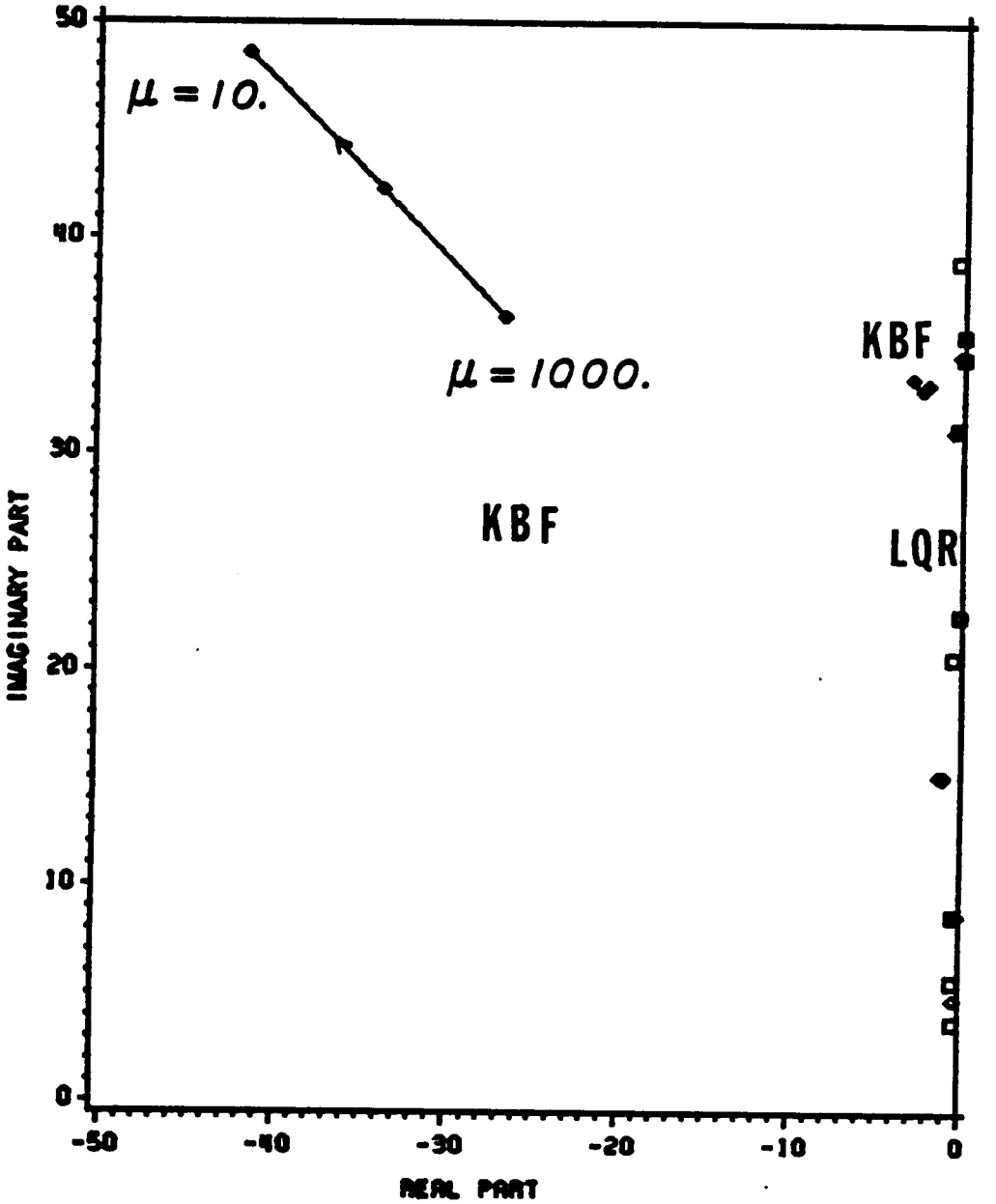

Figure 52. Evolution of the closed-loop poles as a function of the weighting parameter for the MIMO grid structure. [$V_1 = B_c Q_c B_c^T$.]

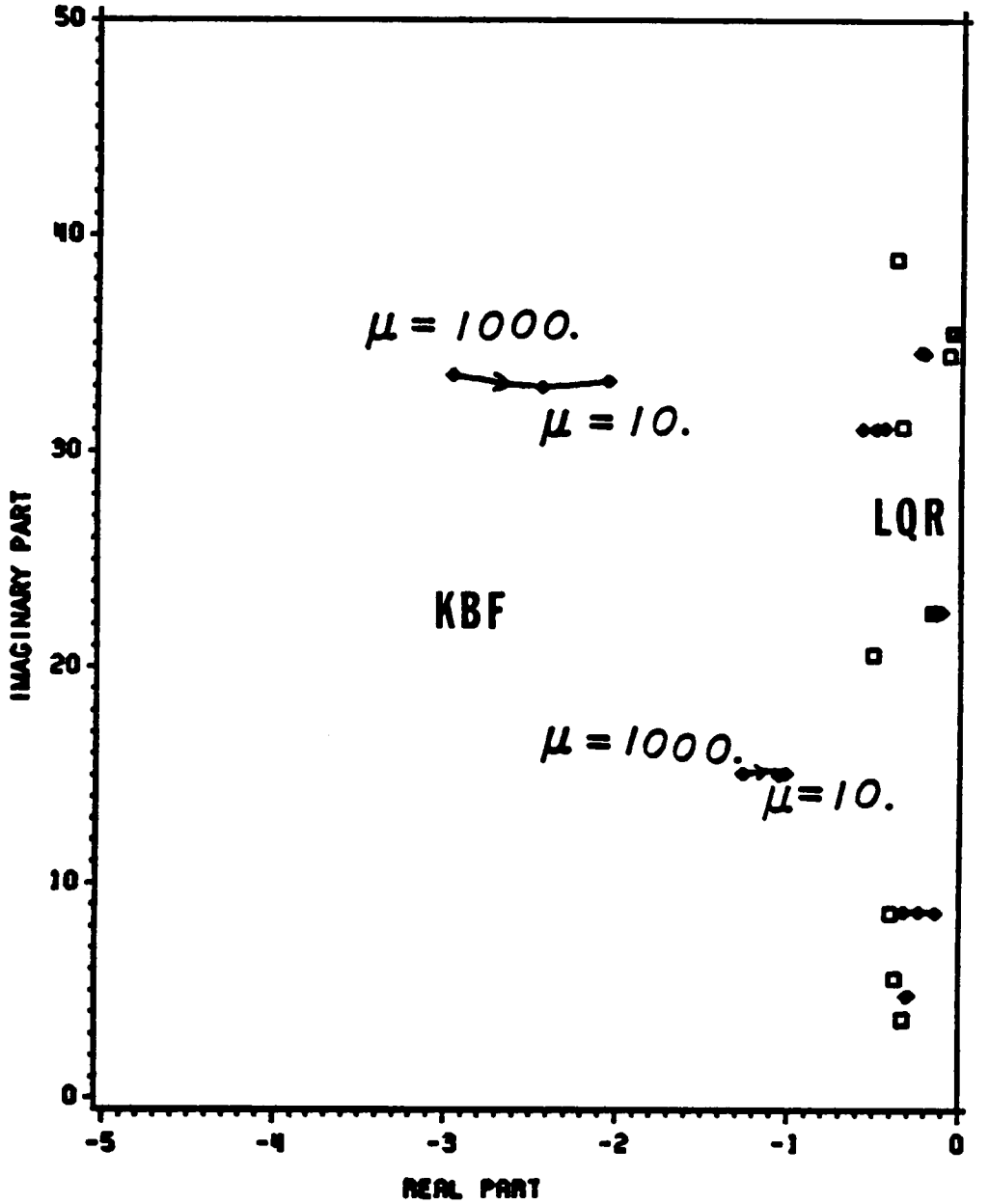

Figure 53. Evolution of the closed-loop poles as a function of the weighting parameter for the MIMO grid structure. [$V_1 = B_c Q_c B_c^T$.]

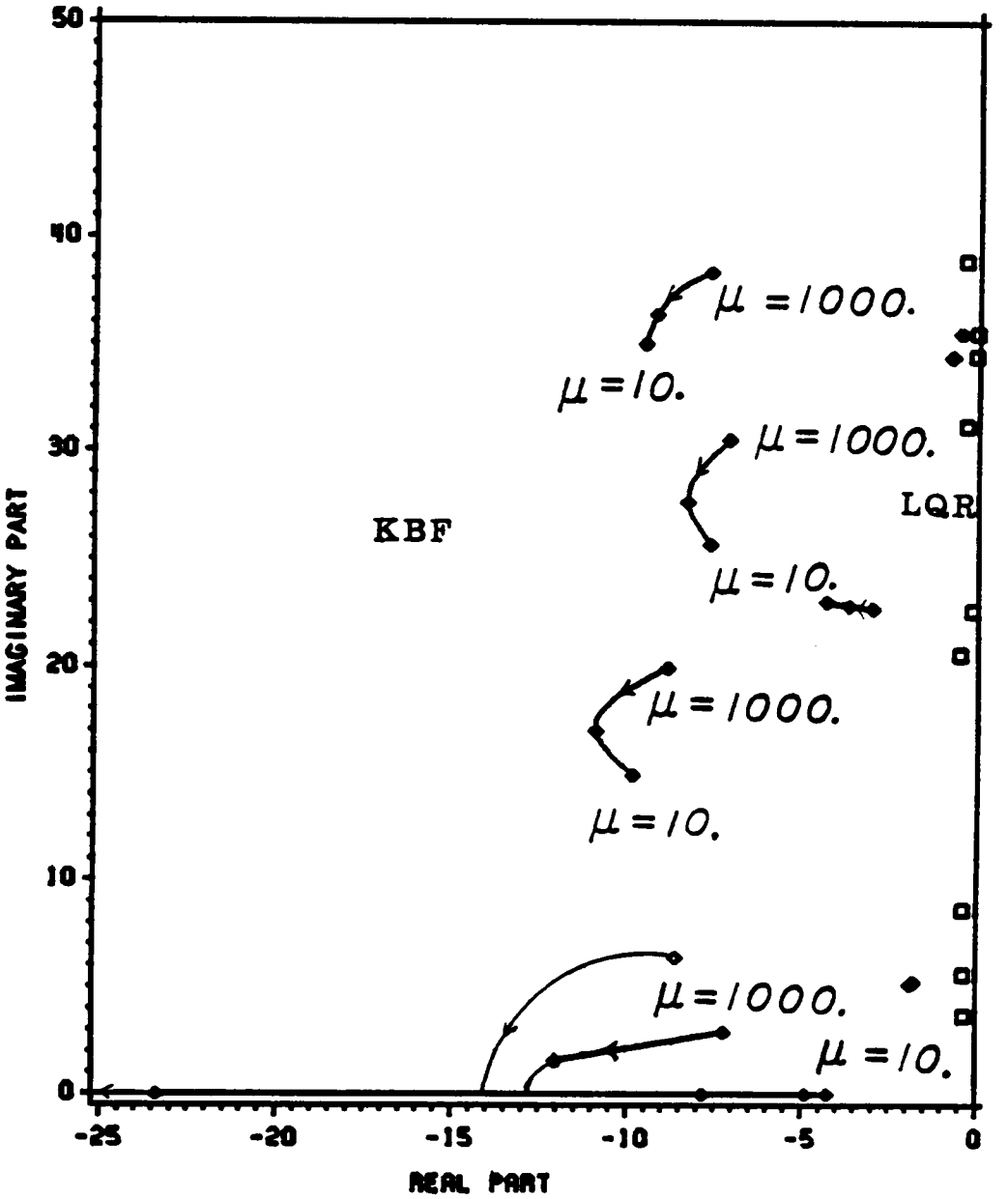

Figure 54. Evolution of the closed-loop poles as a function of the weighting parameter for the MIMO grid structure. $[K_c.]$

(output) multiplicative uncertainties, respectively. Although, the high frequency modes of the (input) multiplicative uncertainty case barely satisfy the robustness criterion (except for modes ten and eleven, of course), for the (output) multiplicative uncertainty case, the high frequency $14th$ mode just barely starts violating the robustness criterion. The case $\mu = 10.$ for $V_1 = B_c Q_c B_c^T$ is shown in Figures 57 and 58 for the (input) and (output) multiplicative uncertainties, respectively. For both cases, the results show appreciable robustness test violations all the way out to the $15th$ mode. All these modes were not explicitly taken into account by the optimization routine. The LTR technique is beginning to recover the loop transfer matrix of the regulator. This is a property of the technique, and, for this combined control/observation spillover problem, it suggests that many more residual modes need to be considered in the design process to insure stability. The case $\mu = 10.$ for K_c is shown in Figures 59 and 60 for the (input) and (output) multiplicative uncertainties, respectively. It, on the other hand, satisfies the high frequency robustness criterion for modes twelve and above for both (input) and (output) multiplicative uncertainty cases. Again, what is typically seen is that the faster observers produce higher observer gain matrices (see Tables 38, 40, and 42), and, therefore, the $\bar{\sigma}\{G(j\omega)K(j\omega)[I + G(j\omega)K(j\omega)]^{-1}\}$ and $\bar{\sigma}\{K(j\omega)G(j\omega)[I + K(j\omega)G(j\omega)]^{-1}\}$ curves go up in magnitude and, thus, have a potential of causing a robustness test violation in the high frequency domain response of low damped structures. Low damped structures produce more appreciable peaks which cause this problem.

Overall, it was demonstrated that the LTR technique is not a good one in terms of spillover alleviation of low-damping structures. It produced small stability margins, high performance degradation, and appreciable robustness test violations.

The computational costs, as measured by the CPU time on an IBM 3084 computer, for all three μ designs combined, are given in Table 43. The diagonal case was the most expensive, followed by the LTR. Both had to solve the nonlinear Riccati Equation for such a high-order problem. The LTR technique, with fewer design variables, had an appreciably lower execution time, i.e., approximately 1/3 of the time for the $V_1 = diag(v_i^2)$ case. The K_c design did not require the solution of a nonlinear Riccati Equation. It solved only the linear Lyapunov Equation which was something $V_1 = diag(v_i^2)$ and $B_c Q_c B_c^T$ also had to solve. As a result, the execution time for the K_c

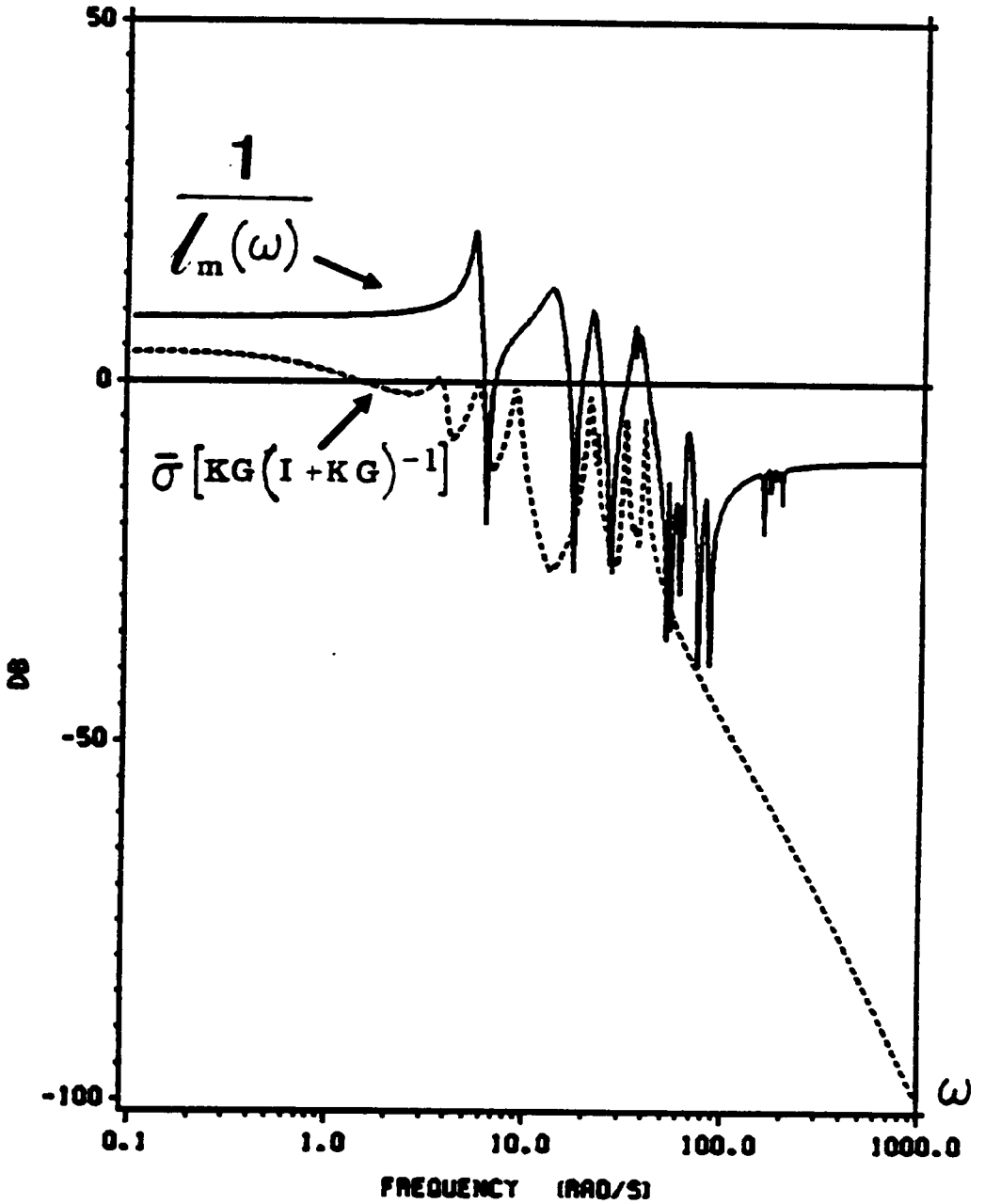

Figure 55. Robustness plot of the loop transfer matrix for (input) multiplicative uncertainty. LQG grid optimized design. [$V_1 = diag(v_i^2)$, $\mu = 10.$, $\zeta = 0.005.$]

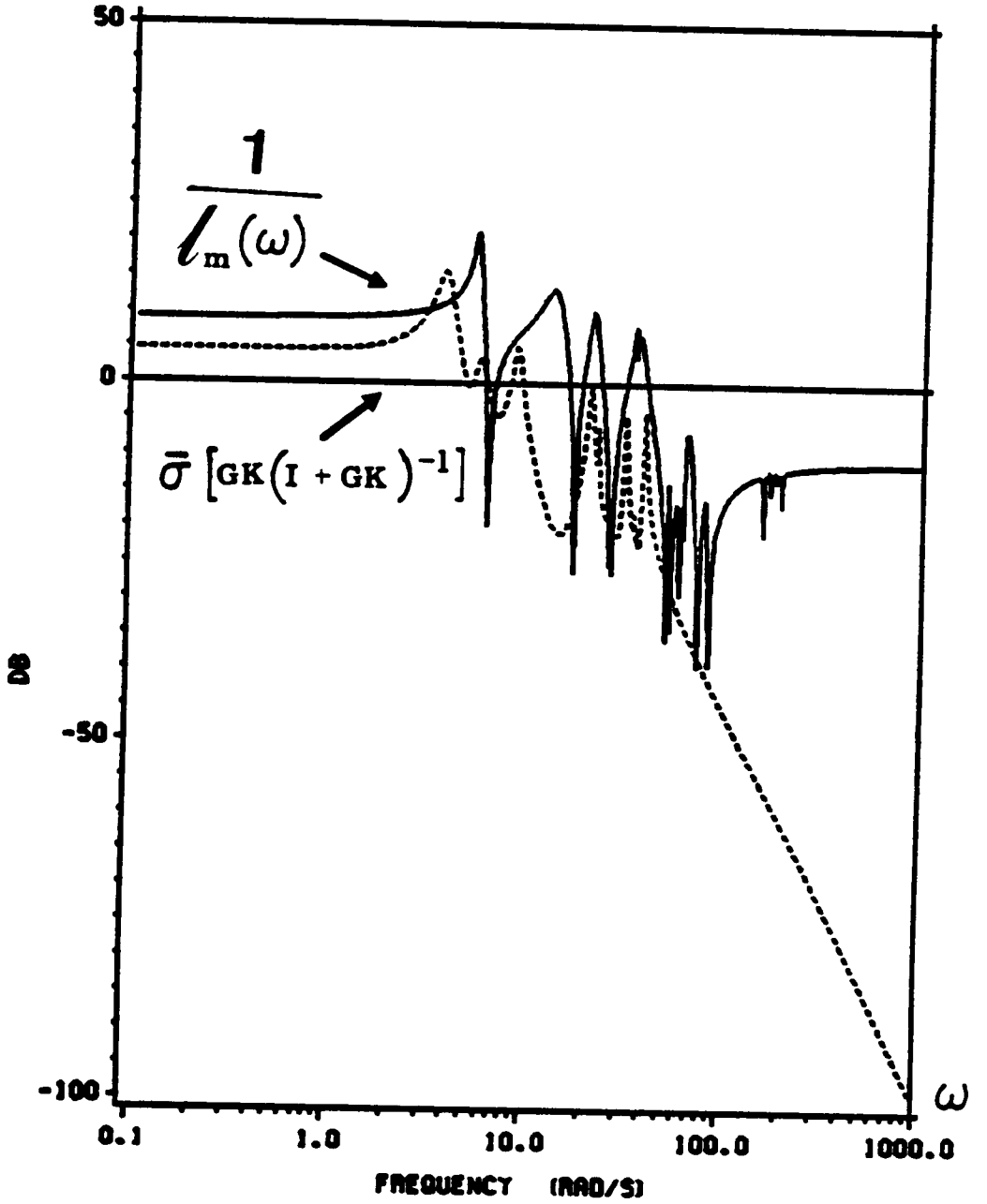

Figure 56. Robustness plot of the loop transfer matrix for (output) multiplicative uncertainty. LQG grid optimized design. [$V_1 = diag(v_i^2)$, $\mu = 10.$, $\zeta = 0.005.$]

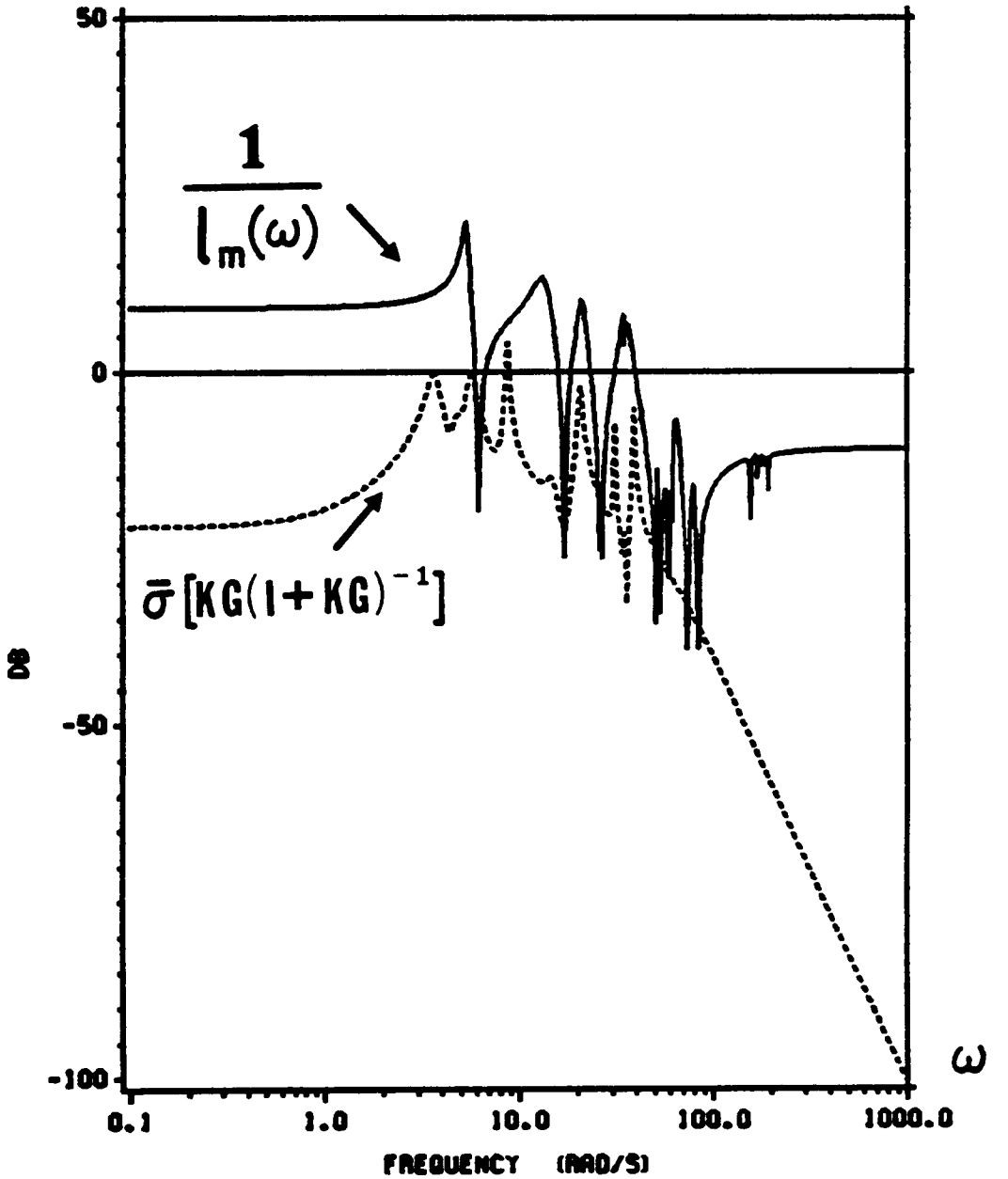

Figure 57. Robustness plot of loop transfer matrix for (input) multiplicative uncertainty. LQG grid optimized design. [$V_1 = B_c Q_c B_c^T$, $\mu = 10, \zeta = 0.005$.]

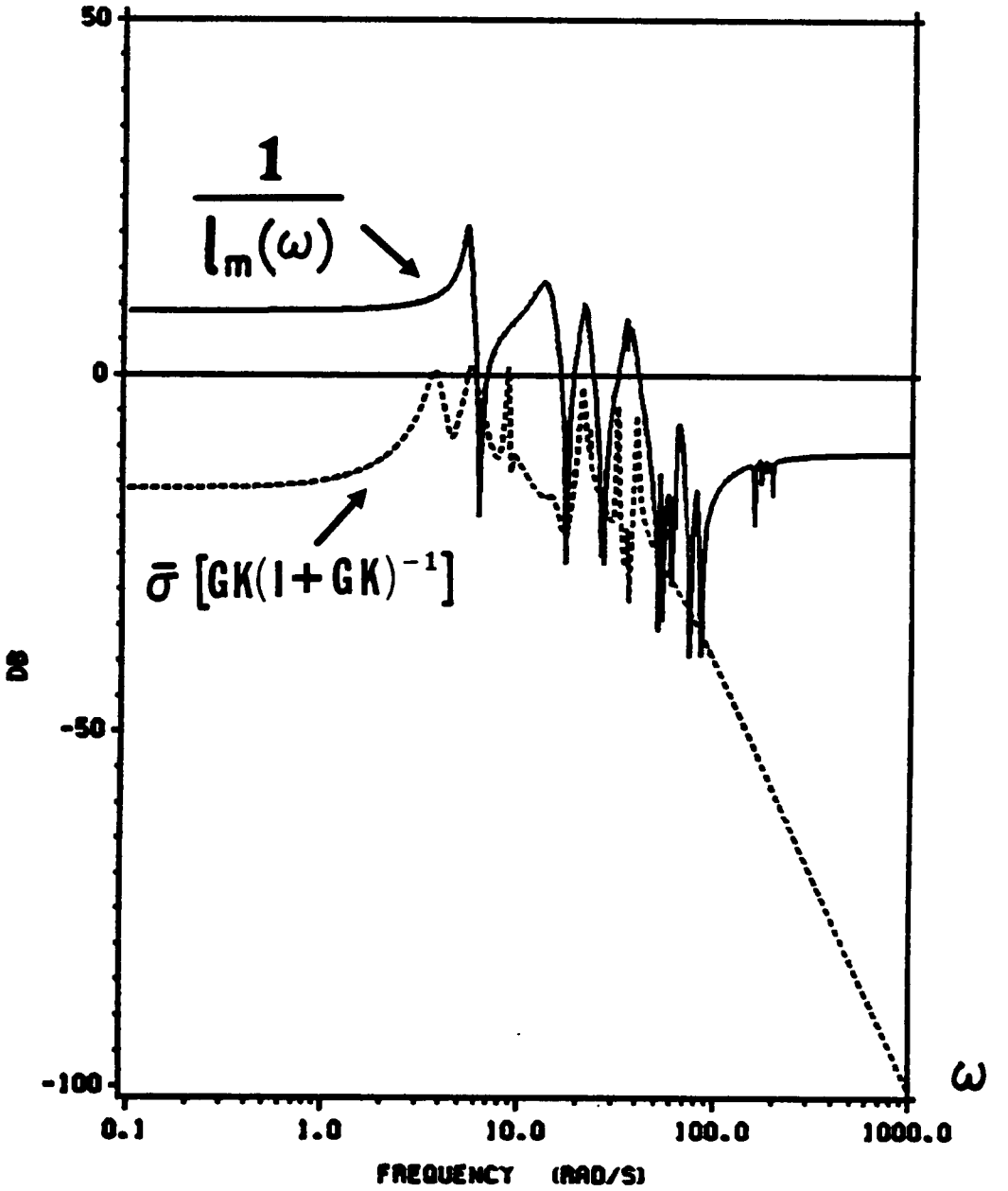

Figure 58. Robustness plot of loop transfer matrix for (output) multiplicative uncertainty. LQG grid optimized design. [$V_1 = B_c Q_\phi B_c^T, \mu = 10, \zeta = 0.005$.]

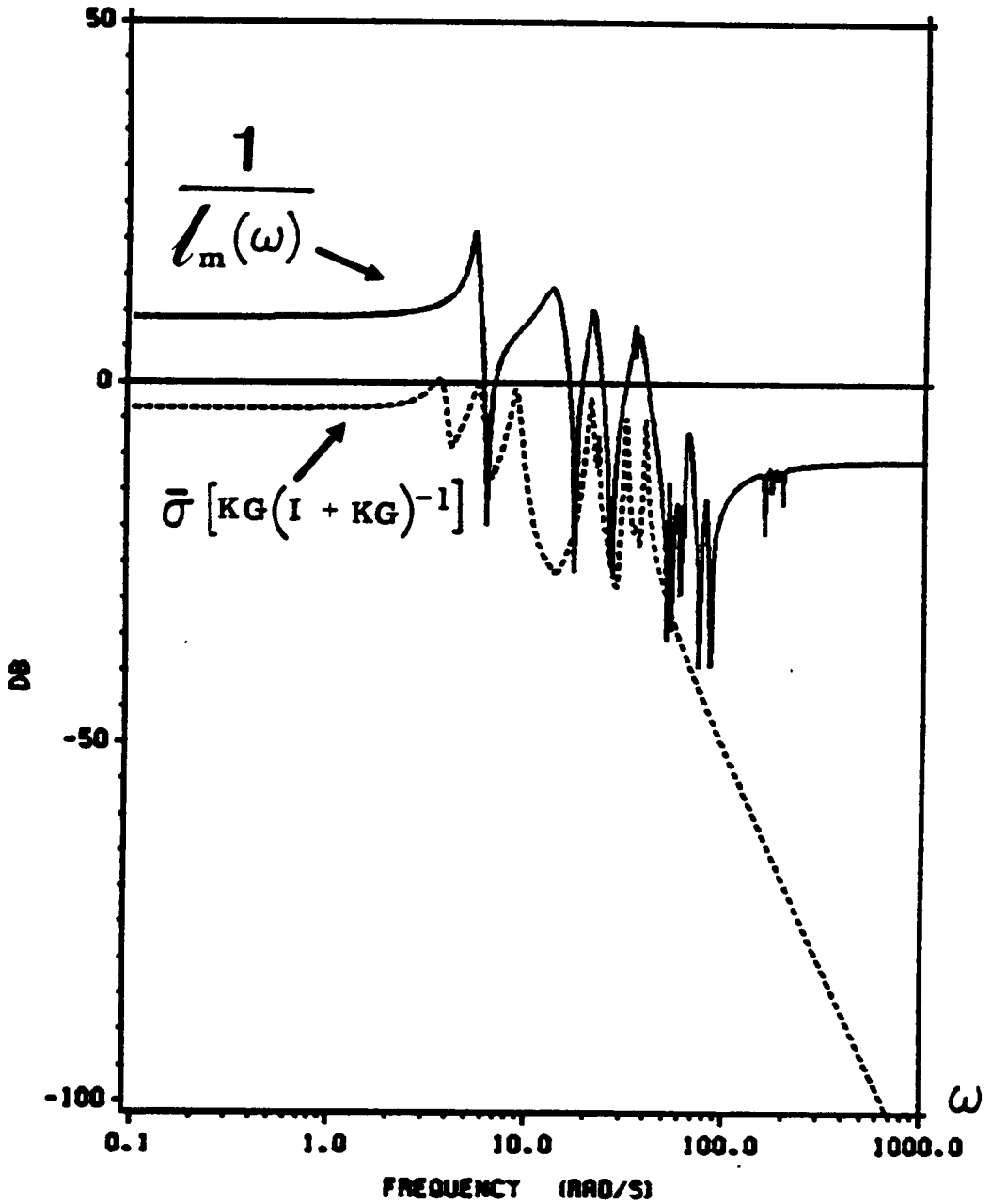

Figure 59. Robustness plot of the loop transfer matrix for (input) multiplicative uncertainty. LQG grid optimized design. [K_c, $\mu = 10.$, $\zeta = 0.005$.]

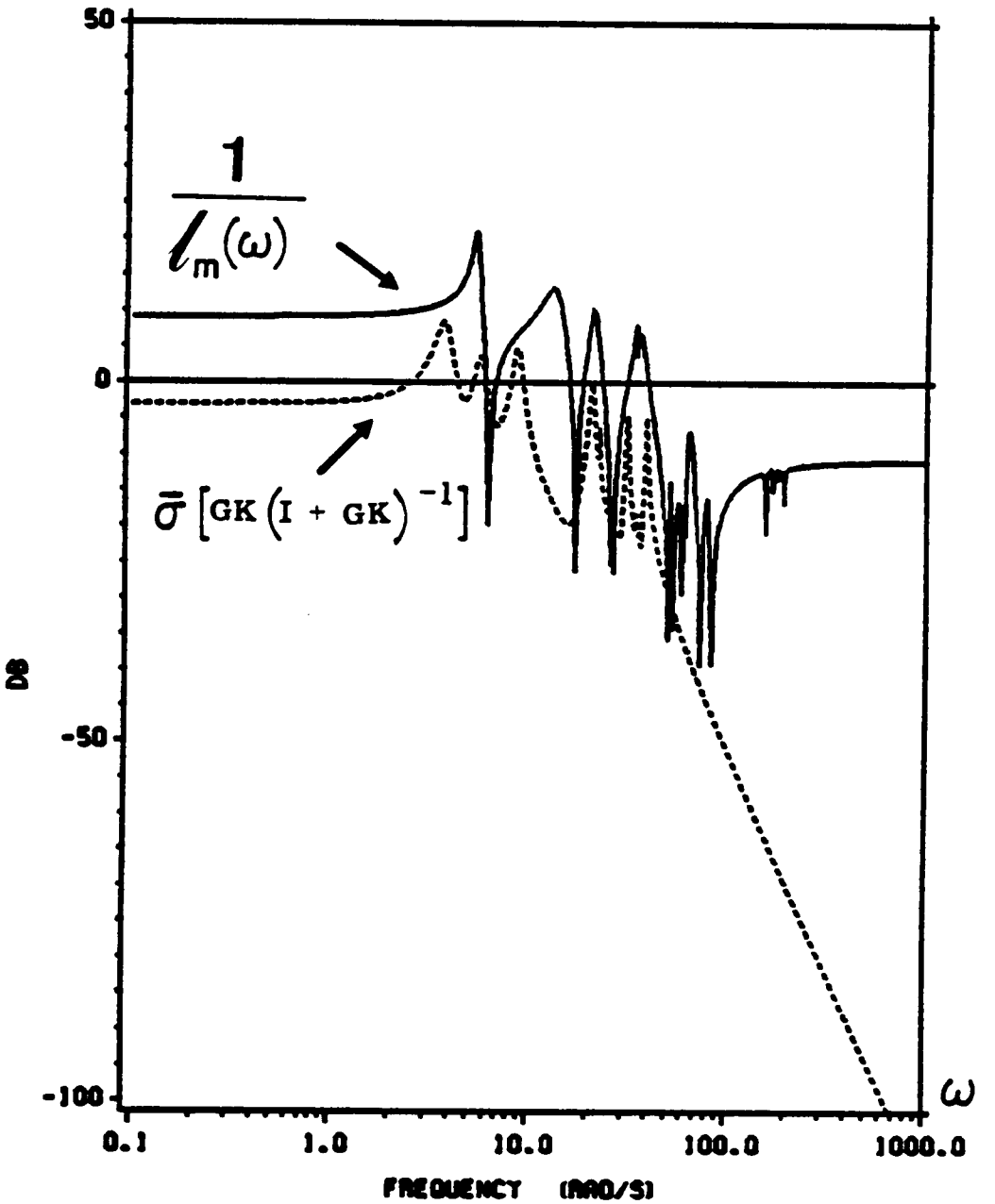

Figure 60. Robustness plot of the loop transfer matrix for (output) multiplicative uncertainty. LQG grid optimized design. [K_c, $\mu = 10.$, $\zeta = 0.005.$]

design was comparatively smaller, i.e., approximately 1/4 of the time for the $V_1 = diag(v_i^2)$ case which had the same number of design variables. The K_c execution time was also smaller than that for the LTR problem which had fewer design variables, i.e., approximately 2/3 of the time for the $V_1 = B_c Q_\phi B_c^T$ case.

7.6. PROPOSED DESIGN PROCEDURE FOR SPILLOVER STABILIZATION

Based on all the results presented, for the centralized controller (i.e., SISO and MIMO), the following design procedure is suggested:

(1) Once the controlled modes have been selected, design an LQR to achieve a reasonable compromise between performance and control requirements, and a KBF with the best available noise statistics.

(2) Apply a robustness test where the uncertainty curve includes all the uncontrolled modes and corresponds to a reasonable value of the structural damping.

(3) Identify the uncontrolled modes which either fail the robustness test or have a small or negative stability margin. The modes (residual) are candidates for spillover destabilization. If there are none, the design is completed.

(4) Apply the foregoing optimization procedure to the design of an observer which stabilizes the modes identified in step (3) with respect to spillover.

(5) Apply the robustness test to the new controller to check that it is satisfied by all the robust modes of the original controller, i.e., the robustness test is violated by at *most* the residual modes identified in step (3) and no more. If it is, the design is completed, if not, go back to step (4) with the new set of residual modes.

Table 43. Computational costs for the MIMO grid structure.

(CPU time in minutes; IBM 3084)

Design	*Time*
$V_1 = diag(v_i^2)$	574.02
$V_1 = B_c Q_q B_c^T$	213.14
K_c	144.67

CHAPTER 8. CONCLUSIONS AND RECOMMENDATIONS

This dissertation considered the stabilization of the neglected dynamics of the higher modes of vibration. The influence of the structure of the plant noise intensity matrix of the Kalman-Bucy Filter on the stability margin of the residual modes has been demonstrated. An optimization procedure was presented which uses information on the residual modes to minimize spillover (i.e., maximize the stability margin) of known residual modes while preserving robustness vis-à-vis the unknown dynamics. This procedure selects either the optimum plant noise intensity matrix or the optimum observer gain matrix directly to maximize the stability margins of the residual modes and properly place the observer poles. The proposed method was demonstrated for both centralized and decentralized modal control. This design procedure is based on minimizing a composite cost functional which includes a contribution from system stability and from performance. The stability of the unknown dynamics (viewed as unstructured) is taken care of by a robustness test. It is the robustness test which decides which modes are robust and which are residual. It was found that only a small number of design variables was necessary in the optimization procedure to achieve large improvements in spillover stability.

Still, much work needs to be done in the area of spillover stabilization. One topic which needs further work is computer efficiency. The design procedure which implemented an optimizer required a considerable amount of computer time in some instances. Some recommendations for future work include investigating the following areas:

- A thorough investigation of the optimization space should be performed. It was found that the optimizer produced different designs for different initial conditions indicating many local optima. As a result, the optimizer sometimes had problems finding solutions. A thorough investigation into the actual space that the optimizer will be searching in would greatly help in the understanding of the problem and in properly formulating the optimization problem for best implementation.

- The derivatives of the objective function and constraints with respect to the design variables can be calculated analytically. These derivatives are used by the optimizer to lead the search in certain directions. These derivatives have been computed by finite differences. Analytical evaluation of these derivatives could considerably decrease the computer time needed by the optimization routine.

This is by no means a complete list of recommendations. There are, of course, many other factors which should be studied in terms of computer efficiency, i.e., computer software, etc.

Other than computer efficiency, the spillover problem is still not totally understood, and much work still needs to be done. Some recommendations for future work include looking at different structures. This dissertation only looked at a simple beam and a grid structure. There are many other structures which need to be analyzed which are currently being considered for launch into orbit. These are extremely large in scale. They include solar arrays, PACOSS representative system, Space Telescope, large flexible antennas, and, of course, the Space Station. Much smaller structures should also be investigated since the spillover problem is still not totally understood, and much information and insight could be obtained from these smaller order models.

Another major issue which was not addressed is the time delay factor. It was assumed that the controller operated instantaneously, yet, in physical systems, time delays do occur, and the delays may produce significant effects on the control system. Understanding this problem can become critical especially when discussing large order systems where the actuators and sensors of a controller may be located far apart. It takes time for a signal to travel from one point to another and to pass along the appropriate control law information. If time delays are not considered, the actual system control mechanism may greatly differ from the originally designed controller.

Other topics for investigation include stochastic decentralized modal control, H_∞ control, robustness test implementations based on *structured* uncertainties, and considering system nonlinearities and different design variables in the optimization routine.

REFERENCES

(1) Balas, M. J., "Active Control of Flexible Systems," *Journal of Optimization Theory and Applications,* Vol. 25, No. 3, July 1978, pp. 415 - 436.

(2) Balas, M. J., "Feedback Control of Flexible Systems," *IEEE Transactions on Automatic Control,* Vol. AC-23, No. 4, August 1978, pp. 673 - 679.

(3) Balas, M. J., "Enhanced Modal Control of Flexible Structures via Innovations Feedthrough," *Int. Journal of Control,* Vol. 32, No. 6, 1980, pp. 983 - 1003.

(4) Balas, M. J., "Trends in Large Space Structure Control Theory. Fondest Hopes, Wildest Dreams.," *IEEE Transactions on Automatic Control,* Vol. AC-27, No. 3, June 1982, pp. 522 - 535.

(5) Balas, M. J., "Enhanced Modal Control of Flexib'e Structures via Innovations Feedthrough," Proceedings of the Second VPI&SU/AIAA Symposium on Dynamics and Control of Large Flexible Spacecraft, Blacksburg, Virginia, June 21 -23, 1979, pp. 677 - 700.

(6) Morgenthaler, D. R., and Gehling, R. N., "Design and Analysis of the PACOSS Representative System," Vibration Damping Workshop II, Las Vegas, March 1986.

(7) Lynch, P. J., and Banda, S. S., "Active Control for Vibration Damping," Vibration Damping Workshop II, Las Vegas, March 1986.

(8) Canavin, J., "Control Technology for Large Space Structures," AIAA Paper 78-1691, Conference on Large Space Platforms, Los Angeles, September 27 - 29, 1978.

(9) Balas, M. J., "Direct Velocity Feedback Control of Large Space Structures," *AIAA Journal of Guidance and Control,* Vol. 2, No. 3, May - June 1979, pp. 252 - 253.

(10) Kosut, R. L., and Salzwedel, H., "Stability and Robustness Control Systems for Large Space Structures," Proceedings of the Third VPI&SU/AIAA Symposium on Dynamics and Control of Large Flexible Spacecraft, Blacksburg, Virginia, June 15 - 17, 1981, pp. 343 - 364.

(11) Canavin, J. R., "The Control of Spacecraft Vibrations Using Multivariable Output Feedback," AIAA Paper 78-1419, AIAA/AAS Astrodynamics Conference, Palo Alto, California, August 7 - 9, 1978.

(12) Elliott, L. E., Mingori, D. L., and Iwens, R. P., "Performance of Robust Output Feedback Controller for Flexible Spacecraft," Proceedings of the Second VPI&SU/AIAA Symposium on Dynamics and Control of Large Flexible Spacecraft, Blacksburg, Virginia, June 21 - 23, 1979, pp. 409 - 420.

(13) Martinovic, Z. N., Haftka, R. T., Hallauer Jr., W. L., and Schamel II, G. C., "A Comparison of Active Vibration Control Techniques: Output Feedback vs. Optimal Control," AIAA-87-0904, AIAA Dynamics Specialists Conference, Monterey, California, April 9 - 10, 1987, pp. 610 - 621.

(14) Sesak, J. R., Likins, P. W., and Coradetti, T., "Flexible Spacecraft Control by Model Error Suppression," *J. Astronautical Sciences,* Vol. 27, No. 2, April - May 1979.

(15) Calico, R. A., and Janiszewski, A. M., "Control of a Flexible Satellite via Elimination of Observation Spillover," Proceedings of the Third VPI&SU/AIAA Symposium on Dynamics and Control of Large Flexible Spacecraft, Blacksburg, Virginia, June 15 - 17, 1981, pp. 15 - 33.

(16) Calico, R. A., and Moore, S., "The Effects of Structural Perturbations on Modal Suppression," Proceedings on the Fifth Symposium on Dynamics and Control of Large Structures, Blacksburg, Virginia, June 12 - 14, 1985, pp. 341 - 351.

(17) Kosut, R. L., Salzwedel, H., and Emami-Naeini, A., "Robust Control of Flexible Spacecraft," *AIAA Journal of Guidance, Control, and Dynamics,* Vol. 6, No. 2, March - April 1983, pp. 104 - 111.

(18) Gupta, N. K., "Frequency-Shaped Cost Functional: Extension of Linear-Quadratic-Gaussian Design Methods," *AIAA Journal of Guidance,* Vol. 3, No. 6, November - December 1980, pp. 529 - 535.

(19) Ridgely, D. B., and Banda, S. S., *Introduction to Robust Multivariable Control,* AFWAL-TR-85-3102, February 1986.

(20) Preumont, A., "Spillover Alleviation in Active Control of Flexible Structures," *AIAA Journal of Guidance and Control,* (to be published), 1987.

(21) Ceballos, D. C., and Neto, A. R., "Truncated Elastic Modes Coupling Effects Minimization Method by Using Special Attitude Control Scheme," Proceedings of the Third International Modal Analysis Conference, Orlando, FL, January 1985, pp. 1227 - 1233.

(22) Calise, A. J., and Moerder, D. D., "Optimal Output Feedback Design of Systems with Ill-conditioned Dynamics," *Automatica,* Vol. 21, No. 3, 1985, pp. 271 - 276.

(23) Sesak, J. R., Likins, P., and Coradetti, T., "Flexible Spacecraft Control by Model Error Sensitivity Suppression," presented at the 2nd VPI/AIAA Symposium on Dynamics and Control of Large Flexible Spacecraft, Blacksburg, VA, July 21 - 23, 1979.

(24) Sesak, J. R., and Coradetti, T., "Decentralized Control of Large Space Structures via Forced Singular Perturbation," AIAA Paper 79-0195, 17th Aerospace Sciences Meeting, New Orleans, January 15 - 17, 1979.

(25) Kwakernaak, H., and Sivan, R., *Linear Optimal Control Systems,* Wiley - Interscience, 1972, pp. 216 - 248, 253 - 264, 281 - 306, 328 - 373, 427 - 434.

(26) Mukhopadhyay, V., Newsom, J. R., and Abel, I., "Reduced Order Optimal Feedback Control Law Synthesis for Flutter Suppression," *AIAA Journal of Guidance, Control, and Dynamics,* Vol. 5, No. 4, July - August 1982, pp. 389 - 395.

(27) Newsom, J. R., and Mukhopadhyay, V., "Application of Constrained Optimization to Active Control of Aeroelastic Response," NASA Technical Memorandum 83150, June 1981.

(28) Craig, R. R., *Structural Dynamics,* John Wiley and Sons, Inc., 1981, pp. 303 - 311, 356 - 357.

(29) Kirk, D. E., *Optimal Control Theory* , Prentice Hall, Inc., 1970, pp. 21 - 22, 90 - 93, 209 - 218.

(30) Ogata, K., *Modern Control Engineering,* Prentice-Hall, Inc., 1970, pp. 407 - 425, 430 - 432, 754 - 771.

(31) Kalman, R. E., "On the General Theory of Control Systems," Proc. First IFAC Congress, 1960, pp. 481 - 493.

(32) Kalman, R. E., "Mathematical Description of Linear Dynamical Systems," *J. SIAM Control,* 1, 1963, pp. 152 - 192.

(33) Kalman, R. E., "A New Approach to Linear Filtering and Prediction Problems," *ASME Journal of Basic Engineering,* 1960, pp. 35 - 45.

(34) Kalman, R. E., and Bucy, R. S., "New Results in Linear Filtering and Prediction Theory," *ASME Journal of Basic Engineering,* 1961, pp. 95 - 108.

(35) Anderson B. D. O., and Moore, J. B., *Linear Optimal Control,* Prentice-Hall, Inc., 1971, pp. 50 - 60, 70 - 77.

(36) Cooper, G. R., and McGillen, C. D., *Probabilistic Methods of Signal and System Analysis,* Holt, Rinehart and Winston, 1986, pp. 59 - 61.

(37) Gelb, A. (ed.), *Applied Optimal Estimation,* The MIT Press, 1974.

(38) Wonham, W. M., "On Pole Assignment in Multi-input Controllable Linear Systems," *IEEE Transactions on Automatic Control,* Vol. AC-12, No. 6, December 1967, pp. 660 - 665.

(39) Kailath, T., *Linear Systems,* Prentice-Hall, Inc., 1980, pp. 198 - 199, 549 - 593.

(40) Luenberger, D. G., "Observing the State of a Linear System," *IEEE Transactions on Military Electronics,* Vol. MIL-8, No. 2, April 1964, pp. 74 - 80.

(41) Luenberger, D. G., "Observers for Multivariable Systems," *IEEE Transactions on Automatic Control,* Vol. AC-11, No. 2, April 1966, pp. 190 - 197.

(42) Luenberger, D. G., "An Introduction to Observers," *IEEE Transactions on Automatic Control,* Vol. AC-16, No. 6, December 1971, pp. 596 - 602.

(43) Poelaert, D. H., "Exact Modal Analysis for Spinning Flexible Spacecraft," ESA Symposium on the Dynamics and Control of Non-Rigid Space Vehicles, ESRIN, Frascati, Italy, ESA-SP-117.

(44) Poelaert, D., "Dynamic Interaction Between Solar Arrays and Controlled Spacecraft," Proc. European Symp. on Photovoltaic Generators in Space (ESTEC, Noordwijk, 11 - 13 Sept. 1978) - ESA SP-140 (Nov. 1978).

(45) Poelaert, D. H. L., "A Guideline for the Analysis and Synthesis of a Nonrigid - Spacecraft Control System," ESA/ASE Scientific & Technical Review (1975) 1, pp. 203 - 218.

(46) Poelaert, D., "Spacecraft Dynamic Analysis Using Cantilever Modes of the Appendages - Application to the Space Telescope," ESA STR-206, October 1981.

(47) Skelton, R. E., and Hughes, P. C., "Modal Cost Analysis for Linear Matrix-Second-Order Systems," *ASME J. Dynamic Systems, Measurement and Control,* Vol. 102, No. 3, September 1980, pp. 151 - 158.

(48) Skelton, R. E., and Hughes, P. C., "Flexible Space Structure Model Reduction by Modal Cost Analysis," Proceedings of the Second VPI&SU/AIAA Symposium on Dynamics and Control of Large Flexible Spacecraft, Blacksburg, Virginia, June 21 - 23, 1979, pp. 641 - 660.

(49) Likins, P., Ohkami, Y., and Wong, C., "Appendage Modal Coordinate Truncation Criteria in Hybrid Coordinate Dynamic Analysis," *Journal of Spacecraft and Rockets,* Vol. 13, No. 10, October 1976, pp. 611 - 617.

(50) Gran, R., and Rossi, M., "Closed Loop Order Reduction for Large Space Structures Control," Proceedings of the Second VPI&SU/AIAA Symposium on Dynamics and Control of Large Flexible Spacecraft, Blacksburg, Virginia, June 21 - 23, 1979, pp. 443 - 457.

(51) Kabamba, P. T., "An Euclidean Approach to the Problem of Parameter Reduction in Large Systems," Proceedings of the Second VPI&SU/AIAA Symposium on Dynamics and Control of Large Flexible Spacecraft, Blacksburg, Virginia, June 21 - 23, 1979, pp. 459 - 474.

(52) Frederick, D. K., and Carlson, A. B., *Linear Systems in Communication and Control,* John Wiley and Sons, Inc., 1971, pp. 417 - 442.

(53) D'Azzo, J. J., and Houpis, C. H., *Linear Control System Analysis and Design: Conventional and Modern,* McGraw-Hill Book Company, 1981, pp. 283 - 306.

(54) Friedland, B., *Control System Design: An Introduction to State-Space Methods,* McGraw-Hill Book Company, 1986, pp. 138 - 143.

(55) DiStefano III, J. J., Stubberud, A. R., and Williams, I. J., *Feedback and Control Systems,* McGraw-Hill Book Company, 1967, pp. 187 - 223.

(56) Rosenbrock, H. H., *Computer Aided Control System Design,* Academic Press, New York, 1974.

(57) Rosenbrock, H. H., *State-Space and Multivariable Theory,* New York, Nelson-Wiley, 1970.

(58) Rosenbrock, H. H., "Design of Multivariable Control Systems, Using the Inverse Nyquist Array," *Proc. Inst. Elec. Eng.,* Vol. 116, 1969, pp. 1929 - 1936.

(59) Rosenbrock, H. H., "The Stability of Multivariable Systems," *IEEE Transactions on Automatic Control,* Vol. AC-17, No. 1, February 1972, pp. 105 - 107.

(60) Doyle, J. C., and Stein, G., "Multivariable Feedback Design: Concepts for a Classical/Modern Synthesis," *IEEE Transactions on Automatic Control,* Vol. AC-26, 1, February 1981, pp. 4 - 16.

(61) Lehtomaki, N. A., Sandell, N. R., and Athans, M., "Robustness Results in Linear-Quadratic Gaussian Based Multivariable Control Designs," *IEEE Transactions on Automatic Control,* Vol. AC-26, No. 1, February 1981, pp. 75 - 93.

(62) Desoer, C. A., and Wang, Y., "On the Generalized Nyquist Stability Criterion," *IEEE Transactions on Automatic Control,* Vol. AC-25, No. 2, April 1980, pp. 187 - 196.

(63) Doyle, J. C., "Guaranteed Margins for LQG Regulators," *IEEE Transactions on Automatic Control,* Vol. AC-23, No. 4, August 1978, pp. 756 - 757.

(64) Doyle, J. C., "Multivariable Design Techniques Based on Singular Value. Generalization of Classical Control.," AGARD-LS-117 on Multivariable Analysis and Design Techniques, 1981.

(65) Yedavalli, R. K. "Robust Control Design for Vibration Suppression of Large Space Structures," Vibration Damping Workshop II, Las Vegas, March 1986.

(66) Yedavalli, R. K., "Improved Measures of Stability Robustness for Linear State Space Models," *IEEE Transactions on Automatic Control,* Vol. AC-30, No. 6, June 1985, pp. 577 - 579.

(67) Yedavalli, R. K., "Perturbation Bounds for Robust Stability in Linear State Space Models," *Int. Journal of Control,* Vol. 42, No. 6, 1985, pp. 1507 - 1517.

(68) Safonov, M. G., *Stability and Robustness of Multivariable Feedback Systems,* The MIT Press, 1980.

(69) Doyle, J. C., "Structured Uncertainties in Control System Design," Proceedings of the 24th Conference on Decision and Control, Ft. Lauderdale, FL, December 1985, pp. 260 - 265.

(70) Curtain, R. F. (ed.), Proceedings of the NATO Advanced Research Workshop on Modelling, Robustness and Sensitivity Reduction in Control Systems, Groningen, The Netherlands, December 1 - 5, 1986, Springer-Verlag Berlin Heidelberg, 1987.

(71) Mukhopadhyay, V., and Newsom, J. R., "Application of Matrix Singular Value Properties for Evaluating Gain and Phase Margins of Multiloop Systems," NASA Technical Memorandum 84524, July 1982.

(72) Sundararajan, N., Joshi, S. M., and Armstrong, E. S., "Robust Controller Synthesis for a Large Flexible Antenna," *AIAA J. Guidance,* Vol. 10, No. 2, March - April 1987, pp. 201 - 208.

(73) Safonov, M. G., Laub, A. J., and Hartmann, G. L., "Feedback Properties of Multivariable Systems: The Role and Use of the Return Difference Matrix," *IEEE Transactions on Automatic Control,* Vol. AC-26, No. 1, February 1981, pp. 47 - 65.

(74) Wie, B., and Bryson, A. E., "Multivariable Control Robustness Examples: A Classical Approach," *AIAA Journal of Guidance, Control and Dynamics,* Vol. 10, No. 1, January - February 1987, pp. 118 - 120.

(75) Mukhopadhyay, V., and Newsom, J. R., "A Multiloop System Stability Margin Study Using Matrix Singular Values," *AIAA Journal of Guidance, Control and Dynamics,* Vol. 7, No. 5, September - October 1984, pp. 582 - 588.

(76) Zames, G., "On the Input-Output Stability of Time-Varying Nonlinear Feedback Systems - Part I," *IEEE Transactions on Automatic Control,* Vol. AC-11, No. 2, April 1966, pp. 228 - 238.

(77) Zames, G., "On the Input-Output Stability of Time-Varying Nonlinear Feedback Systems - Part II," *IEEE Transactions on Automatic Control,* Vol. AC-11, No. 3, July 1966, pp. 465 - 476.

(78) Safonov, M. G., and Athans, M., "Gain and Phase Margin of Multiloop LQG Regulators," *IEEE Transactions on Automatic Control,* Vol. AC-22, No. 2, April 1977, pp. 173 - 179.

(79) Hung, Y. S., and MacFarlane, A. G. J., "Multivariable Feedback: A Quasi-Classical Approach," Lecture Notes in Control and Information Sciences, Springer-Verlag, 1982, pp. 5 - 20, 66 - 77.

(80) Stein, G., and Athans, M., "The LQG/LTR Procedure for Multivariable Feedback Control Design," *IEEE Transactions on Automatic Control,* Vol. AC-32, No. 2, February 1987, pp. 105 - 114.

(81) Ridgely, D. B., Banda, S. S., McQuade, T. E., and Lynch, P. J., "Linear-Quadratic-Gaussian with Loop-Transfer-Recovery Methodology for an Unmanned Aircraft," *AIAA Journal of Guidance, Control and Dynamics,* Vol. 10, No. 1, January - February 1987, pp. 82 - 89.

(82) Athans, M., Kapasouris, P., Kappos, E., and Spang III, H. A., "Linear-Quadratic Gaussian with Loop-Transfer Recovery Methodology for the F-100 Engine," *AIAA Journal of Guidance, Control and Dynamics,* Vol. 9, No. 1, January - February 1986, pp. 45 - 52.

(83) Doyle, J. C., and Stein, G., "Robustness with Observers," *IEEE Transactions on Automatic Control,* Vol. AC-24, No. 4, August 1979, pp. 607 - 611.

(84) Stein, G., "LQG - Based Multivariable Design: Frequency Domain Interpretation," AGARD-LS-117 on Multi-Variable Analysis and Design Techniques, 1981.

(85) Blelloch, P. A., and Mingori, D. L., "Modified LTR Robust Control for Flexible Structures," AIAA/AAS Astrodynamics Conference, Williamsburg, Virginia, August 18 - 20, 1986, AIAA-86-2051, pp. 314 - 318.

(86) Bingulac, S. P., West, P. J., and Perkins, W. R., "Recent Advances in the L-A-S Software Used in CAD of Control Systems," 3rd IFAC Symposium on CAD in Control, Copenhagen, July 1985, pp. 124 - 139.

(87) Bingulac, S., "CAD Package L-A-S: A Research and Educational Tool in Systems and Control," 20th Southeastern Symposium on System Theory, Charlotte, North Carolina, March 20 - 23, 1988, pp. 44 - 49.

(88) Grandhi, R. V., Thareja, R., and Haftka, R. T., "NEWSUMT-A: A General Purpose Program for Constrained Optimization Using Constraint Approximations," *ASME Journal of Mechanics, Transmission and Automation in Design,* Vol. 107, March 1985, pp. 94 - 99.

(89) Thareja, R., and Haftka, R. T., "NEWSUMT-A: A Modified Version of NEWSUMT for Inequality and Equality Constraints," VPI Report 148, March 1985, Aerospace Engineering Department, Virginia Tech, Blacksburg, VA 24061.

(90) Singh, M. G., Titli, A., and Malinowski, K., "Decentralized Control Design: An Overview," *Large Scale Systems - Theory and Applications,* Vol. 9, No. 3, December 1985, pp. 215 - 230.

(91) Emami-Naeini, A., Anex, R. P., and Rock, S. M., "Integrated Control: A Decentralized Approach," Proceedings of the 24th Conference on Decision and Control, Ft. Lauderdale, FL, December 1985, pp. 1836 - 1841.

(92) Lindner, D. K., "A Decentralized Pole Placement: An Example," Proceedings of the 24th Conference on Decision and Control, Ft. Lauderdale, FL, December 1985, pp. 170 - 175.

(93) Bernstein, D. S., "The Optimal Projection Equations for Fixed-Structure Decentralized Dynamic Compensation," Proceedings of the 24th Conference on Decision and Control, Ft. Lauderdale, FL, December 1985, pp. 104 - 107.

(94) Wang, S.-H., and Davison, E. J., "On the Stabilization of Decentralized Control Systems," *IEEE Transactions on Automatic Control,* Vol. AC-18, No. 5, October 1973, pp. 473 - 478.

(95) Davison, E. J., "The Robust Decentralized Control of a General Servomechanism Problem," *IEEE Transactions on Automatic Control,* Vol. AC-21, No. 1, February 1976, pp. 14 - 24.

(96) Sezer, M. E., and Hüseyin, Ö., "Stabilization of Linear Time-Invariant Interconnected Systems Using Local State Feedback," *IEEE Transactions on Systems, Man, and Cybernetics,* Vol. SMC-8, No. 10, October 1978, pp. 751 - 756.

(97) Ramakrishna, A., and Viswanadham, N., "Decentralized Control of Interconnected Dynamical Systems," *IEEE Transactions on Automatic Control,* Vol. AC-27, No. 1, February 1982, pp. 159 - 164.

(98) Sezer, M. E., and Siljak, D. D., "Structurally Fixed Modes," *Systems & Control Letters,* Vol. 1, No. 1, July 1981, pp. 60 - 64.

(99) Corfmat, J. P., and Morse, A. S., "Decentralized Control of Linear Multivariable Systems," *Automatica,* Vol. 12, 1976, pp. 479 - 495.

(100) Siljak, D. D., and Vukcevic, M. B., "Decentrally Stabilizable Linear and Bilinear Large - Scale Systems," *Int. Journal of Control,* Vol. 26, No. 2, 1977, pp. 289 - 305.

(101) Davison, E. J., "The Decentralized Stabilization and Control of a Class of Unknown Non-Linear Time-Varying Systems," *Automatica,* Vol. 10, 1974, pp. 309 - 316.

(102) Ikeda, M., Umefuji, O., and Kodama, S., "Stabilization of Large - Scale Linear Systems," *Systems • Computers • Controls,* Vol. 7, No. 3, 1976, pp. 34 - 41.

(103) Darwish, M., Soliman, H. M., and Fantin, J., "Decentralized Stabilization of Large - Scale Dynamical Systems," *IEEE Transactions on Systems, Man, and Cybernetics,* Vol. SMC-9, No. 11, November 1979, pp. 717 - 720.

(104) Chong, C.-Y., and Athans, M., "On the Stochastic Control of Linear Systems with Different Information Sets," *IEEE Transactions on Automatic Control,* Vol. AC-16, No. 5, October 1971, pp. 423 - 430.

(105) Franklin, J. N., *Matrix Theory,* Prentice-Hall, Inc., 1968, pp. 161 - 163.

(106) Wilkinson, J. H., *The Algebraic Eigenvalue Problem,* Oxford University Press, 1965, pp. 55 - 60, 71 - 81.

(107) Hallauer Jr., W. L., Skidmore, G. R., and Gehling, R. N., "Modal-Space Active Damping of a Plane Grid: Experiment and Theory," *AIAA Journal of Guidance, Control, and Dynamics,* 8, No. 3, May - June 1985, pp. 366 - 373.

(108) Masse, M. A., "A Plane Grillage Model for Structural Dynamics Experiments: Design, Theoretical Analysis, and Experimental Testing," M. S. Thesis, Virginia Polytechnic Institute and State University, February 1983.

(109) Gehling, R. N., "Experimental and Theoretical Analysis of a Plane Grillage Structure with High Model Density," M. S. Thesis, Virginia Polytechnic Institute and State University, March 1984.

(110) Stewart, G. W., *Introduction to Matrix Computations,* Academic Press, Inc., 1973, pp. 160 - 184, 317 - 326, 381 - 387.

(111) Anton, H., *Elementary Linear Algebra,* John Wiley and Sons, Inc., 1977, pp. 94 - 97.

Appendix A. ALPHA-SHIFT STABILITY MARGIN

The α – shift procedure of Anderson and Moore [35] guarantees a *minimum* stability margin of $-\alpha$, yet the system may exhibit a larger stability margin as seen from the examples treated in the dissertation. The stability margin was consistently at -2α. A non-rigorous "proof" of this phenomenon is demonstrated for the *scalar* case.

If the scalar control problem is assumed to have the following governing equation and α – shifted deterministic performance index

$$\dot{x} = a_A x + u \qquad [A.1]$$

and

$$J = \int_{t=0}^{\infty} e^{2\alpha t}(q_Q x^2 + u^2)dt \qquad [A.2]$$

where b_B, the control parameter, and r_R, the weighting parameter on the control, were assumed to be unity. Since this is a scalar case, lower case letters are used in place of the capital letters of the matrix form of the equations. It was shown in Equations [2.6.16] to [2.6.19], that this problem

is equivalent to that of the following where the new system is related to the above system by a co-ordinate transformation

$$\bar{x} = e^{\alpha t}x \qquad [A.3]$$

$$\bar{u} = e^{\alpha t}u \qquad [A.4]$$

producing

$$\dot{\bar{x}} = (a_A + \alpha)\bar{x} + \bar{u} \qquad [A.5]$$

and

$$J = \int_{t=0}^{\infty} (q_Q \bar{x}^2 + \bar{u}^2)dt \qquad [A.6]$$

The minimization of Equation [A.6] produces the following Riccati Equation

$$f_F(a_A + \alpha) + (a_A + \alpha)f_F - f_F^2 + q_Q = 0 \qquad [A.7]$$

whose solution is

$$(f_F)_{1,2} = \frac{2(a_A + \alpha) \pm \sqrt{4(a_A + \alpha)^2 + 4q_Q}}{2} \qquad [A.8]$$

but since f_F must be positive definite

$$f_F = (a_A + \alpha) + \sqrt{(a_A + \alpha)^2 + q_Q} \qquad [A.9]$$

The optimal controller becomes

$$\bar{u} = -f_F\bar{x} \qquad [A.10]$$

or

$$u = -f_F x \qquad [A.11]$$

As a result, Equation [A.1] becomes

$$\dot{x} = (a_A - f_F)x \qquad [A.12]$$

or

$$\dot{x} = -[\alpha + \sqrt{(a_A + \alpha)^2 + q_Q}\,]x \qquad [A.13]$$

For q_Q, $a_A << \alpha$, the stability margin becomes -2α.

The following statements are not mathematically rigorous, but they are interesting to note. In the matrix counterpart of the above equations

$$A = \begin{bmatrix} 0 & \omega \\ -\omega & -2\zeta\omega \end{bmatrix} \qquad [A.14]$$

Recall that when the α – shift procedure is used, it only appears in the diagonal form of

$$\alpha I = \begin{bmatrix} \alpha & 0 \\ 0 & \alpha \end{bmatrix} \qquad [A.15]$$

to produce the $[A + \alpha I]$ term in the Riccati Equation. Therefore, it only affects the *diagonal* elements of A.

If one looks only at the A_{22} element of the matrix A

$$A_{22} = -2\zeta\omega \qquad [A.16]$$

and applies it to Equation [A.13], neglecting the q_Q term, the result is

$$\dot{x} = -[\alpha + \sqrt{(\alpha - 2\zeta\omega)^2}\,]x \qquad [A.17]$$

For $\zeta = 0$ (no damping), the stability margin is -2α, whereas, for $\zeta > 0$ (damping), the stability margin decreases. For a given ω, there is some *critical* ζ, ζ_{CR}, that will make $\alpha - 2\zeta_{CR}\omega = 0$ and produce a $-\alpha$ stability margin. The above is consistent with what was observed during the course of the research.

Though it is mathematically possible to increase the damping beyond $\zeta > \zeta_{CR}$, this produces $\alpha - 2\zeta\omega < 0$ or $\sqrt{(\alpha - 2\zeta\omega)^2} > 0$. The result is that the stability margin once again increases from $-\alpha$. This phenomenon was not observed since the analysis was never done for this high of a damping ratio. The net result is that a minimum stability margin of $-\alpha$ is always guaranteed, yet depending on the amount of damping present, a much higher stability margin may be obtained.

Appendix B. SINGULAR VALUES

Since multivariable feedback control involves dealing with magnitudes of matrices, singular values are introduced as a measure of how large a matrix is [19, 79, 106, 110, 111]. Singular values are a good indicator of the size of a complex matrix. They represent a type of normalized eigenvalue which is *real* and non-negative.

B.1. NORMS

The most common vector norm is the Euclidean norm (l_2 norm), i.e.,

$$||\xi||_E = ||\xi||_2 = \sqrt{\xi_1^2 + \xi_2^2 + \cdots + \xi_n^2} \qquad [B.1.1]$$

where $\xi = (\xi_1, \xi_2, \ldots, \xi_n)$.

The corresponding l_2 norm of a matrix A, known also as the spectral norm, is defined as

$$||A||_2 = \sup_{\xi \neq 0} \frac{||A\xi||_2}{||\xi||_2} \qquad [B.1.2]$$

and can be viewed as the *maximum gain of A*.

The singular values of a matrix A, i.e., $\sigma(A)$, are represented by

$$\sigma_i(A) = \sqrt{\lambda_i(A^*A)} = \sqrt{\lambda_i(AA^*)} \qquad [B.1.3]$$

where (*) stands for the complex conjugate transpose, and the λ_i's are the eigenvalues of the positive semidefinite Hermitian matrix A^*A. The λ_i's are all real and positive (or zero). The maximum and minimum singular values are defined as

$$\overline{\sigma}(A) = \sigma_{\max}(A) = \max_i \sqrt{\lambda_i(A^*A)} \qquad [B.1.4]$$

$$\underline{\sigma}(A) = \sigma_{\min}(A) = \min_i \sqrt{\lambda_i(A^*A)} \qquad [B.1.5]$$

respectively.

It can be shown [19] that

$$\overline{\sigma}(A) = ||A||_2 \qquad [B.1.6]$$

i.e., the maximum singular value corresponds to the spectral norm of the matrix A. It is viewed as a measure of the amplication of the matrix A. On the other hand, $\underline{\sigma}(A)$ is viewed as the measure of attenuation a signal experiences from matrix A. If $\underline{\sigma}(A)$ is equal to zero, the A matrix is singular.

It can also be shown [19] that

$$\underline{\sigma}(A) = \frac{1}{\overline{\sigma}(A^{-1})} = \frac{1}{||A^{-1}||_2} \qquad [B.1.7]$$

$$\overline{\sigma}(A^{-1}) = \frac{1}{\underline{\sigma}(A)} = ||A^{-1}||_2 \qquad [B.1.8]$$

$$\underline{\sigma}(A^{-1}) = \frac{1}{\overline{\sigma}(A)} = \frac{1}{||A||_2} \qquad [B.1.9]$$

provided A^{-1} exists.

$$\underline{\sigma}(A) = 0 \rightarrow A \text{ is singular} \qquad [B.1.10]$$

Since $\underline{\sigma}(A)$ determines the singularity of A, a condition number is defined as

$$cond(A) = \frac{\underline{\sigma}(A)}{\bar{\sigma}(A)} \qquad [B.1.11]$$

If $cond(A)$ is very close to zero, it indicates that A is nearly singular.

B.2. SINGULAR VALUE DECOMPOSITION (SVD)

A square (nxn) matrix A can be written [110] as

$$A = U\Sigma V^* \qquad [B.2.1]$$

where

$$\Sigma = diag(\sigma_1, \sigma_2, \dots, \sigma_n) \qquad [B.2.2]$$

for

$$\sigma_1 \geq \sigma_2 \geq \cdots \geq \sigma_n \geq 0 \qquad [B.2.3]$$

where the σ_i's are the singular values of A, and U and V are unitary matrices, i.e., $U^* = U^{-1}$, $U^*U = UU^* = I$, and $\lambda_i(UU^*) = 1$ for all i, and similarly for V.

U is comprised of column vectors which are the left singular vectors of A

$$u_i^* A^* A = \sigma_i^2(A) u_i^* \qquad [B.2.4]$$

and V is comprised of column vectors which are the right singular vectors of A

$$A^* A v_i = \sigma_i^2(A) v_i \qquad [B.2.5]$$

Finally, if A is rectangular (mxn), the singular value decomposition of A becomes

$$A = U \Sigma V^* \qquad [B.2.6]$$

where

$$\Sigma = \begin{bmatrix} \Sigma_1 \\ 0 \end{bmatrix} \qquad for\ m \geq n \qquad [B.2.7]$$

or

$$\Sigma = [\Sigma_1 \quad 0] \qquad for\ m \leq n \qquad [B.2.8]$$

where Σ_1 is a diagonal matrix containing the singular values. U is dimension mxm, V is dimension nxn, Σ is dimension mxn, and Σ_1 is dimension nxn for $m \geq n$ or mxm for $m \leq n$.

B.3. PROPERTIES OF SINGULAR VALUES

The following properties are found in Reference [19]. This list by no means represents all of the properties of singular values.

$$If\ \underline{\sigma}(A) > \overline{\sigma}(B),\ then\ \underline{\sigma}(A + B) > 0 \qquad [B.3.1]$$

$$\sigma_i(\alpha A) = |\alpha| \sigma_i(A) \qquad [B.3.2]$$

$$\overline{\sigma}(A + B) \leq \overline{\sigma}(A) + \overline{\sigma}(B) \qquad [B.3.3]$$

$\overline{\sigma}(AB) \leq \overline{\sigma}(A)\overline{\sigma}(B)$ [*B*.3.4]

$\underline{\sigma}(AB) \geq \underline{\sigma}(A)\underline{\sigma}(B)$ [*B*.3.5]

Rank(A) *is* the *number* of *nonzero* $\sigma_i(A)$. [*B*.3.6]

$\sigma_i(AB) \neq \sigma_i(BA)$, *in general.* [*B*.3.7]

Appendix C. DECENTRALIZED MODAL CONTROL

The basic idea of decentralized modal control is that separate controllers are designed to independently control various sets of modes which are locally dominant. In Chapter 6, the formulation of this problem was demonstrated for the case when the control vectors u_1 and u_2 were made available simultaneously to both observers. In truly decentralized modal control, this is not the case. The observer of one controller knows absolutely nothing about what is happening at the other controller. The effect of removing this assumption will now be demonstrated. Once again, the governing system of equations to control two sets of modes is:

$$\dot{x}_1 = A_1 x_1 + B_1 u_1 + \beta_1 u_2 \qquad [C.1]$$

$$\dot{x}_2 = A_2 x_2 + \beta_2 u_1 + B_2 u_2 \qquad [C.2]$$

$$y_1 = C_1 x_1 + \gamma_1 x_2 \qquad [C.3]$$

$$y_2 = \gamma_2 x_1 + C_2 x_2 \qquad [C.4]$$

which governs the system dynamics and output.

Since the state of the system is, in general, not fully known, it is reconstructed via a Kalman-Bucy Filter (KBF). The reconstructed states, $\hat{x}_1$ and $\hat{x}_2$, are obtained by integrating

$$\dot{\hat{x}}_1 = A_1\hat{x}_1 + B_1u_1 + K_{c_1}(y_1 - C_1\hat{x}_1) \qquad [\hat{x}_1(0) = 0] \qquad [C.5]$$

$$\dot{\hat{x}}_2 = A_2\hat{x}_2 + B_2u_2 + K_{c_2}(y_2 - C_2\hat{x}_2) \qquad [\hat{x}_2(0) = 0] \qquad [C.6]$$

where K_{c_1} and K_{c_2} are the observer gain matrices.

In truly decentralized modal control, the $\beta_i u_j$ terms are not present in the observer equations as they were in Equations [6.1.5] and [6.1.6]. The observer of one controller knows absolutely nothing about what is happening at the other controller.

The control vectors, u_1 and u_2, are given as

$$u_1 = -G_{c_1}\hat{x}_1 \qquad [C.7]$$

$$u_2 = -G_{c_2}\hat{x}_2 \qquad [C.8]$$

where G_{c_1} and G_{c_2}, the feedback gain matrices, are calculated from the Linear Quadratic Regulator (LQR) design methodology.

The state estimator error is defined as $e_i = \hat{x}_i - x_i$, and the state vector is selected to be $(x_1^T\, x_2^T\, e_1^T\, e_2^T)^T$. The corresponding system matrix for this defined state becomes

$$A_D = \begin{bmatrix} A_1 - B_1G_{c_1} & -\beta_1G_{c_2} & -B_1G_{c_1} & -\beta_1G_{c_2} \\ -\beta_2G_{c_1} & A_2 - B_2G_{c_2} & -\beta_2G_{c_1} & -B_2G_{c_2} \\ 0 & (K_{c_1}\gamma_1 + \beta_1G_{c_2}) & A_1 - K_{c_1}C_1 & \beta_1G_{c_2} \\ (K_{c_2}\gamma_2 + \beta_2G_{c_1}) & 0 & \beta_2G_{c_1} & A_2 - K_{c_2}C_2 \end{bmatrix} \qquad [C.9]$$

which can be written as

$$A_D = A_D^x + A_D^s \qquad [C.10]$$

where

$$A_D^{\times} = \begin{bmatrix} A_1 - B_1 G_{c_1} & 0 & -B_1 G_{c_1} & 0 \\ 0 & A_2 - B_2 G_{c_2} & 0 & -B_2 G_{c_2} \\ 0 & 0 & A_1 - K_{c_1} C_1 & 0 \\ 0 & 0 & 0 & A_2 - K_{c_2} C_2 \end{bmatrix} \qquad [C.11]$$

and

$$A_D^{s} = \begin{bmatrix} 0 & -\beta_1 G_{c_2} & 0 & -\beta_1 G_{c_2} \\ -\beta_2 G_{c_1} & 0 & -\beta_2 G_{c_1} & 0 \\ 0 & (K_{c_1}\gamma_1 + \beta_1 G_{c_2}) & 0 & \beta_1 G_{c_2} \\ (K_{c_2}\gamma_2 + \beta_2 G_{c_1}) & 0 & \beta_2 G_{c_1} & 0 \end{bmatrix} \qquad [C.12]$$

Comparing Equations [C.12] and [6.1.12] shows that in truly decentralized modal control, there are several more perturbation terms in the spillover matrix, A_D^s.

With the global stability requirement being completely analyzed, the next condition to be investigated is that of reliability, i.e., the stability of the disabled control system. This condition requires that the system remain stable even if one of the controllers becomes inoperational.

Consider first the case of subsystem 2 being disabled, and define the state vector as $(x_1^T\, x_2^T\, e_1^T)^T$. It can be shown that the reduced system matrix is found by setting $G_{c_2} = 0$ in the submatrix corresponding to the new state. Denoting the system matrix as $\overline{A}_1^D$, we have

$$\overline{A}_1^D = \begin{bmatrix} A_1 - B_1 G_{c_1} & 0 & -B_1 G_{c_1} \\ -\beta_2 G_{c_1} & A_2 & -\beta_2 G_{c_1} \\ 0 & K_{c_1}\gamma_1 & A_1 - K_{c_1} C_1 \end{bmatrix} \qquad [C.13]$$

which can be written as

$$\overline{A}_1^D = \overline{A}_1^{\times} + \overline{A}_1^{s} \qquad [C.14]$$

where

$$\overline{A}_1^{\times} = \begin{bmatrix} A_1 - B_1 G_{c_1} & 0 & -B_1 G_{c_1} \\ 0 & A_2 & 0 \\ 0 & 0 & A_1 - K_{c_1} C_1 \end{bmatrix} \qquad [C.15]$$

and

$$\overline{A}_1^{s} = \begin{bmatrix} 0 & 0 & 0 \\ -\beta_2 G_{c_1} & 0 & -\beta_2 G_{c_1} \\ 0 & K_{c_1}\gamma_1 & 0 \end{bmatrix} \qquad [C.16]$$

The term A_2 in $\overline{A}_1^{\times}$ has only small stability margin provided by structural damping alone. Therefore, any slight perturbations, $\overline{A}_1^{s}$, can lead to an unstable system.

Similarly, if subsystem 1 is disabled, the state vector becomes $(x_1^T\, x_2^T\, e_2^T)^T$. The corresponding system matrix is

$$\overline{A}_2^{D} = \begin{bmatrix} A_1 & -\beta_1 G_{c_2} & -\beta_1 G_{c_2} \\ 0 & A_2 - B_2 G_{c_2} & -B_2 G_{c_2} \\ K_{c_2}\gamma_2 & 0 & A_2 - K_{c_2} C_2 \end{bmatrix} \qquad [C.17]$$

which can be written as

$$\overline{A}_2^{D} = \overline{A}_2^{\times} + \overline{A}_2^{s} \qquad [C.18]$$

where

$$\overline{A}_2^{\times} = \begin{bmatrix} A_1 & 0 & 0 \\ 0 & A_2 - B_2 G_{c_2} & -B_2 G_{c_2} \\ 0 & 0 & A_2 - K_{c_2} C_2 \end{bmatrix} \qquad [C.19]$$

and

$$\overline{A}_2^x = \begin{bmatrix} 0 & -\beta_1 G_{c_2} & -\beta_1 G_{c_2} \\ 0 & 0 & 0 \\ K_{c_2} y_2 & 0 & 0 \end{bmatrix} \qquad [C.20]$$

Once again, $\overline{A}_2^x$ has small stability margin, therefore, any perturbations can lead to an unstable system.

As it turns out, the reliability condition remains unchanged, i.e., Equations [*C*.13] - [*C*.20] are identical to Equations [6.1.28] - [6.1.35]. As a result, for two controllers, under spillover considerations (i.e., reliability conditions), the two problem formulations are identical.

The vita has been removed from the scanned document